

**CATALYSIS AND LIGAND DESIGN: LIVING RING OPENING
POLYMERIZATION OF LACTIDE WITH CHIRAL DINUCLEAR INDIUM
CATALYSTS AND TEMPLATE SYNTHESIS OF FUNCTIONALIZED
CARBENES ON IRON COMPLEXES**

by

Insun Yu

M.Sc., The University of Manitoba, 2005

A THESIS SUBMITTED IN PARTIAL FULFILLMENT OF
THE REQUIREMENTS FOR THE DEGREE OF

DOCTOR OF PHILOSOPHY

in

THE FACULTY OF GRADUATE STUDIES

(Chemistry)

THE UNIVERSITY OF BRITISH COLUMBIA

(Vancouver)

November 2012

© Insun Yu, 2012

Abstract

A family of indium complexes were synthesized and their catalytic activity towards the ring opening polymerization of lactide to form poly(lactic acid), a biodegradable polymer, were assessed. Racemic and enantiopure mono- and bis-alkoxy-bridged complexes bearing bulky chiral diaminoaryloxy ligands were synthesized and characterized. The reaction of the bis-alkoxy-bridged complexes with water produced mono-hydroxy-alkoxy-bridged dinuclear indium complexes. Investigation of both the mono- and bis-alkoxy-bridged complexes confirmed dinuclear structures in solution and in the solid state. These dinuclear complexes were highly active catalysts for the ring-opening polymerization of lactide to form poly(lactic acid) at room temperature. A detailed mechanistic investigation showed that the selectivities obtained for the ROP of racemic LA with the mono- and bis-alkoxy-bridged complexes are different and, along with kinetics investigations, suggest a dinuclear propagating species for these complexes.

Additionally, neutral and cationic alkyl indium complexes bearing a chiral diaminophenoxy ligand were synthesized and characterized. Investigation of the cationic complexes in solution by NMR spectroscopy showed the counter anions influenced the different chemical environments at the metal center in solution. The preliminary polymerization of methyl methacrylate with neutral dialkyl and cationic alkyl indium complexes produced poly(methyl methacrylate). This is the first demonstration of cationic indium complexes for catalytic reactivity not only in solution but also in neat monomer.

Finally, a family of cyclic and acyclic Fischer-type carbenes were generated via nucleophilic attack at the carbon atom of a coordinated isocyanide on a piano-stool iron(II) complex. All complexes were characterized by IR and NMR spectroscopy and, where possible, by single-crystal X-ray diffraction. In particular, rare donor-functionalized acyclic (phosphino)(amino)- and (silyl)(amino)carbenes were generated by a two-step template synthesis on the iron(II) complex. The methodology involves the initial formation of ylidene complexes followed by reduction of the resulting imine to yield the desired carbene complexes. The reversible conversion of an acyclic (silyl)(amino)carbene complex to its ylidene precursor via slow deprotonation with hydride was demonstrated.

Preface

Chapter 2

I synthesized the majority of the racemic and enantiopure mono- and bis-ethoxy-bridged complexes $[(\text{NNO}_R)\text{InX}(\mu\text{-OEt})]_2$ and $[(\text{NNO}_R)\text{InX}]_2[\mu\text{-Y}][\mu\text{-OEt}]$ ($\text{NNO}_R = 2\text{-}t\text{-butyl-4-R-6-}(((2\text{-}(\text{dimethylamino})\text{cyclohexyl})\text{amino})\text{methyl})\text{phenolate}$, $R = t\text{-Bu, Me}$; $X = \text{Cl, I}$; $Y = \text{Cl, I, OEt}$), respectively, and characterized them using a variety of techniques. I solved all the molecular structures using single-crystal X-ray crystallography and performed the reactivity studies of the dinuclear indium complexes. Dr. Alberto Acosta-Ramirez, a former postdoctoral fellow, synthesized and characterized the racemic dinuclear indium complexes $[(\text{NNO}_{t\text{Bu}})\text{In(I)}(\mu\text{-OEt})]_2$ and $[(\text{NNO}_{t\text{Bu}})\text{In(I)}]_2(\mu\text{-OH})(\mu\text{-OEt})$ and their single crystals that I collected the single crystal X-ray data for these compounds and solved the molecular structure. The work in **Chapter 2** has been published in *the Journal of American Chemical Society*.¹ I was the major contributor to the writing of this manuscript, with significant input from Prof. Mehrkhodavandi.

Chapter 3

I performed all the kinetic and mechanistic studies and the large-scale polymerization of LA, with the exception of the data presented in **Figure 3.16** for a plot of PLA M_n and molecular weight distribution (PDI) as functions of added rac- or L-LA for catalyst $(\pm)\text{-5}$, $(\pm)\text{-}[(\text{NNO}_{t\text{Bu}})\text{InCl}]_2(\mu\text{-Cl})(\mu\text{-OEt})$, **Figure 3.20** for plots of PLA M_n and P_m as functions of conversion for catalysts $(\pm)\text{-5}$ and $(R,R/R,R)\text{-5}$, and **Figure 2.25** for a plot of PLA M_n with $[(\text{NNO}_{t\text{Bu}})\text{In(Cl)}]_2(\mu\text{-Cl})(\mu\text{-OEt})$ in the presence of the different equivalent of $(\text{NNO}_{t\text{Bu}})\text{InCl}_2$ which were performed Dr. Alberto Acosta-Ramirez. **Chapter 3** has been published in its entirety in *the Journal of American Chemical Society*.¹ I also contributed synthesis and characterization of the work with the achiral indium complexes $[(\text{N}_{\text{Me}2}\text{N}_{\text{Me}}\text{O}_{t\text{Bu}})\text{In(Cl)}]_2(\mu\text{-Cl})(\mu\text{-OEt})$ as well as the kinetic and polymerization studies published in *Dalton Transactions*.² Kimberly Osten and I were the major contributors to the writing of this manuscript, with significant input from Prof. Mehrkhodavandi.

Chapter 4

I performed all of the studies in this chapter, and synthesis and single crystal X-ray crystallographic characterization of the indium complex $(\text{NNO}_{\text{tBu}})\text{InMe}_2$ of **Chapter 4** has been published in *Inorganic Chemistry*.³ I was a minor contributor to the writing of the this manuscript, however the remainder of the chapter was written exclusively by myself.

Chapter 5

I performed all of the work in **Chapter 5**, except for DFT calculations performed by professor Paula Diaconescu and molecular structures of **35** and **36** solved by Dr. B. Patrick. This work has been published in *Organometallics* in 2009⁴ and 2010.⁵ I was the major contributor to the writing of the this manuscript, with contributions to the discussion of DFT by Prof. Diaconescu and with significant input from Prof. Mehrkhodavandi.

Table of Contents

Abstract.....	i
Preface.....	ii
Table of Contents	iv
List of Tables	vii
List of Figures.....	ix
List of Schemes	xvi
List of Abbreviations and Symbols	xviii
List of Compounds	xxii
Acknowledgements	xxiv
Dedication	xxvi
Chapter 1: General Introduction	1
Chapter 2: Structural Characterizations of Chiral Alkoxy-Bridged Dinuclear Indium(III) Complexes in Solution and Solid State	6
2.1 Introduction.....	6
2.1.1 Indium catalysts for the polymerization of cyclic esters	6
2.1.2 Comparison with aluminum analogues	10
2.1.3 Determination of catalyst nuclearity in solution	12
2.2 Results.....	14
2.2.1 Synthesis and characterization of proligands	14
2.2.2 Synthesis and characterization of racemic alkoxy-bridged indium complexes.....	16
2.2.3 Synthesis and characterization of enantiopure alkoxy-bridged indium complexes	21
2.2.4 Dinuclear nature of ethoxy-bridged complexes in solution	25
2.3 Conclusion	38
2.4 Experimental section.....	39
Chapter 3: Mechanistic and Selectivity Studies of the Ring Opening Polymerization of Lactide with Chiral Alkoxy-Bridged Dinuclear Indium Catalysts	54
3.1 Introduction.....	54

3.1.1	Lactide	54
3.1.2	Poly(lactic acid).....	56
3.1.3	Metal-catalyzed coordination-insertion mechanisms for ring opening polymerization (ROP) of lactide (LA).....	59
3.2	Results.....	68
3.2.1	Living ring opening polymerization (ROP) of lactide	68
3.2.2	Control of stereoselectivity with dinuclear catalysts.....	76
3.2.3	On the solution structure of the propagating species for catalyst 5 [(NNO _{tBu})InCl] ₂ (μ-Cl)(μ-OEt).....	82
3.3	Discussion and conclusion.....	87
3.4	Experimental section.....	91

Chapter 4: Cationic Chiral Indium Complexes and Their Role in Polymerization of Polar Conjugate Monomers..... 93

4.1	Introduction.....	93
4.1.1	Cationic indium complexes	93
4.1.2	Poly(methyl methacrylate) (PMMA)	95
4.2	Results and discussion	102
4.2.1	Synthesis and characterizations of neutral and cationic indium alkyl complexes.....	102
4.2.2	Reactivity of cationic indium complexes with methyl methacrylate (MMA).....	115
4.3	Conclusion	118
4.4	Experimental section.....	119

Chapter 5: Template Synthesis of Functionalized Carbenes on Iron Complexes 125

5.1	Introduction.....	125
5.1.1	History of singlet carbenes	125
5.1.2	Transition metal carbene complexes	126
5.2	Results and discussion	130
5.2.1	Synthesis of the iron isocyanide template	131
5.2.2	Acyclic diaminocarbene complexes.....	132
5.2.3	Cyclic diaminocarbene complexes	134
5.2.4	(Oxy)(amino)carbene complexes	138
5.2.5	Acyclic (silyl) and (phosphino)(amino)carbene complexes.....	142
5.2.6	Reactivity of acyclic (silyl)(amino) carbene with an unconventional base.....	148
5.3	Conclusion	149

5.4 Experimental section.....	150
Chapter 6: General Conclusion and Future Directions	166
References.....	169
Appendices.....	183
Appendix A	183
A.1 Characterization of indium complexes	183
A.2 Selective crystal data for (\pm)-3, (<i>S,S</i>)-4, (<i>S,S/S,S</i>)-8, meso-9, (\pm)-11, and (<i>R,R/R,R</i>)- [(NNO _{Me})In(I)(μ -OH)] ₂	202
Appendix B	203
B.1 Stereoselectivity.....	203
Appendix C	208
C.1 Characterization of neutral and cationic indium complexes.....	208
C.2 Selective crystal data for 13, 14 and 16.....	224
Appendix D	225
D.1 ¹ H, ¹³ C{ ¹ H} and ³¹ P{ ¹ H} NMR spectra of 35, 36, 37 and 38.....	225
D.2 Overlaid ³¹ P{ ¹ H} NMR spectra.....	233
D.3 IR, ³¹ P{ ¹ H} NMR and ¹³ C{ ¹ H} NMR spectroscopic data for 16-38.....	234
D.4 Selected crystallographic data for compounds 19, 21, 23, 26, 27, 34, 35, 36, and 38. ...	235

List of Tables

Table 2.1. Selected distances (Å) and angles (°) for (±)- 3	18
Table 2.2. Selected distances (Å) and angles (°) for meso- 9	20
Table 2.3. Selected distances (Å) and angles (°) for (±)- 11	20
Table 2.4. Selected distances (Å) and angles (°) for (<i>S,S</i>)- 4	21
Table 2.5. Selected distances (Å) and angles (°) for (<i>S,S/S,S</i>)- 8	24
Table 2.6. Selected distances (Å) and angles (°) for (<i>R,R/R,R</i>)-[(NNO _{Me})In(I)(μ-OH)] ₂	25
Table 2.7. Selective qualitative H-H distance calculated by 1D NOE spectrum of (±)- 5	30
Table 2.8. Selective qualitative H-H distance calculated by 1D NOE spectrum of meso- 9	31
Table 2.9. Comparison of calculated hydrodynamic radii (r _H) by PGSE spectroscopy and estimated r _{x-ray} by X-ray crystallography.....	33
Table 3.1. Rate constants for the ROP of rac-LA using dinuclear indium initiators.....	72
Table 3.2. Polymerization rac-LA by complexes (±)- 5 , (±)- 7 and meso- 8	76
Table 3.3. Effects of catalyst chirality on reaction rates and polymer tacticity by mono-ethoxy bridged complex 5	78
Table 3.4. Effects of catalyst chirality on reaction rates and polymer tacticity by bis-ethoxy bridged complex 8	82
Table 4.1. Selected distances (Å) and angles (°) for complex 12	103
Table 4.2. Selected distances (Å) and angles (°) for complex 13	108
Table 4.3. Selected distances (Å) and angles (°) for complex [(NNO _{tBu})In(CH ₂ SiMe ₃)] [B(C ₆ F ₅) ₄] (14) and 14 •THF.....	113
Table 4.4. Selected distances (Å) and angles (°) for complex 16 [(NNO _{tBu})In(CH ₂ SiMe ₃)] [PF ₆].....	114
Table 4.5. Polymerization of MMA with neutral complexes In(CH ₂ SiMe ₃) ₃ , 13 and 5 and cationic complexes 14-16	117
Table 5.1. Selected distances (Å) and angles (°) for 19 and 21	134
Table 5.2. Selected distances (Å) and angles (°) for 23	136
Table 5.3. Selected distances (Å) and angles (°) for 26	137
Table 5.4. Selected distances (Å) and angles (°) for 27	140
Table 5.5. Selected distances (Å) and angles (°) for 34	142

Table 5.6. Selected distances (Å) and angles (°) for 35 and 36	144
Table 5.7. Selected distances (Å) and angles (°) for 38	147

List of Figures

Figure 2.1. Some indium complexes with chiral ligands for the ROP of lactide. ^{2,23,57,85,86,91}	9
Figure 2.2. Some indium complexes with achiral ligands for the ROP of lactide. ^{2,82,84,86-89}	10
Figure 2.3. Some aluminium complexes with (a) achiral ⁹⁷⁻¹⁰⁴ and (b) chiral ⁹²⁻⁹⁶ ligands for the ROP of lactide.	12
Figure 2.4. Structures of the alkoxy bridged dinuclear Zn complex possible via intramolecular rearrangements or a monomer/dimer equilibrium in solution. ¹¹⁰	14
Figure 2.5. Molecular structure of (\pm)- 3 (depicted with ellipsoids at 50% probability and most H atoms).	17
Figure 2.6. Molecular structure of meso- 9 (depicted with ellipsoids at 50% probability and H atoms omitted for clarity).	19
Figure 2.7. Molecular structure of (\pm)- 11 (depicted with ellipsoids at 50% probability and H atoms as well as solvent molecules omitted for clarity).	20
Figure 2.8. Molecular structure of (<i>S,S</i>)- 4 (depicted with ellipsoids at 50% probability and most H atoms).	21
Figure 2.9. ¹ H spectra (400 MHz, CDCl ₃ , 25 °C) of (a) (\pm)-, (<i>R,R/R,R</i>)-, and (<i>S,S/S,S</i>)- 5 , and (b) meso-, (<i>R,R/R,R</i>)-, and (<i>S,S/S,S</i>)- 8 .	22
Figure 2.10. ¹ H NMR spectra (400 MHz, CDCl ₃ , 25 °C) of a mixture of an equimolar amount of <i>R,R/R,R</i> - and <i>S,S/S,S</i> - 8 . <i>R,R/R,R</i> - and <i>S,S/S,S</i> -[8] = 0.00062 M.	23
Figure 2.11. Molecular structure of (<i>S,S/S,S</i>)- 8 (depicted with ellipsoids at 50% probability and H atoms omitted for clarity).	23
Figure 2.12. Molecular structure of (<i>R,R/R,R</i>)-[(NNO _{Me})In(I)(μ -OH)] ₂ (depicted with ellipsoids at 50% probability and most H atoms).	24
Figure 2.13. ¹ H NMR spectra (400 MHz, C ₆ D ₅ CD ₃) of (\pm)-[(NNO _{tBu})InCl] ₂ (μ -Cl)(μ -OEt) (5) at variable temperatures.	26
Figure 2.14. ¹ H NMR spectra (400 MHz, CDCl ₃) of meso-[(NNO _{Me})In(I)(μ -OEt)] ₂ (8) at variable temperatures.	26
Figure 2.15. 2D NOESY spectra (400 MHz, CDCl ₃ , 25 °C) of (a) (\pm)-[(NNO _{tBu})InCl] ₂ (μ -Cl)(μ -OEt) (5), (b) meso-[(NNO _{Me})In(I)(μ -OEt)] ₂ (8) and (c) meso-[(NNO _{tBu})In(I)(μ -OEt)] ₂	

(9) at the optimized mixing time (400 msec, The diagonal peaks, which have an opposite phase to that of the NOE cross peaks shown in black, are negative and shown in red.).	29
Figure 2.16. Through space interactions expected for mononuclear ethoxy complexes and observed in the ¹ H NOESY-2D NMR spectra of complexes (±)- 5 (left), and meso- 8 and 9 (right) (400 MHz, CDCl ₃ , 25 °C).	29
Figure 2.17. 1D NOE spectrum (400 MHz, CDCl ₃ , 25 °C) of (±)-[(NNO _{tBu})InCl] ₂ (μ-Cl)(μ-OEt) (5).	30
Figure 2.18. 1D NOE spectrum (400 MHz, CDCl ₃ , 25 °C) of meso-[(NNO _{tBu})In(I)(μ-OEt)] ₂ (9).	31
Figure 2.19. Plot of $\ln(I/I_0)$ vs $\gamma^2 \delta^2 G^2 [\Delta - (\delta/3)] \times 10^{10}$ (m ⁻² s) from PGSE experiments (400 MHz, CD ₂ Cl ₂ , 25 °C). The hydrodynamic radius (r _H) of each compound were calculated by using the slopes (<i>D_t</i>) of the linear fits. I = intensity of the observed spin-echo, I ₀ = intensity of the spin-echo in the absence of gradients, G = varied gradient strength, γ = gyromagnetic ratio (2.675 × 10 ⁸ rad s ⁻¹ T ⁻¹), δ = length of the gradient pulse, Δ = delay between the midpoints of the gradients.	32
Figure 2.20. ¹ H NMR spectra (400 MHz, CDCl ₃ , 25 °C) of (a) complex (±)- 5 , [(NNO _{tBu})InCl] ₂ (μ-Cl)(μ-OEt), and complex 5 with 2 equivalents of (b) pyridine, (c) ethyl acetate, and (d) ethanol. [5] = 0.0023 M.	34
Figure 2.21. ¹ H NMR spectra (400 MHz, CD ₂ Cl ₂) of (a) pyridine, (b) (±)- 5 , a mixture of (c) - (s) (±)- 5 with 10 equivalents of pyridine (0.023 M) at variable temperatures, and (t) ¹ H NMR spectrum (400 MHz, CD ₂ Cl ₂ , 25 °C) of (±)- 5 reacted in neat pyridine at 100 °C (the black dot symbol presents new appearing signals.). [5] = 0.0023 M.	35
Figure 2.22. ¹ H NMR spectrum (400 MHz, CD ₂ Cl ₂ , 25 °C) of (±)- 5 reacted in neat pyridine at 100 °C (● represents signals for new complex) [5] = 0.0023 M.	36
Figure 2.23. 2D ¹ H NOESY spectra (400 MHz, CD ₂ Cl ₂ , 25 °C) of (±)- 5 reacted in neat pyridine at 100 °C at the optimized mixing time (400 msec, The diagonal peaks, which have an opposite phase to that of the NOE cross peaks shown in black, are negative and shown in red, and the black dot symbol presents new appearing signals.). [5] = 0.0023 M.	37
Figure 2.24. ¹ H NMR spectra (400 MHz, CDCl ₃ , 25 °C) of (a) complex 5 , (±)-[(NNO _{tBu})InCl] ₂ (μ-Cl)(μ-OEt), and complex (±)- 5 reacted with neat dried (b) methanol and (c) isopropanol for 16 hours at room temperature.	38

Figure 3.1. Schematic life cycle of biodegradable PLA based on renewable biomass (corn or starch).....	55
Figure 3.2. Optical isomers of lactic acid.	55
Figure 3.3. Different optical isomers of lactide.	56
Figure 3.4. Possible microstructures of PLA.	57
Figure 3.5. ^1H NMR and $^1\text{H}\{^1\text{H}\}$ NMR spectra of PLA obtained from rac-LA (600 MHz, CDCl_3 , 25 °C).....	59
Figure 3.6. Proposed mechanism of LA ROP.....	60
Figure 3.7. Possible transesterification side reactions for LA polymerization: (a) intermolecular and (b) intramolecular.	61
Figure 3.8. Proposed mechanism of LA polymerization with (a) the dinuclear BDI zinc alkoxide complex (B) ²¹⁴ and (b) the 1, ω -dithioalkanediyl-bridged bisphenolato (OSSO) scandium complexes (D). ²⁸⁵	62
Figure 3.9. Schematic representation of possible propagation stereoerrors in isospecific and syndiospecific polymerization: (a) enantiomorph-site control errors, (b) chain-end control errors.	63
Figure 3.10. Achiral salen aluminium ethyl complexes. ^{97,233}	65
Figure 3.11. Proposed mechanism for stereoselective LA polymerization using a catalyst generated <i>in-situ</i> from InCl_3 , BnOH , and NEt_3 . ⁹⁰	67
Figure 3.12. The ROP plots of 200 equiv of $[\text{LA}]$ for two different initiators (5 , (\pm)- $[(\text{NNO}_{\text{tBu}})\text{InCl}](\mu\text{-Cl})(\mu\text{-OEt})$, = \blacktriangle ; 6 , (\pm)- $[(\text{NNO}_{\text{tBu}})\text{InCl}](\mu\text{-Cl})(\mu\text{-OEt})$, = \blacksquare) at 25 °C followed to 90% conversion. $[\text{LA}] = 0.91 \text{ M}$. $[\text{catalyst}] = 0.0091 \text{ M}$ in CDCl_3 . 1,3,5-trimethoxybenzene (TMB) was used as internal standard.....	69
Figure 3.13. The ROP plots of rac-LA using dinuclear indium initiators, (a) (\pm)- $[(\text{NNO}_{\text{tBu}})\text{InCl}](\mu\text{-Cl})(\mu\text{-OEt})$ (5), (b) (\pm)- $[(\text{NNO}_{\text{Me}})\text{InI}]_2(\mu\text{-I})(\mu\text{-OEt})$ (7), (c) (\pm)- $[(\text{NNO}_{\text{Me}})\text{In(I)}](\mu\text{-OEt})_2$ (8) and (d) (\pm)- $[(\text{NNO}_{\text{Me}})\text{InI}]_2(\mu\text{-OH})(\mu\text{-OEt})$ (10). All the reactions were carried out in an NMR scale with various ratios of $[\text{LA}]/[\text{initiator}]$ at 25 °C and followed to 90% conversion. For the initiators, (\pm)- 5 , (\pm)- 7 and (\pm)- 10 , $[\text{LA}] = 0.91 \text{ M}$. $[\text{catalyst stock solution}] = 0.0091 \text{ M}$; for the initiator, (\pm)- 8 , $[\text{LA}] = 0.228 \text{ M}$. $[\text{catalyst}] = 0.00228 \text{ M}$ in CDCl_3 . 1,3,5-trimethoxybenzene (TMB) was used as internal standard. The value of k_{obs} was determined from the slope of the plots of $\ln([\text{LA}]/[\text{TMB}])$ vs. time,	

excluding the induction period. The variable concentrations of initiator are shown in the legends. 70

Figure 3.14. Plots of k_{obs} vs. [initiator] for (a) (\pm) - $[(\text{NNO}_{\text{tBu}})\text{InCl}](\mu\text{-Cl})(\mu\text{-OEt})$ (\pm)-**5**, (b) (\pm) - $[(\text{NNO}_{\text{Me}})\text{InI}]_2(\mu\text{-I})(\mu\text{-OEt})$ (\pm)-**7**, (c) (\pm) - $[(\text{NNO}_{\text{Me}})\text{In(I)}](\mu\text{-OEt})_2$ (\pm)-**8** and (d) (\pm) - $[(\text{NNO}_{\text{Me}})\text{InI}]_2(\mu\text{-OH})(\mu\text{-OEt})$ (\pm)-**10**. All the reactions were carried out in an NMR tube with 100, 150, 200, 300, 400, 500 and 600 equivalents of [LA]/[initiator] in CDCl_3 at 25°C and followed to 90% conversion. [LA] = 0.91 M, [catalyst] = 0.0091 M for **5**, **7**, and **10**; [LA] = 0.228 M, [catalyst] = 0.00228 M for **8**. 1,3,5-trimethoxybenzene (TMB) was used as internal standard. The value of k_{obs} was determined from the slope of the plots of $\ln([\text{LA}]/[\text{TMB}])$ vs. time..... 71

Figure 3.15. Activation parameters for the polymerization of rac-LA using (\pm) - $[(\text{NNO}_{\text{tBu}})\text{InCl}]_2(\mu\text{-Cl})(\mu\text{-OEt})$ (**5**) with its variable concentrations, (a) [**5**] = 1.00 mM and (b) [**5**] = 3.00 mM, in CD_2Cl_2 , (c) (\pm) - $[(\text{NNO}_{\text{Me}})\text{InI}]_2(\mu\text{-I})(\mu\text{-OEt})$ (**7**) and (d) meso- $[(\text{NNO}_{\text{Me}})\text{In(I)}](\mu\text{-OEt})_2$ (**8**) in CDCl_3 . Polymerization rate = $k_{obs} \times [\text{LA}]$; $k_{obs} = k[\text{cat}]$, where k is the rate constant used in the Eyring equation to derive activation parameters. Due to solubility constraints, different [cat] were used for (\pm) -**7** and meso-**8**. 74

Figure 3.16. Plot of observed PLA M_n (■) and molecular weight distribution (PDI) (▲) as functions of added rac- or L-LA for catalyst **5** (\pm) - $[(\text{NNO}_{\text{tBu}})\text{InCl}]_2(\mu\text{-Cl})(\mu\text{-OEt})$ (M_n = number averaged molecular weight, PDI = polydispersity index). The line indicates calculated M_n values based on the LA: initiator ratio. All reactions were carried out at room temperature in CH_2Cl_2 and polymer samples obtained at >90% conversion. 75

Figure 3.17. $^1\text{H}\{^1\text{H}\}$ NMR spectra (600 MHz, CDCl_3 , 25°C) of PLA obtained from ROP of rac-LA with (a) (\pm) -**5** ($P_m = 0.61$) and (b) (\pm) -**7** ($P_m = 0.59$). 77

Figure 3.18. Plot of $\ln[\text{LA}]$ vs time for polymerization of rac-LA, L-LA, and D-LA by (a) (R,R,R) -**5** and (b) (R,R,R) -**8**. (400 MHz, CDCl_3 , 25°C). 79

Figure 3.19. Plots of k_{obs} (◆) and P_m (●) as functions of catalyst enantiopurity. All the reactions were carried out with 200 equiv of rac-LA in CDCl_3 at 25°C and followed to 90% conversion. (a); [**5**] = 0.0024 M, [LA] = 0.46 M, (b); [**8**] = 0.00057 M, d [LA] = 0.117 M. .. 80

Figure 3.20. Plots of observed PLA M_n (■) and P_m (●) as functions of conversion for catalysts (\pm) -**5** (a) and (R,R,R) -**5** (b) (M_n = number averaged molecular weight, P_m =

probability of meso linkages in repeating units of a polymer chain). The line indicates calculated M_n values.	80
Figure 3.21. Plot of observed PLA P_m (•) as functions of conversion for catalyst (<i>R,R,R,R</i>)- 5 at 0 °C in CH_2Cl_2 . [<i>R,R,R,R</i>]- 5] = 0.46 mM, [rac-LA] = 0.227 M.	81
Figure 3.22. 1H NMR spectra of (a) 3 , (\pm)-(NNO _{Me})InCl ₂ , (b) 5 , (\pm)-[(NNO _{tBu})InCl](μ -Cl)(μ -OEt), and a mixture of 3 and 5 (c) after 5 minutes, (d) 16 minutes, and (e) 4 hr, (f) 1 , (\pm)-(NNO _{tBu})InCl ₂ , and (g) 6 , (\pm)-[(NNO _{Me})InCl](μ -Cl)(μ -OEt) (400 MHz, CD_2Cl_2 , 25 °C).	83
Figure 3.23. 1H NMR spectra of (a) 7 , (\pm)-[(NNO _{Me})InI](μ -I)(μ -OEt), and a mixture of 2 , (\pm)-(NNO _{tBu})InI ₂ , and 7 , (b) after 5 minutes, (c) 8 minutes, (d) 43 minutes, (e) 2 hr 30 minutes and (f) 2 days, and (g) 8 , (\pm)-[(NNO _{Me})In(I)(μ -OEt)] ₂ (400 MHz, CD_2Cl_2 , 25 °C).	83
Figure 3.24. 1H NMR spectra of (a) complex 8 , (meso)-[(NNO _{Me})In(I)(μ -OEt)] ₂ , (b) complex 2 , (\pm)-(NNO _{tBu})InI ₂ ; a mixture of complexes, 8 and 2 , (c) after 5 minutes, (d) 8 minutes, (e) 2 hr 30 minutes and (f) 2 days, (g) complex (\pm)-[(NNO _{Me})InI](μ -I)(μ -OEt) (7), (h) complex (\pm)- 9 (400 MHz, $CDCl_3$, 25 °C).	84
Figure 3.25. Plots of k_{obs} (♦) and observed PLA M_n (■) as functions of added 1 for polymerization of LA with catalysts 5 ([5] = 0.0024 M, CD_2Cl_2 , room temperature; M_n = number averaged molecular weight).....	85
Figure 3.26. 1H NMR spectra of (a) complex 1 , (\pm)-(NNO _{tBu})InCl ₂ , (b) complex 5 , (\pm)-[(NNO _{tBu})InCl] ₂ (μ -Cl)(μ -OEt) and polymerization of 200 equiv. of rac-LA with complex 5 after 16 minutes (400 MHz, CD_2Cl_2 , 25 °C).	86
Figure 3.27. 1H NMR spectra of (a) (\pm)-(N _{nPr} NO _{tBu})InCl ₂ , and (b) polymerization of 200 equiv. of rac-LA with (\pm)-[(N _{nPr} NO _{tBu})InCl] ₂ (μ -Cl)(μ -OEt) after 5 minutes (400 MHz, CD_2Cl_2 , 25 °C). ²	86
Figure 4.1. Reported cationic indium complexes. ^{304-306,307-314}	94
Figure 4.2. Schematic illustrations of two categories of metal-catalyzed MMA polymerization: (a) monometallic mechanism; (b) bimetallic mechanism. ^{323,338,342}	98
Figure 4.3. Highly stereoselective catalysts for PMMA.....	99
Figure 4.4. Proposed propagation cycle in the coordination-addition mechanism of MMA polymerization with zirconocene mono- and bis(ester enolate) complexes by Chen and coworkers.....	99

Figure 4.5. Cationic and neutral discrete mononuclear aluminum complexes for MMA polymerization. ^{300,302,347-350}	101
Figure 4.6. Molecular structure of 12 (depicted with thermal ellipsoids at 50% probability and most H atoms omitted for clarity).	103
Figure 4.7. ¹ H NMR spectrum of (a) (NNO _{tBu})InMe ₂ (12) and (b) (NNO _{tBu})In(CH ₂ SiMe ₃) ₂ (13) (400 MHz, CDCl ₃ , 25 °C).	104
Figure 4.8. (a) ¹ H- ¹ H COSY and (b) ¹ H- ¹ H NOSEY (optimized mixing time: 400 ms) spectra of (NNO _{tBu})In(CH ₂ SiMe ₃) ₂ (13) (400 MHz, CDCl ₃ , 25 °C).	106
Figure 4.9. Molecular structure of complex 13 (depicted with ellipsoids at 50% probability and H atoms removed for clarity).	107
Figure 4.10. Reported neutral alkyl indium complexes with a trimethylsilyl methyl group. ^{88,309,357}	108
Figure 4.11. ¹ H NMR spectrum of a crude product of [(NNO _{tBu})In(CH ₂ SiMe ₃)] [B(C ₆ F ₅) ₄] (14) (CDCl ₃ , 25 °C).	110
Figure 4.12. ¹⁹ F { ¹ H} NMR spectra of (a) [(NNO _{tBu})In(CH ₂ SiMe ₃)] [B(C ₆ F ₅) ₄] (14), (b) [(NNO _{tBu})In(CH ₂ SiMe ₃)] [BArF] (15) and (c) [(NNO _{tBu})In(CH ₂ SiMe ₃)] [PF ₆] (16) (CDCl ₃ , 25 °C, neat CFC ₃ was externally referenced at 0 ppm).	111
Figure 4.13. Molecular structure of 14 depicted with ellipsoids at 50% probability (H atoms and uncoordinated solvent molecules were removed for clarity). [(NNO _{tBu})In(CH ₂ SiMe ₃)] [B(C ₆ F ₅) ₄] 14 (left) and 14 •THF (right) were found in the unit cell.	112
Figure 4.14. Illustrations of the molecular structures for 14 [(NNO _{tBu})In(CH ₂ SiMe ₃)] [B(C ₆ F ₅) ₄] and 14 •THF.	113
Figure 4.15. Molecular structure of complex 16 [(NNO _{tBu})In(CH ₂ SiMe ₃)] [PF ₆] depicted with ellipsoids at 50% probability (H atoms and solvent molecules removed for clarity)...	114
Figure 5.1. Ground state spin multiplicity and electronic configurations of triplet and singlet carbenes. ^{40,359-361}	125
Figure 5.2. Representations of metal-carbon bonding in a) Fischer carbene complexes ³⁶⁹ and b) Schrock carbene complexes. ³⁷⁶	127
Figure 5.3. Illustration of Bertrand carbenes. ^{50,51,392-396}	128

Figure 5.4. Different modes of stabilization of the carbene center with different types of substituents. ⁵⁰	129
Figure 5.5. Molecular structures of complexes 19 (left) and 21 (right) (depicted with thermal ellipsoids at 50% probability and most H atoms omitted for clarity).	133
Figure 5.6. ¹ H NMR spectra of (a) the acyclic diaminocarbene complexes, 23 (left), 24 (right), and (b) the 5- and 6-membered cyclic diaminocarbene complex, 25 (left), 26 (right) (400 MHz, CDCl ₃ , 25 °C).	135
Figure 5.7. Molecular structure of complex 23 (depicted with thermal ellipsoids at 50% probability and most H atoms omitted for clarity).	136
Figure 5.8. Molecular structure of complex 26 (depicted with thermal ellipsoids at 50% probability and most H atoms as well as solvent molecules omitted for clarity).	136
Figure 5.9. (a) ¹ H NMR spectrum and (b) the nuclear Overhauser effect (NOE) spectrum of complex 23 saturating the N2- <i>H</i> signal at 8.84 ppm (600 MHz, CDCl ₃ , 25 °C).	138
Figure 5.10. Molecular structure of complex 27 (depicted with thermal ellipsoids at 50% probability and all H atoms as well as solvent molecules omitted for clarity).	140
Figure 5.11. Molecular structure of complex 34 (depicted with thermal ellipsoids at 50% probability and all H atoms omitted for clarity).	141
Figure 5.12. Molecular structures of 35 (left) and 36 (right) (thermal ellipsoids at 35% probability). ⁴	144
Figure 5.13. ³¹ P{ ¹ H} NMR spectra of the (phosphino)(amino)carbene complex 37 monitored at different time periods at room temperature.	146
Figure 5.14. Molecular structure of complex 38 (depicted with thermal ellipsoids at 50% probability and most H atoms omitted for clarity).	147
Figure 5.15. ³¹ P{ ¹ H} NMR spectra for conversion of complex 38 to complex 36 by reacting with (a) 6 equivalents, (b) 12 equivalents, and (c) 24 equivalents of NaHB(OAc) ₃	148

List of Schemes

Scheme 1.1. Living ring opening polymerization of lactide catalyzed by the indium complex $[(\text{NNOtBu})\text{InCl}]_2[\mu\text{-Cl}][\mu\text{-OEt}]$.	2
Scheme 1.2. Synthesis of mono- and bis-alkoxy-bridged, chiral dinuclear indium complexes for LA ROP.	3
Scheme 1.3. Polymerization of MMA with cationic indium complexes.	4
Scheme 1.4. Template synthesis of donor-functionalized carbene iron complexes.	5
Scheme 2.1. Synthesis of chiral proligands $\text{H}(\text{NNO}_R)$ ($R = t\text{Bu}, \text{Me}$). ^{23,125}	15
Scheme 2.2. Synthesis of dinuclear indium complexes of the type $[(\text{NNO}_R)\text{InX}]_2(\mu\text{-Y})(\mu\text{-OEt})$ (1 , 2 , and 5 have been reported). ^{23,125}	17
Scheme 2.3. Synthesis of hydroxy-ethoxy bridged complexes $(\pm)\text{-}[(\text{NNO}_R)\text{InI}]_2(\mu\text{-OH})(\mu\text{-OEt})$ ($R = \text{Me}$ (10), $t\text{-Bu}$ (11)).	19
Scheme 2.4. Irreversible reactions of $(\pm)\text{-}[(\text{NNO}_{t\text{Bu}})\text{InCl}]_2(\mu\text{-Cl})(\mu\text{-OEt})$ (5) with donors.	34
Scheme 3.1. Some catalysts for the ROP of lactide.	61
Scheme 3.2. Two mechanistic proposals for ROP of LA by $[(\text{NNO}_{t\text{Bu}})\text{InCl}]_2(\mu\text{-Cl})(\mu\text{-OEt})$.	68
Scheme 3.3. Dissociation of dinuclear catalysts with added lactide. ^{19b}	86
Scheme 3.4. Competing coordination and ring opening in the reactivity of $(R,R/R,R)\text{-5}$ with rac-LA.	90
Scheme 4.1. Synthesis of neutral dialkyl indium complexes $(\text{NNO}_{t\text{Bu}})\text{InMe}_2$ (12) and $(\text{NNO}_{t\text{Bu}})\text{In}(\text{CH}_2\text{SiMe}_3)_2$ (13).	102
Scheme 4.2. Synthesis of cationic indium complexes 14-16 .	109
Scheme 5.1. Synthesis of phosphine-tethered diaminocarbene complexes from 17 . ³⁹⁷	130
Scheme 5.2. Synthesis of phosphinimine phosphine proligands ($R = \text{Ph}, t\text{-Bu}$). ^{397, 64}	131
Scheme 5.3. Synthesis of the phosphino-isocyanide iron (II) complexes, 17 and 18 . ³⁹⁷	131
Scheme 5.4. Synthesis of acyclic diaminocarbene complexes 19-22 .	132
Scheme 5.5. Synthesis of cyclic diaminocarbene complexes 25 and 26 .	135
Scheme 5.6. The two proposed mechanisms for the formation of 25 .	137
Scheme 5.7. Synthesis of acyclic (oxy)(amino)carbanion and carbene complexes, 27-29 and 30-32 , respectively.	139

Scheme 5.8. Synthesis of 5- and 6- membered cyclic (oxy)(amino)carbene complexes, 33-34	141
Scheme 5.9. Methodology for the template synthesis of donor-functionalized NX-Carbenes (X = P, Si).	143
Scheme 5.10. Conversion of carbene complex 37 to 17 and HPPh ₂	145
Scheme 5.11. Reversible reaction of acyclic (silyl)(amino) ylidene (36) and carbene (38) complexes.	148

List of Abbreviations and Symbols

Å	angstrom
$[\alpha]_D$	specific optical rotation measured at the sodium D line (589 nm)
Anal.	Analysis
Ar	aromatic
b	broad
BARF	tetrakis[3,5-bis(trifluoromethyl)phenyl]borate, $B(3,5-(CF_3)_2C_6H_3)_4$
BINAP	2,2'-bis(diphenylphosphino)-1,1'-binaphthyl
Bn	benzyl, $-CH_2(C_6H_5)$
n-Bu	<i>n</i> -butyl, $-CH_2CH_2CH_2CH_3$
t-Bu	<i>tert</i> -butyl, $-CMe_3$
BuLi	<i>n</i> -butyllithium
Calcd	calculated
COSY	Correlation Spectroscopy
Cp	cyclopentadienyl, $(C_5H_5)^-$
Cp*	pentamethylcyclopentadienyl, $(C_5Me_5)^-$
d	doublet
δ	chemical shift downfield from tetramethylsilane in ppm
D_t	translational diffusion coefficient
DACH	diaminocyclohexane
deg, (°)	degree(s)
EA	Elemental Analysis
EI	Electron Impact
eq	equation(s)
equiv	equivalent(s)
Et	ethyl
Et ₂ O	diethyl ether
<i>fac</i>	<i>facial</i>
g	grams
GPC	Gel Permeation Chromatography

ΔH^\ddagger	enthalpy of activation
η	hapticity to describe how a continuous group of atoms on a ligand coordinates a metal center
h	hour(s)
HMBC	Heteronuclear Multiple-Bond Correlation Spectroscopy
HMQC	Heteronuclear Multiple-Quantum Correlation Spectroscopy
HSQC/TOCSY Spectroscopy	Heteronuclear Single Quantum Coherence-Total Correlation Spectroscopy
HPLC	High-Performance Liquid Chromatography
HRMS	High Resolution Mass Spectroscopy
J	coupling constant in Hertz
K	equilibrium constant
κ	kappa
k_{obs}	observed rate constant for polymerization reactions
k_p	propagation rate constant for polymerization propagation
KO ^t Bu	potassium- <i>t</i> -butoxide
KOEt	potassium ethoxide
LA	lactide
LDMS	laser desorption mass spectrometry
LLS	laser light scattering
M	molarity
m	multiplet(s)
M_n	number average molecular weight
M_w	weight average molecular weight
Me	methyl
MeLi	methyllithium
Mes	mesityl, 2,4,6-trimethylphenyl
MMA	methyl methacrylate
MS	mass spectroscopy
NaO ^t Bu	sodium- <i>t</i> -butoxide
NMR	nuclear magnetic resonance

NNO _R	2- <i>t</i> -butyl-4- <i>R</i> -6-(((2-(dimethylamino)cyclohexyl)amino)methyl)phenol
NOE	Nuclear Overhauser Enhancement
NOESY	Nuclear Overhauser Enhancement Spectroscopy
OEt	ethoxy, ethoxide
P _m	probability of meso linkages in a polymer chain
PDI	Polydispersity Index
PDLA	poly(D-lactide)
PGSE	Pulsed Gradient Spin-Echo
Ph	phenyl
Pinner salt	hydrochloric acid salt of an imino ester or an alkyl imidate formed by Pinner reaction, an organic reaction of a nitrile with an alcohol under acid
PLA	poly(lactide)
PLLA	poly(L-lactide)
PMMA	poly(methyl methacrylate)
ppm	parts per million
<i>i</i> -Pr	<i>iso</i> -propyl, -CHMe ₂
<i>n</i> -Pr	<i>n</i> -propyl, -CH ₂ CH ₂ CH ₃
py	pyridine
q	quartet
r _H	hydrodynamic radii
r _{X-ray}	X-ray crystallographic radii
rac	racemic
±	racemic
<i>R</i>	<i>Rectus</i> (Latin for right)
ROP	Ring Opening Polymerization
<i>S</i>	<i>Sinister</i> (Latin for left)
s	singlet
ΔS [‡]	entropy of activation
salan	a compound synthesized by reduction of a salen compound

salen	Schiff bases, usually prepared by the condensation of a salicylaldehyde with an amine
Schiff bases	a compound with a functional group that contains a carbon-nitrogen double bond with the nitrogen atom connected to an aryl or alkyl group, not hydrogen ($R^1R^2C=NR^3$)
sep	septet
t	triplet
T_g	glass transition temperature
T_m	melting temperature
THF	tetrahydrofuran
TMB	1,3,5-trimethoxybenzene
TMS	trimethylsilyl
TMSS	tetrakis(trimethylsilyl)silane
VT	variable temperature
μ	the prefix given in IUPAC nomenclature for a bridging ligand

List of Compounds

Chapter 2 and Chapter 3

- 1 $(\text{NNO}_{\text{tBu}})\text{InCl}_2$
- 2 $(\text{NNO}_{\text{tBu}})\text{InI}_2$
- 3 $(\text{NNO}_{\text{Me}})\text{InCl}_2$
- 4 $(\text{NNO}_{\text{Me}})\text{InI}_2$
- 5 $[(\text{NNO}_{\text{tBu}})\text{InCl}]_2(\mu\text{-Cl})(\mu\text{-OEt})$
- 6 $[(\text{NNO}_{\text{Me}})\text{InCl}]_2(\mu\text{-Cl})(\mu\text{-OEt})$
- 7 $[(\text{NNO}_{\text{Me}})\text{InI}]_2(\mu\text{-I})(\mu\text{-OEt})$
- 8 $[(\text{NNO}_{\text{Me}})\text{In}(\text{I})(\mu\text{-OEt})]_2$
- 9 $[(\text{NNO}_{\text{tBu}})\text{In}(\text{I})(\mu\text{-OEt})]_2$
- 10 $[(\text{NNO}_{\text{Me}})\text{InI}]_2(\mu\text{-OH})(\mu\text{-OEt})$
- 11 $[(\text{NNO}_{\text{tBu}})\text{InI}]_2(\mu\text{-OH})(\mu\text{-OEt})$

Chapter 4

- 12 $(\text{NNO}_{\text{tBu}})\text{InMe}_2$
- 13 $(\text{NNO}_{\text{tBu}})\text{In}(\text{CH}_2\text{SiMe}_3)_2$
- 14 $[(\text{NNO}_{\text{tBu}})\text{In}(\text{CH}_2\text{SiMe}_3)_2][\text{B}(\text{C}_6\text{F}_5)_4]$
- 15 $[(\text{NNO}_{\text{tBu}})\text{In}(\text{CH}_2\text{SiMe}_3)_2][\text{BArF}]$
- 16 $[(\text{NNO}_{\text{tBu}})\text{In}(\text{CH}_2\text{SiMe}_3)_2][\text{PF}_6]$

Chapter 5

- 17 $[\text{CpFe}(\text{CO})(\text{P}_{\text{Ph}}\text{CN})]^{+}\text{I}^{-}$
- 18 $[\text{CpFe}(\text{CO})(\text{P}_{\text{t-butyl}}\text{CN})]^{+}\text{I}^{-}$
- 19 $[\text{CpFe}(\text{CO})(\text{P}_{\text{t-butyl}}\text{C}_{\text{N}(\text{n-butyl})}\text{N}_{\text{H}})]^{+}\text{I}^{-}$
- 20 $[\text{CpFe}(\text{CO})(\text{P}_{\text{Ph}}\text{C}_{\text{NH}(\text{nbutyl})}\text{N}_{\text{H}})]^{+}\text{I}^{-}$
- 21 $[\text{CpFe}(\text{CO})(\text{P}_{\text{Ph}}\text{C}_{\text{N}(\text{nhexyl})_2}\text{N}_{\text{H}})]^{+}\text{I}^{-}$
- 22 $[\text{CpFe}(\text{CO})(\text{P}_{\text{Ph}}\text{C}_{\text{NH}(\text{3-methylphenyl})}\text{N}_{\text{H}})]^{+}\text{I}^{-}$
- 23 $[[\text{CpFe}(\text{CO})(\text{PC}_{\text{N}(\text{chloroethyl})}\text{N}_{\text{H}})]^{+}\text{I}^{-}$

- 24** $[\text{CpFe}(\text{CO})(\text{PC}_{\text{N}(\text{chloropropyl})\text{N}_\text{H}})]^+\text{I}^-$
25 $[[\text{CpFe}(\text{CO})(\text{PC}_{\text{NH}}\text{N}-5\text{Cy})]]^+\text{I}^-$
26 $[\text{CpFe}(\text{CO})(\text{PC}_{\text{NH}}\text{N}-6\text{Cy})]^+\text{I}^-$
27 $\text{CpFe}(\text{CO})(\text{PC}_{\text{O}(\text{Me})}\text{N})$
28 $\text{CpFe}(\text{CO})(\text{PC}_{\text{O}(\text{Et})}\text{N})$
29 $\text{CpFe}(\text{CO})(\text{PC}_{\text{O}(\text{iPr})}\text{N})$
30 $[\text{CpFe}(\text{CO})(\text{PC}_{\text{O}(\text{Me})}\text{N}_\text{H})]^+\text{BF}_4^-$
31 $[\text{CpFe}(\text{CO})(\text{PC}_{\text{O}(\text{Et})}\text{N}_\text{H})]^+\text{BF}_4^-$
32 $[\text{CpFe}(\text{CO})(\text{PC}_{\text{O}(\text{iPr})}\text{N}_\text{H})]^+\text{BF}_4^-$
33 $[\text{CpFe}(\text{CO})(\text{PC}_{\text{NO}}-5\text{Cy})]^+\text{Cl}^-$
34 $[\text{CpFe}(\text{CO})(\text{PC}_{\text{NO}}-6\text{Cy})]^+\text{Cl}^-$
35 $\text{CpFe}(\text{CO})(\text{P}_{\text{Ph}}\text{C}_{\text{P}(\text{Ph})_2}\text{N})$
36 $\text{CpFe}(\text{CO})(\text{P}_{\text{Ph}}\text{C}_{\text{Si}(\text{Ph})_3}\text{N})$
37 $[\text{CpFe}(\text{CO})(\text{P}_{\text{Ph}}\text{C}_{\text{P}(\text{Ph})_2}\text{N}_\text{H})]^+\text{BF}_4^-$
38 $[\text{CpFe}(\text{CO})(\text{P}_{\text{Ph}}\text{C}_{\text{Si}(\text{Ph})_3}\text{N}_\text{H})]^+\text{BF}_4^-$

Acknowledgements

This thesis could not have been completed without the tremendous contributions of the many people who supported me. First of all, I would like to thank my fantastic supervisor, professor Parisa Mehrkhodavandi, who guided me every step of the way. Moreover, I am very grateful for her full support, both emotionally and financially, during a serious illness early in my Ph.D. Without her, I would not have made it through this difficult time. There are so many things that I would like to thank her for, but I unfortunately have a limited number of acknowledgement pages. I just like to say, “She has been my family, friend, boss and supervisor during the whole Ph.D. program.”

I offer many thanks to all the staff of the UBC Chemistry department. In particular, I would like to thank John Ellis in chemistry store who always helped me receive all the chemicals when I needed them, Millan Coschizza in electronic engineering services who fixed the freezer in the glove box and taught me how to fix some of the common electrical problems I experienced, Judy Wrinskelle, Laura Partland and Sheri Harbour in general office who always listened to my complaints, Brian Ditchburn in glassblowing who fixed all of my broken J-young NMR tubes right away so that I was able to finish many kinetics experiments without delay, Jane Cua in IT services who always helped me to fix my computer which enabled me to complete my thesis, Ken Love and Pritesh Padhiar in mechanical engineering services who taught me how to change the catalyst column for the glove box and maintain the pumps in the lab, Marshall Lapawa, David Wong and Derek Luczak in mass spectrometry who ran all my urgent experiments for air-sensitive elemental analysis and MALDI analysis of all the complexes, Dr. Maria Ezhova and Zorana Danilovic in NMR spectroscopy who taught me to run various NMR experiments and offered me their time when I needed it urgently, Dr. Brian Patrick who taught me how to operate the X-ray crystallography equipment to collect the data and solve the molecular structures which were essential to all my projects, and Anita Lam who helped me to collect crystallographic data whenever Brian was absent.

I owe special thanks to all my group members in the past and present. I would first like to thank my past group members and all the undergraduate students. In particular, I thank Dr. Christopher Wallis, the first postdoctoral fellow in the lab, who taught me how to properly

use the Schlenk line and shared his knowledge and inspirations for my first carbene project. I would like to thank the past undergraduate students, Trevor Janes, Karla Rebullar and Stephanie Bishop, who helped me to synthesize all the proligands that I needed for the mechanistic studies. Finally, I really appreciate my lovely current group members, Kimberly Osten and Dinesh Aluthge, who gave their time, encouragement, and companionship to help me to be survived at the last crucial moment of the Ph.D. program.

I would also like to thank my special friends, Dr. Christopher Rohde who encouraged and trusted me to be in the Ph.D. program and gave his time to edit my thesis, Deanne Rohde who offered me her lovely home to stay when I was sick and alone, and Dr. Ivo Krummenacher, Dr. Dominik Nied, Dr. Eamonn Conrad, Sara Vickers, Dr. Paul Sui, Nathan Halcovitch, Dr. Robin Stoodley, and Seongsook Lim for their enduring friendship.

Lastly, special thanks are owed to my parents for their love and support throughout my years of education and my sister, brother and brother-in-law, who have inspired me and believed in me the whole time.

Dedication

This thesis is dedicated to my family for all their support, encouragement, and inspiration.

Chapter 1: General Introduction

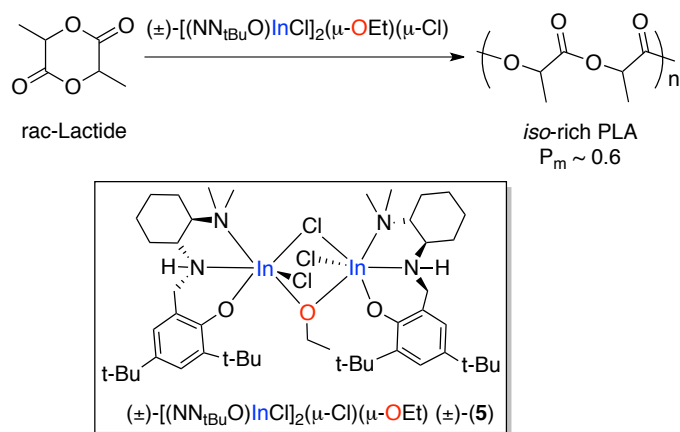
Fundamental research into new catalysts and catalytic processes is of the utmost importance for both academia and industry. A suitable catalyst can transform a reaction from an intellectual curiosity into a vital industrial process. In recent years the development of homogeneous catalysts has been advanced significantly through organometallic chemistry using a variety of metal-containing systems with a diverse range of ligand frameworks.⁶ My Ph.D. research has focused primarily on the mechanism of a family of homogeneous indium catalysts for the ring opening polymerization of lactide as well as development of a new cationic indium system for polymerization of polar vinyl monomers. In a separate project, I have investigated new methodologies for the synthesis of metal complexes bearing common and rare carbene ligands, such as cyclic and acyclic diamino- and (oxy)(amino)carbenes and (phosphino)- and (silyl)(amino)carbenes, respectively, and investigating their reactivities with an eye to the future application of these ligands as non-innocent ligands in catalysis.

Petroleum-derived polymers and plastics, used in beverage and food containers, and packing materials to manufacture toys and furniture play a significant role in our daily lives. Consequently, 31 million tons of plastic waste, representing 12.4 % of the total municipal solid waste, was produced in 2010, and only 8 % of the total plastic waste was recycled.⁷ Biodegradable polymers such as poly(lactic acid) (PLA), which are completely converted either to CO₂ and H₂O or to CH₄ and H₂O by microorganisms in a compost, have been of intense interest in replacing petroleum-derived polymers for efficient plastics waste management on land.⁸⁻¹⁰

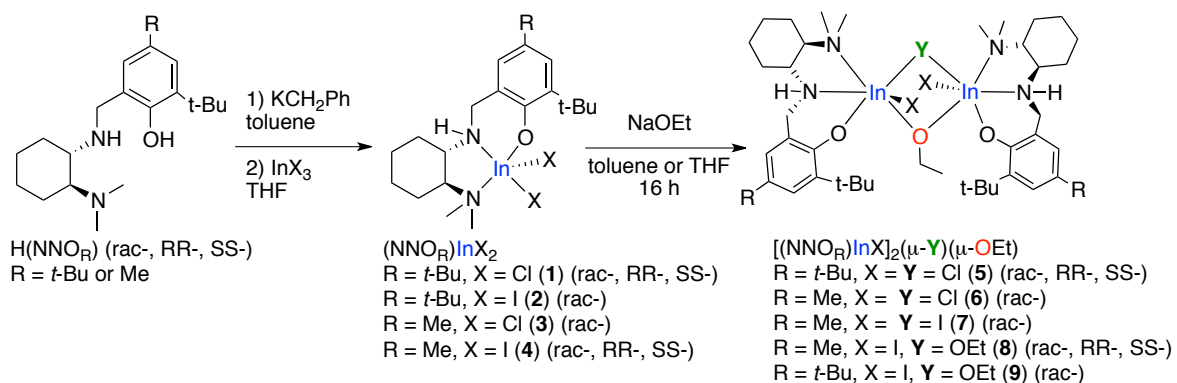
Currently, these polymers are generated on an industrial scale either by condensation of lactic acid or ring opening polymerization of cyclic esters such as lactide (LA), which can be derived from renewable plant sources.¹¹ However, metal-catalysts for the controlled ring opening polymerization (ROP) of LA, such as tin(II) bis(2-ethylhexanoate),¹¹ are the best way to produce well-defined PLA in the presence of monomer impurities, as condensation methods¹² suffer from relatively low molecular weight PLA with a broad molecular weight distribution. The various physical properties of PLA such as phase transition temperatures, T_g, and T_m are dependent on polymer microstructure.¹³⁻¹⁵ These various properties of PLA are what makes the polymer suitable for use in a particular application.¹⁶ These thermal

properties can be tuned by polymer macro- and microstructures. In the past decade, LA ROP catalyzed by many well-defined Lewis acid complexes has been intensively explored to enhance activity and stereoselectivity. A thorough review of relevant literature will be addressed in Chapter 2.

Indium(III) has been chosen because of its use as a versatile, functional-group tolerant Lewis acid catalyst in many organic transformations¹⁷⁻²² and exceptional stability in water. Our group first published a highly active indium-based catalyst for the living ROP of LA in 2008 (**Scheme 1.1**).²³ This unique, mono- and bis-alkoxy-bridged chiral dinuclear indium complex can be synthesized readily after two steps from deprotonated chiral ancillary ligands (**Scheme 1.2**). The unprecedented degree of control in the living polymerization of LA, yielding high molecular weights of PLA with low molecular weight distributions, as well as the promising control of polymer tacticity, led us to investigate the influence of the bridging dinuclear nature on catalyst activity. Chapter 3 provides relevant literature review on the mechanism of LA ROP by known mono- and dinuclear catalysts.



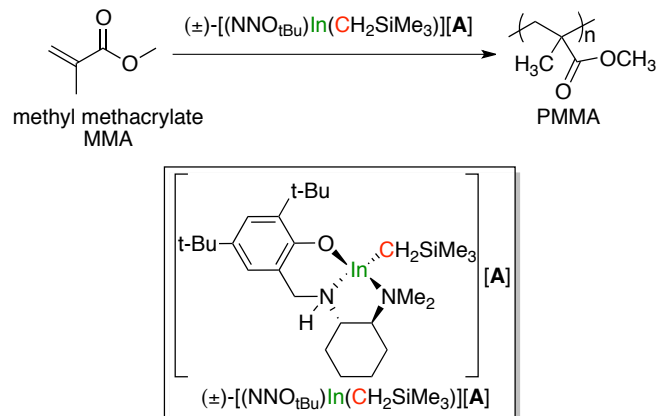
Scheme 1.1. Living ring opening polymerization of lactide catalyzed by the indium complex $[(\text{NNO}_{\text{tBu}})\text{InCl}]_2[\mu\text{-Cl}][\mu\text{-OEt}]$.



Scheme 1.2. Synthesis of mono- and bis-alkoxy-bridged, chiral dinuclear indium complexes for LA ROP.

Changing a metal center from neutral to cationic is another way to tune the inherent properties of organometallic compounds in catalysis. Cationic group 13 metal complexes (Al, Ga, In, Tl)^{24,25} exhibit a highly Lewis acidic nature at the metal center that makes them potentially excellent candidates for many reactions including those performed with neutral group 13 complexes,^{26,27} yet they have been found to be unreactive in all but a handful of catalytic applications.²⁵ Although there have been a number of reports on cationic indium complexes, no catalytic activity has been reported for these species.

Poly(methyl methacrylate) (PMMA) is another important polymer used in numerous industrial applications as well as in biomedical applications.²⁸ To date, transition metal and group 3 catalysts for methyl methacrylate (MMA) polymerization provide highly stereoregular polymers. However, these complexes exhibit low conversions in high concentration of monomer due to impurities. I discuss the synthesis and characterization of a new family of cationic indium complexes supported by chiral diamino-phenolate ligands for the polymerization of polar conjugated alkenes, such as MMA (**Scheme 1.3.**). To the best of my knowledge, no indium complexes have been used for MMA polymerization. All the relevant aspects on this topic in the literature, including cationic group 13 complexes and polymerization, are addressed in Chapter 4.



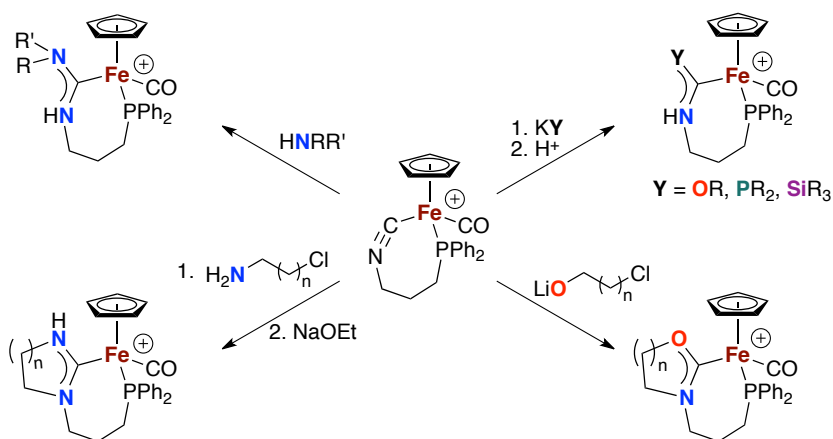
Scheme 1.3. Polymerization of MMA with cationic indium complexes.

It is well known that small changes of ligand backbone and substituents allow for the fine-tuning of intrinsic electronic properties of a metal center in organometallic compounds. The excellent properties of stable, singlet N-heterocyclic carbenes (NHCs) as ligands for transition metals²⁹⁻³¹ have prompted a massive effort to finely control their electronic and steric properties by changing the carbon-bound substituents of stable singlet carbenes. Thereby, a large collection of N-heterocyclic carbenes (NHCs) with varied N-bound substituents and their donor-functionalized analogues have been reported.³²⁻³⁵ Whereas NHCs use two C-bound donors to stabilize the carbene (push-push carbenes), early work on acyclic carbenes³⁶⁻⁴⁰ and recent expansion of the carbene field to stable cyclic (alkyl)(amino)carbenes (CAACs)⁴¹ has demonstrated that “push-spectator” carbenes (NX-carbenes; X = C, P, Si) can be stronger donors than NHCs (“push-push” carbenes) and, with a judicious choice of alkyl substituents, can lead to efficient catalysis.⁴² P- or Si-functionalized carbenes remain largely unexplored as ligands,^{36,39,43,44} although rare examples were shown to be excellent ligands for rhodium.⁴⁵⁻⁵¹ Challenges in the synthesis of the free carbenes and in the formation of complexes via ligand substitution pathways have severely limited the utility of these species as ligands. In the last few years there has been a resurgence of the classic template synthesis of Fischer carbenes to enable formation of unusual and difficult to obtain complexes.⁵²⁻⁵⁶

For this work, a family of cyclic and acyclic donor-functionalized carbene iron complexes with chelating phosphino-carbene ligands is generated by a template synthesis via

nucleophilic attack at the carbon atom of a coordinated isocyanide on a piano-stool iron(II) complex (**Scheme 1.4**).

Importantly, this work demonstrates that the (silyl)(amino)carbene compounds can be converted to their corresponding ylidenes through hydrogen production with hydride. Thus we have a two-electron change on the ligand involving protons and hydrides while the oxidation state of the metal remains unchanged. All the relevant literature on this topic is reviewed in Chapter 5.



Scheme 1.4. Template synthesis of donor-functionalized carbene iron complexes.

Chapter 2: Structural Characterizations of Chiral Alkoxy-Bridged Dinuclear Indium(III) Complexes in Solution and Solid State¹

The first chapter focuses on the synthesis and characterization of new chiral alkoxy-bridged dinuclear indium(III) complexes via modification of halide ligands on the metal center as well as substituents on the ancillary ligands. These complexes are of interest for the controlled ring opening polymerization (ROP) of cyclic esters, in particular, lactide (LA), which is currently the major interest in Mehrkhodavandi group. The emergence of indium as an important Lewis acid catalyst and the relative paucity of indium complexes supported by chiral ligands⁵⁷⁻⁶³ emphasize the importance of developing well-characterized chiral indium complexes.⁶⁴⁻⁶⁹ In this work, we present our investigations into the solution and solid-state structural characteristics of a family of alkoxy-bridged indium(III) complexes supported by a chiral tridentate diaminophenol ligand.

2.1 Introduction

Indium(III) has emerged recently as a versatile, functional-group tolerant Lewis acid in many organic transformations.¹⁷⁻²² Indium(III) salts have proven to be exceptionally stable towards air and water in numerous applications, traits that have allowed them to gain an edge over metals with similar reactivity (zinc and tin).^{18,20} In addition to the numerous reactions in which indium acts as a stoichiometric reagent, indium(III) salts, in conjunction with chiral ligands, have been used to catalyze enantioselective transformations such as allylations,⁷⁰⁻⁷⁶ Diels-Alder reactions,^{77,78} and the formation of homoallylic alcohols.^{70,79}

2.1.1 Indium catalysts for the polymerization of cyclic esters

We have reported the first chiral indium catalyst for the living polymerization of lactide²³ as part of our efforts to develop active catalysts for the controlled ring-opening polymerization of cyclic esters. As well, we have reported some properties and applications of these catalysts and the resulting polymers.^{2,3,14,15,80-83} Prior to our work, an indium catalyst for the polymerization of caprolactone was reported.⁸⁴ Following our contribution, other research groups have reported the synthesis of indium complexes supported by both

¹ The work has been published in *the Journal of American Chemical Society*.¹

chiral^{57,85,86} (**Figure 2.1**) and achiral^{82,85-88} ligands (**Figure 2.2**), as well as simple In(III) salts,^{89,90} that were used as lactide polymerization initiators.

Structurally well-defined chiral^{2,23,57,85,86,91} or achiral^{2,82,84,86-89} indium complexes for single site ROP of LA can be supported with chelating N-, O- and S-donor based ligands (**Figure 2.1** and **Figure 2.2**) in the literature. Among those ligands, the most dominant are Schiff base ligands such as imino-phenolates (salen) and amino-phenolates (salan). The interesting merits of these ligands are their accessibility from relatively cheap starting materials, diamine and salicylaldehyde reagents, and ease of modification for tuning steric and electronic properties of the metal center. The modifications can be achieved by changing the substituents on the phenolate rings or the backbone of the ligand, where both cyclic and acyclic linkages are possible between the two N atoms. Indium complexes with Schiff base proligands are commonly produced by alkane elimination reactions^{86,88} from a trialkyl indium species and the proligand or by salt elimination reactions^{2,23,82,91} from the proligand alkali-metal salts and trihalide indium species. Examples of alcohol elimination reactions from proligand and trialkoxy indium species are rare due to the aggregation tendency of their trialkoxy indium precursors leading to difficulties in controlling the reactivity of these stoichiometric reactions. For instance, reactions of this type have been reported by Okuda and coworkers.⁸⁷

X-ray crystallographic analysis of most indium complexes with alkoxide ligands reveals that there is a tendency for bridging between two metal centers in the presence of these alkoxide ligands,^{85,87,88} which are commonly used as initiators for ROP of LA. This bridging tendency can result in the interesting reactivity and stereoselectivity of indium catalysts for LA polymerization.^{2,23,87,91} The geometry at the indium center is described as distorted octahedral for 6-coordinate,^{2,23,57,85,87,91} distorted square pyramidal or distorted trigonal bipyramidal for 5-coordinate^{57,82,84,86,88} and distorted tetrahedral geometry for 4-coordinate⁸⁶ complexes. Work by Carpentier and coworkers has shown that replacement of electron-donor substituents on the ancillary ligand of a Schiff base indium complex with electron-withdrawing groups (-CF₃), which reduce the electrophilicity of the metal center, thereby preventing the formation of dinuclear complexes via aggregation, instead promoting the formation of mononuclear complexes.⁸⁶ However, their attempts to form a mononuclear indium complex with alkoxide ligands were not successful. In addition, these indium

complexes exhibit significantly less stereoselectivity for ROP of LA as compared to their aluminium analogues, whose solid state structures with isopropoxide ligands show mononuclear species. However, the actual structure of these indium complexes during LA polymerization remains unclear. Okuda and coworkers have reported that achiral monomeric sulfur-containing Schiff base isopropoxide indium complexes can also be obtained by replacement of a *t*-Bu group, $-\text{C}(\text{CH}_3)_3$, with a cumenyl group, $-\text{C}(\text{Ph})(\text{CH}_3)_2$, at the ortho position of the phenolate on the ligand (**Figure 2.2**).⁸⁷

The formation of mononuclear indium complexes via ligand modifications to the parent alkoxy-chloro bridged indium complexes first developed by our group has been of current interest.^{2,91} Two routes have been investigated: one involving changing substituents on the parent half salan-type ancilliary ligand to bulkier groups such as $\text{R} = n\text{-Pr}$,² the second involving changing this tridentate ligand to a tetradentate salen-type ligand.⁹¹ The solid-state structures of the reported indium alkoxide complexes synthesized using these ligands show dinuclear complexes, similar to the parent complexes.

In the case of the tetradentate salen indium complex,⁹¹ pulsed field gradient spin-echo (PGSE) NMR spectroscopic study (see below) was performed to provide a quantitative measure of its solution-state structure. The PGSE data show the hydrodynamic radius (r_{H}) of the In complex (7.6 Å) in solution is significantly larger than that of the monomeric chloro In analogues and the corresponding proligand (6.0 Å and 5.6 Å, respectively) and even slightly larger than its estimated X-ray crystallographic radius ($r_{\text{X-ray}} = 6.6$ Å). This suggests the tetradentate chiral salen indium complex remains as a dimeric species in solution. Interestingly, the stereoselectivity for ROP of LA with the salen indium complex⁹¹ is improved while that of the half salan-type indium complex² with bulky substituents is diminished. Further detailed mechanistic discussion related to the stereoselectivity for ROP of LA will be described in Chapter 3.

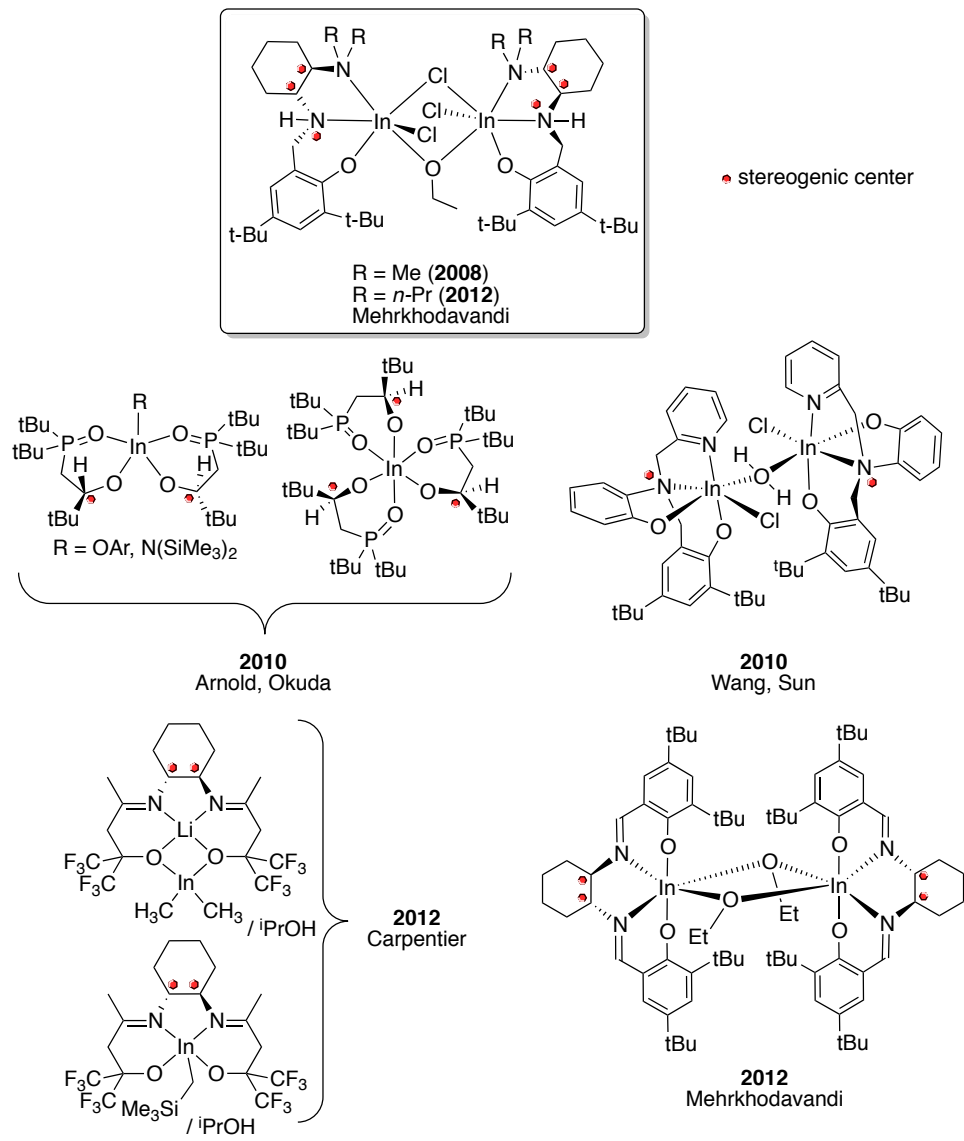


Figure 2.1. Some indium complexes with chiral ligands for the ROP of lactide.^{2,23,57,85,86,91}

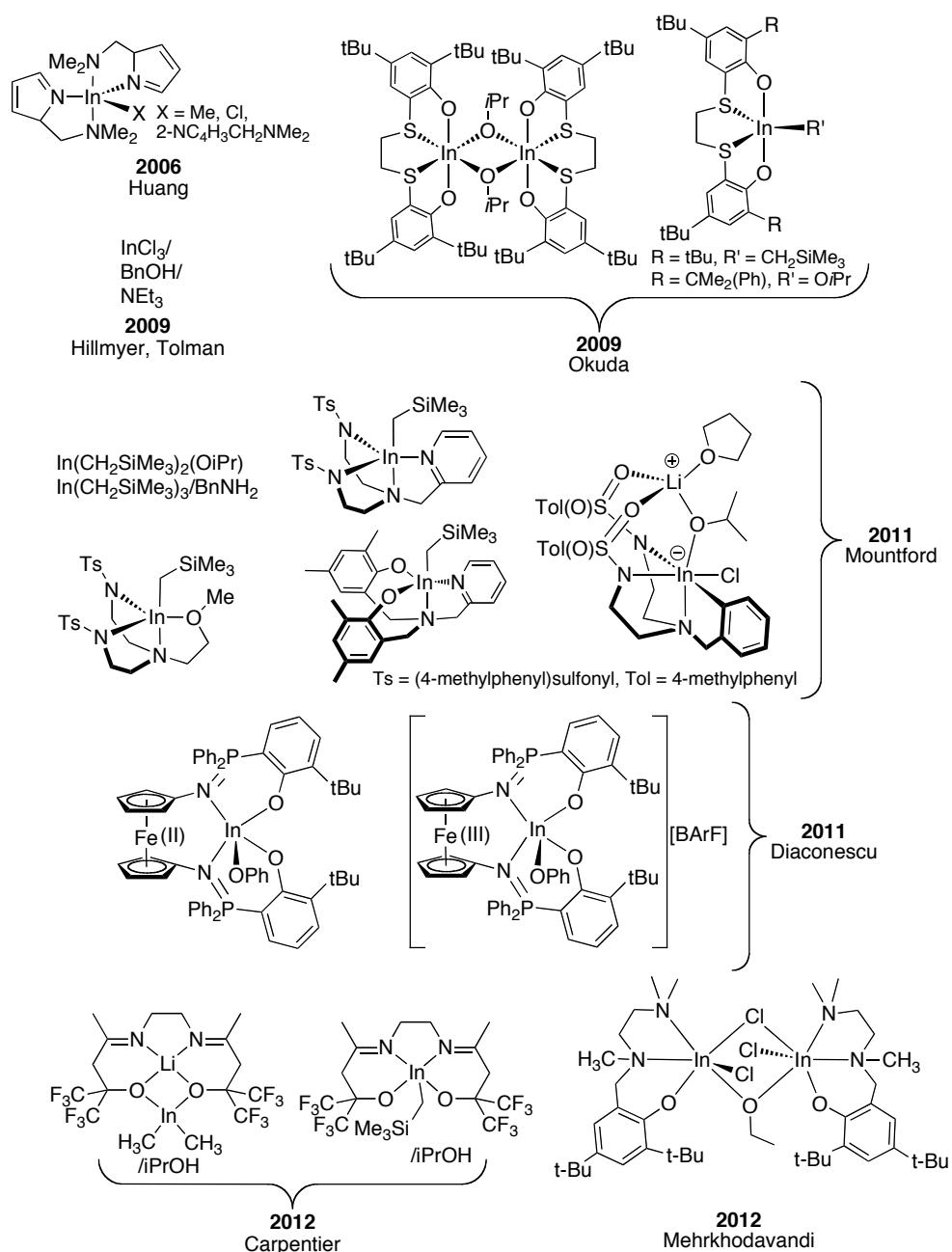


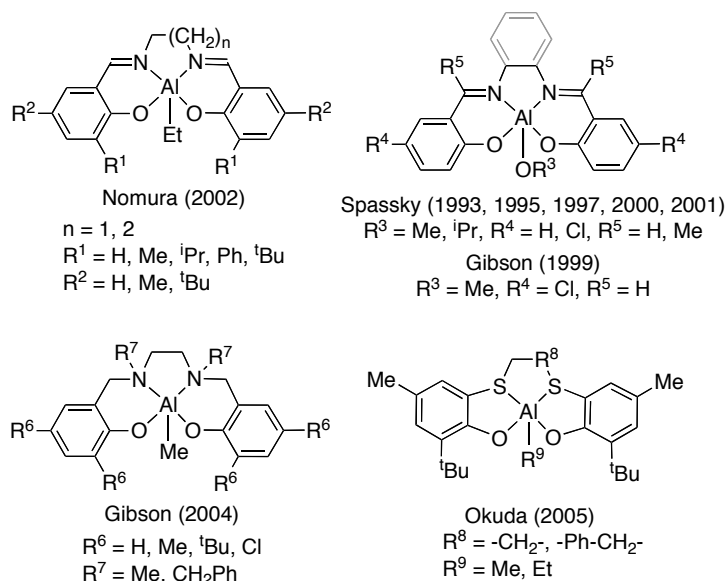
Figure 2.2. Some indium complexes with achiral ligands for the ROP of lactide.^{2,82,84,86-89}

2.1.2 Comparison with aluminum analogues

Along with indium, aluminium complexes featuring chelated chiral⁹²⁻⁹⁶ and achiral⁹⁷⁻¹⁰⁴ ligands are largely reported in the literature as aluminium (Al) complexes, the most naturally abundant metal in the Earth's solid surface (8% by weight of the Earth's crust), is relatively inexpensive and easily accessible from commercial sources. The most prevalent chiral and

achiral aluminium complexes for highly stereoselective ROP of LA possess salen- and salan-type ligands.^{92-94,96,103,105} Unlike indium complexes, aluminium complexes with alkoxide ligands have been studied thoroughly by NMR spectroscopy and mass spectrometry as well X-ray crystallography reveal mononuclear species in solution and solid state.⁹⁴ The structural difference between aluminium and indium complexes may be caused by the relatively smaller ionic radius of aluminium compared to that of indium ($r = 0.80 \text{ \AA}$ for $\text{In}^{3+} > r = 0.53 \text{ \AA}$ for Al^{3+}).¹⁰⁶ However, their electrophilicity is comparable based on the similar 1st, 2nd, and 3rd ionization energies of Al and In (1st, 2nd, and 3rd ionization energies based on the valence shell electron configuration of $ns^2np^1 = 577, 1816, \text{ and } 2744 \text{ kJ mol}^{-1}$ for Al and $558, 1820, 2704 \text{ kJ mol}^{-1}$ for In, respectively); thus, the effective nuclear charge of Al^{3+} and In^{3+} is very similar towards nucleophilic species.¹⁰⁷ Based on the carbonyl shift measurements to determine the acceptor ability of MX_3 ($\text{M} = \text{Al, In; X} = \text{Cl, Br}$) with ethyl acetate ($\nu_{\text{C=O}} = 1735 \text{ cm}^{-1}$ as a reference),^{108,109} the difference between the carbonyl shift frequencies of AlCl_3 and InCl_3 ($\Delta\nu_{\text{C=O}} = 117 \text{ cm}^{-1}$ and 113 cm^{-1} for $\text{EtOAc}\cdot\text{AlCl}_3$ and $\text{EtOAc}\cdot\text{InCl}_3$, respectively) is very small while that between AlBr_3 and InBr_3 ($\Delta\nu_{\text{C=O}} = 138 \text{ cm}^{-1}$ and 107 cm^{-1} for $\text{EtOAc}\cdot\text{AlBr}_3$ and $\text{EtOAc}\cdot\text{InBr}_3$, respectively) is large. Thus, the Lewis acidity of Al and In can be significantly influenced by the surrounding ligands; the order $\text{Cl} < \text{Br}$ for Al is opposite to $\text{Cl} > \text{Br}$ for In.^{108,109}

(a) achiral aluminium complexes



(b) chiral aluminium complexes

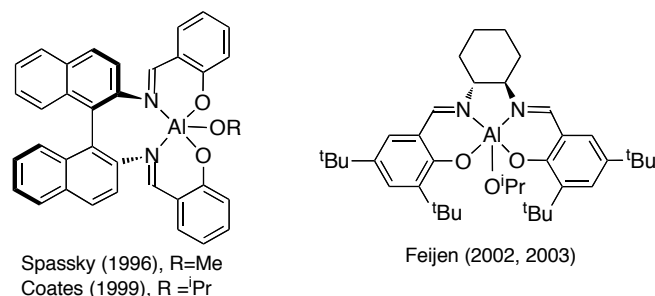


Figure 2.3. Some aluminium complexes with (a) achiral⁹⁷⁻¹⁰⁴ and (b) chiral⁹²⁻⁹⁶ ligands for the ROP of lactide.

2.1.3 Determination of catalyst nuclearity in solution

Determination of molecular architecture in catalytic medium, thus in solution, is very important to understand the mechanism of reactivity and stereoselectivity^{90,110} but frequently problematic in inorganic and organometallic chemistry because of aggregation into polynuclear species.¹¹¹⁻¹¹⁴ Although several classical techniques such as mass spectrometry,^{115,116} colligative property determination,¹¹⁷ light scattering,^{116,118} and X-ray diffraction¹¹⁹ can be used, pulsed field gradient spin-echo (PGSE) NMR measurements have recently become a common methodology to determine molecular volumes of organometallic complexes.^{112-114,120-122} PGSE NMR spectroscopy measures the translational diffusion

coefficient D_t (dipole-dipole relaxation rate), related to the size and shape of the diffusing species in solution.¹²³ When different pulsed magnetic field gradients are applied, the molecules diffusing via Brownian motion experience a different magnetic field strength from the initial strength, providing gradually reduced spin-echo intensities of resonance signals. The hydrodynamic radii of the diffusing species (the size of macromolecules or colloidal particles) can be measured by the translational diffusion coefficient D_t using the Stokes-Einstein equation $\ln(I/I_0) = \gamma^2 \delta^2 G^2 [\Delta - (\delta/3)] (m^{-2} s)$.¹²⁴ Thus, the hydrodynamic radius (r_H) can be calculated by using the slopes (D_t) of the linear fits where I = intensity of the observed spin-echo, I_0 = intensity of the spin-echo in the absence of gradients, G = varied gradient strength, γ = gyromagnetic ratio ($2.675 \times 10^8 \text{ rad s}^{-1} \text{ T}^{-1}$), δ = length of the gradient pulse and Δ = delay between the midpoints of the gradients.

One excellent example of a determination of the solution state structure of a dinuclear complex, which is very significant to understanding our catalytic system, is a highly active Zn complex for controlled ROP of LA reported by Hillmyer and Tolman (**Figure 2.4**).¹¹⁰ Along with variable temperature (VT) NMR spectroscopy, crossover experiments between two alkoxy-bridged dinuclear Zn derivatives and laser desorption mass spectrometry (LDMS), PGSE measurements were used to identify different species in solution accessible through intramolecular rearrangements (the crossover between two alkoxy-bridged dinuclear Zn derivatives) or a monomer/dimer equilibrium. ^1H NMR spectroscopic and LDMS studies of the resulting solid from the crossover experiments of the two alkoxy-bridged dinuclear Zn derivatives ($R = \text{Me, tBu}$) revealed three species: the methyl and tBu substituted dinuclear species and the mixed substituted dinuclear species. PGSE measurements show the hydrodynamic radius of the Zn complex (4.8 Å) in solution is similar to that of the monomeric alkyl Zn analogues (4.2 Å) and 25% smaller than that of its solid state structure (6.8 Å) estimated by X-ray crystallographic data. These results clearly indicate that the Zn complex does not remain as a dimer in solution due to the monomer/dimer equilibrium.

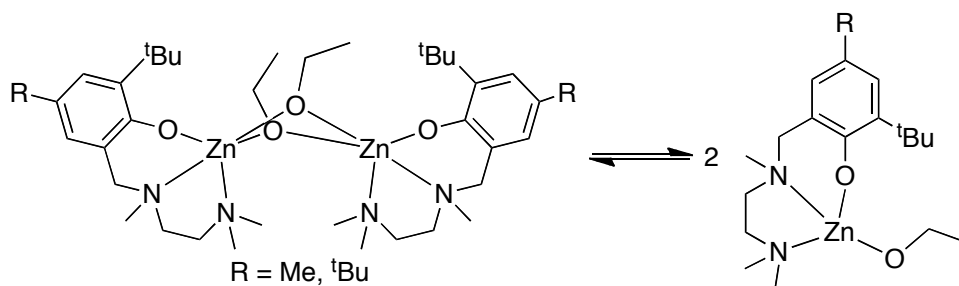


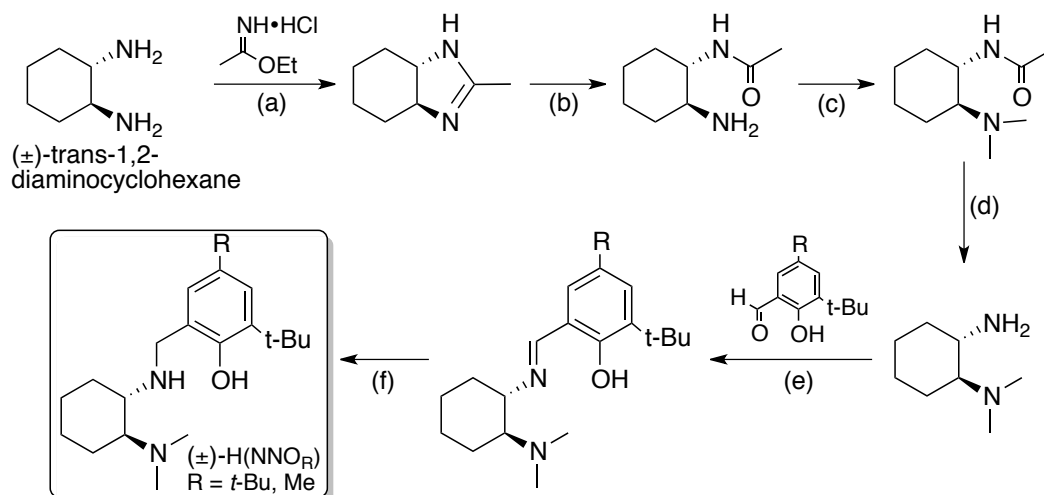
Figure 2.4. Structures of the alkoxy bridged dinuclear Zn complex possible via intramolecular rearrangements or a monomer/dimer equilibrium in solution.¹¹⁰

As mentioned above, we have reported the first chiral indium catalyst $[(\text{NNO}_{\text{tBu}})\text{InCl}]_2[\mu\text{-Cl}][\mu\text{-OEt}]$ for fast, living polymerization of lactide, and its solid-state structure confirmed by single crystal X-ray crystallography exhibits two octahedral indium centers asymmetrically bridged with both ethoxy and chloro ligands.²³ The interesting finding from our initial kinetic and mechanistic work is a significant decrease in the activity and stereoselectivity of the polymerization of rac-LA with an enantiopure catalyst, suggesting enantiomeric-site control competes with chain-end control in this system. However, the structure of the active propagating species (monomeric or dimeric) in the polymerization medium has not been clear. To understand the stereoselectivity of LA polymerization the solution state structures of a family of mono-alkoxy bridged dinuclear complexes $[(\text{NNO}_{\text{tBu}})\text{InCl}]_2(\mu\text{-Cl})(\mu\text{-OEt})$ (**5**) and $[(\text{NNO}_{\text{Me}})\text{InX}]_2(\mu\text{-X})(\mu\text{-OEt})$ ($\text{X} = \text{Cl}$ (**6**), **I** (**7**)) and their enantiopure analogues will be investigated by VT NMR spectroscopy, 2D NOESY spectroscopy and PGSE experiments as well as their solid-state structures by single crystal X-ray crystallography in this chapter.

2.2 Results

2.2.1 Synthesis and characterization of proligands

Racemic 2-*t*-butyl-4-*R*-6-(((2-(dimethylamino)cyclohexyl)amino)methyl)phenol proligands (\pm)-H(NNO_R), where R is a para methyl or *t*-butyl substituent on the phenol, were synthesized according to previously reported methods (**Scheme 2.1**).^{23,125}



(a) dry EtOH; (b) EtOH/H₂O (1:1), reflux; (c) Formaldehyde (37% w/w aq. soln.), NaBH₃CN, AcOH, CH₃CN; (d) 4M HCl, reflux; (e) dry MeOH; (f) NaBH₄, AcOH, CH₃CN

Scheme 2.1. Synthesis of chiral proligands H(NNO_R) (R= tBu, Me).^{23,125}

The first step of the proligand synthesis was the formation of a 1H-benzimidazole compound via condensation of (±)-trans-1,2-diaminocyclohexane referred to (±)-DACH with ethyl acetimidate hydrochloride (a Pinner salt). The ¹H NMR spectrum of the imidazole compound (CDCl₃) shows a singlet signal at 1.91 ppm for -CH₃, which indicates the cyclic formation of (±)-DACH with the Pinner salt. Hydrolysis of the imidazole compound by heating to reflux in neutral 1:1 EtOH-H₂O provided the asymmetric acylated diamine, N-(2-aminocyclohexyl)acetamide.

In the ¹H NMR spectrum of the asymmetric acylated diamine (CDCl₃) two singlet signals appear at 5.76 ppm and 1.99 ppm for the -NH- and -CH₃ protons of the -NHC(O)CH₃ group resulting from the ring opening of the imidazole compound, respectively. The asymmetric acylated diamine was then converted to the corresponding N,N-dimethylated diamine, N-(2-dimethylaminocyclohexyl)acetamide, via reductive amination using sodium cyanoborohydride and aqueous formaldehyde. Hydrolysis of the N,N-dimethylated product by heating to reflux in an acidic aqueous solution (1M HCl) removed the acyl functional group to afford the asymmetric N,N-dimethylated amine, N-(1-dimethylcyclohexyl)-1,2-diamine. The ¹H NMR spectrum of the asymmetric N,N-dimethylated amine has a singlet at 1.83 ppm for the methyl protons of the tertiary amine, -N(CH₃)₂, and a singlet peak at 2.35 ppm disappears for the acyl group of the asymmetrically bound dimethylated amine.

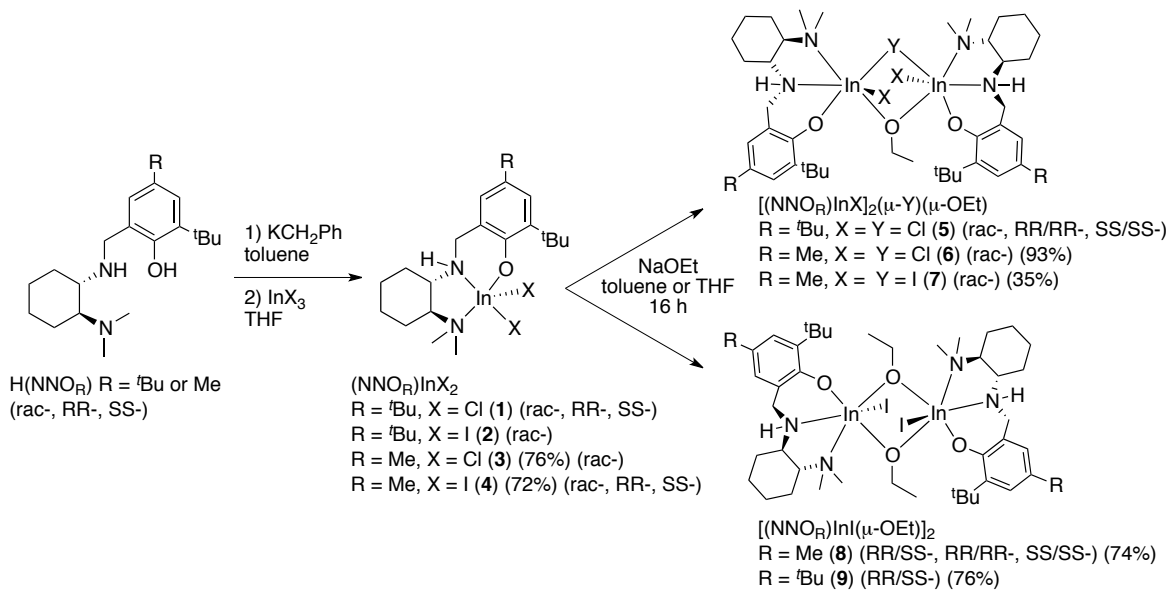
Condensation of the N,N-dimethyl diamine with 3,5-di-tert-butylsalicylaldehyde formed the corresponding *para-t*-butyl salicaldimine as a yellow precipitate. After filtration to collect the yellow solid, the pure product was obtained in 68% yield. However, in the case of the *para*-methyl substituted salicaldimine obtained in 58% yield, recrystallization in acetonitrile was necessary to purify the crude product. The ¹H NMR spectra of the *para*-methyl and *t*-Bu substituted salicaldimine exhibit the very indicative resonance peak at 8.27 ppm and 8.33 ppm for -N=CH-Ar, respectively.

The final step in the synthesis of the chiral tridentate ligand (±)-H(NNO_R) is the reduction of the imine to the amine using sodium borohydride. Sodium cyanoborohydride can also be used to afford the product in better yield after recrystallization in acetonitrile rather than sodium borohydride, however this route is not utilized for this work. The ¹H NMR spectrum of the chiral tridentate ligand (±)-H(NNO_R) (CDCl₃) shows only one set of signals, suggesting both of the enantiomers, which possess a symmetric environment, identical chemical and physical properties, exist in solution. For the synthesis of enantiopure proligands, (1*R*,2*R*)- or (1*S*,2*S*)-1,2-diaminocyclohexane was resolved from (±)-trans-1,2-diaminocyclohexane with L- and D-tartaric acid, respectively, via literature procedures and used.¹²⁶

2.2.2 Synthesis and characterization of racemic alkoxy-bridged indium complexes

Dihalide indium complexes bearing 2-*t*-butyl-4-*R*-6-(((2-(dimethylamino)cyclohexyl)amino)methyl)phenolate ligands, (±)-(NNO_{tBu})InX₂ (**1**: X = Cl, **2**: X = I) and (±)-(NNO_{Me})InX₂ (**3**: X = Cl, **4**: X = I), were prepared by addition of the potassium salts of the proligands, (±)-K(NNO_R), to the appropriate indium trihalide via salt metathesis (**Scheme 2.2**).³ Crystallization from a solution of tetrahydrofuran (THF) and diethyl ether at room temperature afforded yellow crystals of (±)-**3** which were suitable for single crystal X-ray diffraction. The solid-state molecular structure of (±)-**3** shows a distorted square-pyramidal geometry around the indium center (**Figure 2.5**). Addition of 2 equivalents of NaOEt to complexes **1-4** formed mono-alkoxy bridged dinuclear complexes (±)-[(NNO_{tBu})InCl]₂(μ-Cl)(μ-OEt) (**5**) and (±)-[(NNO_{Me})InX]₂(μ-X)(μ-OEt) (X = Cl (**6**), I (**7**)). The NMR spectra (CD₂Cl₂) of (±)-**6** and **7** prepared from (±)-H(NNO_{Me}) show signals corresponding to one compound, as did the previously reported (±)-[(NNO_{tBu})InCl]₂(μ-Cl)(μ-

OEt) (**5**) (**Figure A-1** - **Figure A-2** in Appendix A). The solid state structure of (\pm)-**5** shows a homochiral dimer with (*R,R,R,R*) centers, implying that the (*S,S,S,S*) enantiomer also exists in solution.²³



Scheme 2.2. Synthesis of dinuclear indium complexes of the type $[(\text{NNO}_R)\text{InX}_2]_2(\mu\text{-Y})(\mu\text{-OEt})$ (**1**, **2**, and **5** have been reported).^{23,125}

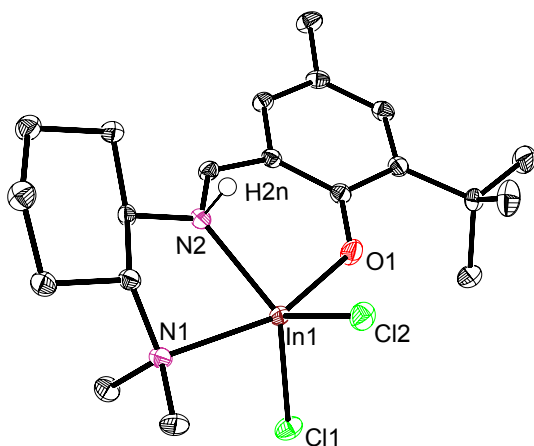
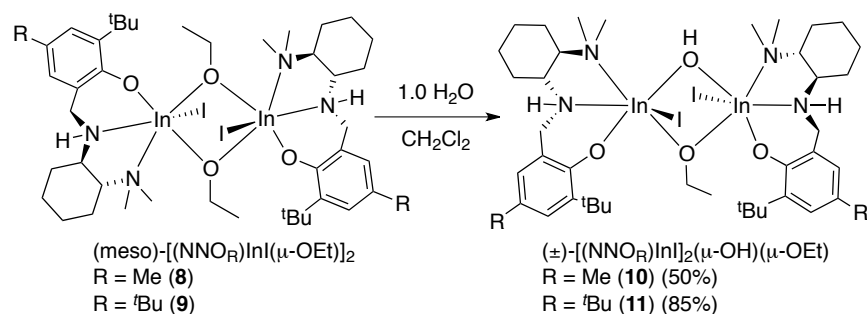


Figure 2.5. Molecular structure of (\pm)-**3** (depicted with ellipsoids at 50% probability and most H atoms).

Table 2.1. Selected distances (Å) and angles (°) for (±)-**3**.

(±)- 3				
Bond Lengths	In1-Cl1	1.742(4)	In1-N1	1.146(5)
	In1-Cl2	1.976(5)	In1-N2	1.322(9)
	In1-O1	2.185(7)		
Bond Angles	O1-In1-Cl1	97.75(5)	N1-In1-Cl1	95.16(4)
	O1-In1-Cl2	96.04(4)	N1-In1-Cl2	93.04(4)
	O1-In1-N2	84.84(5)	Cl1-In1-N2	115.91(6)
	O1-In1-N1	159.65(5)	N2-In1-Cl2	129.63(6)
	N1-In1-N2	75.36(5)	Cl2-In1-Cl1	113.839(18)

Addition of **4** to a suspension of a two-fold excess of NaOEt in toluene forms a mixture of (±)-**7** and a bis-ethoxy bridged complex, meso-[(NNO_{Me})InI(μ-OEt)]₂ (**8**) (**Scheme 2.2**). Unlike the chloro analogues, synthetic routes involving the reaction of complex (±)-**4** with NaOEt always resulted in a mixture of (±)-**7** and meso-**8**, which can be easily separated with a 1:1 solution of acetonitrile and THF. Alternatively, KOEt can be used to generate complex **8** as the major product. The analogous, highly insoluble complex with a *t*-Bu group at the *para* position of phenolate, meso-[(NNO_{tBu})InI(μ-OEt)]₂ (**9**), is synthesized in a similar manner. Upon addition of 1 equivalent of water, the bis-ethoxy bridged complexes meso-**8** and **9** convert to the hydroxy-ethoxy bridged dinuclear complexes (±)-[(NNO_R)InI]₂(μ-OH)(μ-OEt) (R = Me (**10**), *t*-Bu (**11**)) (**Scheme 2.3**). The ¹H NMR spectra (CD₂Cl₂) of (±)-**10** and (±)-**11** display signals corresponding to one compound which are similar to the spectra obtained for the asymmetrically-bridged complexes (±)-**5**, (±)-**6** and (±)-**7** (**Figure A-3-Figure A-4** in Appendix A).



Scheme 2.3. Synthesis of hydroxy-ethoxy bridged complexes $(\pm)\text{-}[(\text{NNO}_R)\text{InI}]_2(\mu\text{-OH})(\mu\text{-OEt})$ ($R = \text{Me}$ (**10**), $t\text{-Bu}$ (**11**)).

The molecular structure of **9**, which was synthesized from $(\pm)\text{-H}(\text{NNO}_{t\text{Bu}})$, shows a heterochiral dimer (*meso*-**9**) with $(R,R/S,S)$ configuration (**Figure 2.6**). In contrast, the solid-state structure of **11**, synthesized from $(\pm)\text{-H}(\text{NNO}_{t\text{Bu}})$, shows a homochiral dimer with $(R,R/R,R)$ configuration, implying that the $(S,S/S,S)$ analogue of $(\pm)\text{-11}$ exists in solution (**Figure 2.7**). Complexes $(\pm)\text{-5}$ and **11** have similar In-N bond distances and there is a “*cis*” relationship between the phenoxy moieties of the ligand (the phenoxy groups are on the same hemisphere of the molecule). Addition of excess water to these complexes forms the previously described hydroxy-bridged complexes $(\pm)\text{-}[(\text{NNO}_R)\text{InX}(\mu\text{-OH})]_2$.³

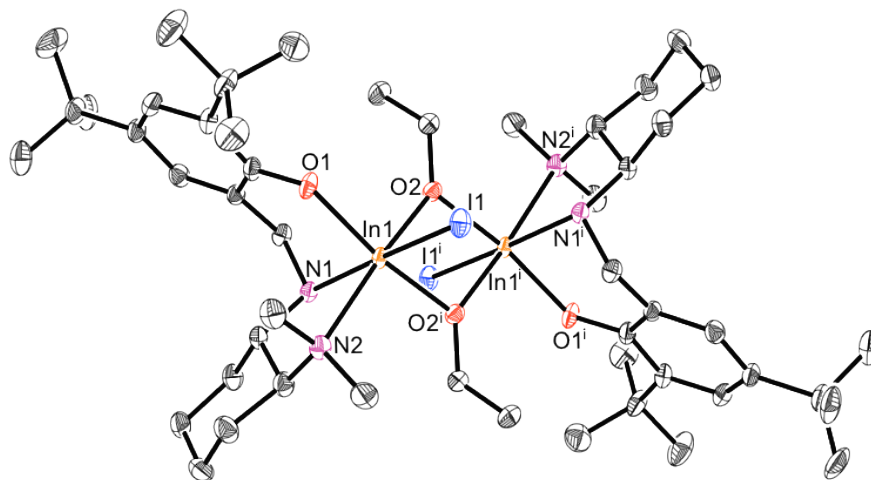
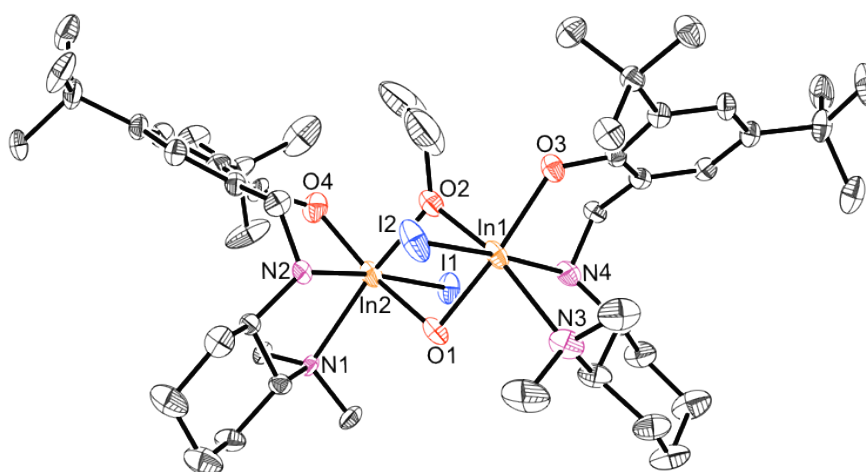


Figure 2.6. Molecular structure of *meso*-**9** (depicted with ellipsoids at 50% probability and H atoms omitted for clarity).

Table 2.2. Selected distances (Å) and angles (°) for meso-**9**.

meso- 9				
Bond Lengths	In1-I1	1.742(4)	In1-N1	1.146(5)
	In1-O1	1.976(5)	In1-N2	1.322(9)
	In1-O2	2.185(7)		
Bond Angles	O1-In1-O2 ⁱ	91.22(8)	N1-In1-N2	75.97(9)
	O1-In1-O2	163.88(8)	N2-In1-O2	98.69(9)
	O1-In1-I1	92.77(6)	N ⁱ -In1-I1	171.11(6)
	O1-In1-N1	85.06(8)	In1-O2-In1 ⁱ	105.84(8)
	O1-In1-N2	94.93(9)		

**Figure 2.7.** Molecular structure of (±)-**11** (depicted with ellipsoids at 50% probability and H atoms as well as solvent molecules omitted for clarity).**Table 2.3.** Selected distances (Å) and angles (°) for (±)-**11**.

(±)- 11				
Bond Lengths	In1-O1	2.180(3)	In1-N4	2.273(4)
	In2-O1	2.211(3)	In1-I2	2.8030(4)
	In1-O2	2.142(3)	In2-I1	2.7923(4)
	In2-O2	2.146(3)	In2-O4	2.099(5)
	In1-O3	2.090(3)	In2-N1	2.338(9)
	In1-N3	2.336(4)	In2-N2	2.265(5)
	Bond Angles	O1-In1-O2	92.49(12)	O1-In2-O2
N3-In1-I2		96.20(10)	In1-O1-In2	103.26(13)
N3-In1-O3		103.29(14)	In1-O2-In2	106.90(14)
N1-In2-I1		98.20(15)	O2-In1-O3	165.62(12)
N1-In2-O4		100.14(5)		

2.2.3 Synthesis and characterization of enantiopure alkoxy-bridged indium complexes

(*R,R*)- and (*S,S*)-H(NNO_R), where R is a para-methyl or *t*-butyl substituent on the phenol group, were synthesized in an analogous manner to (±)-H(NNO_R),^{23,125} as were the dihalide complexes (NNO_{tBu})InX₂ ((*R,R*)- and (*S,S*)-**1**: X = Cl) and (NNO_{Me})InX₂ ((*R,R*)- and (*S,S*)-**4**: X = I). The NMR spectra of the enantiomers are identical to those of the racemic complexes (**Figure A-1-Figure A-4**). The solid state structure of (*S,S*)-**4** shows a distorted trigonal bipyramid with the iodo ligands in the axial and equatorial positions, while in (±)-**3** both chloro ligands are in the equatorial position (**Figure 2.5** and **Figure 2.8**).

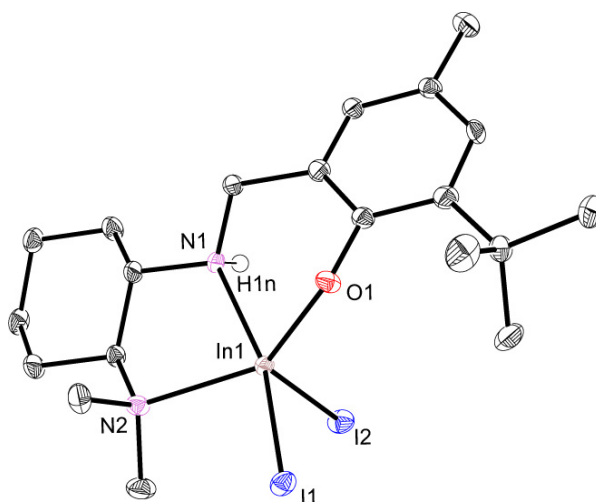


Figure 2.8. Molecular structure of (*S,S*)-**4** (depicted with ellipsoids at 50% probability and most H atoms).

Table 2.4. Selected distances (Å) and angles (°) for (*S,S*)-**4**.

(S,S)-4				
Bond Lengths	In1-I1	2.7627(4)	In1-N1	2.294(4)
	In1-I2	2.7370(4)	In1-N2	2.328(4)
	In1-N1	2.061(3)		
Bond Angles	O1-In1-I1	89.49(8)	N1-In1-I1	158.57(10)
	O1-In1-I2	114.76(9)	N1-In1-I2	95.12(10)
	O1-In1-N2	141.49(13)	I1-In1-N2	93.12(9)
	O1-In1-N1	86.37(12)	N2-In1-I2	101.45(10)
	N1-In1-N2	77.46(13)	I2-In1-I1	105.685(13)

Enantiopure mono- and bis-ethoxy bridged complexes (*R,R*-, *S,S*-**5**) and (*R,R*-, *S,S*-**8**) were synthesized in an analogous manner to their racemic counterparts. The ^1H NMR spectra of complex **5** generated from (\pm)-, (*R,R*)- and (*S,S*)- $\text{H}(\text{NNO}_{\text{tBu}})$ are identical, suggesting that the species observed in solution for (\pm)-**5** are indeed the two homochiral enantiomers (*R,R/R,R*)- and (*S,S/S,S*)-**5** (**Figure 2.9a**). In contrast, while the ^1H NMR spectra of (*R,R/R,R*)- and (*S,S/S,S*)-**8** are identical, the ^1H NMR spectrum of meso-**8** is different and shows only two signals for each of $\text{Ar-CH}_2\text{-N}$ and $\text{O-CH}_2\text{CH}_3$, as would be expected from a centrosymmetric complex (**Figure 2.9b**).

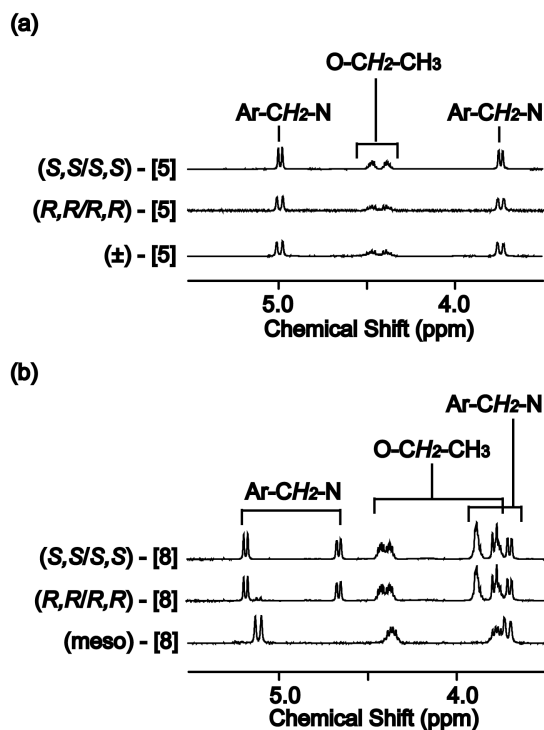


Figure 2.9. ^1H spectra (400 MHz, CDCl_3 , 25 $^\circ\text{C}$) of (a) (\pm)-, (*R,R/R,R*)-, and (*S,S/S,S*)-**5**, and (b) meso-, (*R,R/R,R*)-, and (*S,S/S,S*)- **8**.

The molecular structure of (*S,S/S,S*)-**8**, obtained by single-crystal X-ray diffraction, shows two homochiral octahedral indium centers with no center of symmetry in the molecule (**Figure 2.11**). This is in contrast to the structure of meso-**9** (**Figure 2.6**) that shows a centrosymmetric heterochiral dimer. Meso-**8** is the thermodynamically-favored form of the complex: a 1:1 mixture of (*R,R/R,R*)- and (*S,S/S,S*)-**8** converts to (*R,R/S,S*)-**8** in a few hours at room temperature (**Figure 2.10**).

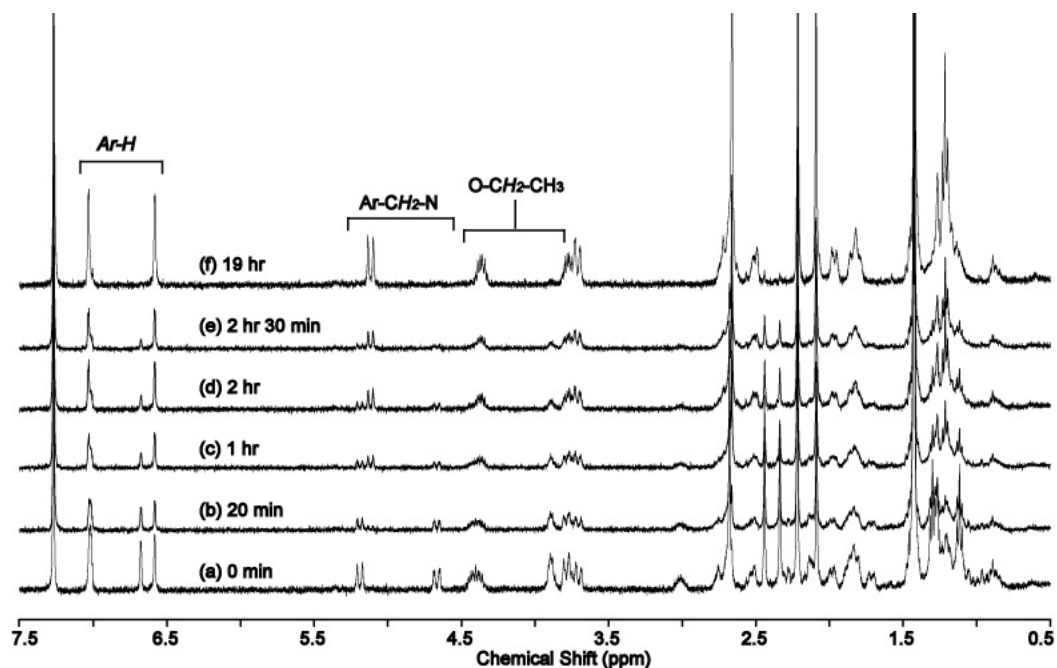


Figure 2.10. ^1H NMR spectra (400 MHz, CDCl_3 , 25°C) of a mixture of an equimolar amount of $R,R/R,R$ - and $S,S/S,S$ -**8**. $R,R/R,R$ - and $S,S/S,S$ -[**8**] = 0.00062 M.

Reaction of $(R,R/R,R)$ -**8** with adventitious water forms the nearly isostructural bis-hydroxy-bridged complex $(R,R/R,R)$ - $[(\text{NNO}_{\text{Me}})\text{In}(\text{I})(\mu\text{-OH})_2]$ (**Figure 2.12**). Again, this is in contrast to the bis-hydroxy bridged dimers in this series, which have been isolated in the centrosymmetric meso-forms.^{3,23}

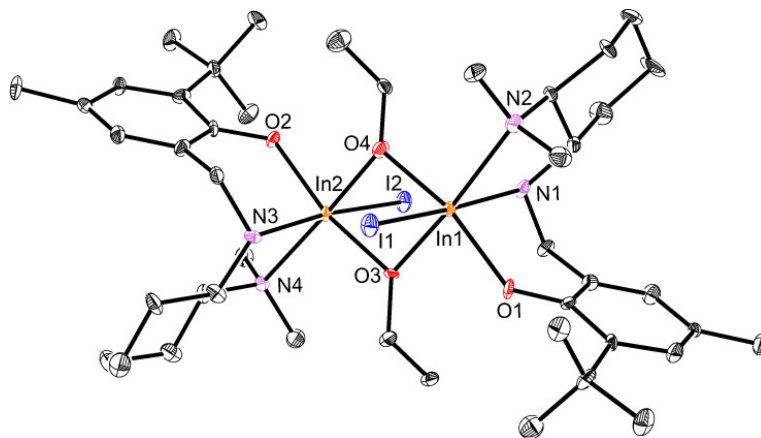


Figure 2.11. Molecular structure of $(S,S/S,S)$ -**8** (depicted with ellipsoids at 50% probability and H atoms omitted for clarity).

Table 2.5. Selected distances (Å) and angles (°) for (*S,S/S,S*)-**8**.

(<i>S,S/S,S</i>)-8				
Bond Lengths	In1-O1	2.101(4)	In1-N1	2.270(5)
	In2-O2	2.100(4)	In1-N2	2.387(5)
	In1-O3	2.187(4)	In2-N3	2.259(5)
	In2-O3	2.174(3)	In2-I4	2.379(4)
	In1-O4	2.176(3)	In1-I1	2.8052(5)
	In2-O4	2.174(4)	In2-I2	2.7980(5)
	Bond Angles	O1-In1-O4	162.29(15)	O2-In2-O4
O1-In1-O3		87.89(14)	O2-In2-O3	163.08(14)
O4-In1-O3		75.07(11)	O4-In2-O3	75.38(11)
O1-In1-N1		85.27(16)	O2-In2-N3	89.10(16)
O4-In1-N1		92.39(16)	O4-In2-N3	95.78(16)
O3-In1-N1		98.38(17)	O3-In2-N3	88.24(15)
O1-In1-N2		98.69(14)	O2-In2-N4	92.31(14)
O4-In1-N2		97.80(14)	O4-In2-N4	172.58(17)
O3-In1-N2		171.12(15)	O3-In2-N4	103.33(14)
N1-In1-N2		76.36(18)	N3-In2-N4	76.84(16)
O1-In1-I1		92.23(12)	O2-In2-I2	93.25(12)
O4-In1-I1		93.22(12)	O4-In2-I2	92.14(12)
O3-In1-I1		92.35(11)	O3-In2-I2	91.74(11)
N1-In1-I1		168.87(12)	N3-In2-I2	171.81(11)
N2-In1-I1		93.35(13)	N4-In2-I2	95.22(12)

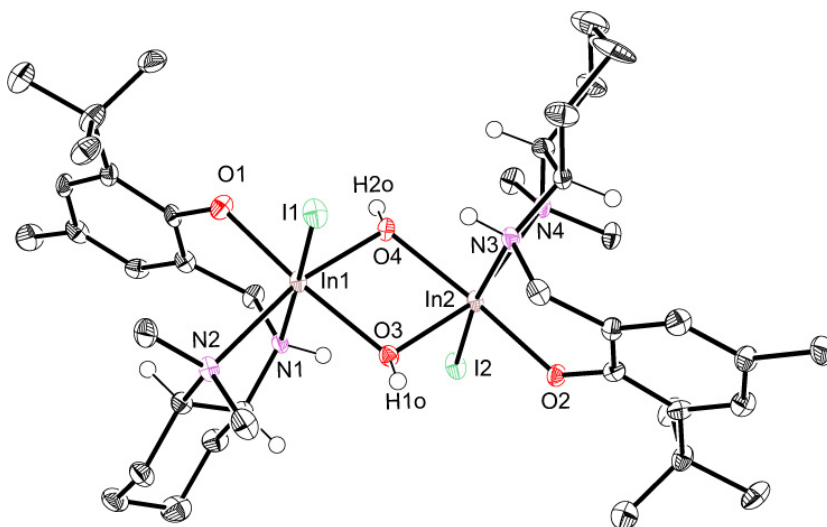


Figure 2.12. Molecular structure of (*R,R/R,R*)-[(*NNO*_{Me})In(I)(μ -OH)]₂ (depicted with ellipsoids at 50% probability and most H atoms).

Table 2.6. Selected distances (Å) and angles (°) for (*R,R/R,R*)-[(NNO_{Me})In(I)(μ-OH)]₂.

(<i>R,R/R,R</i>)-[(NNO_{Me})In(I)(μ-OH)]₂				
Bond Lengths	In1-I1	2.8033(4)	In2-I2	2.8143(4)
	In1-O1	2.097(3)	In2-O2	2.105(3)
	In1-O3	2.160(3)	In2-O3	2.144(4)
	In1-O4	2.146(4)	In2-O4	2.158(3)
	In1-N1	2.269(5)	In2-N3	2.269(4)
	In1-N2	2.367(4)	In2-N4	2.375(4)
Bond Angles	O1-In1-O4	162.29(15)	O2-In2-O4	88.28(14)
	O1-In1-O3	87.89(14)	O2-In2-O3	163.08(14)
	O4-In1-O3	75.07(11)	O4-In2-O3	75.38(11)
	O1-In1-N1	85.27(16)	O2-In2-N3	89.10(16)
	O4-In1-N1	92.39(16)	O4-In2-N3	95.78(16)
	O3-In1-N1	98.38(17)	O3-In2-N3	88.24(15)
	O1-In1-N2	98.69(14)	O2-In2-N4	92.31(14)
	O4-In1-N2	97.80(14)	O4-In2-N4	172.58(17)
	O3-In1-N2	171.12(15)	O3-In2-N4	103.33(14)
	N1-In1-N2	76.36(18)	N3-In2-N4	76.84(16)
	O1-In1-I1	92.23(12)	O2-In2-I2	93.25(12)
	O4-In1-I1	93.22(12)	O4-In2-I2	92.14(12)
	O3-In1-I1	92.35(11)	O3-In2-I2	91.74(11)
	N1-In1-I1	168.87(12)	N3-In2-I2	171.81(11)
N2-In1-I1	93.35(13)	N4-In2-I2	95.22(12)	

2.2.4 Dinuclear nature of ethoxy-bridged complexes in solution

All alkoxy-containing complexes in this family have a dinuclear structure in the solid state, and we show above that the solution structures of (*S,S/S,S*)- and (*R,R/S,S*)- reflect the differences observed in the analogous solid state structures. Additional data, below, support the dinuclear nature of the alkoxy-bridged complexes in solution.

(1) Variable temperature ¹H NMR spectra of (±)-**5** and meso-**8** show no changes over a wide temperature range (Figure 2.13 and Figure 2.14).

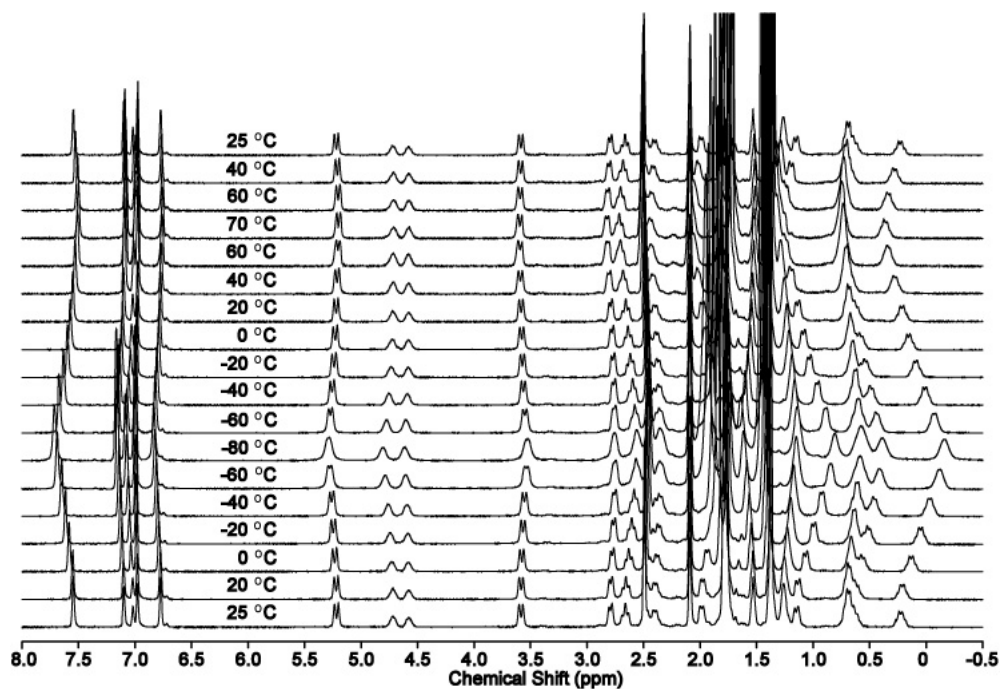


Figure 2.13. ¹H NMR spectra (400 MHz, C₆D₅CD₃) of (±)-[(NNO_{tBu})InCl]₂(μ-Cl)(μ-OEt) (**5**) at variable temperatures.

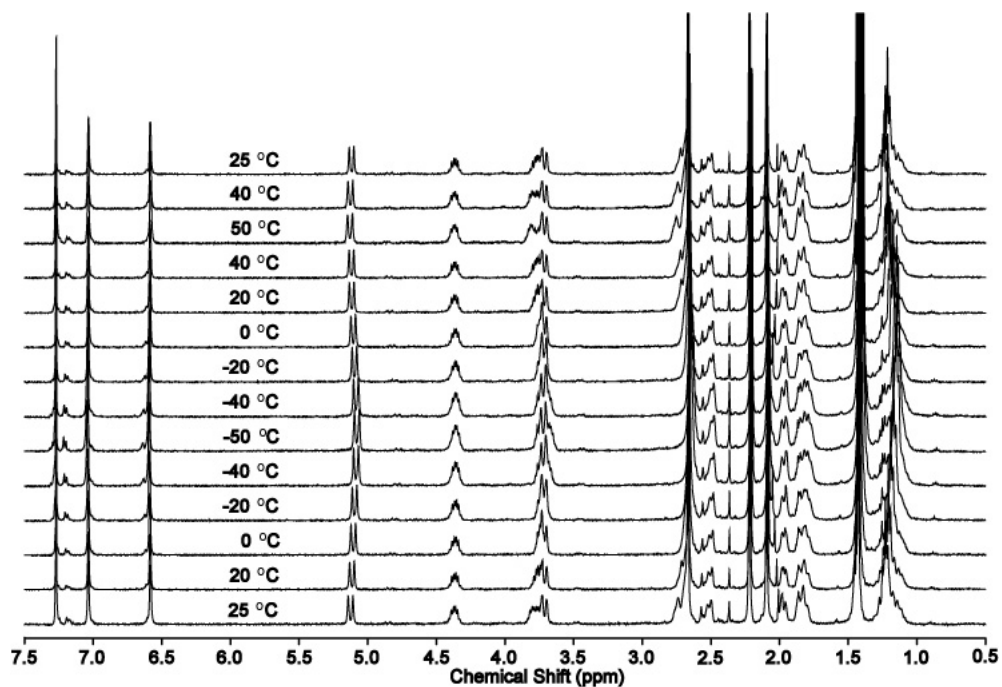
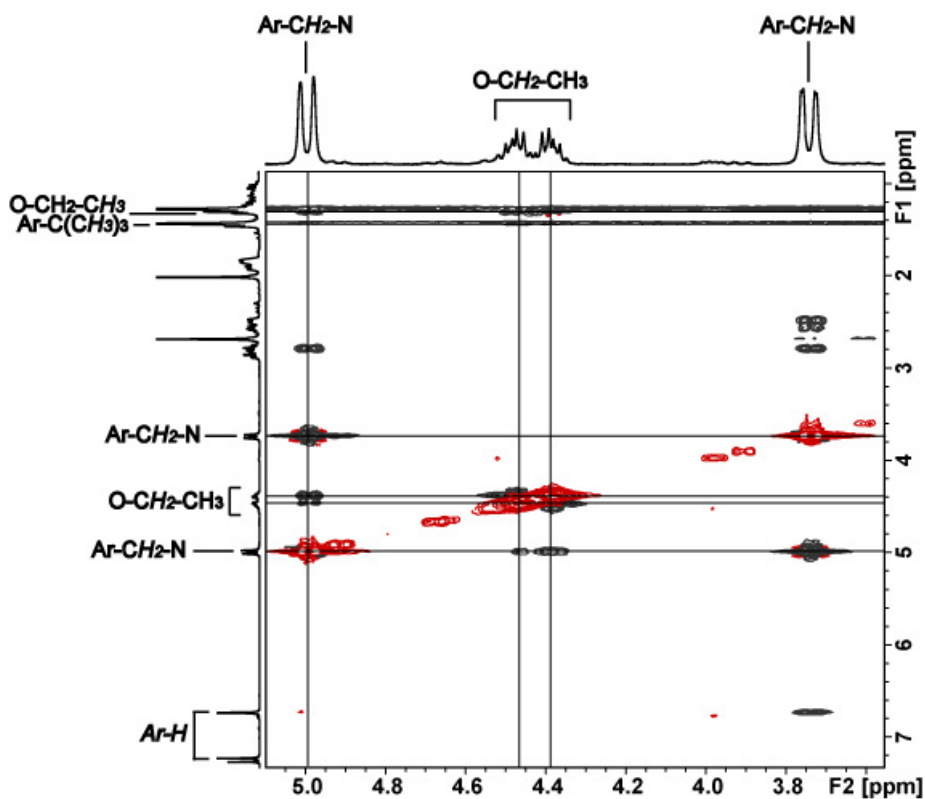


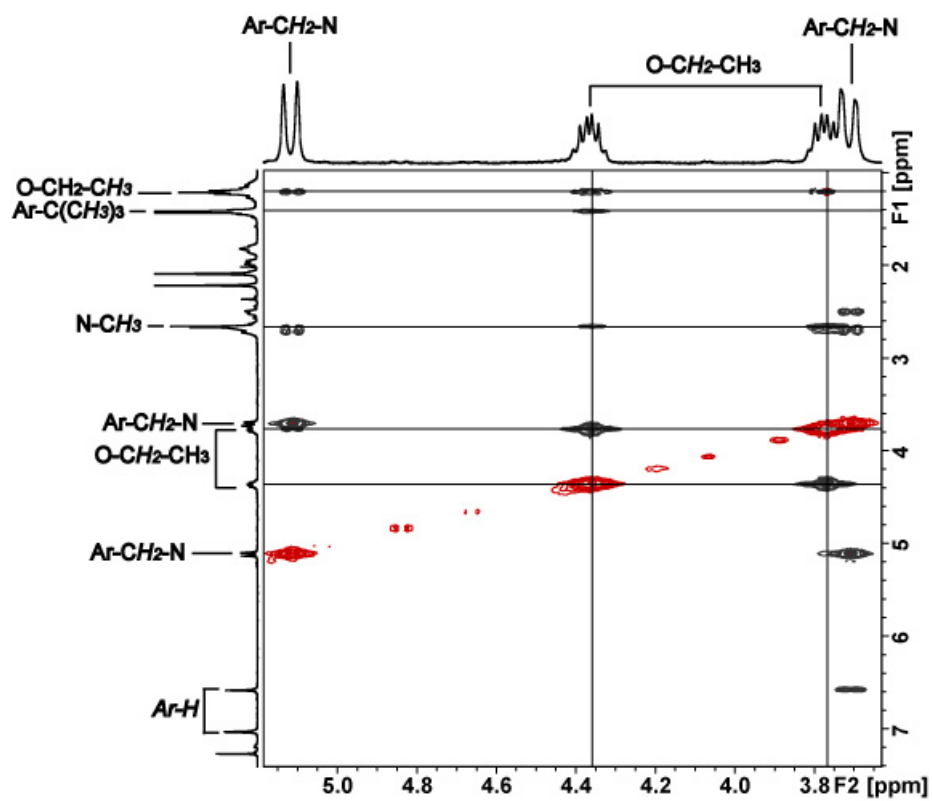
Figure 2.14. ¹H NMR spectra (400 MHz, CDCl₃) of meso-[(NNO_{Me})In(I)(μ-OEt)]₂ (**8**) at variable temperatures.

(2) NOE experiments with (\pm) -**5** and *meso*-**8** support dinuclear structures. The ^1H NOESY-2D NMR spectrum of **5** shows through space interactions between $\text{In-OCH}_2\text{CH}_3$ and the phenolate *ortho*- $\text{C}(\text{CH}_3)_3$ protons only (**Figure 2.15a**). Importantly, cross peaks are not observed between $\text{In-OCH}_2\text{CH}_3$ and the protons of $\text{N}(\text{CH}_3)_2$, indicating an asymmetric environment around $\text{In-OCH}_2\text{CH}_3$ (**Figure 2.16** left). There is also a clear through-space interaction between $\text{In-OCH}_2\text{CH}_3$ and only one of the $\text{NCH}_2\text{-Ar}$ protons of the ancillary ligand. In contrast, the ^1H NOESY-2D NMR spectrum of *meso*-**8** (**Figure 2.16** right) shows through space interactions between OCH_2CH_3 and the phenolate *ortho*- $\text{C}(\text{CH}_3)_3$ as well as between $\text{In-OCH}_2\text{CH}_3$ and the protons of $\text{N}(\text{CH}_3)_2$ (**Figure 2.15b**). Similar cross peaks are observed for complex *meso*-**9** (**Figure 2.15c**). The calculated distances between $\text{In-OCH}_2\text{CH}_3$ and ligand protons for (\pm) -**5** and *meso*-**9** using ^1H NOESY-1D spectroscopy are in good agreement with the values obtained from the solid-state structures ((\pm) -**5**; **Figure 2.17** and **Table 2.7**, *meso*-**9**; **Figure 2.18** and **Table 2.8**).

(a) (\pm) - $[(\text{NNO}_{\text{tBu}})\text{InCl}]_2(\mu\text{-Cl})(\mu\text{-OEt})$ (**5**)



(b) meso-[(NNO_{M_c})In(I)(μ-OEt)₂] (8)



(c) meso-[(NNO_{tBu})In(I)(μ-OEt)]₂ (**9**)

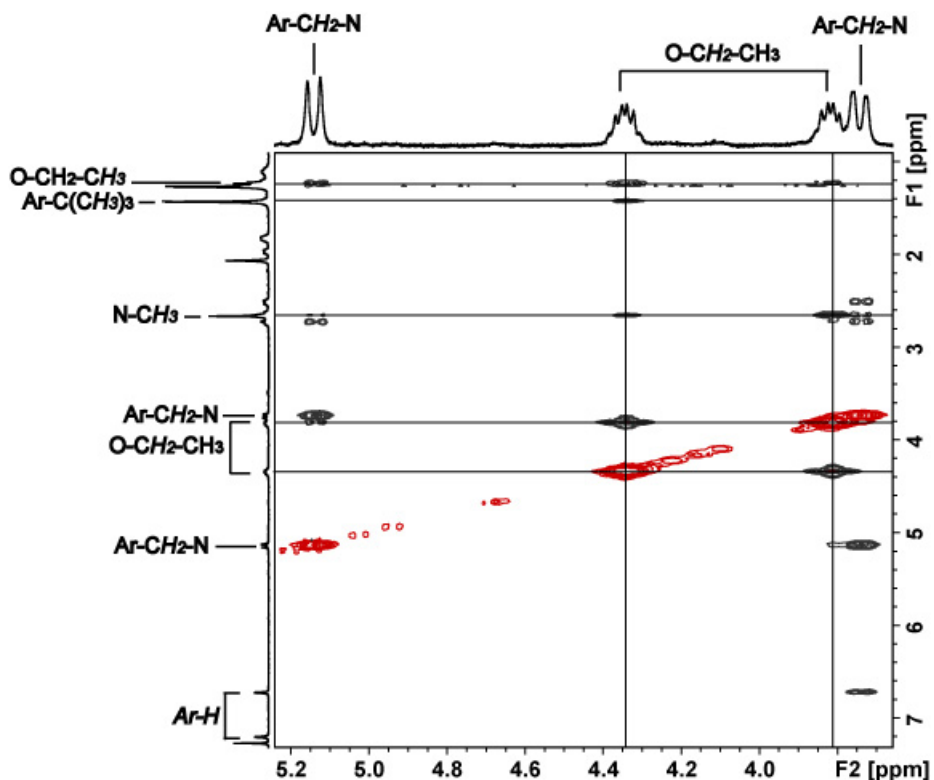


Figure 2.15. 2D NOESY spectra (400 MHz, CDCl₃, 25 °C) of (a) (±)-[(NNO_{tBu})InCl]₂(μ-Cl)(μ-OEt) (**5**), (b) meso-[(NNO_{Me})In(I)(μ-OEt)]₂ (**8**) and (c) meso-[(NNO_{tBu})In(I)(μ-OEt)]₂ (**9**) at the optimized mixing time (400 msec, The diagonal peaks, which have an opposite phase to that of the NOE cross peaks shown in black, are negative and shown in red.).

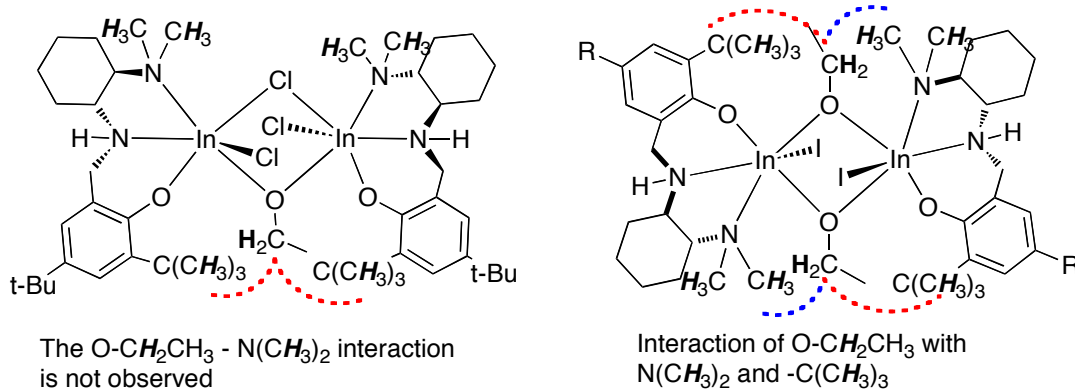


Figure 2.16. Through space interactions expected for mononuclear ethoxy complexes and observed in the ¹H NOESY-2D NMR spectra of complexes (±)-**5** (left), and meso-**8** and **9** (right) (400 MHz, CDCl₃, 25 °C).

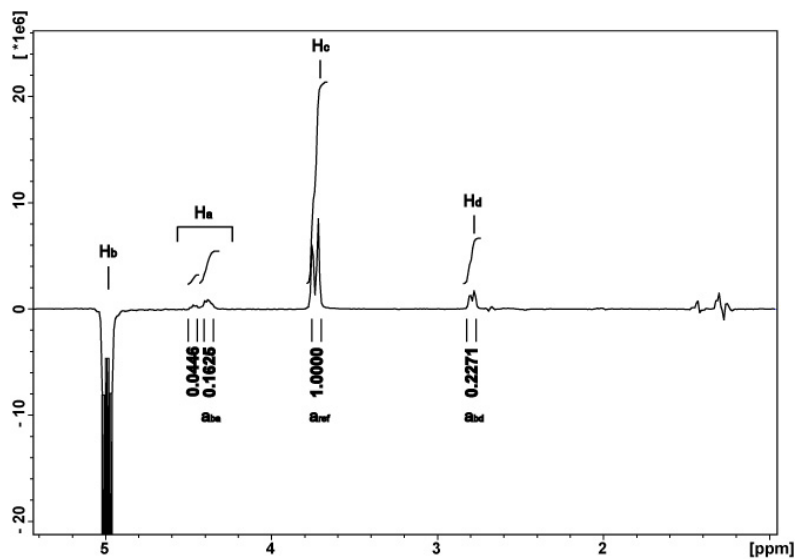
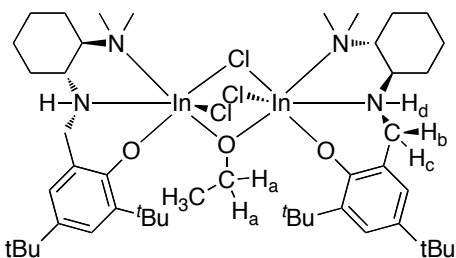


Figure 2.17. 1D NOE spectrum (400 MHz, CDCl_3 , 25 °C) of (\pm) - $[(\text{NNO}_{\text{tBu}})\text{InCl}]_2(\mu\text{-Cl})(\mu\text{-OEt})$ (**5**).

Table 2.7. Selective qualitative H-H distance calculated by 1D NOE spectrum of (\pm) -**5**.

complex [5]	r_{ref} (Å)	r_{ij} (Å)	
	r_{bc} ($\text{H}_b\text{-H}_c$)	r_{ba} ($\text{H}_b\text{-H}_a$)	r_{bd} ($\text{H}_b\text{-H}_d$)
X-ray ^a	1.599	2.118	2.236
NOE ^b		2.16 (0.11)	2.05 (0.10)

^a An obtained distance between two protons (r_{ref}) obtained from X-ray crystallographic data. ^b a calculated distance from NOE spectroscopic data based on the equation, $r_{ij} = r_{\text{ref}}(a_{\text{ref}}/a_{ij})^{1/6}$, where a_{ij} is the NOE cross-peak volume and r_{ij} is the interproton distance of the two protons i and j , a known distance between two protons (r_{ref}) and its NOE volume (a_{ref}).

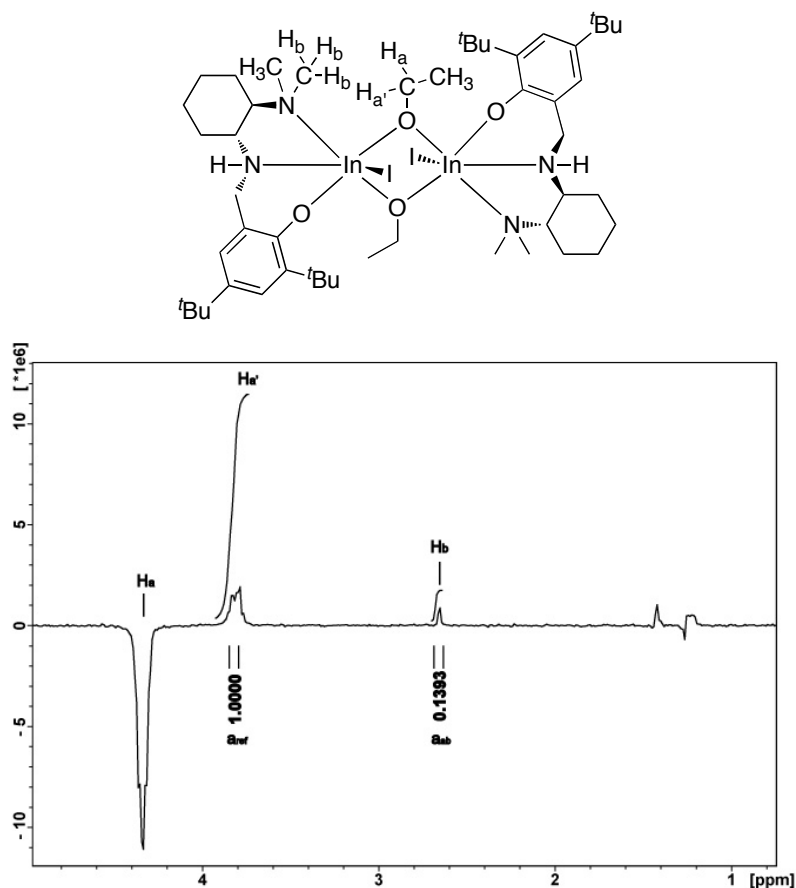


Figure 2.18. 1D NOE spectrum (400 MHz, CDCl_3 , 25 °C) of meso- $[(\text{NNO}_{t\text{Bu}})\text{In}(\text{I})(\mu\text{-OEt})]_2$ (**9**).

Table 2.8. Selective qualitative H-H distance calculated by 1D NOE spectrum of meso-**9**.

complex [9]	r_{ref} (Å)	r_{ij} (Å)
	r_{bc} ($\text{H}_a\text{-H}_{a'}$)	r_{ba} ($\text{H}_a\text{-H}_b$)
X-ray ^a	1.601	2.295
NOE ^b		2.22 (0.11)

^a An obtained distance between two protons (r_{ref}) obtained from X-ray crystallographic data. ^b a calculated distance from NOE spectroscopic data based on the equation, $r_{ij} = r_{ref}(a_{ref}/a_{ij})^{1/6}$, where a_{ij} is the NOE cross-peak volume and r_{ij} is the interproton distance of the two protons i and j , a known distance between two protons (r_{ref}) and its NOE volume (a_{ref}).

(3) Pulsed-gradient spin-echo (PGSE) NMR experiments³³ are in agreement with the solid state structures and support dinuclear solution structures for (\pm)-**5** and meso-**8**. The diffusion coefficients (D) of the proligand ($12.0 \times 10^{-10} \text{ m}^2\text{s}^{-1}$), the mononuclear complex **1** ($10.4 \times 10^{-10} \text{ m}^2\text{s}^{-1}$), and the previously reported complex $(\text{NNO}_{t\text{Bu}})\text{In}(\text{CH}_3)_2$ ($11.1 \times 10^{-10} \text{ m}^2\text{s}^{-1}$)²³ are significantly faster than those of (\pm)-**5** ($7.8 \times 10^{-10} \text{ m}^2\text{s}^{-1}$) and meso-**8** ($7.9 \times 10^{-10} \text{ m}^2\text{s}^{-1}$).

¹⁾ (Figure 2.19). The hydrodynamic radii values (r_H) of the dinuclear species ((\pm)-**5**, 7.5 Å, meso-**8** 7.4 Å) calculated from the modified Stokes-Einstein equation³³ are consistent with the structurally determined values ((\pm)-**5**, 7.3 Å, meso-**8**, 6.7 Å) estimated from the X-ray crystallographic data (Table 2.9).

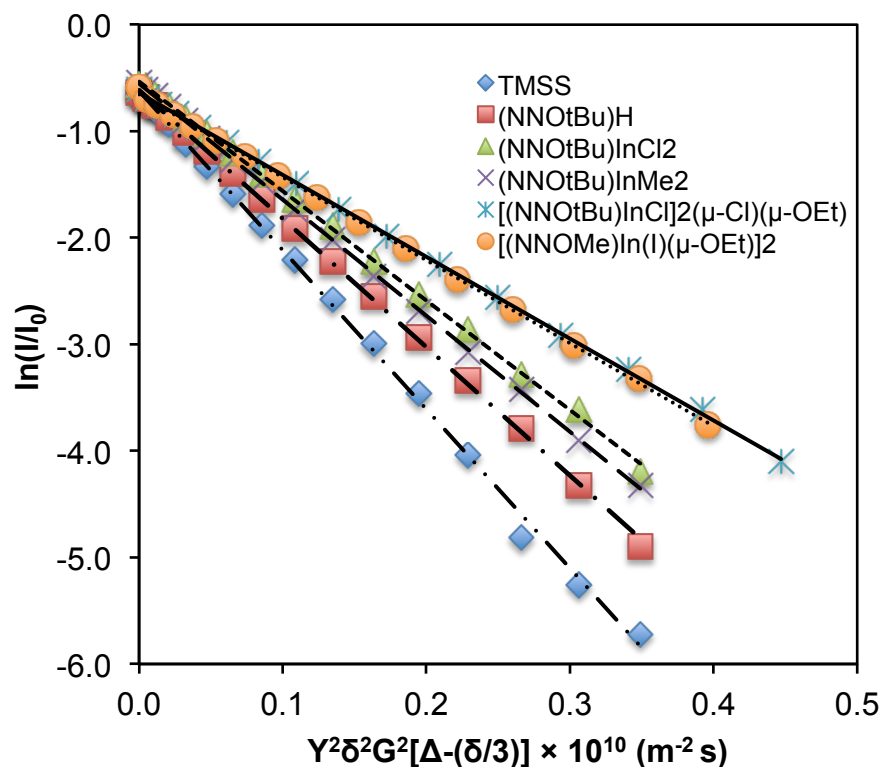


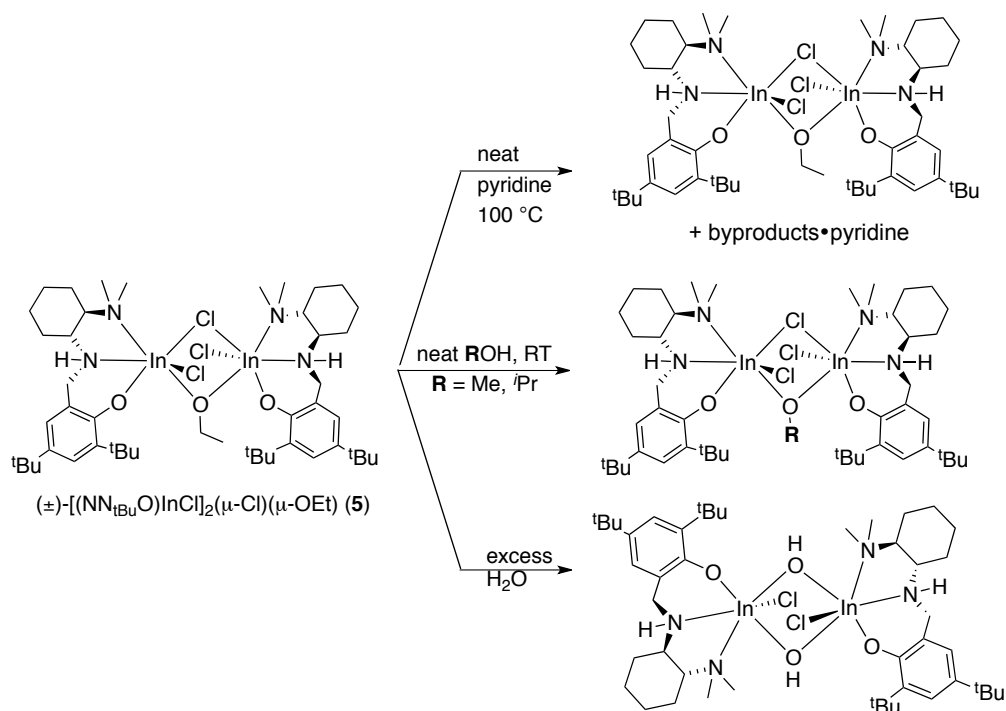
Figure 2.19. Plot of $\ln(I/I_0)$ vs $\gamma^2\delta^2G^2[\Delta-(\delta/3)] \times 10^{10}$ ($m^2 s$) from PGSE experiments (400 MHz, CD_2Cl_2 , 25 °C). The hydrodynamic radius (r_H) of each compound were calculated by using the slopes (D_i) of the linear fits. I = intensity of the observed spin-echo, I_0 = intensity of the spin-echo in the absence of gradients, G = varied gradient strength, γ = gyromagnetic ratio ($2.675 \times 10^8 \text{ rad s}^{-1} \text{ T}^{-1}$), δ = length of the gradient pulse, Δ = delay between the midpoints of the gradients.

Table 2.9. Comparison of calculated hydrodynamic radii (r_H) by PGSE spectroscopy and estimated $r_{x\text{-ray}}$ by X-ray crystallography.

	D_t^{sa} ($\times 10^{-10} \text{ m}^2 \text{ s}^{-1}$)	r_H (\AA) ^a	$r_{x\text{-ray}}$ (\AA)
(\pm)-(NNO _{tBu})H ^b	12.05 (0.17)	5.19 (0.07)	-
(\pm)-(NNO _{tBu})InCl ₂ (1) ^b	10.37 (0.17)	5.89 (0.10)	-
(\pm)-(NNO _{tBu})InMe ₂ ^b	11.07 (0.63)	5.57 (0.32)	5.38
(\pm)-[(NNO _{tBu})InCl] ₂ (μ -Cl)(μ -OEt) (5) ^b	7.80 (0.31)	7.53 (0.30)	7.30
meso-[(NNO _{Me})In(I)(μ -OEt)] ₂ (8) ^c	7.93 (0.32)	7.42 (0.30)	6.71 ^d

^a Calculated hydrodynamic Radius (r_H) from translational diffusion coefficients (D_t) (0.9 mM TMSS used as internal standard). ^b 4.5 mM in CD₂Cl₂. ^c Saturated solution was used due to low solubility in CD₂Cl₂. ^d X-ray crystallographic data of *RR/RR*-**8** was used to calculate $r_{x\text{-ray}}$ using the equation $r_{x\text{-ray}} = ((3/4)\pi V)^{1/3}$ where V is a volume of a unit cell.

(4) Examination of the dissociation of (\pm)-**5** in the presence of added donors reveals the high stability of the dinuclear architecture. Complex (\pm)-**5** remains unchanged 24 hours after the addition of 2 equivalents of pyridine, ethyl acetate, and ethanol, as observed by ¹H NMR spectroscopy (CDCl₃, 25 °C, **Figure 2.20**). Irreversible changes are observed upon addition of a larger excess of a donor (**Scheme 2.4**). Variable temperature ¹H NMR spectra (25 - -82 °C, CD₂Cl₂) of a mixture of (\pm)-**5** and 10 equivalents of pyridine show new signals for coordinated pyridine, which can be observed below -30 °C (**Figure 2.21**). When complex (\pm)-**5** is heated to 100 °C in neat pyridine for 48 h, signals for at least two new complexes as well as pyridine are observed in the ¹H NMR spectra; however, complex (\pm)-**5** remains the major species in solution (**Figure 2.22**). A 2D NOESY spectrum of this mixture shows no correlations between the proton signals of pyridine and (\pm)-**5**, while correlations between pyridine and at least one of the new by-products is observed (**Figure 2.23**). We have reported that in a similar reaction with (\pm)-(NNO_{tBu})InCl₂ (**1**) the pyridine adduct forms quantitatively.¹⁷ Therefore, dinuclear complex (\pm)-**5** may be dissociated in the presence of a strong base under forcing conditions to form base-adducts; however, the majority of the parent complex (\pm)-**5** remains unreacted, attesting to the stability of the dinuclear structure in solution.



Scheme 2.4. Irreversible reactions of $(\pm)\text{-}[(\text{NNO}_{\text{tBu}})\text{InCl}]_2(\mu\text{-Cl})(\mu\text{-OEt})$ (**5**) with donors.

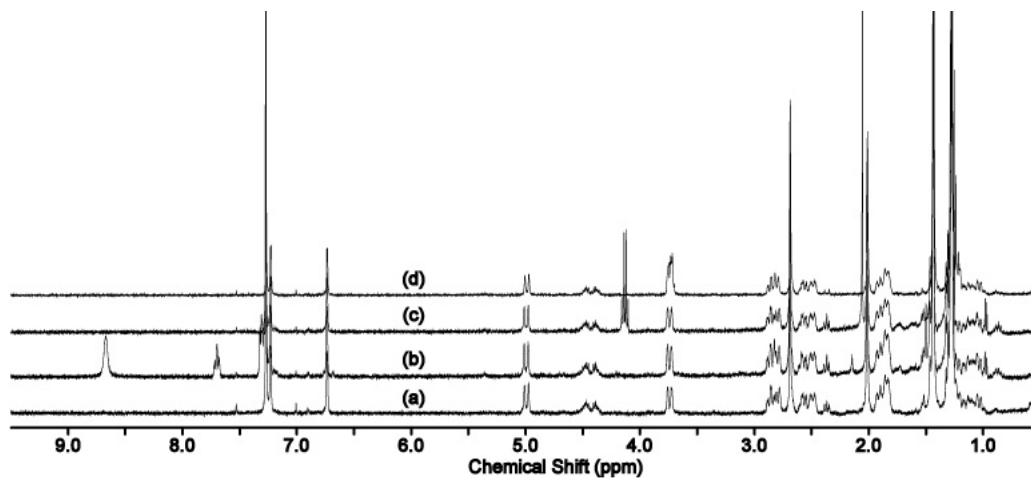


Figure 2.20. ^1H NMR spectra (400 MHz, CDCl_3 , 25 °C) of (a) complex **5**, $[(\text{NNO}_{\text{tBu}})\text{InCl}]_2(\mu\text{-Cl})(\mu\text{-OEt})$, and complex **5** with 2 equivalents of (b) pyridine, (c) ethyl acetate, and (d) ethanol. $[\mathbf{5}] = 0.0023$ M.

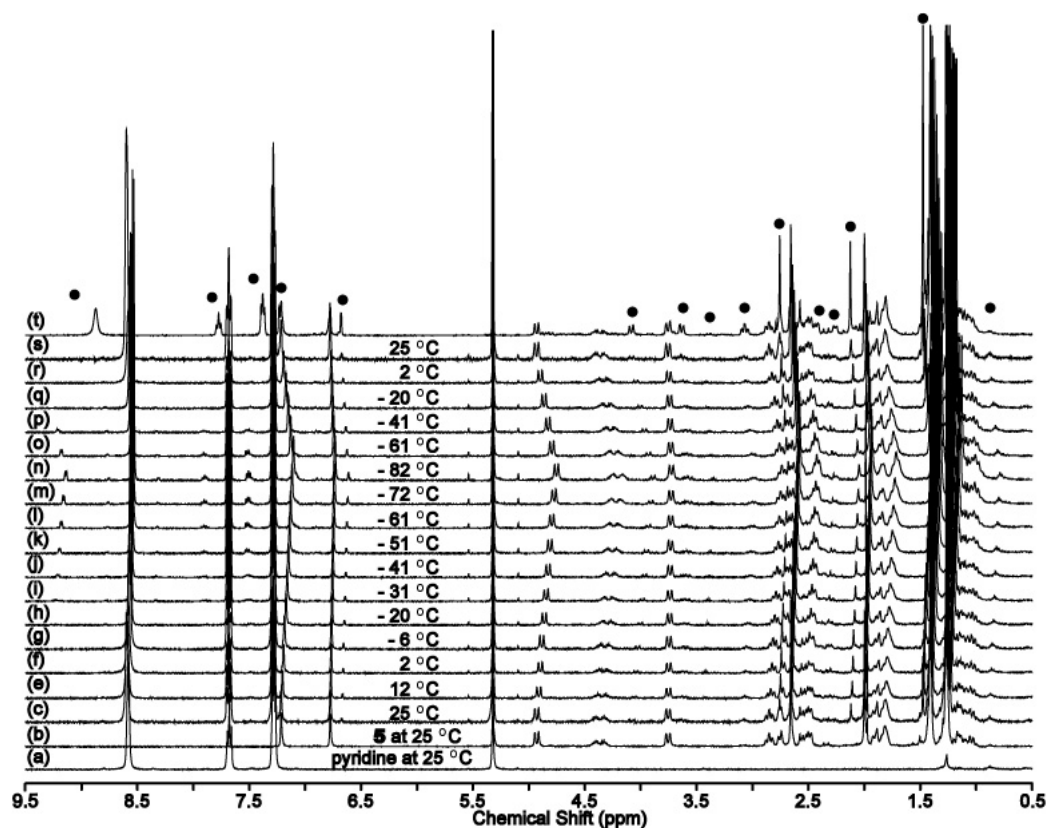


Figure 2.21. ^1H NMR spectra (400 MHz, CD_2Cl_2) of (a) pyridine, (b) $(\pm)\text{-5}$, a mixture of (c) - (s) $(\pm)\text{-5}$ with 10 equivalents of pyridine (0.023 M) at variable temperatures, and (t) ^1H NMR spectrum (400 MHz, CD_2Cl_2 , 25 °C) of $(\pm)\text{-5}$ reacted in neat pyridine at 100 °C (the black dot symbol presents new appearing signals.). $[\text{5}] = 0.0023 \text{ M}$.

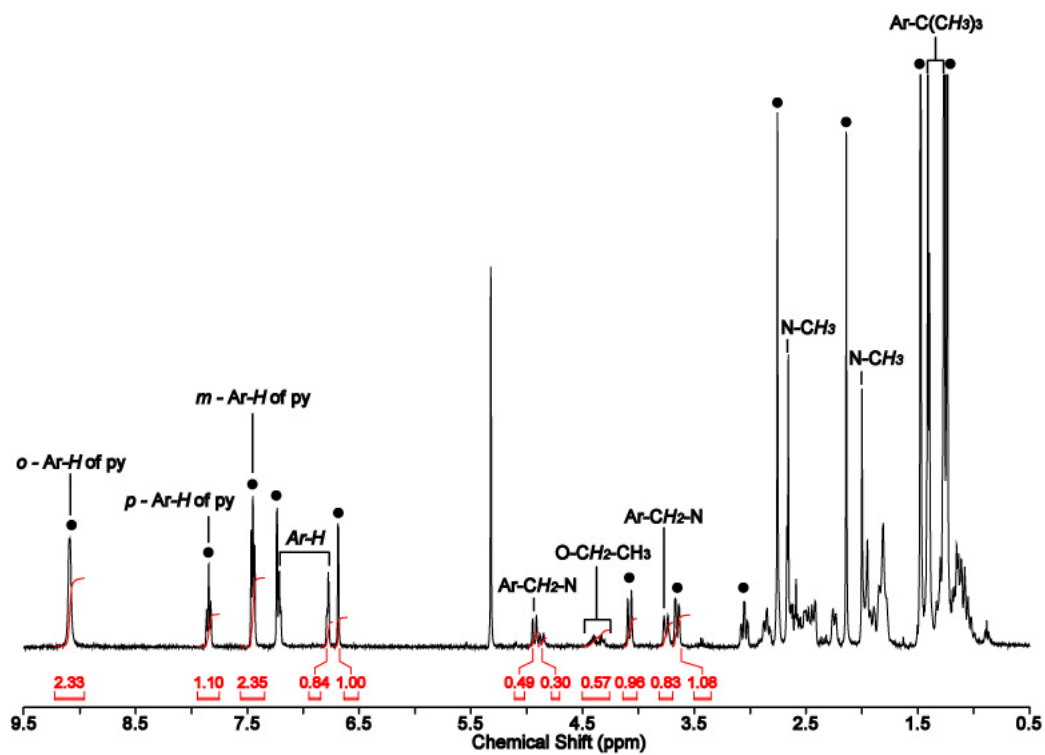


Figure 2.22. ^1H NMR spectrum (400 MHz, CD_2Cl_2 , 25 °C) of (\pm)-**5** reacted in neat pyridine at 100 °C (● represents signals for new complex) [**5**] = 0.0023 M.

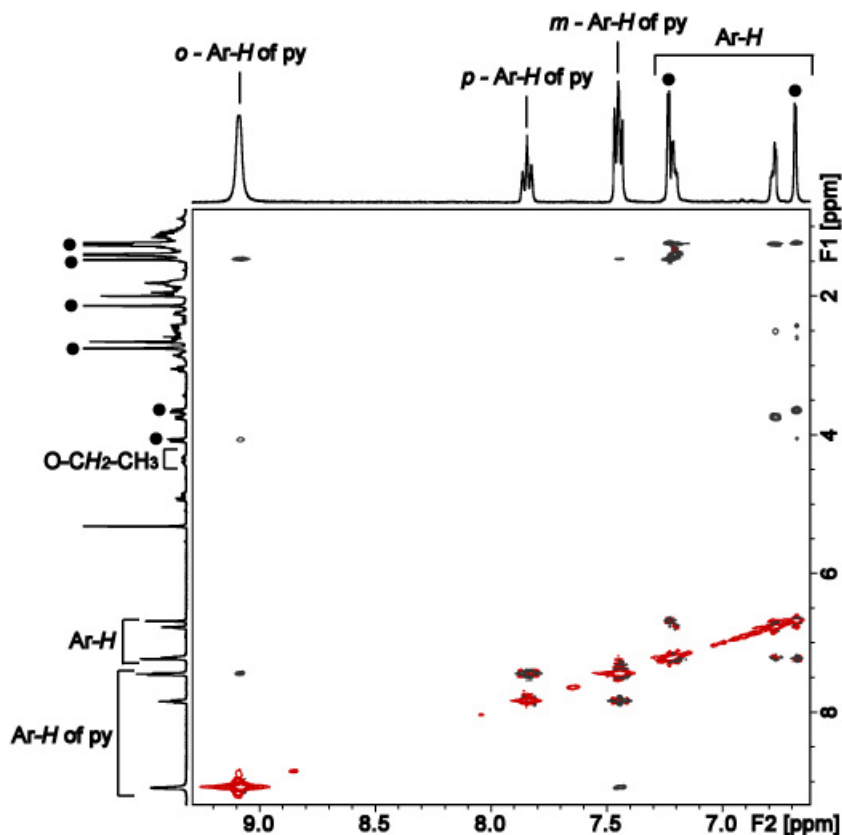


Figure 2.23. 2D ^1H NOESY spectra (400 MHz, CD_2Cl_2 , 25 $^\circ\text{C}$) of (\pm)-**5** reacted in neat pyridine at 100 $^\circ\text{C}$ at the optimized mixing time (400 msec, The diagonal peaks, which have an opposite phase to that of the NOE cross peaks shown in black, are negative and shown in red, and the black dot symbol presents new appearing signals.). $[\mathbf{5}] = 0.0023 \text{ M}$.

(5) *The thermodynamic stability of the dinuclear complex does not preclude reactivity.* As previously reported, reaction of (\pm)-**5** with water yields the meso form of the bis-hydroxy bridged complex $(R,R/S,S)\text{-}[(\text{NNO}_{\text{tBu}})\text{In}(\text{Cl})(\mu\text{-OH})]_2$.^{3,23} The meso complex can only be formed if the $(R,R/R,R)$ - and $(S,S/S,S)$ -**5** dissociate during the reaction. Also, when **5** is dissolved in neat methanol or isopropanol at room temperature, the NMR spectra of the resulting products show resonances corresponding to the quantitative formation of new metal methoxide and isopropoxide complexes (**Figure 2.24**). Integrals of the alkoxy groups in ^1H NMR spectra of these new species clearly show that the complexes maintain a mono-alkoxy bridged dinuclear structure analogous to complex **5**.

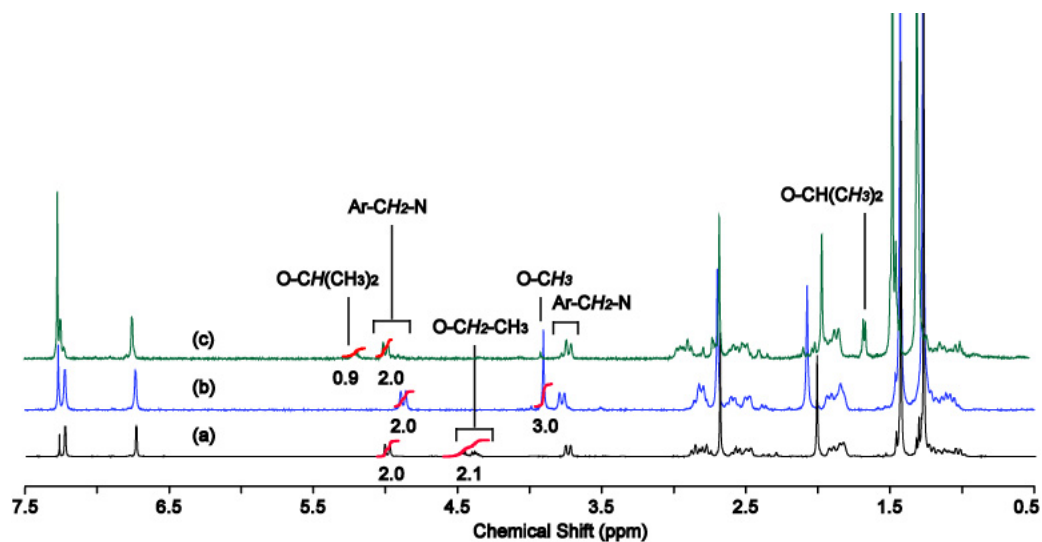


Figure 2.24. ^1H NMR spectra (400 MHz, CDCl_3 , 25 $^\circ\text{C}$) of (a) complex **5**, $(\pm)\text{-}[(\text{NNO}_{\text{tBu}})\text{InCl}]_2(\mu\text{-Cl})(\mu\text{-OEt})$, and complex $(\pm)\text{-5}$ reacted with neat dried (b) methanol and (c) isopropanol for 16 hours at room temperature.

2.3 Conclusion

We have synthesized dihalide indium complexes bearing chiral 2-*t*-butyl-4-*R*-6-(((2-(dimethylamino)cyclohexyl)amino)methyl)phenolate ligands, $(\pm)\text{-}(\text{NNO}_{\text{tBu}})\text{InX}_2$ (**1**: X = Cl, **2**: X = I) and $(\pm)\text{-}(\text{NNO}_{\text{Me}})\text{InX}_2$ (**3**: X = Cl, **4**: X = I) and a family of mono-alkoxy bridged dinuclear complexes $(\pm)\text{-}(\text{NNO}_{\text{tBu}})\text{InCl}]_2(\mu\text{-Cl})(\mu\text{-OEt})$ (**5**) and $(\pm)\text{-}[(\text{NNO}_{\text{Me}})\text{InX}]_2(\mu\text{-X})(\mu\text{-OEt})$ (X = Cl (**6**), I (**7**)) and their enantiopure analogues. Indium alkoxide complexes in this family are invariably dinuclear in the solid state by X-ray crystallography. A variety of techniques (VT NMR spectroscopy, 2D NOESY spectroscopy, PGSE experiments) confirm that the complexes are also dinuclear in solution and that the solution structures correlate closely to the solid state structures. This is most striking when comparing the enantiopure analogues of the bis-ethoxy bridged complex. The solid state structure of meso- $[(\text{NNO}_{\text{tBu}})\text{In}(\text{I})(\text{OEt})]_2$ **9** derived from $(\pm)\text{-H}(\text{NNO}_{\text{tBu}})$ (**Figure 2.6**) is in the centrosymmetric meso form, while the enantiopure $(S,S/S,S)\text{-8}$ derived from $(S,S)\text{-H}(\text{NNO}_{\text{Me}})$ has lost the center of symmetry (**Figure 2.11**). These differences are reflected in the solution structures of the compounds: $(R,R/R,R)\text{-}$ and $(S,S/S,S)\text{-8}$ have a different ^1H NMR signature than meso-**8** (**Figure 2.9b**).

There is ample evidence that the dinuclear complexes dissociate in solution and can react with added donors under forcing conditions; however, the dinuclear complexes are the thermodynamic sinks in these systems. All irreversible reactions with added donors / (\pm)-(NNO_R)InX₂ complexes (**Scheme 2.4**) as well as conversion of enantiopure to meso complexes (**Figure 2.10**) result in the formation of more stable dinuclear complexes. The most telling experiment is the low reactivity of complex (\pm)-**5** with neat pyridine at 100 °C. Thus, addition of a large concentration of a donor such as lactide does not necessarily lead to dissociation of the dimer. These complexes have been used to investigate the kinetic and mechanistic studies of mono- (Y = Cl, I) and bis-alkoxy bridged (Y = OEt) complexes for the living ring opening polymerization (ROP) of lactide (LA) in Chapter 3. The effects of varying the steric properties of the ligand on the structure and reactivity of the complexes are being investigated in the group.²

2.4 Experimental section

General Considerations. Unless otherwise indicated, all air- and/or water-sensitive reactions were carried out under dry nitrogen using either an MBraun glove box or standard Schlenk line techniques. NMR spectra were recorded on a Bruker Avance 400 MHz or 600 MHz spectrometer. ¹H NMR chemical shifts are reported in ppm versus residual protons in deuterated solvents as follows: δ 7.27 CDCl₃, δ 5.32 CD₂Cl₂. ¹³C{¹H} NMR chemical shifts are reported in ppm versus residual ¹³C in the solvent: δ 77.2 CDCl₃, δ 54.0 CD₂Cl₂. Diffraction measurements for X-ray crystallography were made on a Bruker X8 APEX II diffraction with graphite monochromated Mo-K α radiation. The structures (Table S3) were solved by direct methods and refined by full-matrix least-squares using the SHELXTL crystallographic software of Bruker-AXS. Unless specified, all non-hydrogens were refined with anisotropic displacement parameters, and all hydrogen atoms were constrained to geometrically calculated positions but were not refined. EA CHN analysis was performed using a Carlo Erba EA1108 elemental analyzer. The elemental composition of unknown samples was determined by using a calibration factor. The calibration factor was determined by analyzing a suitable certified organic standard (OAS) of a known elemental composition. Molecular weights were determined by triple detection gel permeation chromatography coupled with laser light scattering (GPC-LLS) using a Waters liquid chromatograph

equipped with a Water 515 HPLC pump, Waters 717 plus autosampler, Waters Styragel columns (4.6 × 300 mm) HR5E, HR4 and HR2, Water 2410 differential refractometer, Wyatt tristar miniDAWN (laser light scattering detector) and a Wyatt ViscoStar viscometer. A flow rate of 0.5 mL min⁻¹ was used and samples were dissolved in THF (2 mg mL⁻¹). Narrow molecular weight polystyrene standards were used for calibration purposes.

Materials. Solvents (THF, toluene, hexane and diethyl ether) were collected from an MBraun Solvent Purification System packed with activated alumina. CH₂Cl₂ and CHCl₃ were dried over CaH₂ and degassed through a series of freeze-pump-thaw cycles. CD₂Cl₂, CDCl₃, methanol, ethanol, isopropanol, ethyl acetate, pyridine and acetonitrile (CH₃CN) were dried over CaH₂, collected by vacuum distillation and degassed through a series of freeze-pump-thaw cycles. rac-LA ([α]_D = -0.1°, toluene, 25 °C), D-LA ([α]_D = +287 - +300°, toluene, 25 °C) and L-LA ([α]_D = -288.1°, toluene, 25 °C) were obtained from PURAC America Inc. and were recrystallized twice from hot dried toluene prior to use. (1*R*,2*R*)- or (1*S*,2*S*)-1,2-diaminocyclohexane were resolved from (±)-trans-1,2-diaminocyclohexane using known literature procedures.¹²⁶ KOEt was generated by reacting KO^tBu with dried ethanol. The solvent was removed under high vacuum, and the addition of hexane to the residual precipitated a white solid. The white solid, KOEt, was isolated by vacuum filtration and dried *in vacuo* for 4 h. 1,3,5-trimethoxybenzene and tetrakis(trimethylsilyl)silane (TMSS) were purchased from Aldrich and Alfa Aesar, respectively, and used as received. Para-methyl salicaldimine, proligand H(NNO_(tBu)) and complexes **1**, **2**, and **5**, were synthesized according to previously reported procedures.^{23,125}

Synthesis of 2-methyl-3a,4,5,6,7,7a-hexahydro-1H-benzimidazole. 2-Methyl-3a,4,5,6,7,7a-hexahydro-1H-benzimidazole was synthesized according to the reported routes.¹ A 500 mL round bottom flask was charged with ethyl ethanecarboximidate hydrochloride (15.0 g, 0.121 mol) in a glovebox. A 300 mL solution of dry EtOH was added to the flask to dissolve the salt via cannula transfer with the use of the Schlenk line. The solution was then cooled in an ice bath, and then 1,2-diaminocyclohexane (15.8 mL, 0.131 mol) was added to the stirring solution. After the addition, a white solid was formed, and the suspension changed into a clear yellow solution after about 5 minutes of stirring. The reaction mixture was warmed to room temperature and left overnight. Then a 200 mL

solution of 1M NaOH was added to dilute the reaction mixture, and the organic layer was extracted using 5% MeOH/CH₂Cl₂ (3 × 120 mL). The collected organic fraction was then dried over Na₂SO₄ and filtered through a Buchner funnel. The filtrate was evaporated to dryness using a rotary evaporator to yield a pale yellow oily solid (13.6 g, 75%). The product was then used in the next step without any further purification. ¹H NMR (300 MHz, CDCl₃) δ 2.88-2.91 (2H, m, -CH- of DACH), 1.91 (3H, s, CH₃), 1.14-1.81 (8H, m, -CH₂- of DACH).

Synthesis of N-(2-aminocyclohexyl)acetamide. N-(2-aminocyclohexyl)acetamide was synthesized according to the reported routes.¹ A 1 L round bottom flask was charged with the 1H-benzimidazole compound (7.65g, 0.0558 mol). Ethanol (100 mL) and distilled H₂O (100 mL) was added to the flask, and the mixture was heated to reflux at 120°C overnight. Then the mixture was cooled to room temperature. The solution was evaporated to dryness using a rotary evaporator. The resulting product was a pale yellow solid (7.32 g, 84%). The product was then methylated in the next step without further purification. ¹H NMR (400 MHz, CDCl₃) δ 5.76 (1H, br. s, -NHC(O)CH₃), 3.45-3.50 (1H, m, -CH- of DACH), 2.34-2.38 (1H, m, -CH- of DACH), 1.99 (3H, s, -C(O)CH₃), 1.95 (2H, m, -CH₂- of DACH), 1.72 (2H, m, -CH₂- of DACH), 1.10-1.29 (4H, m, -CH₂- of DACH).

Synthesis of N-(2-dimethylaminocyclohexyl)acetamide. N-(2-dimethylaminocyclohexyl)acetamide was synthesized according to the reported routes.¹ A 500 mL round bottom flask was charged with N-(2-aminocyclohexyl)acetamide (20.4 g, 0.131 mol) and formaldehyde (53.1 mL of 37% weight in H₂O, 0.655 mol) in acetonitrile (500 mL). The reaction mixture was stirred for 30 minutes. Then, NaBH₃CN (17.2 g, 0.275 mol) was added, and the reaction mixture was stirred for additional 30 minutes. Glacial acetic acid (37.4 mL, 0.654 mol) was added dropwise to the stirring solution. The mixture was left to stir at room temperature overnight. Then, the solution was diluted with 2% CH₃OH/CH₂Cl₂ (400 mL). The organic layer was extracted and washed with 1 M NaOH (3 × 300 mL). The organic fraction was collected and dried over MgSO₄. The solvent was dried *in vacuo*. The resulting product was a dark brown oil (22.3 g, 92%), which was then used without further purification. ¹H NMR (300 MHz, CDCl₃) δ 6.22 (1H, s, NHC(O)CH₃), 3.43-3.51 (1H, m, -CH- of DACH), 2.46-2.49 (1H, m, -CH- of DACH), 2.35 (3H, s, -C(O)CH₃), 2.21 (6H, s, -N(CH₃)₂), 1.01-1.34 (8H, m, -CH₂- of DACH).

Synthesis of N-(1-dimethylcyclohexyl)-1,2-diamine. N-(1-dimethylcyclohexyl)-1,2-diamine was synthesized according to the reported routes.¹ N-(2-Dimethylaminocyclohexyl)acetamide (22.3 g, 0.121 mol) was dissolved in a 600 mL of 4M HCl, and the reaction mixture was heated to reflux at 110°C overnight. The mixture was cooled to room temperature, basified with 700mL of 4 M NaOH and then extracted with 5 % MeOH/CH₂Cl₂ (3 × 500 mL) from the aqueous layer. The collected organic fractions were dried over MgSO₄ and filtered through a Buchner funnel. The filtrate was evaporated to dryness using a rotary evaporator to yield a dark brown liquid (11.5 g, 67.1%). The resulting product was then used without further purification. ¹H NMR (300 MHz, CDCl₃) δ 2.16-2.21 (1H, m, -CH- of DACH), 1.98 (1H, t, -CH- of DACH), 1.87 (2H, d, -NH₂), 1.83 (6H, s, -N(CH₃)₂), 0.68-0.80 (8H, m, -CH₂- of DACH).

Synthesis of (±)-*para*-methyl salicaldimine. *Para*-methyl substituted salicaldimine was synthesized according to the reported routes.¹ 6-*tert*-Butyl-2-hydroxy-3-methylbenzaldehyde (3.98 g, 20.7 mmol) synthesized by reported procedures² was added to a solution of *trans*-N,N-dimethylcyclohexyldiamine (4.41 g, 31.0 mmol) in methanol (30 mL). The reaction mixture was stirred for 16 h at room temperature. The solvent was removed under vacuum to give a yellow solid, which was recrystallized from pentane to yield yellow crystals of salicaldimine (4.87 g, 58%). ¹H NMR (600 MHz, CDCl₃): δ 8.27 (1H, s, N=CH-Ar), 7.13 (1H, br. s., ArH), 6.92 (1H, br. s., ArH), 3.22 (1H, td, ³J_{H-H} = 10.2 Hz ⁴J_{H-H} = 4.3 Hz, N-CH-CH₂ of DACH), 2.58 - 2.66 (1H, m, N-CH-CH₂ of DACH), 2.31 (3H, s, Ar-CH₃), 2.29 (6H, s, -N-(CH₃)₂) 1.89 (4H, dd, ³J_{H-H} = 5.4 Hz ⁴J_{H-H} = 3.7 Hz, -CH₂- of DACH), 1.80 - 1.86 (2H, m, -CH₂- of DACH), 1.76 (1H, dd, ³J_{H-H} = 6.0 Hz ⁴J_{H-H} = 4.6 Hz, -CH₂- of DACH), 1.59 - 1.71 (1H, m, -CH₂- of DACH), 1.46 (9H, br. s., Ar-(CH₃)₃) 1.23-1.37 (3H, m, , -CH₂- of DACH); ¹³C{¹H} NMR (151 MHz, CDCl₃) δ 163.8 (-N=CHAr), 158.4 (Ar C-OH), 136.9 (Ar C-C(CH₃)₃), 129.9 (Ar C-H), 129.3 (Ar C-H), 126.1 (Ar C-CH₃), 118.6 (Ar HN=C-C), 69.6 (-CH-N(CH₃)₂), 66.7 (-CH-N=), 40.8 (-N(CH₃)₂), 34.9 (-C(CH₃)₃), 34.7 (-CH₂- of DACH), 29.4 (-C(CH₃)₃), 25.2(-CH₂- of DACH), 24.6 (-CH₂- of DACH), 24.1 (-CH₂- of DACH), 20.6 (-CH₃). Anal. Calcd for C₂₀H₃₂N₂O: C 75.90; H 10.19; N 8.85. Found: C 75.35; H 10.03; N 9.08. **6-*tert*-Butyl-2-hydroxy-3-methylbenzaldehyde.** ¹H NMR (600 MHz, CDCl₃) δ 11.63 (1H, s, ArCHO), 9.84 (1H, s, ArOH), 7.31 - 7.39 (1H, m, ArH), 7.19 (1H, s, ArH), 2.34 (3H,

s, ArCH₃), 1.44 (9H, s, ArC(CH₃)₃); ¹³C{¹H} NMR (151 MHz, CDCl₃) δ 197.0 (ArCHO), 159.1 (Ar C-OH), 137.9 (Ar C-C(CH₃)₃), 135.4 (Ar C-H), 131.4 (Ar C-CH₃), 128.1 (Ar C-CHO), 120.3 (Ar C-H), 34.7 (-C(CH₃)₃), 29.2 (-C(CH₃)₃), 20.5 (-CH₃). Anal. Calcd for C₁₂H₁₆O₂: C 74.97; H 8.39. Found: C 74.82; H 8.46.

Synthesis of (R,R)- and (S,S)-*para*-methyl salicaldimine. With either of (1*R*,2*R*)- or (1*S*,2*S*)-1,2-diaminocyclohexane resolved from (±)-trans-1,2-diaminocyclohexane, enantiopure *para*-methyl substituted salicaldimines were synthesized according to the above routes for (±)-*para*-methyl salicaldimine.¹ They have identical NMR spectra. ¹H NMR (400 MHz, CDCl₃): δ 8.26 (1H, s, N=CH-Ar), 7.12 (1H, d, ⁴J_{H-H} = 2.0 Hz, ArH), 6.91 (1H, d, ⁴J_{H-H} = 1.7 Hz, ArH), 3.21 (1H, td, ³J_{H-H} = 10.2 Hz ⁴J_{H-H} = 4.3 Hz, N-CH-CH₂ of DACH), 2.62 (1H, td, ³J_{H-H} = 10.3 Hz ⁴J_{H-H} = 3.6 Hz, N-CH-CH₂ of DACH), 2.30 (3H, s, Ar-CH₃), 2.28 (6H, s, -N-(CH₃)₂), 1.71 - 1.94 (4H, m, -CH₂- of DACH), 1.56 - 1.71 (1H, m, -CH₂- of DACH), 1.45 (9H, s, Ar-(CH₃)₃) 1.22-1.39 (3H, m, -CH₂- of DACH); ¹³C{¹H} NMR (101 MHz, CDCl₃) δ 163.8 (-N=CHAr), 158.4 (Ar C-OH), 137.0 (Ar C-C(CH₃)₃), 130.0 (Ar C-H), 129.3 (Ar C-H), 126.1 (Ar C-CH₃), 118.6 (Ar HN=C-C), 69.6 (-CH-N(CH₃)₂), 66.8 (-CH-N=), 40.8 (-N(CH₃)₂), 34.9 (-C(CH₃)₃), 34.7 (-CH₂- of DACH), 29.4 (-C(CH₃)₃), 25.2(-CH₂- of DACH), 24.6 (-CH₂- of DACH), 24.2 (-CH₂- of DACH), 20.6 (-CH₃). **(R,R)-*para*-methyl salicaldimine.** Yield (1.13 g, 58%) based on 0.84 g of (R,R)-*N,N*-(dimethylcyclohexyl)-1,2-diamine. Anal. Calcd for C₂₀H₃₂N₂O: C 75.90; H 10.19; N 8.85. Found: C 75.84; H 10.29; N 8.74. **(S,S)-*para*-methyl salicaldimine.** Yield (0.83 g, 48%) based on 0.75 g of (S,S)-*N,N*-(dimethylcyclohexyl)-1,2-diamine. Anal. Calcd for C₂₀H₃₂N₂O: C 75.90; H 10.19; N 8.85. Found: C 75.98; H 10.28; N 8.80.

Synthesis of (R,R)- and (S,S)-*para*-tert-butyl salicaldimine. With either of (1*R*,2*R*)- or (1*S*,2*S*)-1,2-diaminocyclohexane resolved from (±)-trans-1,2-diaminocyclohexane, *para*-tert-butyl substituted salicaldimine was synthesized according to reported routes.¹ They have identical NMR spectra. ¹H NMR (400 MHz, CDCl₃): δ 8.33 (1H, s, N=CH-Ar), 7.38 (1H, d, ⁴J_{H-H} = 2.2 Hz, ArH), 7.09 (1H, d, ⁴J_{H-H} = 2.2 Hz, ArH), 3.22 (1H, td, ³J_{H-H} = 10.1 ⁴J_{H-H} = 4.3 Hz, N-CH-CH₂ of DACH), 2.63 (1H, td, ³J_{H-H} = 10.1 Hz ⁴J_{H-H} = 3.3 Hz, N-CH-CH₂ of DACH), 2.30 (6H, s, -N-(CH₃)₂), 1.71 - 1.97 (4H, m, -CH₂- of DACH), 1.56 - 1.71 (1H, m, -CH₂- of DACH), 1.47 (9H, s, Ar-(CH₃)₃) 1.23-1.40 (12H, m, -CH₂- of DACH and Ar-

(CH₃)₃); ¹³C{¹H} NMR (101 MHz, CDCl₃) δ 164.1 (-N=CHAr), 158.4 (Ar C-OH), 139.6 (Ar C-C(CH₃)₃), 139.5 (Ar C-C(CH₃)₃), 126.5 (Ar C-H), 125.6 (Ar C-H), 118.6 (Ar HN=C-C), 69.6 (-CH-N(CH₃)₂), 66.8 (-CH-N=), 40.8 (-N(CH₃)₂), 35.0 (-C(CH₃)₃), 34.1 (-C(CH₃)₃), 31.5 (-C(CH₃)₃), 29.4 (-C(CH₃)₃), 25.2(-CH₂- of DACH), 24.6 (-CH₂- of DACH), 24.1 (-CH₂- of DACH). **(R,R)-para-tert-butyl salicaldimine**. Yield (2.90 g, 58%) based on 1.92 g of (R,R)-N,N-(dimethylcyclohexyl)-1,2-diamine. Anal. Calcd for C₂₃H₃₈N₂O: C 77.04; H 10.68; N 7.81. Found: C 77.08; H 10.86; N 7.60. **(S,S)-para-tert-butyl salicaldimine**. Yield (2.00 g, 40%) based on 1.92 g of (S,S)-N,N-(dimethylcyclohexyl)-1,2-diamine. Anal. Calcd for C₂₃H₃₈N₂O: C 77.04; H 10.68; N 7.81. Found: C 77.08; H 10.86; N 7.60.

Synthesis of 6-tert-butyl-2-{N-[2-(N,N-dimethyl)aminocyclohexyl]salicaldimino}-4-methylphenol (±)-H(NNO_{Me}), (R,R)- and (S,S)-H(NNO_{Me}). A 500 mL round bottom flask was charged with *para*-methyl salicaldimine (2.87 g, 9.08 mmol) in 150 mL of acetonitrile. NaBH₄ (2.51 g, 66.3 mmol) was added to the stirring mixture. The reaction mixture was stirred for 30 min, and a 1.5 mL of glacial acetic acid was added drop-wise to the stirring mixture. The reaction mixture was stirred for 16 h. After the basic aqueous work-up with 1M NaOH and 5% MeOH/CH₂Cl₂, the organic layer was collected, and an off-white solid was obtained by removal of the solvent under vacuum. The solid was recrystallized from acetonitrile (2.17 g, 78%). ¹H NMR (600 MHz, CDCl₃): δ 7.01 (1H, br. s., ArH), 6.74 (1H, br. s., ArH), 4.01 (d, 1H, ⁴J_{H-H} = 13.4 Hz, NH-CH₂-Ar), 3.81 (1H, d, ⁴J_{H-H} = 13.4 Hz, NH-CH₂-Ar), 3.38 (1H, br. s., -NH-), 2.36-2.43 (1H, m, -CH- of DACH), 2.25-2.33 (4H, m, Ar-CH₃; -CH- of DACH), 2.23 (6H, s, -N(CH₃)₂), 2.14-2.20 (1H, m, -CH₂- of DACH), 1.80-1.89 (2H, m, -CH₂- of DACH), 1.68-1.75 (1H, m, -CH₂- of DACH), 1.45 (9H, br. s., Ar-(CH₃)₃), 1.11-1.29 (4H, m, -CH₂- of DACH); ¹³C{¹H} NMR (151 MHz, CDCl₃) δ 154.8 (Ar C), 136.4 (Ar C), 126.6 (Ar C-H), 126.5 (Ar C-H), 126.1 (Ar C), 124.3 (Ar C), 66.6 (CH-N(CH₃)₂), 58.9 (CH-NH-CH₂), 51.1 (N-CH-CH₂), 40.0 (N(CH₃)₂), 34.5 (N(CH₃)₂), 34.5 (Ar-C(CH₃)₃), 31.7 (Ar-CH₃), 29.6 (Ar-C(CH₃)₃), 25.3 (-CH₂- of DACH), 20.9 (-CH₂- of DACH), 20.8 (-CH₂- of DACH). **(±)-H(NNO_{Me})**. Anal. Calcd. For C₂₀H₃₄N₂O: C 75.42; H 10.76; N 8.80. Found: C 75.36; H 10.72; N 8.87. **(R,R)-H(NNO_{Me})**. Yield (0.75 g, 52%) based on 1.44 g of (R,R)-*para*-tert-butyl salicaldimine. Anal. Calcd. For C₂₀H₃₄N₂O: C 75.42; H 10.76; N 8.80. Found: C 75.25; H 10.76; N 8.69. **(S,S)-H(NNO_{Me})**. Yield (0.42 g, 50%) based on 0.83 g of (S,S)-

para-methyl salicaldimine. Anal. Calcd. For C₂₀H₃₄N₂O: C 75.42; H 10.76; N 8.80. Found: C 75.07; H 10.62; N 8.45.

Synthesis of 4,6-di-*tert*-butyl-2-{*N*-[2-(*N,N*-dimethyl)aminocyclohexyl]salicaldimino}phenol (*R,R*)- and (*S,S*)-H(NNO_{tBu}). The syntheses were carried out in an analogous manner to the racemic compound above and have identical NMR signatures.¹⁷ (*R,R*)-H(NNO_{tBu}). Yield (1.88 g, 59%) based on 3.14 g of (*R,R*)-*para*-*tert*-butyl salicaldimine. Anal. Calcd. For C₂₃H₄₀N₂O: C 76.61; H 11.18; N 7.77. Found: C 76.44; H 11.29; N 7.65. (*S,S*)-H(NNO_{tBu}). Yield (0.35 g, 50%) based on 0.70 g of (*S,S*)-*para*-*tert*-butyl salicaldimine. Anal. Calcd. For C₂₃H₄₀N₂O: C 76.61; H 11.18; N 7.77. Found: C 75.10; H 11.23; N 7.84.

Synthesis of (*R,R*)- and (*S,S*)-(NNO_{tBu})InCl₂ (1**).** The syntheses of (±)- and (*R,R*)-NNO_{tBu}InCl₂ were published previously in the literature.¹⁷ (*S,S*)-(NNO_{tBu})InCl₂ was carried out in an analogous manner to (±)- and (*R,R*)-(**1**) and has an identical NMR signature. A 20 mL scintillation vial was charged with H(NNO_{Me}) (198 mg, 0.62 mmol) in toluene (5 mL) at room temperature. A slurry of benzyl potassium (76.8 mg, 0.59 mmol) in toluene (5 mL) was added drop-wise to the stirring solution at room temperature. The reaction mixture was stirred for 16 h. An off-white solid was isolated by removal of the solvent under high vacuum. The product, K(NNO_{tBu}), was used without further purification and characterization. A suspension of InCl₃ (81.6 mg, 0.37 mmol) in THF (3 mL) was added drop-wise to a slurry of K(NNO_{Me}) (147 mg, 0.37 mmol) in THF (10 mL). The mixture was stirred for 16 h at room temperature resulting in a white solid (KCl) and yellow solution. The white solid was filtered through Celite and the pale yellow filtrate was concentrated under vacuum. The residue was taken up in 3 mL Et₂O, from which an off-white solid precipitated. The solid was isolated by vacuum filtration and dried *in vacuo* for a few hours. ¹H NMR (600 MHz, CD₂Cl₂): δ 7.28 (1H, br. s., ArH), 6.89 (1H, br. s., ArH), 4.14 (2H, br. s., NH-CH₂-Ar), 2.73 (3H, s, N-(CH₃)₂), 2.54 - 2.69 (3H, m, -NH- and -CH- of DACH), 2.44 (3H, br. s., -N-(CH₃)₂), 2.01 - 2.13 (2H, m, -CH₂- of DACH), 1.82 - 1.98 (2H, m, -CH₂- of DACH), 1.42 (9H, br. s., Ar-(CH₃)₃), 1.16 - 1.36 (13H, m, -CH₂- of DACH and Ar-(CH₃)₃). ¹³C{¹H} NMR (151MHz, CD₂Cl₂): δ 164.1 (Ar C), 140.2 (Ar C), 130.4 (Ar C-H), 125.3 (Ar C-H), 125.3 (Ar C), 121.9 (Ar C), 66.7 (N-CH-CH₂), 56.0 (N-CH-CH₂), 52.4 (N-CH₂-Ar), 44.6

(N(CH₃)₂), 38.1 (N(CH₃)₂), 35.6 (Ar-C(CH₃)₃), 34.5 (Ar-C(CH₃)₃), (32.0 (Ar-C(CH₃)₃), 31.9 (-CH₂- of DACH), 30.2 (Ar-C(CH₃)₃), 25.0 (2C, -CH₂- of DACH), 22.5 (-CH₂- of DACH). **(R,R)-1**. Yield (231 mg, 80%) based on 211 mg of (R,R)- K(NNO_{tBu}). Anal. Calcd. For C₂₃H₃₉Cl₂InN₂O: C 50.66; H 7.21; N 5.14. Found: C 50.39; H 7.20; N 5.39. **(S,S)-1**. Yield (153 mg, 76%) based on 211 mg of (S,S)- K(NNO_{tBu}). Anal. Calcd. For C₂₃H₃₉Cl₂InN₂O: C 50.66; H 7.21; N 5.14. Found: C 50.57; H 7.06; N 5.14.

Synthesis of (±)-(NNO_{Me})InCl₂ (3). A 100 mL round bottom flask was charged with H(NNO_{Me}) (309 mg, 0.97 mmol) in toluene (30 mL) at room temperature. Benzyl potassium (126 mg, 0.97 mmol) in toluene (30 mL) was added drop-wise to the stirring solution at room temperature. The reaction mixture was stirred for 16 h. An off-white solid was isolated by removal of the solvent under high vacuum. The product, K(NNO_{Me}), was used without further purification and characterization. A suspension of InCl₃ (239 mg, 1.08 mmol) in THF (3 mL) was added drop-wise to a slurry of K(NNO_{Me}) in THF (10 mL). The mixture was stirred for 16 h at room temperature resulting in a white solid (KCl) and yellow solution. The white solid was filtered through Celite and the pale yellow filtrate was concentrated under vacuum. The residue was taken up in 5 mL Et₂O, from which an off-white solid precipitated. The solid was isolated by vacuum filtration and dried *in vacuo* for a few hours. Recrystallization with a solution of THF and ether at room temperature afforded yellow crystals of **3** (380 mg, 76%). ¹H NMR (400 MHz, CD₂Cl₂): δ 7.04 (1H, d, ⁴J_{H-H} = 2.0 Hz, ArH), 6.68 (1H, d, ⁴J_{H-H} = 1.7 Hz, ArH), 4.46 (1H, d, ²J_{H-H} = 12.6 Hz, NH-CH₂-Ar), 3.97 (1H, dd, ²J_{H-H} = 12.5 Hz ³J_{H-H} = 6.7 Hz, NH-CH₂-Ar), 2.73-2.82 (1H, m, -CH- of DACH), 2.71 (3H, s, -N-(CH₃)₂), 2.63-2.61 (1H, m, -CH- of DACH), 2.54 (1H, br. s., -NH- of DACH), 2.38-2.48 (1H, m, -CH₂- of DACH), 2.27 (3H, s, -N-(CH₃)₂), 2.21 (3H, s, Ar-CH₃), 1.94-2.04 (m, 1H, -CH₂- of DACH), 1.78-1.94 (2H, m, -CH₂- of DACH), 1.40 (9H, Ar-(CH₃)₃), 1.18-1.29 (4H, m, -CH₂- of DACH); ¹³C{¹H} NMR (151 MHz, CD₂Cl₂): δ 161.9 (Ar C), 140.2 (Ar C), 129.7 (Ar C-H), 125.0 (Ar C-H), 128.9 (Ar C), 121.4 (Ar C), 66.2 (N-CH₂-Ar), 54.8 (N-CH-CH₂), 51.0 (N-CH-CH₂), 44.7 (N(CH₃)₂), 38.4 (N(CH₃)₂), 35.3 (Ar-C(CH₃)₃), 31.5 (Ar-CH₃), 30.3 (Ar-C(CH₃)₃), 25.0 (-CH₂- of DACH), 22.4 (-CH₂- of DACH), 20.9 (-CH₂- of DACH). Anal. Calcd. For C₂₀H₃₃Cl₂InN₂O: C 47.74; H 6.61; N 5.57. Found: C 47.48; H 6.60; N 5.51.

Synthesis of (\pm)-(NNO_{Me})InI₂ (4**).** Complex **4** was synthesized in a similar manner to **3** by adding a suspension of InI₃ (973 mg, 1.96 mmol) in THF (3 mL) to a slurry of K(NNO_{Me}) (700 mg, 1.96 mmol) in THF (20 mL). Complex **4** was filtered through a glass frit and dried *in vacuo* for few hours (965 mg, 72%). ¹H NMR (600 MHz, CD₂Cl₂): δ 7.04 (1H, d, ⁴J_{H-H} = 1.8 Hz, ArH), 6.70 (1H, d, ⁴J_{H-H} = 1.5 Hz, ArH), 4.05-4.11 (1H, m, NH-CH₂-Ar), 3.94 (1H, d, ²J_{H-H} = 11.1 Hz, NH-CH₂-Ar), 2.72-2.78 (1H, m, -CH- of DACH), 2.63-2.69 (1H, m, -CH- of DACH), 2.61 (3H, s, -N-(CH₃)₂), 2.54-2.58 (1H, m, -CH₂- of DACH), 2.45 (3H, s, -N-(CH₃)₂), 2.21 (3H, s, Ar-CH₃), 2.06-2.11 (1H, m, -CH₂- of DACH), 1.81-1.96 (2H, m, -NH-; -CH₂- of DACH), 1.76 (1H, m, -CH₂- of DACH), 1.42 (9H, Ar-(CH₃)₃), 1.17-1.40 (4H, m, -CH₂- of DACH); ¹³C{¹H} NMR (151 MHz, CD₂Cl₂): δ 161.3 (Ar C), 140.9 (Ar C), 129.0 (Ar C-H), 128.6 (Ar C-H), 125.6 (Ar C), 122.7 (Ar C), 65.5 (N-CH₂-Ar), 56.7 (N-CH-CH₂), 52.4 (N-CH-CH₂), 43.9 (N(CH₃)₂), 37.7 (N(CH₃)₂), 35.1 (Ar-C(CH₃)₃), 32.4 (Ar-CH₃), 30.6 (Ar-C(CH₃)₃), 25.1 (-CH₂- of DACH), 25.0 (-CH₂- of DACH), 23.1 (-CH₂- of DACH), 21.0 (-CH₂- of DACH). Anal. Calcd. For C₂₀H₃₃I₂InN₂O: C 35.01; H 4.85; N 4.08. Found: C 35.11; H 4.79; N 4.08.

Synthesis of (*R,R*)- and (*S,S*)-4**.** The syntheses were carried out in an analogous manner to the racemic compound above and have identical NMR signatures. (*R,R*)-**4**. Yield (286 mg, 85%) based on 173 mg of (*R,R*)- K(NNO_{Me}). Anal. Calcd. For C₂₀H₃₃I₂InN₂O: C 35.01; H 4.85; N 4.08. Found: C 34.90; H 4.85; N 4.03. (*S,S*)-**4**. Yield (162 mg, 80%) based on 105 mg of (*S,S*)- K(NNO_{Me}). Anal. Calcd. For C₂₀H₃₃I₂InN₂O•CH₃CN : C 36.34; H 4.99; N 5.78. Found: C 36.32; H 4.97; N 5.23.

Synthesis of (*R,R/R,R*)- and (*S,S/S,S*)-[(NNO_{tBu})InCl]₂(μ-Cl)(μ-OEt) (5**).** The syntheses were carried out in an analogous manner to the racemic compound and have identical NMR signatures.¹⁷ (*R,R/R,R*)-**5**. Yield (28 mg, 87%) based on 32 mg of (*R,R*)-(NNO_{tBu})InCl₂. Anal. Calcd. For C₄₈H₈₄Cl₃In₂N₄O₃: C 52.40; H 7.60; N 5.09. Found: C 51.97; H 7.54; N 4.95. (*S,S/S,S*)-**5**. Yield (53 mg, 85%) based on 61 mg of (*S,S*)-(NNO_{tBu})InCl₂. Anal. Calcd. For C₄₈H₈₄Cl₃In₂N₄O₃: C 52.40; H 7.60; N 5.09. Found: C 52.16; H 7.51; N 5.34.

Synthesis of (\pm)-[(NNO_{Me})InCl]₂(μ-Cl)(μ-OEt) (6**).** A solution of NaOEt (20 mg, 0.30 mmol) in toluene (1.5 mL) was added dropwise to a stirring suspension of complex **3** (150

mg, 0.30 mmol) in toluene (3 mL) at room temperature. The reaction mixture was stirred for 12 h. The resulting white precipitate was filtered through Celite to yield a pale yellow filtrate. All volatiles were removed in *vacuo*, and ether (5 mL) was added to the residue to precipitate an off-white solid. The product was collected on a glass frit by vacuum filtration, washed with ether at least twice, and dried in *vacuo* for few hours (140.8 mg, 93%). ¹H NMR (400 MHz, CD₂Cl₂): δ 6.99 (1H, br. s., ArH), 6.60 (1H, br. s., ArH), 4.91 (1H, d, ²J_{H-H} = 13.5 Hz, NH-CH₂-Ar), 4.25-4.45 (1 H, m, O-CH₂-CH₃), 3.72 (1H, dd, ²J_{H-H} = 13.6 Hz ³J_{H-H} = 1.7 Hz, NH-CH₂-Ar), 2.86 (1H, td, ³J_{H-H} = 11.3 ⁴J_{H-H} = 3.1 Hz, -CH- of DACH), 2.73-2.74 (1H, br. m, -NH-), 2.66 (3H, s, -N(CH₃)₂), 2.52-2.63 (1H, m, -CH- of DACH), 2.48-2.50 (1H, m, -CH₂- of DACH), 2.18 (3H, s, Ar-CH₃), 2.03 (3H, s, -N(CH₃)₂), 1.86-1.99 (1H, m, -CH₂- of DACH), 1.82 (2H, br. m, -CH₂- of DACH), 1.39 (9H, Ar-(CH₃)₃), 1.01-1.31 (6H, m, -CH₂- of DACH; O-CH₂-CH₃); ¹³C{¹H} NMR (101 MHz, CD₂Cl₂): δ 163.2 (Ar C), 139.9 (Ar C), 130.6 (Ar C-H), 128.6 (Ar C-H), 123.3 (Ar C), 120.0 (Ar C), 65.3 (N-CH₂-Ar), 63.0 (O-CH₂-CH₃), 53.2 (N-CH-CH₂), 50.8 (N-CH-CH₂), 44.6 (N(CH₃)₂), 38.5 (N(CH₃)₂), 35.5 (Ar-C(CH₃)₃), 31.5 (Ar-CH₃), 30.2 (Ar-C(CH₃)₃), 25.4 (-CH₂- of DACH), 25.2 (-CH₂- of DACH), 22.4 (-CH₂- of DACH), 20.9 (-CH₂- of DACH), 19.8 (O-CH₂-CH₃). Anal. Calcd. For C₄₂H₇₁Cl₃In₂N₄O₃: C 49.65; H 7.04; N 5.51. Found: C 48.91; H 6.89; N 5.29.

Synthesis of (±)-[(NNO_{Me})InI]₂(μ-I)(μ-OEt) (7). NaOEt (61.3 mg, 0.90 mmol) suspended in toluene (6 mL) were added dropwise to a stirring suspension of complex **4** (309.4 mg, 0.45 mmol) in toluene (8 mL) (both of the suspensions were stirred for 5 minutes separately). The reaction mixture was stirred for 16 h. The resulting white precipitate was filtered through glass filter paper to collect the pale yellow filtrate. All volatiles were removed from the filtrate in *vacuo* and the residue was completely dissolved in THF (2 mL). Acetonitrile (5 mL) was added to this solution after which complex **8** is isolated as a white solid via filtration. The solvent was removed from the filtrate to yield complex **7** as an off-white solid. Both complexes were washed with acetonitrile (2 × 1 mL) and dried in *vacuo* for several hours. (complex **7**: 100.5 mg, 35% yield; complex **8**: 39.5 mg, 14% yield) ¹H NMR (400 MHz, CD₂Cl₂): δ 7.00 (1H, d, ⁴J_{H-H} = 1.9 Hz, ArH), 6.63 (1H, d, ⁴J_{H-H} = 1.9 Hz, ArH), 4.79-4.86 (1H, m, NH-CH₂-Ar), 4.15-4.41 (1 H, m, O-CH₂-CH₃), 3.65-3.77 (1H, m, NH-CH₂-Ar), 3.41 (1H, d, ³J_{H-H} = 10.8 Hz, -NH-), 2.60-2.72 (1H, m, , -CH- of DACH), 2.57 (3H,

s, -N(CH₃)₂), 2.51-2.55 (1H, m, -CH₂- of DACH), 2.46 (1H, td, ³J_{H-H} = 11.4 Hz ⁴J_{H-H} = 3.2 Hz, -CH- of DACH), 2.20 (3H, s, - Ar-CH₃), 1.96 (3H, s, -N(CH₃)₂), 1.84 (2H, t, ³J_{H-H} = 12.1 Hz, -CH₂- of DACH), 1.43 (9H, Ar-(CH₃)₃), 1.37 (2H, t, ³J_{H-H} = 12.1 Hz, O-CH₂-CH₃), 1.05-1.33 (5H, m, -CH₂- of DACH); ¹³C{¹H} NMR (101 MHz, CD₂Cl₂): δ 163.4 (Ar C), 139.7 (Ar C), 130.5 (Ar C-H), 128.4 (Ar C-H), 122.9 (Ar C), 120.3 (Ar C), 67.4 (N-CH₂-Ar), 61.9 (O-CH₂-CH₃), 53.2 (N-CH-CH₂), 50.0 (N-CH-CH₂), 46.0 (N(CH₃)₂), 38.1 (N(CH₃)₂), 35.3 (Ar-C(CH₃)₃), 31.2 (Ar-CH₃), 30.4 (Ar-C(CH₃)₃), 25.4 (-CH₂- of DACH), 25.2 (-CH₂- of DACH), 22.6 (-CH₂- of DACH), 20.9 (-CH₂- of DACH), 19.5 (O-CH₂-CH₃). Anal. Calcd. For C₄₂H₇₁I₃In₂N₄O₃: C 39.09; H 5.55; N 4.34. Found: C 42.69; H 6.22; N 5.48.

Synthesis of (meso)-[(NNO_{Me})In(I)(μ-OEt)]₂ (8). A suspension of KOEt (24.5 mg, 0.29 mmol) in toluene (4 mL) was added dropwise to a stirring suspension of **4** (125.4 mg, 0.14 mmol) in toluene (6 mL) at room temperature (both of the solutions were stirred for 5 minutes separately prior to addition). The pale yellow color of the reaction mixture changed to white in 5 min after the addition of KOEt. The white solid was filtered through a glass fibre filter paper to collect the colorless filtrate of complex **8**, which was dried *in vacuo* to yield an off white residue. THF (1 mL) was added to the white residue forming a suspension. Subsequently acetonitrile (2 mL) was added to this stirring suspension to solubilize any remaining impurities. The suspension was filtered through a glass frit and the solid was washed with acetonitrile (2 × 1 mL) and dried under vacuum to obtain the desired complex **8** as a white solid. (81.2 mg, 74% yield) ¹H NMR (400 MHz, CD₂Cl₂): δ 6.98 (1H, br. s., ArH), 6.59 (1H, br. s., ArH), 5.08 (1H, d, ²J_{H-H} = 13.3 Hz, NH-CH₂-Ar), 4.30-4.42 (1H, m, O-CH₂-CH₃), 3.65-3.80 (2H, m, O-CH₂-CH₃, NH-CH₂-Ar), 2.60-2.75 (5H, br. s., -CH- of DACH; -CH- of DACH; -N(CH₃)₂), 2.49 (1H, m, -NH- of DACH), 2.18 (3H, s, Ar-CH₃), 2.06 (3H, s, -N(CH₃)₂), 1.97 (1H, br. m, -CH₂- of DACH), 1.74-1.87 (2H, m, -CH₂- of DACH), 1.39 (9H, Ar-(CH₃)₃), 1.05-1.23 (8H, m, -CH₂- of DACH and O-CH₂-CH₃); ¹³C{¹H} NMR (151 MHz, CD₂Cl₂): δ 163.5 (Ar C), 139.7 (Ar C), 130.4 (Ar C-H), 128.4 (Ar C-H), 122.4 (Ar C), 120.0 (Ar C), 68.3 (N-CH-CH₂), 60.8 (O-CH₂-CH₃), 52.6 (N-CH₂-Ar), 51.4 (N-CH-CH₂), 49.9 (N(CH₃)₂), 40.0 (N(CH₃)₂), 35.3 (Ar-C(CH₃)₃), 31.1 (Ar-CH₃), 30.4 (Ar-C(CH₃)₃), 25.4 (-CH₂- of DACH), 25.1 (-CH₂- of DACH), 23.3 (-CH₂- of DACH), 20.9 (-

CH₂- of DACH), 19.7 (O-CH₂-CH₃). (**meso**)-**8**; Anal. Calcd. For C₄₄H₇₆I₂In₂N₄O₄: C 43.73; H 6.34; N 4.64. Found: C 44.09; H 6.36; N 4.84.

(R,R/R,R)- and **(S,S/S,S)**-**8**. The syntheses were carried out in an analogous manner to the racemic compound above. **(R,R/R,R)**- and **(S,S/S,S)**-**8** have identical NMR spectra: ¹H NMR (600 MHz, CDCl₃): δ 7.02 (2H, m, ArH), 6.65-6.70 (1H, m ArH), 6.53 - 6.61 (1H, m, ArH), 5.19 (1H, d, ²J_{H-H} = 13.6 Hz, NH-CH₂-Ar), 4.63-4.72 (1H, m, NH-CH₂-Ar), 4.33-4.49 (2H, m, O-CH₂-CH₃), 3.82-3.96 (2H, m, O-CH₂-CH₃), 3.70-3.82 (2H, m, NH-CH₂-Ar), 2.95-3.09 (1H, m, -CH- of DACH), 2.73-2.80 (1H, m, -CH- of DACH), 2.60-2.73 (m, 4 H, -NH- of DACH and -N(CH₃)₂), 2.52 (1H, d, ³J_{H-H} = 10.9 Hz, -NH- of DACH), 2.44 (3H, s, -N(CH₃)₂), 2.34 (3H, s, -N(CH₃)₂), 2.27 (1H, td, ³J_{H-H} = 3.8, 11.7 Hz, -NH- of DACH), 2.19-2.25 (6H, m, Ar-CH₃), 2.10-2.19 (2H, m -CH₂- of DACH), 2.09 (3H, s, -N(CH₃)₂), 1.98 (1H, m, -CH₂- of DACH), 1.78-1.91 (4H, m, -CH₂- of DACH), 1.42 (19H, m, -CH₂- of DACH, Ar-C(CH₃)₃), 1.30 (3H, t, ³J_{H-H} = 6.7 Hz, O-CH₂-CH₃), 1.14-1.28 (6H, m, -CH₂- of DACH), 1.11 (3H, t, ³J_{H-H} = 6.6 Hz, O-CH₂-CH₃), 1.07 (1H, m, -CH₂- of DACH), 0.93-1.00 (1H, m, -CH₂- of DACH); ¹³C{¹H} NMR (151 MHz, CD₂Cl₂): δ 164.0 (Ar C), 163.0 (Ar C), 139.4 (Ar C), 138.7 (Ar C), 130.0 (Ar C-H), 129.6 (Ar C-H), 128.0 (Ar C-H), 127.8 (Ar C-H), 122.1 (Ar C), 121.9 (Ar C), 121.2 (Ar C), 119.4 (Ar C), 67.8 (N-CH-CH₂), 64.6 (N-CH-CH₂), 60.9 (O-CH₂-CH₃), 60.5 (O-CH₂-CH₃), 56.2 (N-CH-CH₂), 52.1 (N-CH-CH₂), 51.2 (N-CH₂-Ar), 47.4 (N-CH₂-Ar), 46.6 (-N(CH₃)₂), 45.3 (-N(CH₃)₂), 39.7 (-N(CH₃)₂), 38.5 (-N(CH₃)₂), 35.0 (Ar-C(CH₃)₃), 34.9 (-CH₂- of DACH), 30.7 (Ar-C(CH₃)₃), 30.4(Ar-C(CH₃)₃), 30.1 (Ar-C(CH₃)₃), 28.8 (-CH₂- of DACH), 25.1 (-CH₂- of DACH), 25.1 (-CH₂- of DACH), 24.7 (-CH₂- of DACH), 24.6 (-CH₂- of DACH), 23.9 (-CH₂- of DACH), 22.7 (-CH₂- of DACH), 20.8 (Ar-CH₃), 20.7 (Ar-CH₃), 20.1 (O-CH₂-CH₃), 19.5(O-CH₂-CH₃). **(R,R/R,R)**-**8**. Yield (48 mg, 60%) based on 90 mg of **(R,R)**-(NNO_{Me})InI₂. Anal. Calcd. For C₄₄H₇₆I₂In₂N₄O₄: C 43.73; H 6.34; N 4.64. Found: C 44.11; H 6.31; N 4.65. **(S,S/S,S)**-**8**. Yield (44 mg, 68%) based on 73 mg of **(S,S)**-(NNO_{Me})InI₂. Anal. Calcd. For C₄₄H₇₆I₂In₂N₄O₄: C 43.73; H 6.34; N 4.64. Found: C 43.96; H 6.34; N 4.67.

Synthesis of (meso)-[(NNO_{tBu})In(I)(μ-OEt)]₂ (9). A 25 mL round bottom flask was charged with a suspension of NaOEt (56 mg, 0.84 mmol) in 5 mL of THF. A solution of **2** (300 mg, 0.42 mmol) dissolved in 10 mL of THF was added dropwise to this mixture. After

stirring the reaction mixture for 2 h at room temperature, NaI formation was observed. The salt was removed by filtration through glass fibre filter paper and the remaining yellow solution was evaporated to dryness. The residue was washed with hexane and dried for 2 h *in vacuo* to yield complex **9** as a white powder (208 mg, 76% yield). ^1H NMR (600MHz, CD_2Cl_2): δ 7.20 (1H, br. s., ArH), 6.76 (1H, br. s., ArH), 5.10 (1H, d, $^2J_{\text{H-H}} = 13.4$ Hz, $\text{NH-CH}_2\text{-Ar}$), 4.28-4.40 (1H, m, $\text{O-CH}_2\text{-CH}_3$) 3.69 - 3.82 (2H, m, $\text{O-CH}_2\text{-CH}_3$, $\text{NH-CH}_2\text{-Ar}$), 2.67-2.71 (5H, m, $-\text{CH-}$ of DACH; $-\text{CH-}$ of DACH; $-\text{N}(\text{CH}_3)_2$), 2.48-2.50 (1H, m, $-\text{NH-}$), 2.18 (3H, s, Ar- CH_3), 2.04 (3H, s, $-\text{N}(\text{CH}_3)_2$), 1.96 (1H, br. m, $-\text{CH}_2\text{-}$ of DACH), 1.76-1.90 (2H, m, $-\text{CH}_2\text{-}$ of DACH), 1.40 (9H, Ar- $(\text{CH}_3)_3$), 1.26 (9H, m, Ar- $(\text{CH}_3)_3$), 1.13-1.23 (5H, m, $-\text{CH}_2\text{-}$ of DACH; $\text{O-CH}_2\text{-CH}_3$), 1.02-1.13 (3H, $-\text{CH}_2\text{-}$ of DACH); $^{13}\text{C}\{^1\text{H}\}$ NMR (151 MHz, CD_2Cl_2): δ 162.2 (Ar C), 137.7 (Ar C), 135.0 (Ar C-H), 125.8 (Ar C-H), 123.3 (Ar C), 118.5 (Ar C), 67.1 (N- $\text{CH}_2\text{-Ar}$), 59.8 (O- $\text{CH}_2\text{-CH}_3$), 51.6 (N- CH-CH_2), 50.7 (N- CH-CH_2), 44.7 ($\text{N}(\text{CH}_3)_2$), 39.0 ($\text{N}(\text{CH}_3)_2$), 34.6 (Ar-C(CH_3) $_3$), 33.2 (Ar-C(CH_3) $_3$), 31.1 (Ar-C(CH_3) $_3$), 30.0 (Ar-C(CH_3) $_3$), 29.5 ($-\text{CH}_2\text{-}$ of DACH), 24.6 ($-\text{CH}_2\text{-}$ of DACH), 24.2 ($-\text{CH}_2\text{-}$ of DACH), 22.3 ($-\text{CH}_2\text{-}$ of DACH), 18.9 (O- $\text{CH}_2\text{-CH}_3$). Anal. Calcd. For $\text{C}_{50}\text{H}_{86}\text{I}_2\text{In}_2\text{N}_4\text{O}_4$: C 46.44; H 6.65, N 4.33. Found: C 46.41; H 6.60; N 4.34.

Synthesis of (\pm) -[(NNO_{Me}) $\text{InI}_2(\mu\text{-OH})(\mu\text{-OEt})$ (10**).** Deoxygenated H_2O (0.6 μL , 0.033 mmol) was added to a stirring suspension of complex **8** (50 mg, 0.041 mmol) in THF (3 mL) at room temperature. The reaction mixture was stirred for 16 h. The solvent was removed *in vacuo* and dried under vacuum to yield complex **10** as a white solid. To purify the compound, this solid was redissolved in THF (2 mL), and a 3 mL solution of acetonitrile was added to the solution to precipitate the unreacted starting complex. This suspension was filtered through a frit and complex **8** was collected as a solid and reused for other reactions. The filtrate was isolated and the solvent removed to yield complex **10** as a white solid (19.5 mg, 50% yield). ^1H NMR (600 MHz, CD_2Cl_2): δ 6.97 (1H, d, $^4J_{\text{H-H}} = 1.9$ Hz, ArH), 6.61 (1H, d, $^4J_{\text{H-H}} = 1.7$ Hz, ArH), 4.77-4.82 (1H, m, $\text{NH-CH}_2\text{-Ar}$), 4.13-4.39 (1H, m, $\text{O-CH}_2\text{-CH}_3$), 3.69 (1H, dd, $^2J_{\text{H-H}} = 13.6$ Hz $^3J_{\text{H-H}} = 2.2$ Hz, $\text{NH-CH}_2\text{-Ar}$), 3.39 (1H, d, $J = 10.9$ Hz, $-\text{NH-}$), 2.61-2.66 (1H, m, $-\text{CH-}$ of DACH), 2.55 (3H, s, $-\text{N}(\text{CH}_3)_2$), 2.47-2.53 (1H, m, $-\text{CH}_2\text{-}$ of DACH), 2.43 (1H, td, $^3J_{\text{H-H}} = 11.4$ Hz $^4J_{\text{H-H}} = 3.3$ Hz, $-\text{CH-}$ of DACH), 2.18 (3H, s, Ar- CH_3), 1.94 (3H, s, $-\text{N}(\text{CH}_3)_2$), 1.82 (2H, t, $^3J_{\text{H-H}} = 15.9$ Hz, $-\text{CH}_2\text{-}$ of DACH), 1.41 (9H, Ar- $(\text{CH}_3)_3$), 1.34

(2H, t, $^3J_{H-H} = 7.0$ Hz, O-CH₂-CH₃), 1.01-1.33 (5H, m, -CH₂- of DACH). $^{13}\text{C}\{^1\text{H}\}$ NMR (101 MHz, CD₂Cl₂): δ 163.3 (Ar C), 139.7 (Ar C), 130.5 (Ar C-H), 128.4 (Ar C-H), 122.9 (Ar C), 120.3 (Ar C), 67.3 (N-CH₂-Ar), 61.9 (O-CH₂-CH₃), 53.2 (N-CH-CH₂), 49.9 (N-CH-CH₂), 46.0 (N(CH₃)₂), 38.1 (N(CH₃)₂), 35.3 (Ar-C(CH₃)₃), 31.2 (Ar-CH₃), 30.3 (Ar-C(CH₃)₃), 25.4 (-CH₂- of DACH), 25.1 (-CH₂- of DACH), 22.6 (-CH₂- of DACH), 20.9 (-CH₂- of DACH), 19.5 (O-CH₂-CH₃). Anal. Calcd. For C₄₂H₇₁I₃In₂N₄O₃: C 42.73; H 6.15; N 4.75. Found: C 43.26; H 6.20; N 5.40.

Synthesis of (\pm)-[(NNO_{tbu})InI]₂(μ -OH)(μ -OEt) (11**).** A 25 mL round bottom flask was charged with a solution of **5** (250 mg, 0.19 mmol) in 10 mL CH₂Cl₂, and then water (3.5 μ L, 0.19 mmol) was added to the solution. The reaction was stirred for 1 h and after that the mixture was evaporated to dryness *in vacuo*. The residue was washed with diethyl ether and dried for 2 h *in vacuo*, to yield complex **11** as a white powder. Suitable crystals for X-ray diffraction were grown by slow diffusion of diethyl ether into a CH₂Cl₂ solution of the complex (204.1 mg, 85% yield). ^1H NMR (600 MHz, CD₂Cl₂): δ 7.20 (1H, d, $^4J_{H-H} = 3$ Hz, ArH), 6.78 (1H, d, $^4J_{H-H} = 3$ Hz, ArH), 4.81 (1H, d, $^2J_{H-H} = 13.2$ Hz, NH-CH₂-Ar), 4.14-4.44 (1H, m, O-CH₂-CH₃), 3.73 (1H, d, $^2J_{H-H} = 13.3$ Hz, NH-CH₂-Ar), 3.42 (1H, d, $^3J_{H-H} = 10.8$ Hz, -NH-), 2.56-2.65 (1H, m, -CH- of DACH), 2.54 (3H, s, -N(CH₃)₂), 2.50 (1H, m, -CH₂- of DACH), 2.39-2.47 (1H, m, -CH- of DACH), 1.91 (3H, s, -N(CH₃)₂), 1.82 (2H, m, -CH₂- of DACH), 1.36-1.47 (12H, m, Ar-(CH₃)₃; O-CH₂-CH₃), 1.20-1.32 (11H, m, Ar-(CH₃)₃; -CH₂- of DACH), 1.02-1.18 (3H, m, -CH₂- of DACH). $^{13}\text{C}\{^1\text{H}\}$ NMR (151 MHz, CD₂Cl₂): δ 163.1 (Ar C), 138.8 (Ar C), 136.6 (Ar C-H), 126.8 (Ar C-H), 124.5 (Ar C), 119.8 (Ar C), 67.2 (N-CH₂-Ar), 62.0 (O-CH₂-CH₃), 53.2 (N-CH-CH₂), 50.2 (N-CH-CH₂), 46.0 (N(CH₃)₂), 38.1 (N(CH₃)₂), 35.6 (Ar-C(CH₃)₃), 34.3 (Ar-C(CH₃)₃), 32.1 (Ar-C(CH₃)₃), 31.1 (Ar-C(CH₃)₃), 30.4 (-CH₂- of DACH), 25.4 (-CH₂- of DACH), 25.2 (-CH₂- of DACH), 22.7 (-CH₂- of DACH), 19.6 (O-CH₂-CH₃). Elem. Anal. Calcd C₄₈H₈₄I₃In₂N₄O₄: C 45.46; H 6.64, N 4.43. Found: C 45.13; H 6.64; N 4.40.

Procedure for *in situ* crossover between (*R,R/R,R*)- and (*S,S/S,S*)-8**.** ^1H NMR spectroscopy (400 MHz NMR spectrometer, CDCl₃ at room temperature) was used to monitor the crossover of (*R,R/R,R*)- and (*S,S/S,S*)-**8**. In a glovebox, a solution of (*R,R/R,R*)-**8** (0.5 mL, 0.62 mM) was loaded to a teflon-sealed NMR tube and frozen in a liquid N₂ cold

well ($-90\text{ }^{\circ}\text{C}$). A solution of (*S,S/S,S*)-**8** (0.5 mL, 0.62 mM) was added to the frozen solution of (*R,R/R,R*)-**8** and frozen again, forming a bilayer. The two solutions were thawed and quickly mixed before the NMR tube was loaded into the NMR spectrometer.

Representative sample preparation with (\pm)-5** for PGSE NMR studies.** Each sample of (\pm)-(NNO_{tBu})H (1.4 mg, 0.0045M), (\pm)-**1** (2.4 mg, 0.0045M), (\pm)-(NNO_{tBu})InMe₂ (2.3 mg, 0.0045M), and (\pm)-**5** (5 mg, 0.0045 M) was made up with a sample of tetrakis(trimethylsilyl)silane (TMSS) (0.94 mM, CD₂Cl₂), used as internal standard. Due to the low solubility of (*meso*)-**8** in CD₂Cl₂, a saturated solution was made up with a sample of tetrakis(trimethylsilyl)silane (0.94 mM, CD₂Cl₂).

Procedure for reactivity of (\pm)-5** with neat methanol, isopropanol, and pyridine.** A 20 mL scintillation vial was charged with (\pm)-**5** (5.0 mg, 0.0045 mmol), and approximately 5 mL alcohol was added to the vial. The mixture was stirred for 16 hours at room temperature. The solvent was removed under vacuum and the resulting white solid was washed with hexane and further dried *in vacuo* for a few hours prior to analysis by ¹H NMR spectroscopy.

Chapter 3: Mechanistic and Selectivity Studies of the Ring Opening Polymerization of Lactide with Chiral Alkoxy-Bridged Dinuclear Indium Catalysts²

In Chapter 2, the synthesis of alkoxy-bridged dinuclear indium complexes and their structural characterizations in solution and the solid state were discussed. Chapter 3 outlines the mechanistic and stereoselectivity investigations of alkoxy-bridged dinuclear indium complexes for the ring opening polymerization of lactide.

3.1 Introduction

3.1.1 Lactide

Lactide (LA) is a 6-membered cyclic dimer of lactic acid and can be generated from biological sources of lactic acid.¹²⁷ Recently, lactide has become widely used for the production of biodegradable and biocompatible polymers, poly(lactides) (PLA), for use in the packaging and pharmaceutical fields.¹²⁸⁻¹³¹

Lactic acid¹³², (2-hydroxy propionic acid), was first discovered by Scheele in 1780 in sour milk. The term lactic acid comes from the French word “acide lactique”. In 1857 Pasteur claimed that lactic acid was not a milk component, but a metabolite produced by fermentation via microorganisms. Lactic acid is a simple carboxylic acid with a hydroxy group adjacent to the carboxyl group. It can be degraded to carbon dioxide (CO₂), which plants absorb through photosynthesis (**Figure 3.1**). Lactic acid is a chiral compound due to the stereogenic center at carbon and possesses two stereoisomers, D-(-)-, which is harmful to humans,¹³³ and L-(+)-lactic acid (**Figure 3.2**).¹³²,

Lactic acid can be generated by either chemical synthesis¹³³⁻¹³⁶ or biochemical synthesis.^{134,137,138} Commercially, the biological production of lactic acid is preferable for two major reasons. One is that the availability of petrochemical resources (54 years: the length of the time that the oil remaining reserves would last) is relatively limited compared to

² The work with the achiral indium complexes [(N_{Me}2N_{Me}O_{tBu})In(Cl)]₂(μ-Cl)(μ-OEt) as well as the kinetic and polymerization studies published in *Dalton Transactions*.² **Chapter 3** has been published in *the Journal of American Chemical Society*.¹

biorenewable resources (carbohydrate-rich materials such as sugar cane, whey, molasses, starch waste, and beets) (**Figure 3.1**).¹³⁹ The second is that biological production is the most effective way to produce either an enantiopure form of lactic acid (D-(-)-lactic acid or L-(+)-lactic acid) or a racemic mixture of isomers depending upon the microorganism,¹³⁷ while chemical processes only produce a racemic mixture.

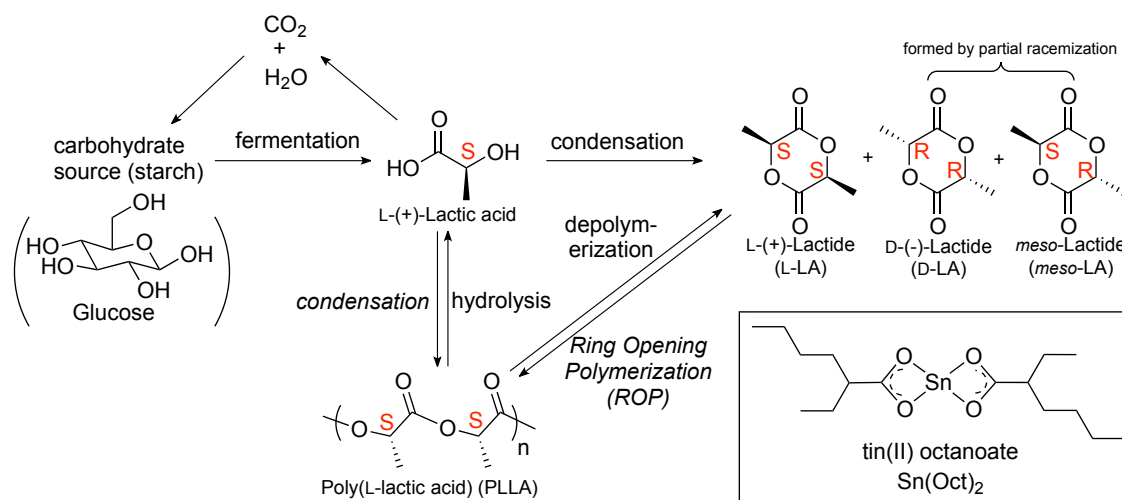


Figure 3.1. Schematic life cycle of biodegradable PLA based on renewable biomass (corn or starch).

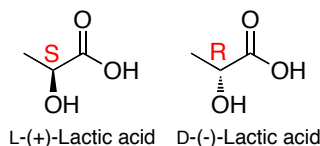


Figure 3.2. Optical isomers of lactic acid.

As mentioned, lactide is a 6-membered cyclic dimer produced from the optical isomers of lactic acid and possesses three stereoisomers: L-(+)-LA, its enantiomer D-(-)-LA, and the diastereomer meso-LA (**Figure 3.3**).^{140,141} Industrially, lactide is prepared by oligomerization of linear PLA possessing from ten to seventy repeating units produced by condensation of L-lactic acid (naturally occurring isomer) at high temperature (110-180 °C) in vacuum, followed by depolymerization and cyclization of the PLA oligomers in the presence of tin carboxylate or alkoxides.¹³ The major isomer is L-LA (>98% purity), which is usually contaminated with small amounts of D-(-)-lactide and meso-lactide that form by racemization (**Figure 3.1**). 99.9% Pure L-LA can be obtained by repetition of distillation or

crystallization. In general, racemic lactide (DL-LA) is obtained from a 50:50 blend of the two enantiomers, L-(+)-lactide and D-(-)-LA. Therefore, the most commercially available, optically pure PLA is the homochiral poly(L-lactide) (PLLA) produced from L-LA.

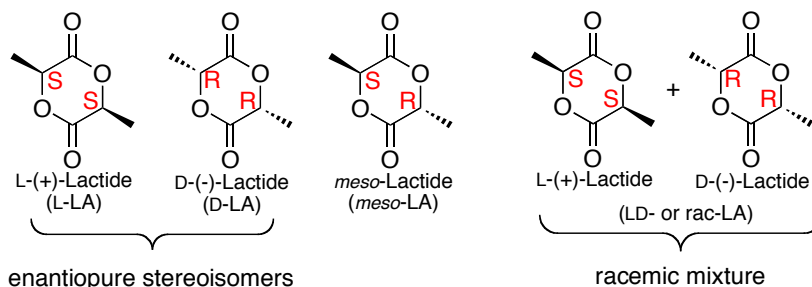


Figure 3.3. Different optical isomers of lactide.

3.1.2 Poly(lactic acid)

Poly(lactic acid) (PLA),^{16,142} a biodegradable polyester, has been studied for the past two decades because of its biodegradability and biocompatibility in applications ranging from packaging and agricultural materials to drug delivery and medical devices.¹²⁸⁻¹³¹ PLA can be produced by either by condensation of lactic acid or ring-opening polymerization of lactide (LA) (**Figure 3.1**).¹¹ However, metal-catalysts for the controlled ring opening polymerization (ROP) of LA such as tin(II) bis(2-ethylhexanoate)¹¹ (the most commonly used catalyst for industrial production of PLA) is the best way to produce well-defined PLA, as condensation methods¹² tend to form relatively low molecular weight PLA with a broad molecular weight distribution unless highly pure lactic acid is used. A more detailed description of metal-catalyzed LA ROP will be provided later in this chapter.

The various physical properties of PLA such as phase transition temperatures, T_g and T_m , are dependent on the stereochemistry in the polymer chains (**Figure 3.4**).¹³⁻¹⁵ These various properties are what make the polymer suitable for use in a particular application.¹⁶ The most important physical properties of thermoplastic materials, which can retain their properties after repeated processes of softening by heating and hardening by cooling, are phase transition temperatures, glass transition temperature T_g at where a hard and brittle polymer (glassy) turns a elastic and flexible polymer (rubbery) and melting point T_m at where a solid

becomes a liquid because these temperatures determine the maximum and minimum temperatures for handling and use of the material.

Another important factor in determining polymer properties is the polymer stereochemistry or tacticity.¹⁶ Tacticity is the relative spatial arrangement to form meso (the same chirality in a linkage of two repeating units) and racemo (the opposite chirality in a linkage of two repeating units) sequences in repeating units of a polymer chain.¹⁴³⁻¹⁴⁵ Polymerization of enantiopure L- or D-LA produces isotactic PLLA or PDLA (semicrystalline, $T_g = 55-65\text{ }^\circ\text{C}$, $T_m = 169-190\text{ }^\circ\text{C}$),^{14,15,146} whereas polymerization of racemic LA^{105,147} can result in four different microstructures of PLA: predominately atactic PLA (amorphous, $T_g = 50-60\text{ }^\circ\text{C}$), heterotactic PLA (amorphous, $T_g = \sim 40\text{ }^\circ\text{C}$), stereoblock isotactic PLA (crystalline, $T_m = 179-205\text{ }^\circ\text{C}$) and stereocomplex isotactic PLA (semicrystalline, $T_g = 65-72\text{ }^\circ\text{C}$, $T_m = 220-279\text{ }^\circ\text{C}$). Polymerization of meso LA can produce two forms of PLA: atactic PLA (amorphous, $T_g = \sim 46\text{ }^\circ\text{C}$) and syndiotactic PLA (semicrystalline, $T_g = \sim 40\text{ }^\circ\text{C}$, $T_m = \sim 152\text{ }^\circ\text{C}$).^{146,147} With respect to the thermal properties of PLAs, isotactic PLAs are the most desirable for many industrial and pharmaceutical applications.

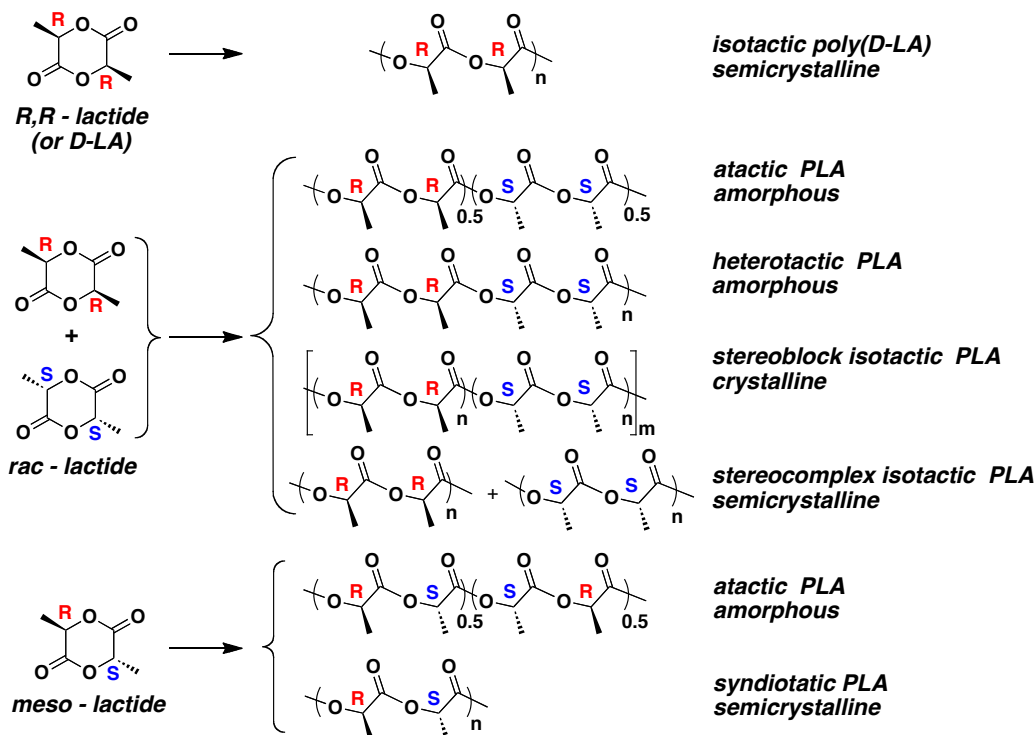


Figure 3.4. Possible microstructures of PLA.

The tacticity of PLA is determined by homonuclear decoupled high resolution ^1H NMR spectroscopy, which is used to simplify multiplet patterns.¹⁴⁸ The ^1H NMR spectrum of PLA exhibits two-resonance multiplet signals at approximately 1.58 ppm and 5.18 ppm assigned to the methyl and methine protons, respectively. In homonuclear ^1H decoupling of a PLA sample a constant radio-frequency irradiation of the proton isotope at the methyl region during the collection time saturates the excited state nuclei for the methyl protons and diminishes the scalar coupling relaxation processes (interaction between neighbouring nuclei) of the methine protons (**Figure 3.5**). PLA obtained from rac LA possess five distinguishable tetrad sequences in five constitutional units, *mmm*, *mmr(rmm)*, *rmm(mmr)*, *mrm* and *rmr*, although eight tetrad sequences including *rrr*, *mrr* and *rrm* exist in theory. The microstructure of the polymer is determined by examining the relative integrals of these tetrad signals.^{148,149} There are the two most common mathematical methods, Bernoullian and first-order Markov statistics, to calculate the probability of meso and racemo linkages in the repeating units of the polymer, depending on a chain-end controlling and enantiomorphous-site controlling model, respectively.²⁸

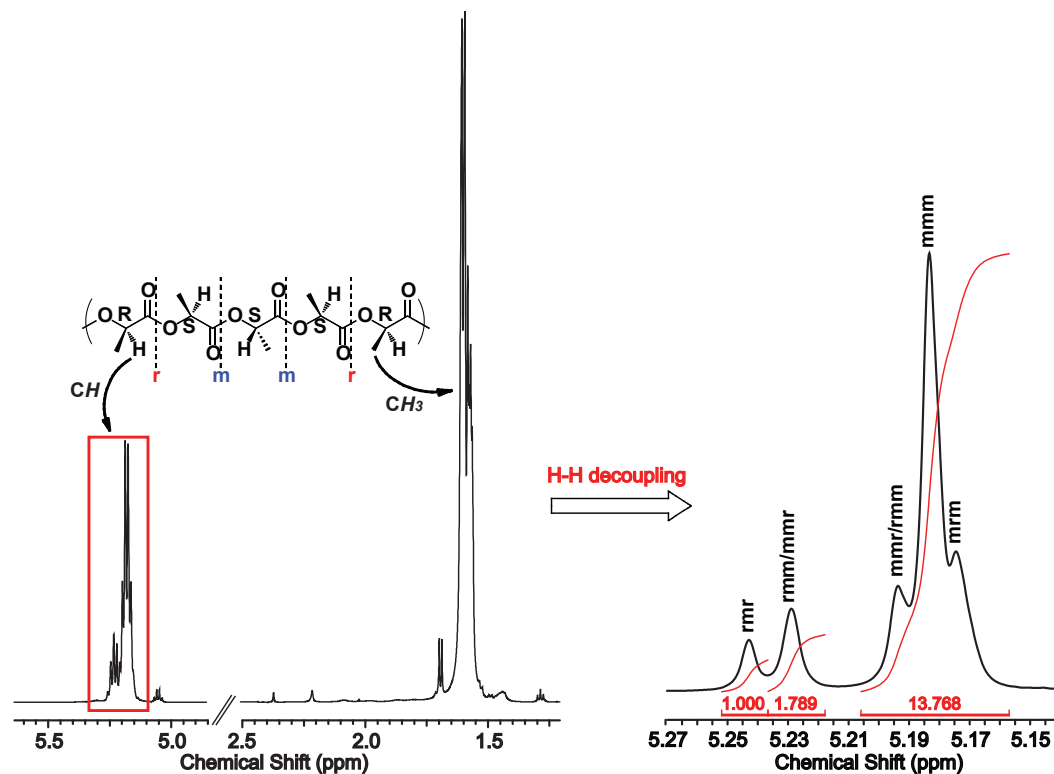


Figure 3.5. ^1H NMR and $^1\text{H}\{^1\text{H}\}$ NMR spectra of PLA obtained from rac-LA (600 MHz, CDCl_3 , 25 °C).

3.1.3 Metal-catalyzed coordination-insertion mechanisms for ring opening polymerization (ROP) of lactide (LA)

In recent years, the ring opening polymerization (ROP) of cyclic esters such as lactide (LA), catalyzed by organocatalysts¹⁵⁰⁻¹⁶⁵ as well as discrete metal complexes bearing various ligand architectures,^{130,166-168} has been heavily explored in an attempt to control polymer micro- and macrostructures and limit transesterification or other uncontrolled chain transfer events.^{146,169-173} In particular, there has been a strong concentration on Lewis acidic centers such as alkali metals,¹⁷⁴⁻¹⁸⁰ alkaline earth metals and Zn,^{110,181-214} Al,^{92,95,97,98,103-105,147,187,196,215-237} Ga,²³⁸ Ge,²³⁹ Sn,²⁴⁰⁻²⁴⁷ Bi,²⁴⁸ Fe²⁴⁹⁻²⁵⁴ and other transition metals²⁵⁵⁻²⁶⁸ as well as rare earth metals.^{80,82,269-279} The generally accepted mechanism for the metal-catalyzed controlled ring opening polymerization of lactides is the coordination-insertion mechanism (**Figure 3.6**).^{280,281} The initial step of the mechanism involves the coordination of lactide to a Lewis acidic metal center to form a dative / covalent bond between the metal and the carbonyl oxygen. Then, the activated lactide inserts into the initiator-metal bond via nucleophilic

addition of the initiator (alkoxide as depicted in **Figure 3.6**) at the carbonyl carbon. The most active initiator groups are generally alkoxides, but alkyls, amides, and halides have been used for LA polymerization. The next step is the ring opening of the lactide via cleavage of the acyl-cyclic oxygen bond leading generation of a new alkoxy-metal species that can repeat the cycle. Finally, the polymerization reaction is terminated by hydrolysis of the active propagating chain. In this mechanism ring opening of lactide involves the cleavage of the acyl-cyclic oxygen bond yielding an ester end group on the polymer chain. Kricheldorf²⁸¹ in 1988 and Teyssie²⁸² in 1991 demonstrated experimental evidence for the ester end group in polymers resulting from the coordination-insertion mechanism.

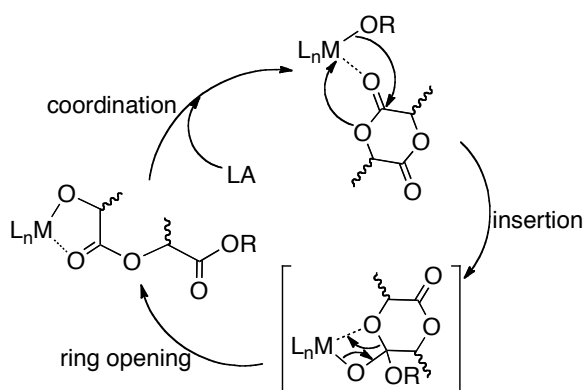


Figure 3.6. Proposed mechanism of LA ROP.

Transesterification side reactions are one of the main drawbacks in ROP of LA with both intermolecular and intramolecular transesterification being possible (**Figure 3.7**). Intermolecular transesterification is a random exchange of two growing polymer chain ends leading to a broadening of the molecular weight distribution. Intramolecular transesterification can occur through a backbiting process, a random attack on the growing polymer chain, to form cyclic oligomers. The tendency of these transesterifications to occur depends on the metallic initiator or the presence of a protic solvent such as water or alcohols in the polymerization.

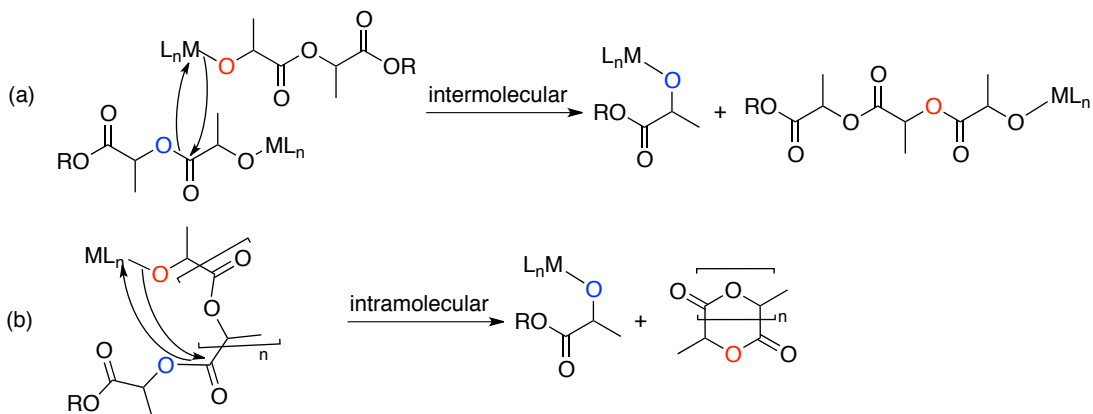
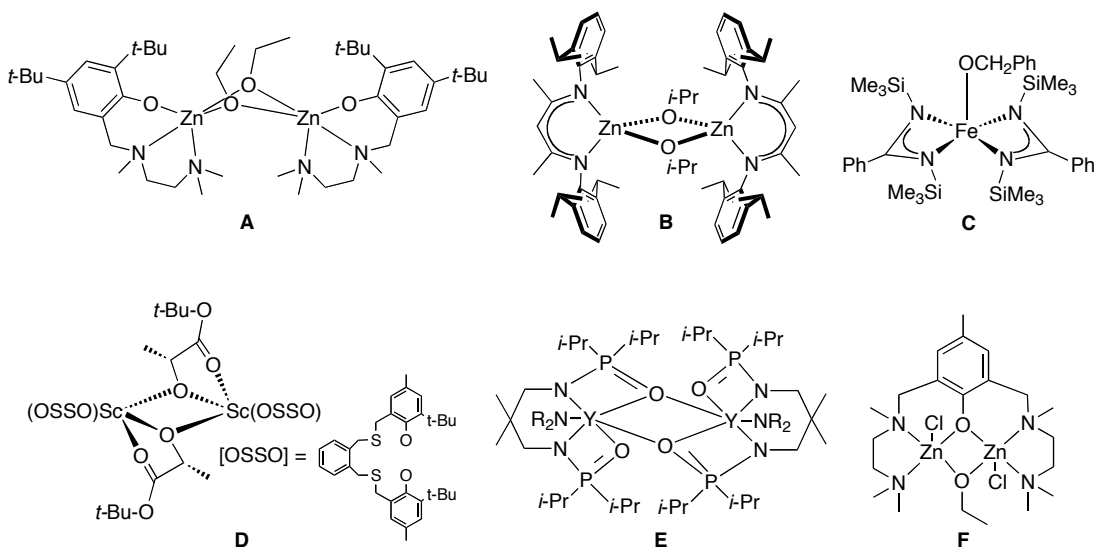


Figure 3.7. Possible transesterification side reactions for LA polymerization: (a) intermolecular and (b) intramolecular.



Scheme 3.1. Some catalysts for the ROP of lactide.

Early reports of catalysts bearing iron,^{251,283} zinc,^{110,214,284} and rare earth metals^{278,285} demonstrate a range of possibilities for the role of multiple metal centers in lactide ROP (**Scheme 3.1**). One possibility is a catalyst that is dinuclear in the solid state but is mononuclear in solution, as in the case of diaminophenolate zinc alkoxide (**A**) (**Figure 3.8a**).¹¹⁰ In this case, the plot of $-d[\text{LA}]/dt$ is proportional to $[\text{A}/2]^n$ with $n = 1.33$ (0 °C) or 1.75 (25 °C) indicating a possible fractional dependence on catalyst, although plots of k_{obs} vs $[\text{A}/2]^0$ are linear. The dinuclear BDI zinc alkoxide (**B**) also exhibited a fractional order in catalyst: $-d[\text{LA}]/dt = k_p[\text{Zn}]^{1.56}[\text{LA}]$.²¹⁴ A catalyst that is mononuclear in solution as well as in the solid state, such as iron alkoxide catalyst (**C**) can also exhibit fractional order in

catalyst.²⁵¹ This fractional dependence was interpreted by using a model of active chain aggregation.²⁸⁶ In contrast, the scandium complexes bearing 1, ω -dithioalkanediyl-bridged bisphenolato (OSSO)-type ligands (**D**) are dinuclear in solution as well as in the solid state (**Figure 3.8b**).²⁸⁵ A slow dissociation of this dimer to an active lactide adduct **D/2**•lactide similar to those obtained in analogous yttrium complexes was proposed.²⁸⁷ Phosphine oxide bridged dinuclear yttrium amido complexes (**E**) remain dinuclear in solution as well as in the solid state but can change from a single to a double site catalyst based on the steric bulk of the amido initiator.²⁷⁸ Finally, the dizinc monoalkoxide complex supported by a dinucleating ligand (**F**) is first order in the dinuclear catalyst and does not show significant aggregation phenomena.²⁸⁴

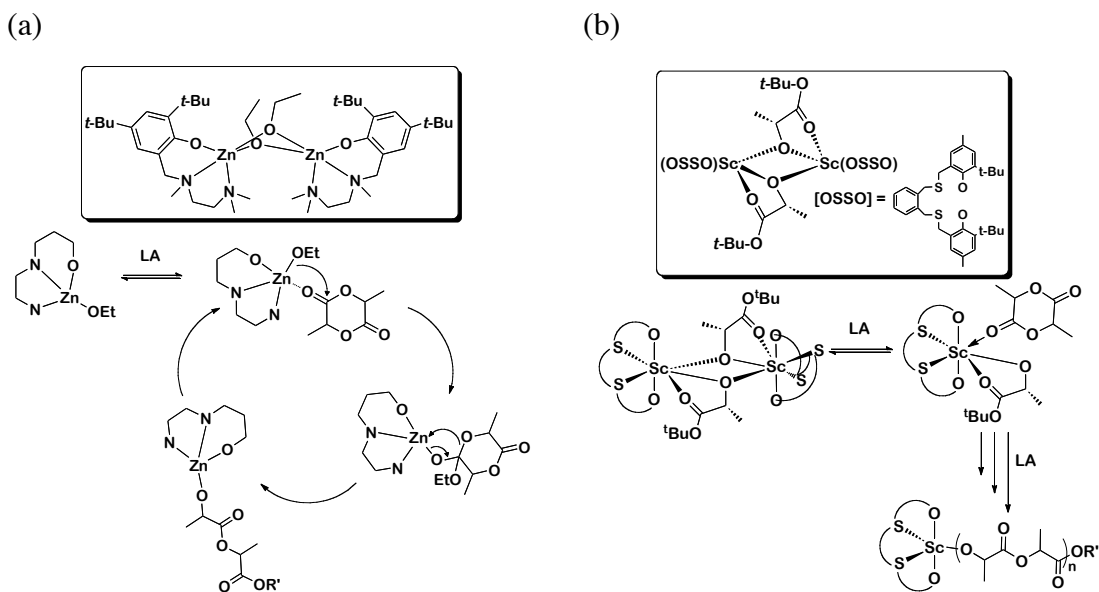


Figure 3.8. Proposed mechanism of LA polymerization with (a) the dinuclear BDI zinc alkoxide complex (**B**)²¹⁴ and (b) the 1, ω -dithioalkanediyl-bridged bisphenolato (OSSO) scandium complexes (**D**).²⁸⁵

The mechanism of stereoselectivity of LA polymerization in a metal-based catalytic system is explained by either enantiomeric-site control or chain-end control.^{288,289} Single-site catalysts have demonstrated a significantly high stereoselectivity as a result of enantiomeric-site control although the line between stereoselectivity resulting from enantiomeric-site control and chain-end control is not well understood. In enantiomeric-site control, the chirality of the catalyst preferentially directs the

polymerization of one enantiomer of the chiral monomer. In this type of selectivity *rr* triad and *mm* triad stereoerrors can occur when the non-preferred monomer isomer is polymerized in isospecific and syndiospecific polymerization, respectively. These errors are then corrected with the next incoming monomer by the stereoselectivity of the catalyst (**Figure 3.9a**). In chain-end control, the chirality of the last incorporated monomer unit directs the stereochemistry of the following monomer, and *r* dyad and *m* dyad stereoerrors in isospecific and syndiospecific polymerization, respectively, are not corrected but propagated in the growing polymer chain (**Figure 3.9b**). Evidence of stereoerrors resulting from different stereoselective polymerization is detectable by high-resolution NMR analysis (^1H and ^{13}C NMR spectroscopy).²⁹⁰

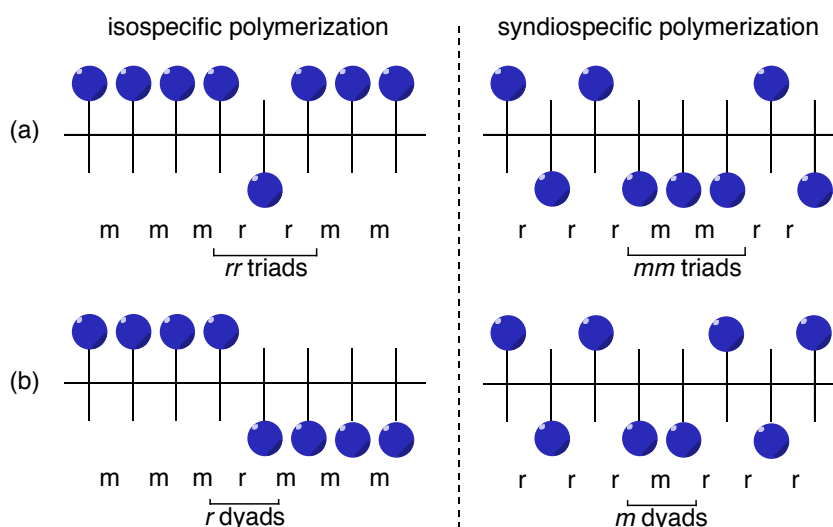


Figure 3.9. Schematic representation of possible propagation stereoerrors in isospecific and syndiospecific polymerization: (a) enantiomorph-site control errors, (b) chain-end control errors.

Some of the most successful stereoselective metal complexes for the controlled living ROP of rac-LA to produce highly isotactic PLA are alkoxy aluminium complexes supported by achiral and chiral tetradentate Schiff base salen ligands, although they tend to have slower rates of polymerization (**Figure 2.3** in Chapter 2).^{92-94,96,103,105} For example, Spassky reported the highly stereoselective polymerization of rac-LA with a chiral aluminium methoxide complex stabilized by a (*R,R*)-BINAP salen ligand ((*R,R*)-[2,2'-(1,1'-binaphthy-2,2'-diylbis(nitrileomethylidene)]diphenolate) to produce an isotactic stereocomplex PLA ($T_g =$

53 °C. $T_m = 185\text{-}187$ °C) via a predominantly site-controlled mechanism.⁹² In contrast, an achiral ethylsalen aluminum methoxide complex polymerized rac-LA to form an iso-rich PLA via a predominantly chain-end controlled mechanism. Separately, Coates⁹³ demonstrated that both rac-BINAP salen Al(OⁱPr) and (*R,R*)-BINAP salen Al(OMe) for polymerization of rac-LA form an isotactic stereoblock PLA ($T_m = 179\text{-}191$ °C) not the isotactic stereocomplex PLA previously reported to have been formed by Spassky.⁹² Unfortunately, the lack of molecular structural information for BINAP salen Al(OⁱR) complexes leads to a limited understanding of their stereoselectivity mechanism in LA polymerization.

In Feijen's work, a rac-cyclohexylsalen aluminium isopropoxide complex (rac-(cyclohexylsalen)Al(OiPr)) in solution (tolene, $T_{rxn} = 70$ °C, $P_m = 0.93$) and in the melt ($T_{rxn} = 130$ °C, $P_m = 0.88$) polymerized rac-LA to isotactic stereoblock PLA ($T_m = 184$ °C).^{94,95} The polymerization kinetics of rac-LA with rac-(cyclohexylsalen)Al(OiPr) revealed the plot of $-d[LA]/dt$ is first order in [LA] and [mononuclear Al] ($k_p = 9.02 \times 10^{-3} \text{ M}^{-1}\cdot\text{min}^{-1}$), while the ratio (k_{L-LA}/k_{D-LA}) of the relative polymerization rates of enantiopure L-LA and D-LA with (*R,R*)-(cyclohexylsalen)Al(OiPr) is ~ 25 (k_{rel} is a stereoselective factor that evaluates the efficiency of stereoselectivity in the catalyst: $k_{rel} = k_{D-LA}/k_{L-LA}$ when $k_{D-LA} > k_{L-LA}$, but $k_{rel} = k_{L-LA}/k_{D-LA}$ when $k_{L-LA} > k_{D-LA}$). These results indicated the stereoselectivity in this system is governed by predominantly enantiomeric-site control. The active propagating chain in the polymerization was considered to be a mononuclear species based on NMR and MALDI-TOF mass spectral studies of the resulting polymer. The solid-state structure of rac-(cyclohexylsalen)Al(OiPr) later reported by Chisholm showed a monomeric square pyramidal geometry at the Al center.

Nomura⁹⁷ and Chen,²³³ individually, reported a family of achiral salen aluminium alkoxide complexes, which were generated from their corresponding ethyl precursors in alcohols (**Figure 3.10**), for polymerization of rac-LA and showed various degrees of stereoselectivity via modest chain-end control ($T_m = 142\text{-}191$ °C). In their work the achiral salen aluminum complexes exhibit interesting features that influence stereoselectivity and activity in LA polymerization: they have active single-site propagating species, five-coordinate metal center geometries (square pyramidal or trigonal bipyramidal), and relatively flexible ligand backbones (the linkage group between the two nitrogen atoms) on the salen ligand. Without

steric hinderance from a bulky substituent (*t*-Bu) at the ortho position on the phenolate ring the formation of the dimeric alkoxy-bridged aluminium species is accelerated in the solid state and in solution. Moreover, enhancing the electrophilicity of the metal center with electron-withdrawing substituents (Cl) at the para and ortho positions of the phenolate ring increases the formation of the dimeric species via aggregation. According to kinetic and mechanistic studies of LA polymerization, the dinuclear aluminum catalysts in the solid state and in solution show a plot of $-d[LA]/dt$ that is proportional to $[Al]^n$ with $n = 1.81$, and the molecular weights of the resulting polymers determined by GPC analysis is much lower than the theoretical values, indicating a possible fractional dependence on catalyst due to an equilibrium of monomeric and dimeric species in the polymerization medium. In the case of the monomeric salen aluminium alkoxide complex with the bulky substituent (*t*-Bu) at the ortho position on the phenolate ring (**Figure 3.10** right), kinetic studies show a first-order dependence with respect to both $[LA]$ and $[Al]$, and the molecular weights of the resulting polymers are much higher than the estimated ones due to significant transesterification. The stereoselectivity of the mononuclear species in rac-LA polymerization is much higher ($P_m = 0.90$) than that of the dinuclear species ($P_m = 0.71$).²³³

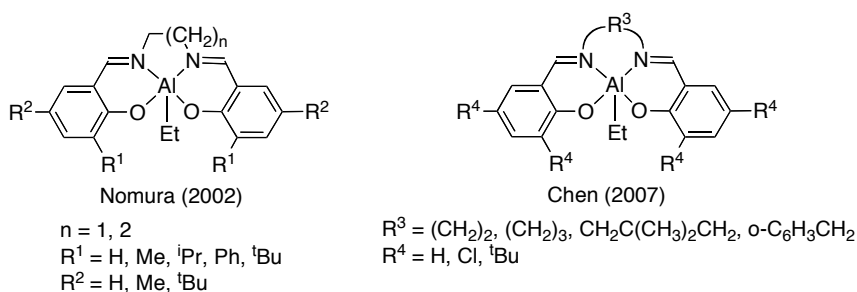


Figure 3.10. Achiral salen aluminium ethyl complexes.^{97,233}

Apart from the aluminum catalysts, another group 13 catalyst for LA polymerization that produces isotactic PLA is the chiral dinuclear half-salan indium complex reported by our group.²³ Since our initial report, other research groups have reported the synthesis of indium complexes supported by both chiral⁵⁷ and achiral^{82,85-88} ligands, as well as simple In(III) salts,^{89,90} that were used as lactide polymerization initiators (**Figures 2.1** and **Figure 2.2** in Chapter 2).⁹⁰ Unlike aluminum complexes, the indium complexes exhibit a relatively high tendency for aggregation to form dimeric species in the solid state, even with the presence of sterically

bulky groups at the ortho position of the phenolate ring, due to the relatively larger size of the In^{3+} ion. A number of these indium catalysts are dinuclear^{85,87,88} or are postulated to have multinuclear active centers based on model initiators in the polymerization medium.⁹⁰

In a subsequent publication we reported a highly active chiral indium complex, *rac*-(cyclohexylsalen)In(OEt), for polymerization of *rac*-LA to form isotactic stereoblock PLA ($P_m = 0.77$).⁹¹ Unlike the analogous aluminium isopropoxide complex, the solid-state structure of *rac*-(cyclohexylsalen)In(OEt) shows a dinuclear species with a bridging alkoxide (X-ray diffraction data), which is also confirmed in solution (kinetics and PGSE NMR spectral studies). Based on kinetic data, the ratio ($k_{L-LA}/k_{D-LA} = 5$) of the relative polymerization rates of enantiopure L-LA and D-LA with (*R,R*)-(cyclohexylsalen)In(OiPr) is lower than that with the less active analogue salen Al system ($k_{L-LA}/k_{D-LA} = 25$). Based on GPC analysis of the resulting polymers with *rac*-(cyclohexylsalen)In(OEt), both of the alkoxides are involved as initiators in LA polymerization. In addition, we have published the synthesis and characterization of achiral and chiral analogues of the parent dinuclear indium complex [(NNO_{tBu})InCl]₂(μ -Cl)(μ -OEt) by introducing a more flexible backbone linkage (ethylene) between the two N atoms and bulky substituents (*n*-propyl) at the tertiary amine, respectively, for LA polymerization (**Figure 2.1** and **Figure 2.2** in Chapter 2).² In kinetic studies, the rate of polymerization with the achiral dinuclear indium complex [(N_{Me2}N_{Me}O_{tBu})InCl]₂(μ -Cl)(μ -OEt) ($k_{\text{obs}} = 1.1 \times 10^{-5} \text{ s}^{-1}$) is much slower than that with the analogous dinuclear zinc alkoxide (**B**) complex ($k_{\text{obs}} = 0.16 \text{ s}^{-1}$) under the same conditions ([LA]/[initiator] = 200, CH₂Cl₂, 25 °C), while that of the chiral dinuclear indium complex [(N_{nPr2}NO_{tBu})InCl]₂(μ -Cl)(μ -OEt) ($k_{\text{obs}} = 2.1 \times 10^{-3} \text{ s}^{-1}$) is consistent with that of the parent complex [(NNO_{tBu})InCl]₂(μ -Cl)(μ -OEt) within error ($k_{\text{obs}} = 2.2 \times 10^{-3} \text{ s}^{-1}$). Interestingly, both of the achiral and chiral analogues produced atactic PLA, suggesting a dissociative mechanism in the polymerization to generate a mononuclear propagating species, similar to what was described in Hillymer and Tolman's Zn system.¹¹⁰

Unlike the discrete indium catalysts stabilized by an ancillary ligand, Hillymer and Tolman reported a highly stereoselective and controlled polymerization of *rac*-LA using an indium catalyst generated *in situ* from InCl₃, benzyl alcohol and triethylamine to form heterotactic PLA ($P_r = 0.86$ -0.97).^{89,90} In kinetic studies, the rate of LA polymerization exhibited a first order dependence on both the indium salt and the monomer ($-d[\text{LA}]/dt = k_p[\text{InCl}_3]_0[\text{LA}]$,

CH₂Cl₂, 21 °C) with the propagation rate constant $k_p = 0.3 \text{ M}^{-1}\cdot\text{s}^{-1}$, which is similar to that of [(NNO_{tBu})InCl]₂(μ-Cl)(μ-OEt) ($k_p = 0.56 \text{ M}^{-1}\cdot\text{s}^{-1}$). Based on a detailed investigation with a dinuclear model system showing similar stereoselectivity ($P_r = 0.92$), they proposed that a dinuclear propagating active species is involved in the coordination-insertion mechanism for LA polymerization (**Figure 3.11**). PGSE NMR experiments were used to support the idea that the true catalytically active species in solution is dimeric. The radius of the hydrated model complex estimated by X-ray crystallography ($r_{x\text{-ray}} = 5.9 \text{ \AA}$) is similar to that of the anhydrous model complex calculated by PGSE NMR data ($r_H = 5.8 \text{ \AA}$), which is approximately twice that of the proligand radius ($r_H = 3.4 \text{ \AA}$). The stereoselectivity is controlled via a predominantly chain end controlled mechanism due to both the steric and electronic effects from the halide ligands and the growing polymer chain.⁹⁰

From the above sample kinetic and mechanistic studies it is clear that significant work is necessary to shed light on the subtle mechanistic aspects of polymerization by Lewis acid catalysts capable of aggregation.

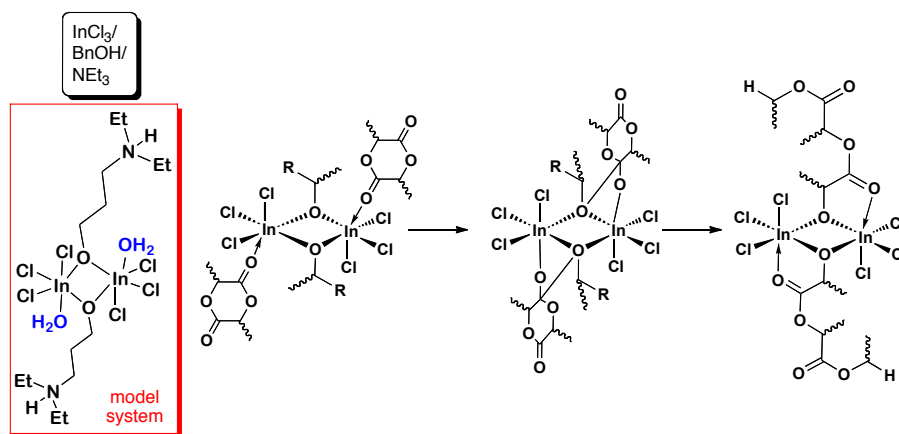
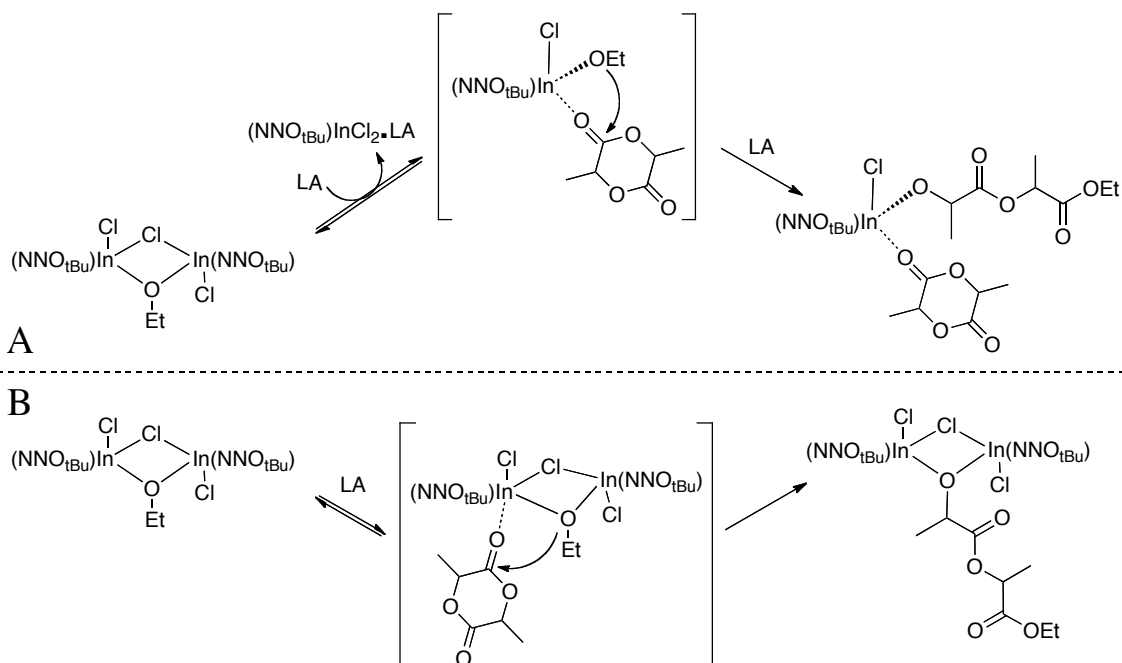


Figure 3.11. Proposed mechanism for stereoselective LA polymerization using a catalyst generated *in-situ* from InCl₃, BnOH, and NEt₃.⁹⁰

In our early work we proposed a mechanism for ROP of LA with an ethoxy-chloro bridged dinuclear indium complex, [(NNO_{tBu})InCl]₂(μ-Cl)(μ-OEt), involving the dissociation of the dinuclear complex to yield an active mononuclear propagating species (NNO_{tBu})In(Cl)(OEt) and an inactive complex (NNO_{tBu})InCl₂ (**Scheme 3.2A**).²³ In this chapter, we present our full investigation into the polymerization of rac-LA by this family of dinuclear alkoxy-bridged catalysts and rule out this dissociative mechanism. Our investigations strongly indicate that

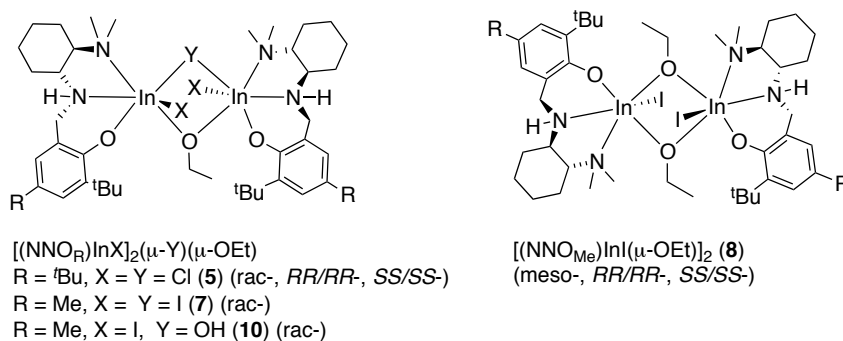
the propagating species is dinuclear. We propose an alternative mechanism, involving two metal centers that can stabilize the propagating polymer chain (**Scheme 3.2B**), which explains the highly living character of the catalyst. Extensive studies of the stereoselectivity of the catalyst for the ROP of rac-, L- and D-LA support this mechanism and provide a more nuanced picture of the various processes involved.



Scheme 3.2. Two mechanistic proposals for ROP of LA by $[(\text{NNO}_{\text{tBu}})\text{InCl}_2](\mu\text{-Cl})(\mu\text{-OEt})$.

3.2 Results

3.2.1 Living ring opening polymerization (ROP) of lactide



Dinuclear complexes **5**, **7**, **8**, and **10** are excellent initiators for lactide polymerization and were studied in depth. The choice of solvent for carrying out comparative experiments was

complicated by the limited solubility of the bis-ethoxy bridged complex **8** in all solvents except CDCl_3 . The role of the solvent will be discussed further below.

The rates of LA ROP with the para-*t*-Bu and -Me substituted complexes (\pm)-**5** and (\pm)-**6** are identical under the same conditions (**Figure 3.12**). The change to a less bulky and weaker electron donor group, -Me, versus -*t*-Bu at the para position of the phenolate group has no significant impact on the reactivity of LA ROP.

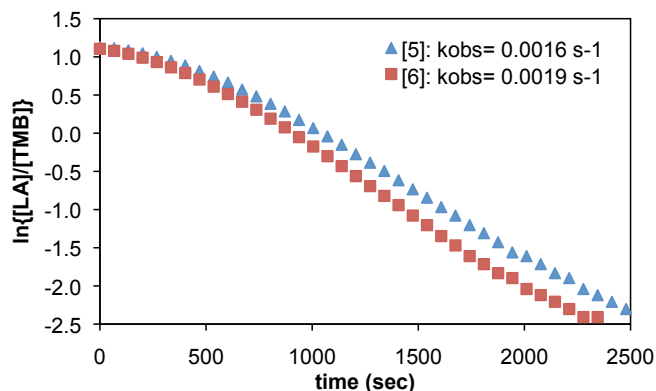


Figure 3.12. The ROP plots of 200 equiv of [LA] for two different initiators (**5**, (\pm)- $[(\text{NNO}_{t\text{Bu}})\text{InCl}](\mu\text{-Cl})(\mu\text{-OEt})$, = \blacktriangle ; **6**, (\pm)- $[(\text{NNO}_{t\text{Bu}})\text{InCl}](\mu\text{-Cl})(\mu\text{-OEt})$, = \blacksquare) at 25 °C followed to 90% conversion. [LA] = 0.91 M. [catalyst] = 0.0091 M in CDCl_3 . 1,3,5-trimethoxybenzene (TMB) was used as internal standard.

The reactions of rac-LA with catalysts (\pm)-**5**, (\pm)-**6**, meso-**8**, and (\pm)-**10** were monitored by ^1H NMR spectroscopy at 25 °C up to 90% conversion of 200 equiv of rac-LA (~50 min), with variations in rate depending on the initiator and reaction conditions. In all cases, an induction period was observed (**Figure 3.13**). In all the reactions, the relative integration of the methine proton of the monomer consumption to an internal standard, 1,3,5-trimethoxybenzene (TMB), was monitored during the polymerization.

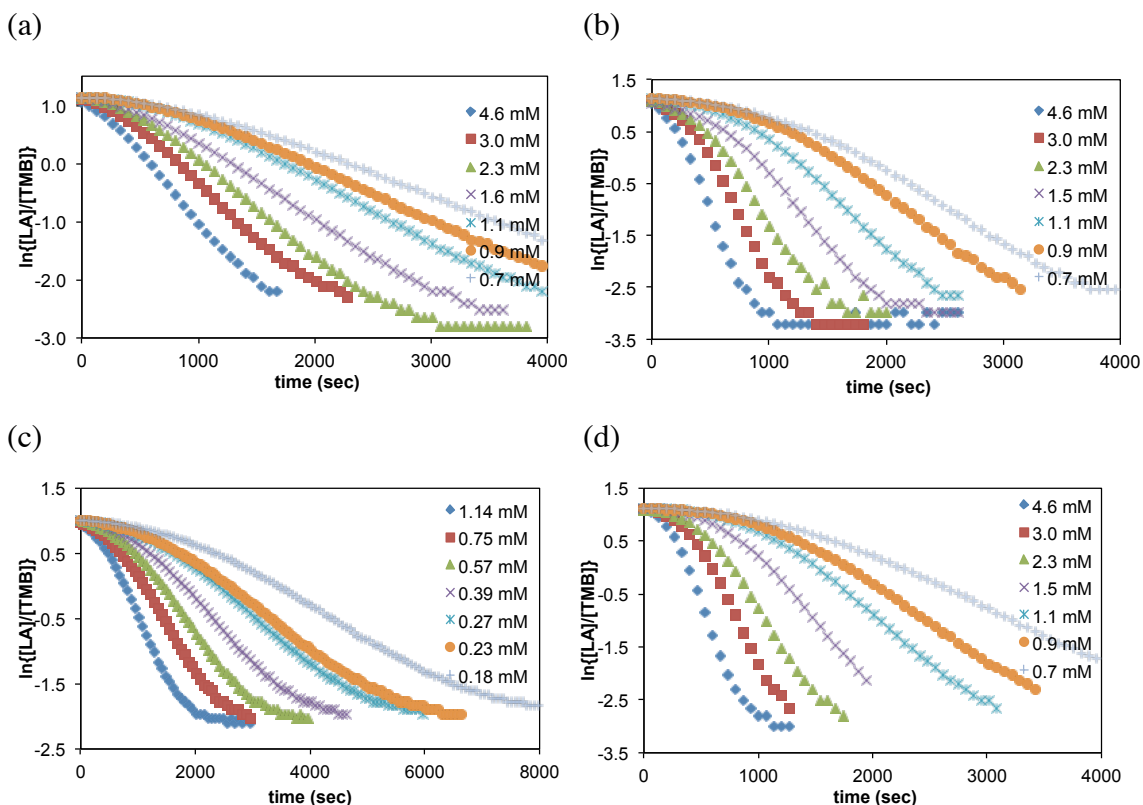


Figure 3.13. The ROP plots of rac-LA using dinuclear indium initiators, (a) (\pm) - $[(\text{NNO}_{\text{tBu}})\text{InCl}](\mu\text{-Cl})(\mu\text{-OEt})$ (**5**), (b) (\pm) - $[(\text{NNO}_{\text{Me}})\text{InI}_2](\mu\text{-I})(\mu\text{-OEt})$ (**7**), (c) (\pm) - $[(\text{NNO}_{\text{Me}})\text{In}(\text{I})(\mu\text{-OEt})_2]$ (**8**) and (d) (\pm) - $[(\text{NNO}_{\text{Me}})\text{InI}_2](\mu\text{-OH})(\mu\text{-OEt})$ (**10**). All the reactions were carried out in an NMR scale with various ratios of $[\text{LA}]/[\text{initiator}]$ at 25 °C and followed to 90% conversion. For the initiators, (\pm) -**5**, (\pm) -**7** and (\pm) -**10**, $[\text{LA}] = 0.91 \text{ M}$. $[\text{catalyst stock solution}] = 0.0091 \text{ M}$; for the initiator, (\pm) -**8**, $[\text{LA}] = 0.228 \text{ M}$. $[\text{catalyst}] = 0.00228 \text{ M}$ in CDCl_3 . 1,3,5-trimethoxybenzene (TMB) was used as internal standard. The value of k_{obs} was determined from the slope of the plots of $\ln([\text{LA}]/[\text{TMB}])$ vs. time, excluding the induction period. The variable concentrations of initiator are shown in the legends.

After the induction period, the polymerization rates are first order in LA concentration (rate = $k_{\text{obs}}[\text{LA}]$). The polymerization rate is also first order in the concentration of dinuclear complexes (\pm) -**5**, (\pm) -**7**, meso-**8**, and (\pm) -**10**, indicating that there is one initiating species for all complexes, and give an overall second-order rate law (rate = $k[\text{catalyst}][\text{LA}]$) (**Figure 3.14**). This allows us to directly compare k values for the four catalysts in question (**Table 3.1**).

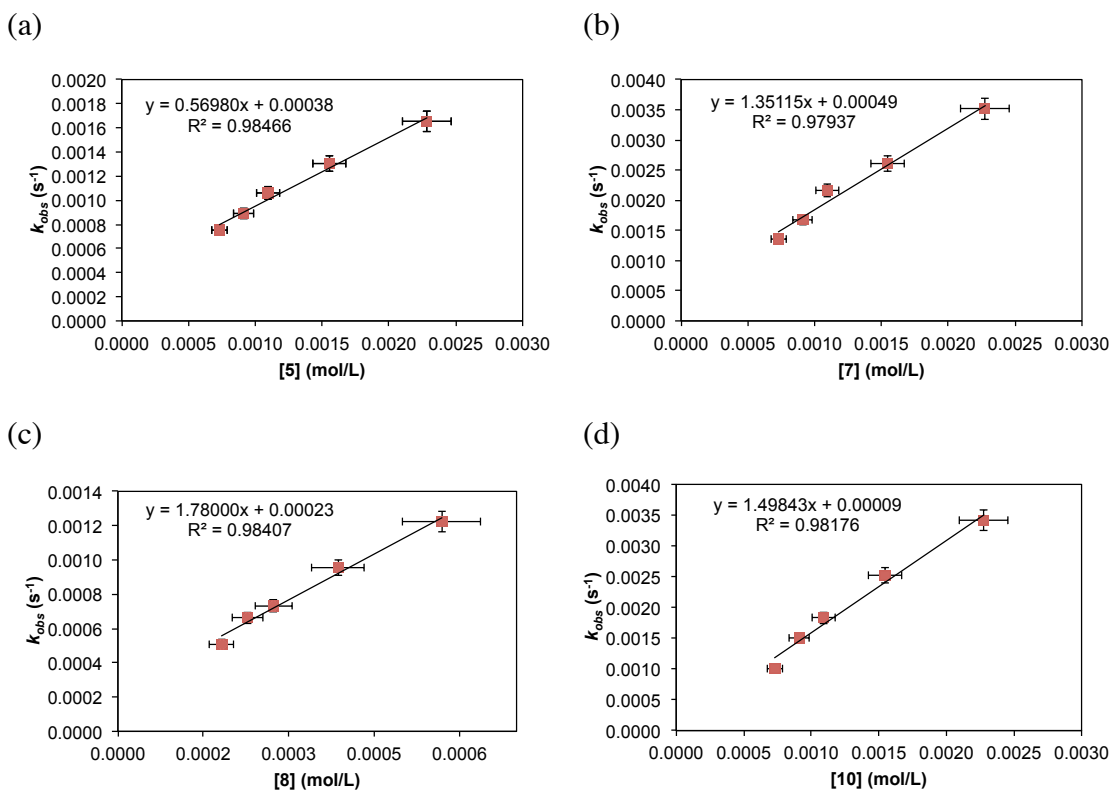


Figure 3.14. Plots of k_{obs} vs. [initiator] for (a) (\pm) -[(NNO_{tBu})InCl](μ -Cl)(μ -OEt) (\pm)-**5**, (b) (\pm) -[(NNO_{Me})InI]₂(μ -I)(μ -OEt) (\pm)-**7**, (c) (\pm) -[(NNO_{Me})In(I)(μ -OEt)]₂ (\pm)-**8** and (d) (\pm) -[(NNO_{Me})InI]₂(μ -OH)(μ -OEt) (\pm)-**10**. All the reactions were carried out in an NMR tube with 100, 150, 200, 300, 400, 500 and 600 equivalents of [LA]/[initiator] in CDCl₃ at 25 °C and followed to 90% conversion. [LA] = 0.91 M, [catalyst] = 0.0091 M for **5**, **7**, and **10** ; [LA] = 0.228 M, [catalyst] = 0.00228 M for **8**. 1,3,5-trimethoxybenzene (TMB) was used as internal standard. The value of k_{obs} was determined from the slope of the plots of $\ln([LA]/[TMB])$ vs. time.

Table 3.1. Rate constants for the ROP of rac-LA using dinuclear indium initiators.

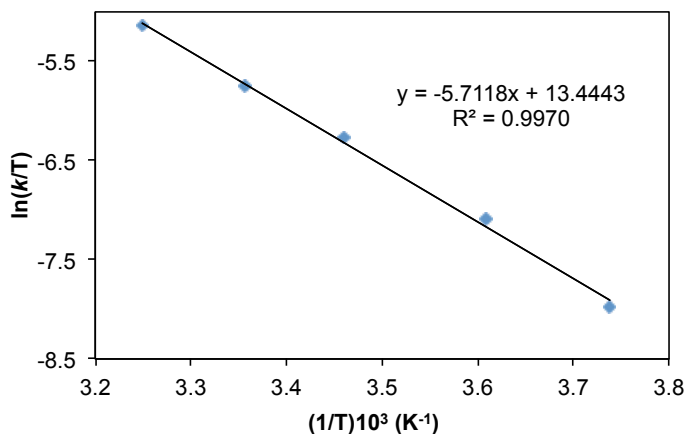
Entry	Catalyst	k (M ⁻¹ s ⁻¹)
1 ^a	(±)-[(NNO _{tBu})InCl] ₂ (μ-OEt)(μ-Cl) (5)	0.57(0.05)
2 ^a	(±)-[(NNO _{Me})InI] ₂ (μ-OEt)(μ-I) (7)	1.35(0.11)
3 ^b	Meso-[(NNO _{Me})InI(μ-OEt)] ₂ (8)	1.78(0.26)
4 ^a	(±)-[(NNO _{Me})InI] ₂ (μ-OEt)(μ-OH) (10)	1.50(0.13)

All the reactions were carried out in an NMR tube in CDCl₃ at 25 °C and followed to 90% conversion. ^a[LA] = 0.91 M. [catalyst] = 0.0091 M ; ^b[LA] = 0.228 M. [catalyst] = 0.00228 M. 1,3,5-trimethoxybenzene (TMB) was used as internal standard. The value of k_{obs} was determined from the slope of the plots of ln([LA]/[TMB]) vs. time.

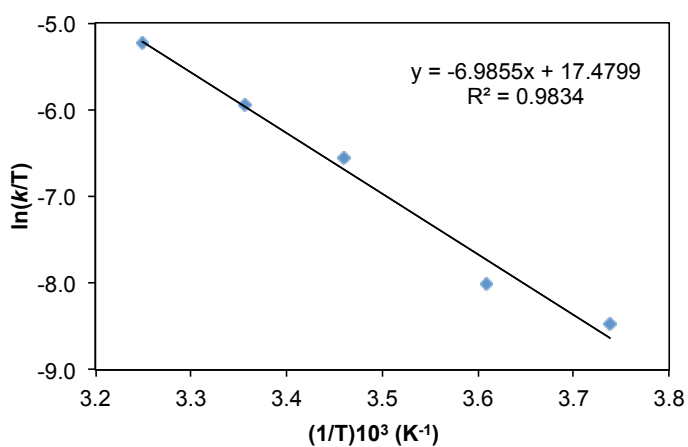
The rate constant for the ROP of LA with (±)-**5** in CDCl₃ ($k = 0.57(0.05) \text{ M}^{-1}\text{s}^{-1}$) is comparable to the reported value in CD₂Cl₂ ($k = 0.56(0.18) \text{ M}^{-1}\text{s}^{-1}$).²³ The rates of propagation for the iodo analogues (±)-**7**, meso-**8**, and (±)-**10** are significantly higher than that for (±)-**5**. In particular, the rate for meso-**8** ($k = 1.78(0.26) \text{ M}^{-1}\text{s}^{-1}$) is very similar with that for the fastest known lactide polymerization catalyst, the dinuclear zinc alkoxide (**B**) complex ($k = 2.2 \text{ M}^{-1}\text{s}^{-1}$). Based on our previous studies on the role of halides in dinuclear indium complexes,³ we believe that this increase is due to the greater electrophilicity of the indium centers in the chloro analogues. This enhanced electrophilicity is expected to strengthen the initiator-LA interaction and slow down ring opening and propagation. Importantly, the monoalkoxy complexes (±)-**7** and (±)-**10** have nearly identical rates, within error, to the bis-alkoxy bridged complex meso-**8** (Table 3.1, entries 2-4). This would not be expected if complex meso-**8** dissociated to form two initiating species. The activation parameters of the mono- and bis-ethoxy bridged complexes (±)-**7** ($\Delta H^\ddagger = 47(3) \text{ kJmol}^{-1}$, $\Delta S^\ddagger = -83(7) \text{ JK}^{-1}\text{mol}^{-1}$) and meso-**8** ($\Delta H^\ddagger = 62(4) \text{ kJmol}^{-1}$, $\Delta S^\ddagger = -30(3) \text{ JK}^{-1}\text{mol}^{-1}$)²⁹¹ are in agreement with reported values for complex (±)-**5** ($\Delta H^\ddagger = 49(2) \text{ kJmol}^{-1}$, $\Delta S^\ddagger = -87(4) \text{ JK}^{-1}\text{mol}^{-1}$, [5] = 2 mM) and other indium catalysts for LA ROP and indicate similar ordered transition states in a coordination-insertion mechanism (Figure 3.15).^{23,87} Surprisingly, the activation parameters for complex (±)-**5** show different values in terms of the concentrations of the catalyst (±)-**5**: $\Delta H^\ddagger = 47(3) \text{ kJ mol}^{-1}$ and $\Delta S^\ddagger = -86(4) \text{ J mol}^{-1}\text{K}^{-1}$ for [5] = 1 mM and $\Delta H^\ddagger = 58(4) \text{ kJ mol}^{-1}$ and $\Delta S^\ddagger = -52(5) \text{ J mol}^{-1}\text{K}^{-1}$ for [5] = 3 mM. Thus, the values are

significantly different at the higher concentration of catalyst, suggesting aggregation of the indium complex may not be negligible in the rate of LA polymerization.

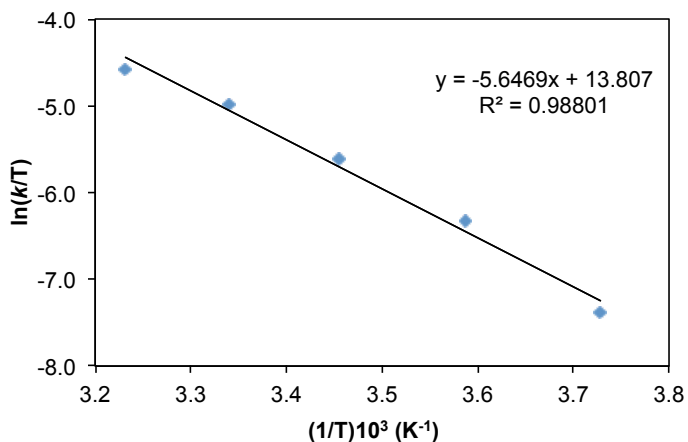
(a) $(\pm)\text{-}[(\text{NNO}_{\text{tBu}})\text{InCl}_2(\mu\text{-Cl})(\mu\text{-OEt})]$ (**5**) ($[\mathbf{5}] = 1.00 \text{ mM}$, $[\text{LA}] = 0.46 \text{ M}$, CD_2Cl_2); $\Delta H^\ddagger = 47(1) \text{ kJ mol}^{-1}$ $\Delta S^\ddagger = -86(4) \text{ J mol}^{-1}\text{K}^{-1}$



(b) $(\pm)\text{-}[(\text{NNO}_{\text{tBu}})\text{InCl}_2(\mu\text{-Cl})(\mu\text{-OEt})]$ (**5**) ($[\mathbf{5}] = 3.00 \text{ mM}$, $[\text{LA}] = 0.46 \text{ M}$, CD_2Cl_2); $\Delta H^\ddagger = 58(4) \text{ kJ mol}^{-1}$ $\Delta S^\ddagger = -52(5) \text{ J mol}^{-1}\text{K}^{-1}$



(c) (\pm) -[(NNO_{Me})InI]₂(μ -I)(μ -OEt) (**7**) ([**7**] = 2.27 mM, [LA] = 0.46 M, CDCl₃); $\Delta H^\ddagger = 47(3)$ kJ mol⁻¹ $\Delta S^\ddagger = -83(7)$ J mol⁻¹K⁻¹



(d) meso-[(NNO_{Me})In(I)(μ -OEt)]₂ (**8**) ([**8**] = 0.57 mM, [LA] = 0.11 M, CDCl₃); $\Delta H^\ddagger = 62(4)$ kJ mol⁻¹ $\Delta S^\ddagger = -30(3)$ J mol⁻¹K⁻¹

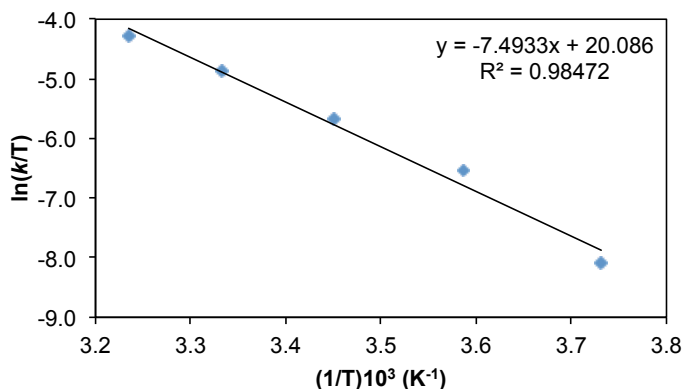


Figure 3.15. Activation parameters for the polymerization of rac-LA using (\pm) -[(NNO_{tBu})InCl]₂(μ -Cl)(μ -OEt) (**5**) with its variable concentrations, (a) [**5**] = 1.00 mM and (b) [**5**] = 3.00 mM, in CD₂Cl₂, (c) (\pm) -[(NNO_{Me})InI]₂(μ -I)(μ -OEt) (**7**) and (d) meso-[(NNO_{Me})In(I)(μ -OEt)]₂ (**8**) in CDCl₃. Polymerization rate = $k_{\text{obs}} \times [\text{LA}]$; $k_{\text{obs}} = k[\text{cat}]$, where k is the rate constant used in the Eyring equation to derive activation parameters. Due to solubility constraints, different [cat] were used for (\pm) -**7** and meso-**8**.

In our communication,²³ we reported that the ROP of LA with (\pm) -**5** was a living process, with a linear increase of M_n values and low molecular weight distributions for monomer:initiator (M/I) ratios up to 500. We have expanded this range to M/I ratios of over 2100 with the same control, obtaining polymers with molecular weights up to 350 kDa with very low PDI values (**Figure 3.16**). These results confirm that complex (\pm) -**5** is one of the most controlled catalysts reported for the ROP of LA.^{130,146,172,173,279}

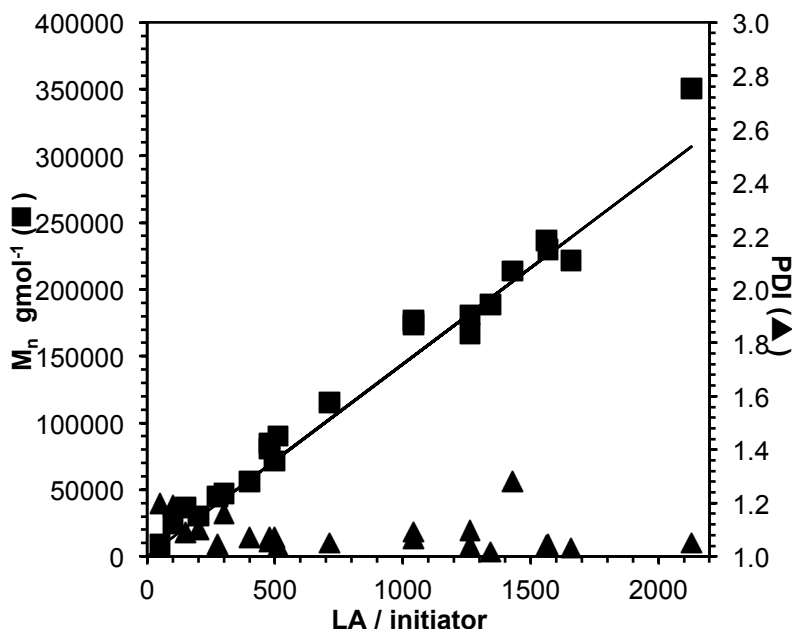


Figure 3.16. Plot of observed PLA M_n (■) and molecular weight distribution (PDI) (▲) as functions of added rac- or L-LA for catalyst **5** (\pm)-[(NNO_{tBu})InCl₂(μ -Cl)(μ -OEt) (M_n = number averaged molecular weight, PDI = polydispersity index). The line indicates calculated M_n values based on the LA: initiator ratio. All reactions were carried out at room temperature in CH₂Cl₂ and polymer samples obtained at >90% conversion.

Due to the low solubility of meso-**8** in CD₂Cl₂, all the NMR spectroscopic studies were conducted in CDCl₃. These solvents, however, do not affect the large scale polymerization of LA with complex **5** as well as its rate constant (Table 3.2, entries 1-2). Although the rates of polymerization for the mono- and bis-ethoxy bridged complexes (\pm)-**7** and meso-**8** are identical, the molecular weight of polymers obtained using the two catalysts depends on the number of alkoxides in the molecule (Table 3.2). Polymers obtained with the mono-ethoxy bridged catalysts (\pm)-**5** and (\pm)-**7** show a good correlation between the theoretical M_n based on dimer concentration (Table 3.2, entries 1-4). In contrast, those obtained with the bis-ethoxy bridged complex meso-**8** show M_n values roughly half of the theoretical values, indicating the presence of two propagation sites for meso-**8** (Table 3.2, entries 5-7). Thus for the bis-ethoxy bridged catalyst meso-**8** polymer molecular weights are indicative of one polymer chain per ethoxide. This result is consistent with that in LA polymerization using the bis-alkoxy bridged dinuclear indium system generated *in-situ* from InCl₃, BnOH, and NEt₃ reported by Hillmyer and Tolman.⁸⁹

Table 3.2. Polymerization rac-LA by complexes (\pm)-**5**, (\pm)-**7** and meso-**8**.

Entry	Initiator	[LA] ₀ : [Dimer]	Solvent	Conv. ^a (%)	M _{n,theo} ^b / g mol ⁻¹	M _{n,GPC} ^c / g mol ⁻¹	M _w /M _n ^c
1	(\pm)- 5	1005	CH ₂ Cl ₂	93	134 760	129800	1.04
2	(\pm)- 5	1002	CHCl ₃	98	141 580	148400	1.04
3	(\pm)- 7	510	CH ₂ Cl ₂	95	68 880	50050	1.17
4	(\pm)- 7	976	CH ₂ Cl ₂	95	133 680	141700	1.12
5	meso- 8	500	CH ₂ Cl ₂	92	66 350	35940	1.16
6	meso- 8	1000	CH ₂ Cl ₂	93	134 090	61490	1.14
7	meso- 8	2001	CH ₂ Cl ₂	95	273 960	154900	1.26

^a Monomer conversion, determined by ¹H NMR spectroscopy. ^b Calculated from [LA]₀/[initiator] × LA conversion × M_{LA} + M_{EiOH}. ^c Determined by GPC-LALLS (gel permeation chromatography-low angle laser light scattering) to the polystyrene standard calibration curve via the Mark–Houwink equation in THF at 25 °C ([η] = KM^a while [η] = intrinsic viscosity, M = molecular weight, and K and a are Mark–Houwink parameters, K = 1.832 × 10⁻⁴ dl/g and a = 0.69, dn/dc = 0.042 mL/g).³⁵ All the reactions were carried out for 16 h.

3.2.2 Control of stereoselectivity with dinuclear catalysts

We have previously communicated that (\pm)-**5** exerts moderate isoselectivity for the ROP of rac-LA (P_m = 0.62).²³ In the current study, we investigate the stereoselectivity of racemic and enantiopure dinuclear complexes (\pm)-, (*R,R/R,R*)- and (*S,S/S,S*)-**5** and meso-, (*R,R/R,R*)-, and (*S,S/S,S*)-**8** for the polymerization of rac-, D- and L-LA (CDCl₃, 25 °C) in depth (Appendix B). Unlike the halide effect on reactivity for LA ROP (**5**; k = 0.57(0.05) M⁻¹s⁻¹, **7**; k = 1.35(0.11) M⁻¹s⁻¹), we do not observe a halide effect on selectivities for (\pm)-[(NNO_{tBu})InCl]₂(μ-OEt)(μ-Cl) (**5**) (P_m = 0.61) and (\pm)-[(NNO_{Me})InI]₂(μ-OEt)(μ-I) (**7**) (P_m = 0.59) which are identical (**Figure 3.17**).

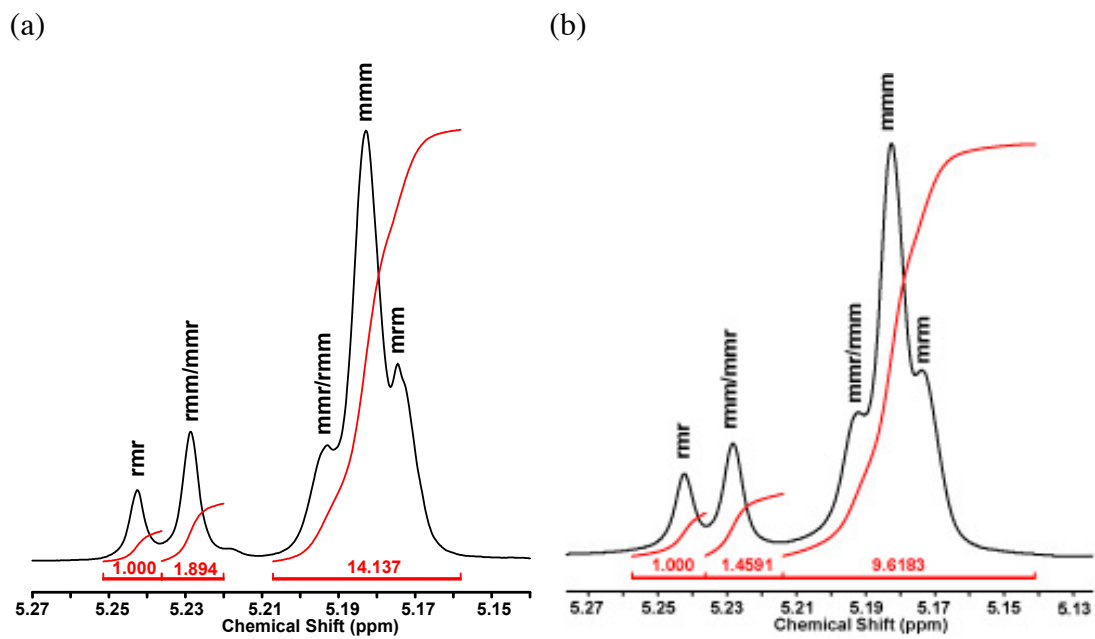


Figure 3.17. $^1\text{H}\{^1\text{H}\}$ NMR spectra (600 MHz, CDCl_3 , 25 °C) of PLA obtained from ROP of rac-LA with (a) (±)-**5** ($P_m = 0.61$) and (b) (±)-**7** ($P_m = 0.59$).

Table 3.3. Effects of catalyst chirality on reaction rates and polymer tacticity by monoethoxy bridged complex **5**.

Entry	Catalyst	Monomer	k_{obs} ($\times 10^{-3} \text{ s}^{-1}$) ^a	P_m
1	(<i>R,R/R,R</i>)- 5	L-LA	3.4 (0.6)	1
2	(<i>R,R/R,R</i>)- 5	D-LA	0.25 (0.14)	1
3	(<i>S,S/S,S</i>)- 5	L-LA	0.27 (0.04)	1
4	(<i>S,S/S,S</i>)- 5	D-LA	3.8 (0.8)	1
5	(<i>R,R/R,R</i>)- 5	rac-LA	0.62 (0.16) ^b 0.21 (0.06) ^c	0.48
6	(<i>S,S/S,S</i>)- 5	rac-LA	0.70 (0.05) ^b 0.24 (0.01) ^c	0.49
7	(\pm)- 5	L-LA	2.98 (0.09)	1
8	(\pm)- 5	D-LA	2.95 (0.08)	1
9	(\pm)- 5	rac-LA	1.72 (0.16)	0.61

All reactions were carried out with 200 equiv of LA in CDCl_3 at 25 °C and followed to 90% conversion by ^1H NMR spectroscopy, unless otherwise stated. [catalyst] = 0.0023 M, [LA] = 0.45 M, ^a Average of two experiments. ^b k_{obs} from 0 to 64% conversion. ^c k_{obs} from 73 to 90% conversion.

The rates of polymerization for enantiopure **5** reveal strong site selectivity. Comparison of the ROP rates for D- and L-LA with (*R,R/R,R*)-**5** shows a k_L/k_D value of ~ 14 ; the reverse value ($k_D/k_L \sim 14$) is obtained for (*S,S/S,S*)-**5** (Table 3.3, entries 1-4).³⁶ This k_{rel} value is similar to those reported for highly selective chiral aluminum salen complexes.⁹ Despite this high selectivity, and in contrast to the aluminum systems, polymerization of rac-LA with enantiopure **5** forms atactic PLA (Table 3.3, entries 5, 6). Polymerization of rac-LA with (*R,R/R,R*)-**5** follows two rate regimes (Figure 3.18a). In the early stages of the polymerization, a rate of $0.62 \times 10^{-3} \text{ s}^{-1}$ is observed; however, after ~ 30 min there is a sharp decrease in the rate to $0.21 \times 10^{-3} \text{ s}^{-1}$. This is the rate observed for the disfavored monomer. Similar values are observed for (*S,S/S,S*)-**5** indicating that the favored monomer is polymerized first, at a faster rate, than the disfavored monomer (Appendix B). In contrast, the k_{obs} values for polymerization of L- and D-LA with (\pm)-**5** (Table 3.3, entries 7, 8) are identical to the analogous enantiopure complexes within error (Table 3.3, entries 1, 4). Importantly, the rate of polymerization of rac-LA with (\pm)-**5** (Table 3.3, entry 1) is

significantly lower than the rates for enantiopure monomers indicating catalyst inhibition by the mismatched monomer.

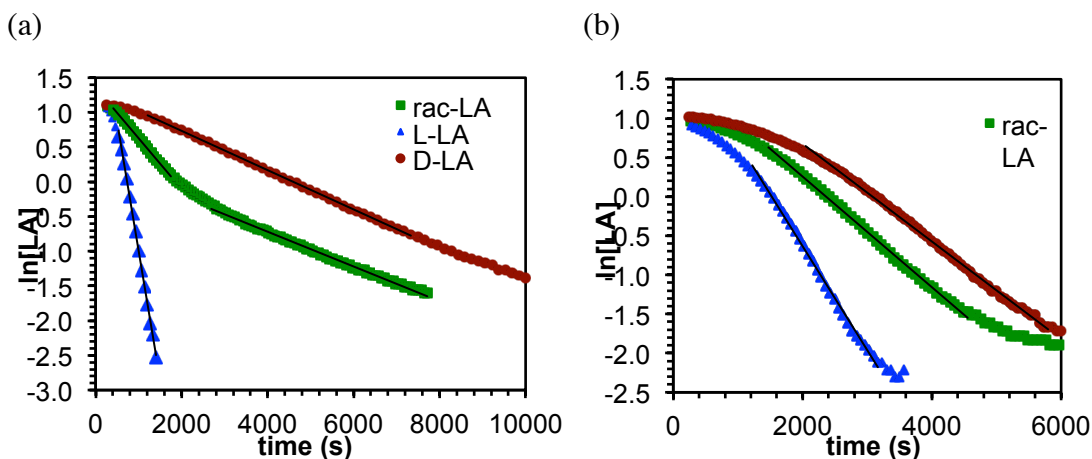


Figure 3.18. Plot of $\ln[LA]$ vs time for polymerization of rac-LA, L-LA, and D-LA by (a) (R,R,R,R) -5 and (b) (R,R,R,R) -8. (400 MHz, $CDCl_3$, 25 °C).

There is a non-linear relationship between the observed rate constant and percent (R,R,R,R) -5. In asymmetric catalysis, nonlinearity, which shows the enantiopurity of a product is not directly correlated to that of an enantiomeric chiral catalyst, may be caused by diastereomeric perturbations of the initial chiral species of the catalyst. As the enantiopurity of the samples increases from (\pm) -5 (50%) to (R,R,R,R) -5 (100%) the observed rate constants decrease an order of magnitude in a non-linear fashion, while P_m values decrease from ~ 0.6 to 0.5, again in a non-linear fashion (**Figure 3.19a**). Such non-linear relationships are a characteristic of dinuclear stereoselective catalysts.²⁹² This suggests the homochiral dimeric species of complex **5** possesses a possible greater stability versus its monomeric species. P_m values for ROP of rac-LA with (\pm) - and (R,R,R,R) -5 remain essentially unchanged with increasing conversion (at 25 °C and 0 °C) confirming that the resulting polymers are not stereoblock (**Figure 3.20** and **Figure 3.21**).

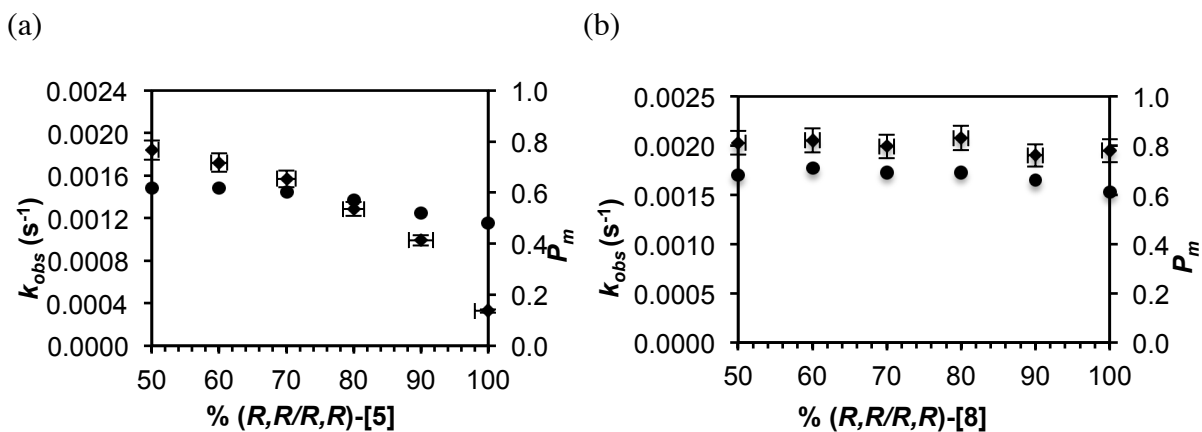


Figure 3.19. Plots of k_{obs} (◆) and P_m (●) as functions of catalyst enantiopurity. All the reactions were carried out with 200 equiv of rac-LA in CDCl₃ at 25 °C and followed to 90% conversion. (a); **[5]** = 0.0024 M, [LA] = 0.46 M, (b); **[8]** = 0.00057 M, ^d[LA] = 0.117 M.

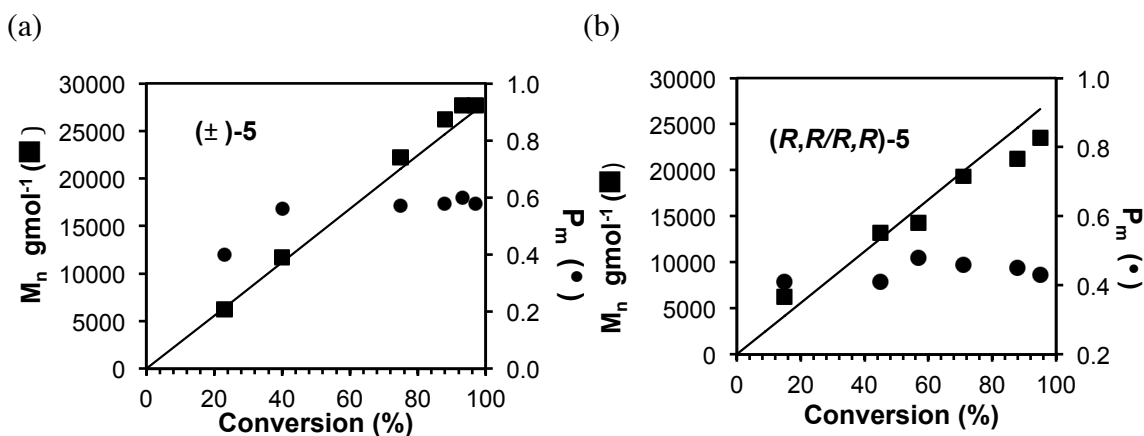


Figure 3.20. Plots of observed PLA M_n (■) and P_m (•) as functions of conversion for catalysts (±)-**5** (a) and (R,R/R,R)-**5** (b) (M_n = number averaged molecular weight, P_m = probability of meso linkages in repeating units of a polymer chain). The line indicates calculated M_n values.

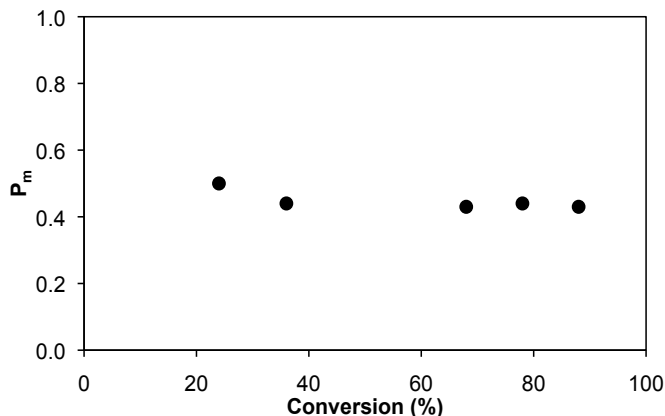


Figure 3.21. Plot of observed PLA P_m (•) as functions of conversion for catalyst $(R,R/R,R)$ -**5** at 0 °C in CH_2Cl_2 . $[(R,R/R,R)$ -**5**] = 0.46 mM, [rac-LA] = 0.227 M.

In contrast to the mono-ethoxy bridged complex **5**, polymerizations of LA with bis-ethoxy bridged complex **8** do not show significant site selectivity. The k_t/k_D value for ROP of L-LA with $(R,R/R,R)$ -**8** is only ~ 2 , with the opposite selectivity of the same magnitude observed for $(S,S/S,S)$ -**8** (Table 3.4, entries 1-4). P_m values for the polymerizations of rac-LA with meso- or enantiopure **8** are the same (Table 3.4, entries 5-7). The rate constants for ROP of rac-, D-, and L-LA with meso-**8** are identical within experimental error (Table 3.4, entries 7-9). Observed rate constants and P_m values do not change with increasing enantiopurity of the catalyst (Figure 3.18b). These data suggest that the observed selectivity ($P_m = 0.65$) with catalyst **8** is not affected by catalyst chirality and thus must be dominated by chain end control.

Table 3.4. Effects of catalyst chirality on reaction rates and polymer tacticity by bis-ethoxy bridged complex **8**.

Entry	Catalyst	Monomer	k_{obs} ($\times 10^{-3} \text{ s}^{-1}$) ^a	P_m
1	(<i>R,R/R,R</i>)- 8	L-LA	1.25 (0.21)	1
2	(<i>R,R/R,R</i>)- 8	D-LA	0.64 (0.01)	1
3	(<i>S,S/S,S</i>)- 8	L-LA	0.67 (0.16)	1
4	(<i>S,S/S,S</i>)- 8	D-LA	1.29 (0.30)	1
5	(<i>R,R/R,R</i>)- 8	rac-LA	0.72 (0.01)	0.65
6	(<i>S,S/S,S</i>)- 8	rac-LA	0.66 (0.09)	0.64
7	(meso)- 8	rac-LA	1.73 (0.76)	0.62
8	(meso)- 8	L-LA	1.24 (0.03)	1
9	(meso)- 8	D-LA	1.23 (0.02)	1

All reactions were carried out with 200 equiv of LA in CDCl₃ at 25 °C and followed to 90% conversion by ¹H NMR spectroscopy. [catalyst] = 0.00052 M, [LA] = 0.114 M. ^aAverage of two experiments.

3.2.3 On the solution structure of the propagating species for catalyst **5**

[(NNO_{tBu})InCl]₂(μ-Cl)(μ-OEt)

The P_m values obtained for the ROP of rac-LA with (*R,R/R,R*)-**5** (0.48) and (*R,R/R,R*)-**8** (0.65) are significantly different. This would not be possible if the polymers were derived from identical mononuclear initiators. Indeed, the kinetics and selectivity data discussed above strongly suggest a dinuclear propagating species for catalyst **5**.

As described in Chapter 1, the reactivity with alcohols and water shows that dinuclear complexes such as **5** [(NNO_{tBu})InCl]₂(μ-Cl)(μ-OEt) are undergoing some dissociation in the presence of added species. Indeed, cross over reactions between (±)-[(NNO_{tBu})InCl]₂(μ-Cl)(μ-OEt) (**5**) and (NNO_{Me})InCl₂ (**3**), as well as [(NNO_{Me})InI]₂(μ-I)(μ-OEt) (**7**) and the (NNO_{tBu})InI₂ (**2**), are observed in 5 min (**Figure 3.22** and **Figure 3.23**, respectively). A similar crossover reaction was observed between meso-[(NNO_{Me})In(I)(μ-OEt)]₂ (meso-**8**) and (±)-[(NNO_{tBu})InI]₂ (**2**) (**Figure 3.24**).

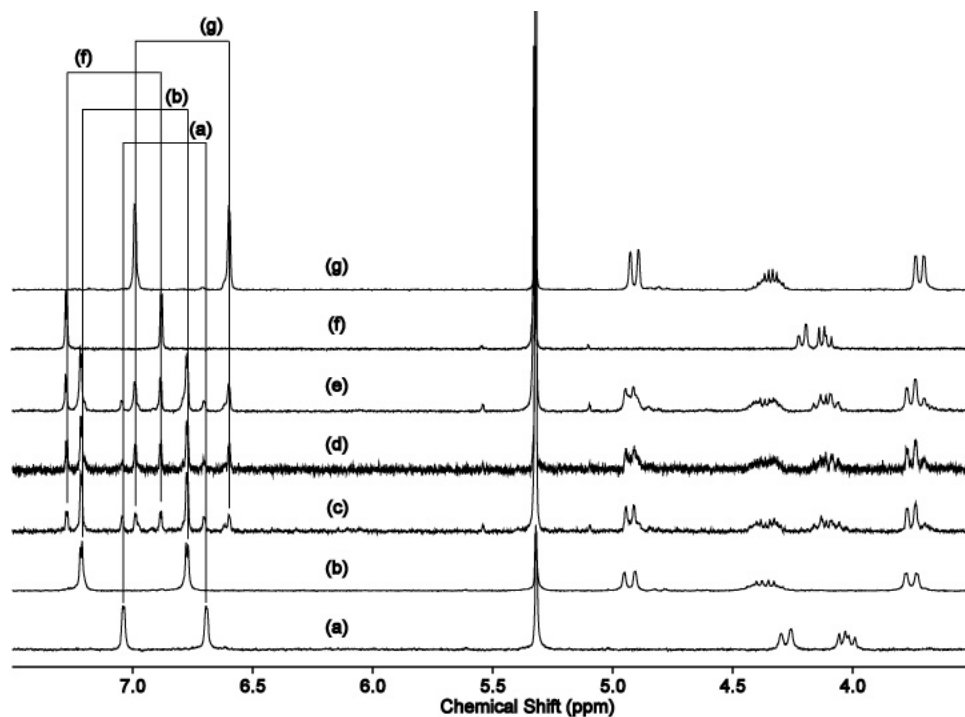


Figure 3.22. ^1H NMR spectra of (a) **3**, $(\pm)\text{-(NNO}_{\text{Me}})\text{InCl}_2$, (b) **5**, $(\pm)\text{-}[(\text{NNO}_{\text{tBu}})\text{InCl}](\mu\text{-Cl})(\mu\text{-OEt})$, and a mixture of **3** and **5** (c) after 5 minutes, (d) 16 minutes, and (e) 4 hr, (f) **1**, $(\pm)\text{-}(\text{NNO}_{\text{tBu}})\text{InCl}_2$, and (g) **6**, $(\pm)\text{-}[(\text{NNO}_{\text{Me}})\text{InCl}](\mu\text{-Cl})(\mu\text{-OEt})$ (400 MHz, CD_2Cl_2 , 25 °C).

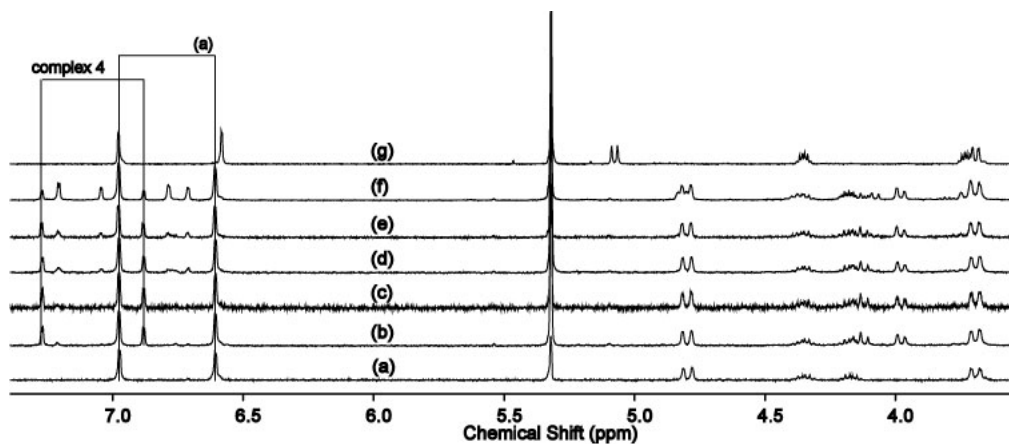


Figure 3.23. ^1H NMR spectra of (a) **7**, $(\pm)\text{-}[(\text{NNO}_{\text{Me}})\text{InI}](\mu\text{-I})(\mu\text{-OEt})$, and a mixture of **2**, $(\pm)\text{-}(\text{NNO}_{\text{tBu}})\text{InI}_2$, and **7**, (b) after 5 minutes, (c) 8 minutes, (d) 43 minutes, (e) 2 hr 30 minutes and (f) 2 days, and (g) **8**, $(\pm)\text{-}[(\text{NNO}_{\text{Me}})\text{In(I)}](\mu\text{-OEt})_2$ (400 MHz, CD_2Cl_2 , 25 °C).

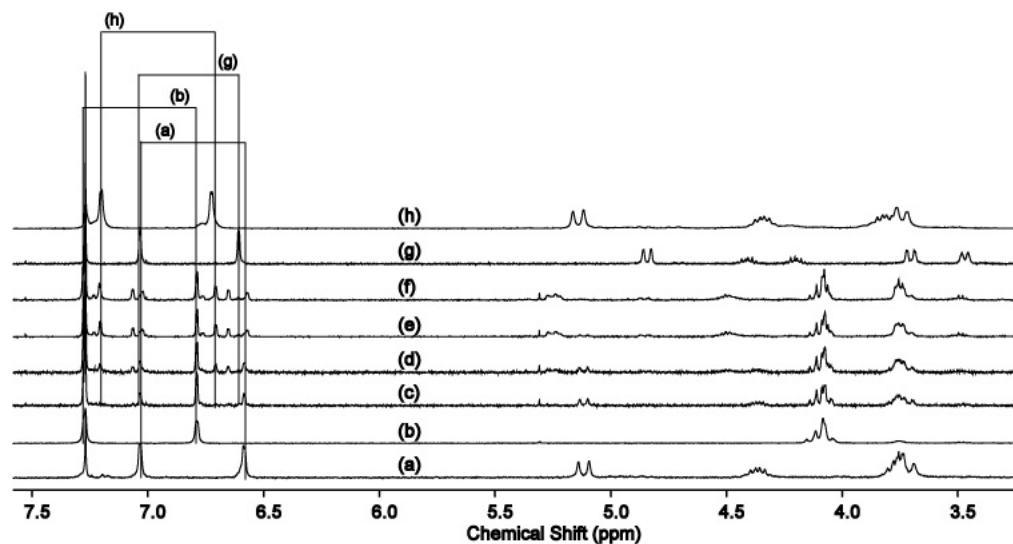


Figure 3.24. ^1H NMR spectra of (a) complex **8**, (meso)- $[(\text{NNO}_{\text{Me}})\text{In}(\text{I})(\mu\text{-OEt})]_2$, (b) complex **2**, $(\pm)\text{-}(\text{NNO}_{\text{tBu}})\text{InI}_2$; a mixture of complexes, **8** and **2**, (c) after 5 minutes, (d) 8 minutes, (e) 2 hr 30 minutes and (f) 2 days, (g) complex $(\pm)\text{-}[(\text{NNO}_{\text{Me}})\text{InI}](\mu\text{-I})(\mu\text{-OEt})$ (**7**), (h) complex $(\pm)\text{-9}$ (400 MHz, CDCl_3 , 25°C).

However, the potential lability of the dinuclear catalysts is not a factor in lactide polymerization. If the dinuclear complex **5** is dormant and dissociation to an active mononuclear species is required for polymerization (**Scheme 3.2a**), addition of $[\text{NNO}_{\text{tBu}}]\text{InCl}_2$ (**1**) should shift the equilibrium towards the unreactive species and affect polymerization rates and/or polymer molecular weights. In a series of experiments, different amounts of **1** were added to a solution of **5** (CD_2Cl_2 , 25°C) prior to the addition of monomer to the catalyst mixture and the polymerization was monitored by ^1H NMR spectroscopy. In an identical set of reactions the polymer was isolated and analyzed. The resulting values of k_{obs} and M_n remain constant with up to 5 additional equivalents of **1** (**Figure 3.25**). At the higher equivalents of **1** the solution becomes saturated for the complex to be dissolved. These experiments indicate that although complex **5** can dissociate in the presence of donors, this dissociation does not play a role in the polymerization of lactide.

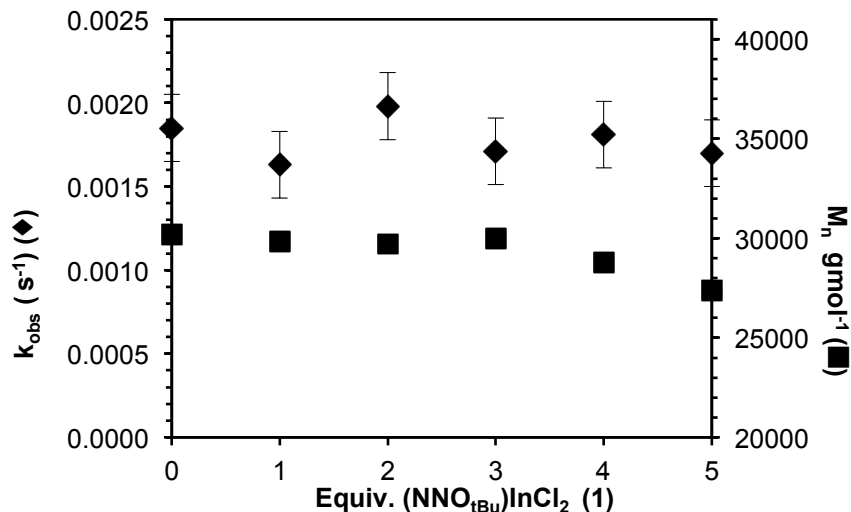


Figure 3.25. Plots of k_{obs} (◆) and observed PLA M_n (■) as functions of added **1** for polymerization of LA with catalysts **5** ($[\mathbf{5}] = 0.0024$ M, CD_2Cl_2 , room temperature; M_n = number averaged molecular weight).

The mechanism in **Scheme 3.2A** assumes that the induction period is caused by the dissociation of $[(\text{NNO}_{\text{tBu}})\text{InCl}]_2(\mu\text{-Cl})(\mu\text{-OEt})$ (**5**) to give lactide adducts of $(\text{NNO}_{\text{tBu}})\text{In}(\text{Cl})(\text{OEt})$, the proposed active catalyst, and $(\text{NNO}_{\text{tBu}})\text{InCl}_2$ (**1**) in the presence of lactide. However, we have never observed complex **1** in solution during polymerization (**Figure 3.26**). However, we have observed such a dissociation in bulkier systems (**Figure 3.27**). In related work with bulky N-alkylated ligands, the dinuclear catalyst $[(\text{N}_{\text{nPr}}\text{NO})\text{InCl}]_2(\mu\text{-Cl})(\mu\text{-OEt})$ dissociates in the presence of added lactide to form $[(\text{N}_{\text{nPr}}\text{NO}_{\text{tBu}})\text{In}(\text{Cl})(\text{O-Polymer})]$ and $(\text{N}_{\text{nPr}}\text{NO}_{\text{tBu}})\text{InCl}_2$ (**Scheme 3.3**).² Interestingly, in the bulkier systems that dissociate, all selectivity is lost; thus, the resulting polymer is atactic. This suggests that the selectivity that is observed for complex **5** is a result of its dinuclear nature.

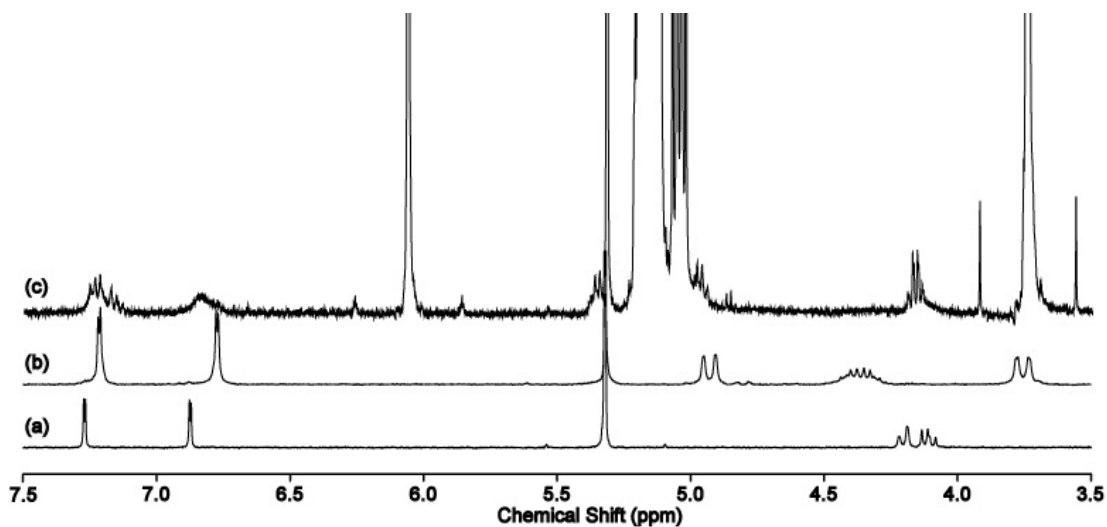
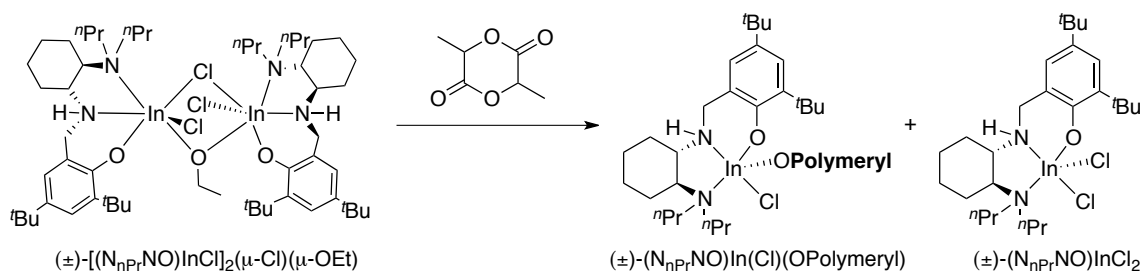


Figure 3.26. ^1H NMR spectra of (a) complex **1**, $(\pm)\text{-}(\text{NNO}_{t\text{Bu}})\text{InCl}_2$, (b) complex **5**, $(\pm)\text{-}[(\text{NNO}_{t\text{Bu}})\text{InCl}_2(\mu\text{-Cl})(\mu\text{-OEt})]$ and polymerization of 200 equiv. of rac-LA with complex **5** after 16 minutes (400 MHz, CD_2Cl_2 , 25°C).



Scheme 3.3. Dissociation of dinuclear catalysts with added lactide.^{19b}

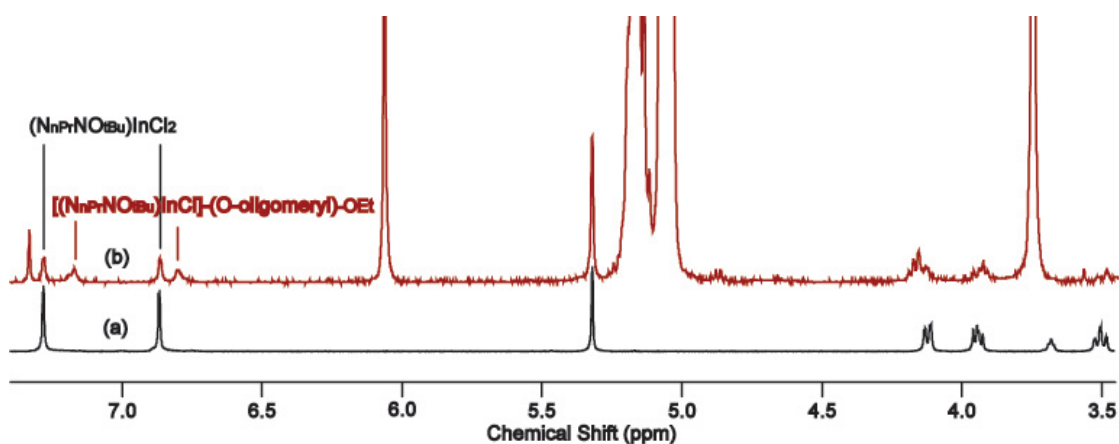


Figure 3.27. ^1H NMR spectra of (a) $(\pm)\text{-}(\text{N}_{n\text{Pr}}\text{NO}_{t\text{Bu}})\text{InCl}_2$, and (b) polymerization of 200 equiv. of rac-LA with $(\pm)\text{-}[(\text{N}_{n\text{Pr}}\text{NO}_{t\text{Bu}})\text{InCl}]_2(\mu\text{-Cl})(\mu\text{-OEt})$ after 5 minutes (400 MHz, CD_2Cl_2 , 25°C).²

3.3 Discussion and conclusion

We have conducted the ring opening polymerization (ROP) of lactide (LA) with a family of dinuclear ethoxy bridged indium complexes $[(\text{NNO}_R)\text{InX}]_2(\mu\text{-OEt})(\mu\text{-Y})$ ($R = t\text{-Bu, Me}$; $X = \text{Cl, I}$; $Y = \text{Cl, I, OH, OEt}$) and their enantiopure analogues, and compared the reactivity of mono- ($Y = \text{Cl, I}$) and bis-alkoxy bridged ($Y = \text{OEt}$) complexes for the ring opening polymerization (ROP) of lactide (LA). In particular, the chloro-ethoxy-bridged derivative $(\pm)\text{-}[(\text{NNO}_{t\text{Bu}})\text{InCl}]_2(\mu\text{-OEt})(\mu\text{-Cl})$ (**5**) is one of the most successful catalysts for controlled LA ROP and generates PLA samples of up to 300 kDa with predictable molecular weights and low molecular weight distributions. The living nature of the propagation was confirmed by *in situ* monitoring of reactions as well as by analysis of bulk polymer samples. Kinetic studies show that after an induction period, the rate of lactide polymerization is first order in the concentration of lactide and also first order in the concentration of catalyst, regardless of whether one or two bridging ethoxy groups are present.

Complex $(\pm)\text{-5}$ is a unique asymmetrically bridged dinuclear catalyst with excellent potential as a commercial catalyst for the ring opening polymerization (ROP) of lactide (LA).²⁹³ The dinuclear nature of the catalyst raises an important mechanistic question: is the propagating species derived from the dissociation of the dimer in the presence of a large concentration of lactide or does the dinuclear complex act as the propagating species? The data support a dinuclear propagating species.

1) *The ethoxy-bridged indium complexes are dinuclear in solution (Chapter 2).*

The structures of the indium alkoxide complexes in this family are invariably dinuclear in solution confirmed by VT NMR spectroscopy, 2D NOESY spectroscopy, and PGSE experiments and also dinuclear in solution and in the solid state as observed by X-ray crystallography.

2) *Polymerization rate and polymer molecular weight are not affected by addition of **1** $(\pm)\text{-}(\text{NNO}_{t\text{Bu}})\text{InCl}_2$.*

Although an equilibrium between $(\pm)\text{-5}$, $(\pm)\text{-1}$, and an ethoxy mononuclear complex $(\text{NNO}_{t\text{Bu}})\text{In}(\text{Cl})(\text{OEt})$ is possible, it does not affect the rate of polymerization nor the molecular weights of the resulting polymers (**Figure 3.25**). If complex $(\pm)\text{-5}$ was a dormant species requiring dissociation to complex $(\pm)\text{-1}$ and an active $(\text{NNO}_{t\text{Bu}})\text{In}(\text{Cl})(\text{OEt})$ complex,

then addition of (\pm)-**1** would be expected to shift the equilibrium towards complex (\pm)-**5** and, in turn, lower rates of polymerization and lead to higher observed molecular weights. The lack of influence of added **5** on the reaction rates and polymer properties confirms that an equilibrium between the dinuclear complex (\pm)-**5** and the monometallic compounds (\pm)-**1** and $(\text{NNO}_{\text{tBu}})\text{In}(\text{Cl})(\text{OEt})$, if it is indeed present, is not important to propagation and thus complex (\pm)-**5** is not a dormant species, but rather a dinuclear active catalyst as shown in **Scheme 3.2B**.

3) *There is no evidence for dissociation of (\pm)-**5** during polymerization.*

Unlike the bulkier systems (\pm)- $[(\text{N}_{\text{nPr}}\text{NO})\text{InCl}]_2(\mu\text{-Cl})(\mu\text{-OEt})$ where a dissociative mechanism is applied for LA polymerization to produce atactic PLA, the mechanism of LA polymerization with (\pm)- $[(\text{NNO}_{\text{tBu}})\text{InCl}]_2(\mu\text{-Cl})(\mu\text{-OEt})$ (**5**) does not involve dissociation. Thus, the selectivity observed for complex (\pm)-**5** is a result of its dinuclear nature.

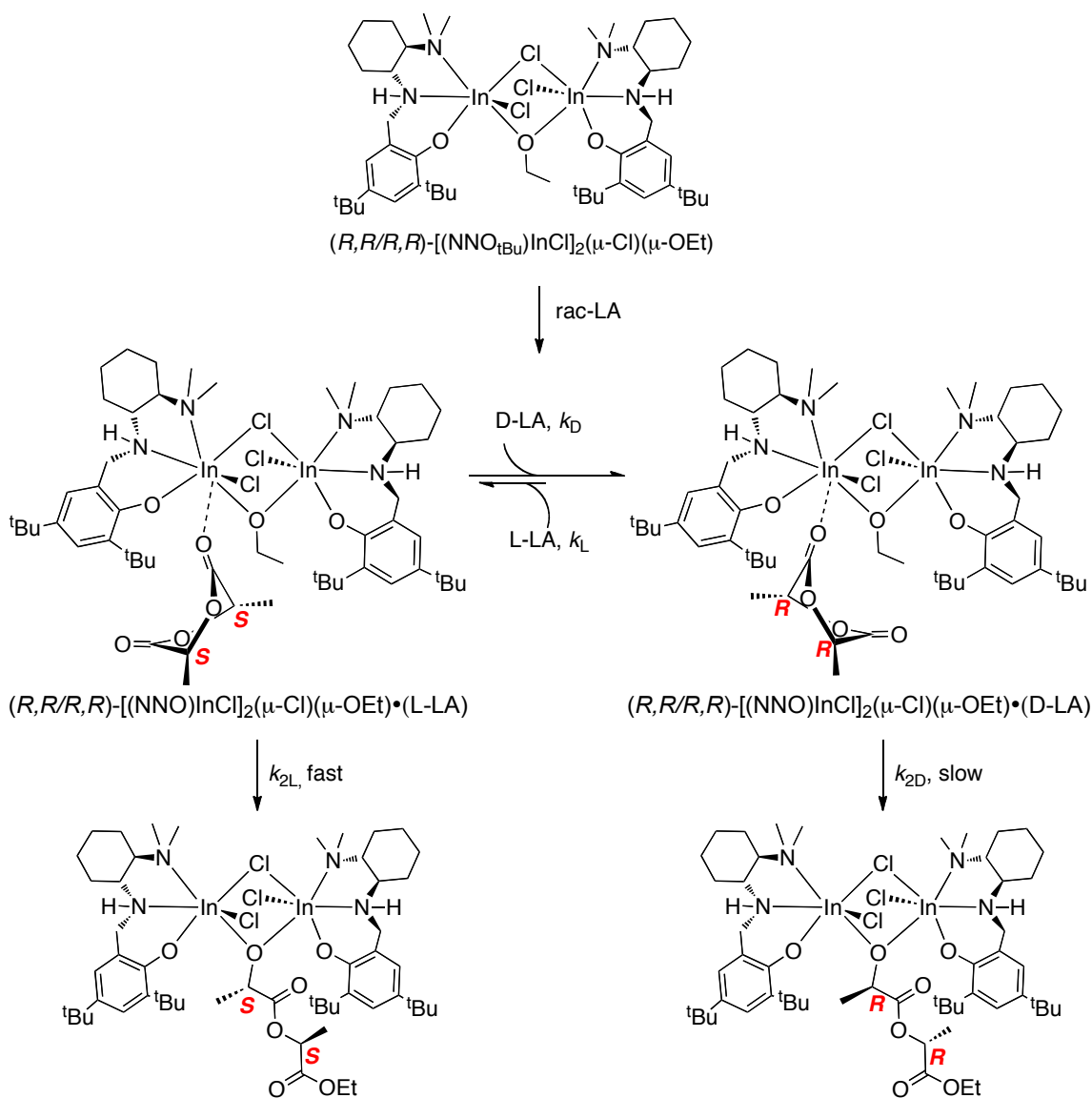
4) *The mono- and bis alkoxy complexes show different selectivities for the ROP of lactide.*

One of the most striking pieces of evidence for the dinuclear nature of the propagating species is the difference of selectivities observed for complexes (\pm)-**5** and meso-**8**. If the propagating species is a mononuclear alkoxide, then these complexes should have identical selectivities. A comparison of polymerization rates with (*R,R/R,R*)-**5** (**Table 3.3**, entry 5) and (*R,R/R,R*)-**8** (**Table 3.4**, entry 5) shows P_m values of 0.48 and 0.65, respectively. Indeed, the different k_{rel} values for **5** and **8** (14 vs 2), and the general independence of selectivity on catalyst chirality for complex **8**, indicates that the two catalysts cannot have identical propagating species. The different solution structures of the dinuclear complexes, matched by the solid state structures, are a strong justification for their different selectivities. The non-linear nature of the dependence of the observed rate constant on enantiopurity of **5** (**Figure 3.18a**) also supports a dinuclear propagating species.

These observations lead us to propose an alternate mechanism for the ring opening polymerization of lactide by our dinuclear catalysts. It is clear that ethoxy-bridged dinuclear indium complexes $[(\text{NNO}_{\text{R}})\text{InX}]_2(\mu\text{-OEt})(\mu\text{-Y})$ ($\text{X} = \text{Cl, I}$; $\text{Y} = \text{Cl, I, OH, OEt}$) remain dinuclear during the ROP of LA. However, our studies show that the mechanism depicted in **Scheme 3.2B** is too simplistic to explain the selectivities observed for this system. In particular, there is a high k_{rel} value for polymerization of L-LA compared to D-LA with

(*R,R/R,R*)-**5**, however, the polymer obtained in the polymerization of rac-LA with this catalyst is atactic.

An alternate mechanism that explains this phenomenon involves two competing rates: the rate of coordination of L- and D-LA to the catalyst (k_L and k_D) and the rates of propagation of these monomers (k_{2L} and k_{2D}) (**Scheme 3.4**). We know that k_{2L}/k_{2D} is 14 for (*R,R/R,R*)-**5**. However, these values were determined using enantiopure catalyst and enantiopure monomer. When *racemic* lactide is added, there will be a competition between coordination of D- or L-LA to (*R,R/R,R*)-**5**. We propose that $k_D > k_L$ and that the equilibrium favors the formation of the adduct (*R,R/R,R*)-**5**•D-LA, which goes on to ring open D-LA. If the rates k_D and k_{2L} are on the same order, we would expect an equal incorporation of L- and D-LA into the polymer to form atactic PLA. This mechanism is compatible with the non-linear decrease in the polymerization rate for rac-LA with increasing enantiopurity of catalyst (**Figure 3.19a**). We are assuming that for ROP of rac-LA with (*R,R/R,R*)-**5** chain end control is surpassed by the high selectivity of the catalyst. With (\pm)-**5** and with all isomers of **8**, chain end control dominates to yield similar P_m values (~ 0.6).



Scheme 3.4. Competing coordination and ring opening in the reactivity of $(R,R/R,R)$ -**5** with rac-LA.

In this work we studied the polymerization behavior and selectivity of chiral alkoxy-bridged dinuclear indium complexes for the ring opening polymerization of lactide. We were able to show that the complexes remain dinuclear during lactide polymerization, with a stable dinuclear polymeryl-bridged steady state that resists chain termination and leads to a highly controlled system. The dinuclear nature of the chiral catalyst has a significant effect on the stereoselectivity of the catalysts and will impact the design of future indium-based catalysts.

3.4 Experimental section

Representative NMR scale polymerization with 5, 6, 7, 8 and 10. A teflon-sealed NMR tube was charged with a 0.25 mL solution of a catalyst stock solution (0.25 mL, **5, 6, 7, 10**: 0.0091 M, 0.0023 mmol; **8**, 0.00228 M, 0.00057 mmol) in CDCl₃ and made up to 0.5 mL with 0.25 mL of CDCl₃, and the solution was mixed and frozen in the glovebox using a liquid N₂ cold wall. A stock solution of rac-lactide (0.91 M, 0.46 mmol for **5, 6, 7, 10**; 0.228 M, 0.114 mmol for **8**) and an internal standard 1,3,5-trimethoxybenzene (5 mg, 0.03 mmol for **5, 6, 7, 10**; 1.2 mg, 0.0075 mmol for **8**) in 0.5 mL of CDCl₃ was added to the frozen complex solution and frozen again, forming a bilayer. The NMR tube was sealed and quickly evacuated by vacuum to remove N₂ gas from the NMR tube. The two solutions were thawed and quickly mixed before the NMR tube was loaded into the NMR spectrometer (400MHz Avance Bruker Spectrometer). The polymerization was monitored to 90% conversion.

Representative large-scale polymerization with complex 5. A 20 mL scintillation vial was charged with a solution of complex **5** (1.0 mg, 0.00091 mmol) in 2 mL CH₂Cl₂. A solution of rac-lactide (131 mg, 0.91 mmol) in 2 mL of CH₂Cl₂ was added dropwise to the vial. The resulting mixture was stirred at room temperature for 16 h. The resulting clear solution was concentrated to dryness. A sample of the residue was dissolved in CDCl₃ to be analyzed by ¹H NMR spectroscopy to determine conversion. The remaining polymeric material was dissolved in a minimum amount of CH₂Cl₂ (1 mL) and added to cold wet methanol (0 °C, 7 mL). The polymer precipitated from solution and was isolated by centrifugation. The supernatant was decanted and the polymer was dried under high vacuum for 2 h prior to analysis.

Procedure for *in situ* crossover between 3 and 5. ¹H NMR spectroscopy (400 MHz NMR spectrometer, CD₂Cl₂ at room temperature) was used to monitor the crossover of complexes **3** and **5**. In a glovebox, a solution of complex **3** (0.5 mL, 0.0045 M) was loaded into a teflon-sealed NMR tube and frozen in a liquid N₂ cold well (−90 °C). A solution of complex **5** (0.5 mL, 0.0046 M) was added to the frozen solution of complex **3** and frozen again, forming a bilayer. The two solutions were thawed and quickly mixed before the NMR tube was loaded into the NMR spectrometer.

Representative large-scale polymerization of rac-lactide using mixtures of **5 and **1**.** A 20 mL scintillation vial was charged with a solution of rac-lactide (129.3 mg, 0.92 mmol) in 3 mL of CH₂Cl₂. A solution consisting of complex **5** (5 mg, 0.0046 mmol) and **1** (2.5 mg, 0.0046 mmol) in 2 mL CH₂Cl₂ was added to the vial and the resulting mixture was stirred at room temperature for 16 h. The resulting clear solution was concentrated to dryness. A sample of the residue was dissolved in CDCl₃ to be analyzed by ¹H NMR spectroscopy to determine conversion. The remaining polymeric material was dissolved in a minimum amount of CH₂Cl₂ (1 mL) and added to cold wet methanol (0 °C, 7 mL). The polymer precipitated from solution and was isolated by centrifugation. The supernatant was decanted and the polymer was dried under high vacuum for 2 h prior to analysis.

Representative polymerization for variable conversions of rac-LA with (*R,R/R,R*)-5** at 0°C.** A Schlenk flask (a bomb flask) was charged with 0.25 mL of catalyst stock solution (0.25 mL, **5**: 0.0032 M, 0.0008 mmol) in CH₂Cl₂ and made up to 0.5 mL with 0.25 mL CH₂Cl₂, and the solution was mixed and frozen in the glovebox using a liquid N₂ cold wall. A stock solution of rac-lactide (0.32 M, 0.398 mmol) in 1.25 mL of CH₂Cl₂ was added to the frozen complex solution and frozen again, forming a bilayer. The Schlenk flask was sealed and the two solutions were thawed and quickly mixed before the flask was immersed into an ice bath to maintain the reaction temperature at 0°C. At a certain time the resulting clear solution was concentrated to dryness. A 1 mL solution of HCl (1.5 M HCl in Et₂O) was added to the reaction mixture to quench the polymerization and the solvents were removed under vacuum. The sample of the residue was dissolved in CDCl₃ to be analyzed by ¹H NMR spectroscopy (600 MHz) to determine conversion and tacticity of the resulting polymer.

Chapter 4: Cationic Chiral Indium Complexes and Their Role in Polymerization of Polar Conjugate Monomers³

4.1 Introduction

The third chapter demonstrates the synthesis and characterization of new chiral neutral and cationic indium(III) complexes possessing a chiral diaminophenolate ligand. These complexes show catalytic polymerization of polar vinyl monomer.

4.1.1 Cationic indium complexes

Cationic group 13 metal complexes (Al, Ga, In, Tl)^{24,25} provide a unique challenge: their highly Lewis acidic nature makes them potentially excellent candidates for a myriad of reactions including those performed with neutral group 13 complexes^{26,27}, yet they have been found to be unreactive in all but a handful of catalytic applications.²⁵ Examples of reactivity include the polymerization of isobutene,²⁹⁴ ethylene,^{295,296} alkene oxide^{297,298} and rac-lactide²⁹⁹ as well as the dimerization of terminal alkynes,^{300,301} and these examples are dominated by aluminum cations. Among group 13 cations four-coordinate cations are the most common due to an electronically saturated metal center, which adopts its preferred tetrahedral geometry.²⁵ In particular, recent interest in four-coordinate Al alkyl cationic species¹ with various geometries incorporating mono- and/or bidentate ligands has been growing, as they appear to possess not only good stability but also a highly Lewis acidic nature in catalytic polymerization of polar conjugated monomers,³⁰² epoxides³⁰³ and cyclic esters³⁰².

³ Synthesis and single crystal X-ray crystallographic characterization of the indium complex (NNO_{tBu})InMe₂ of **Chapter 3** has been published in the journal *Inorganic Chemistry*.³

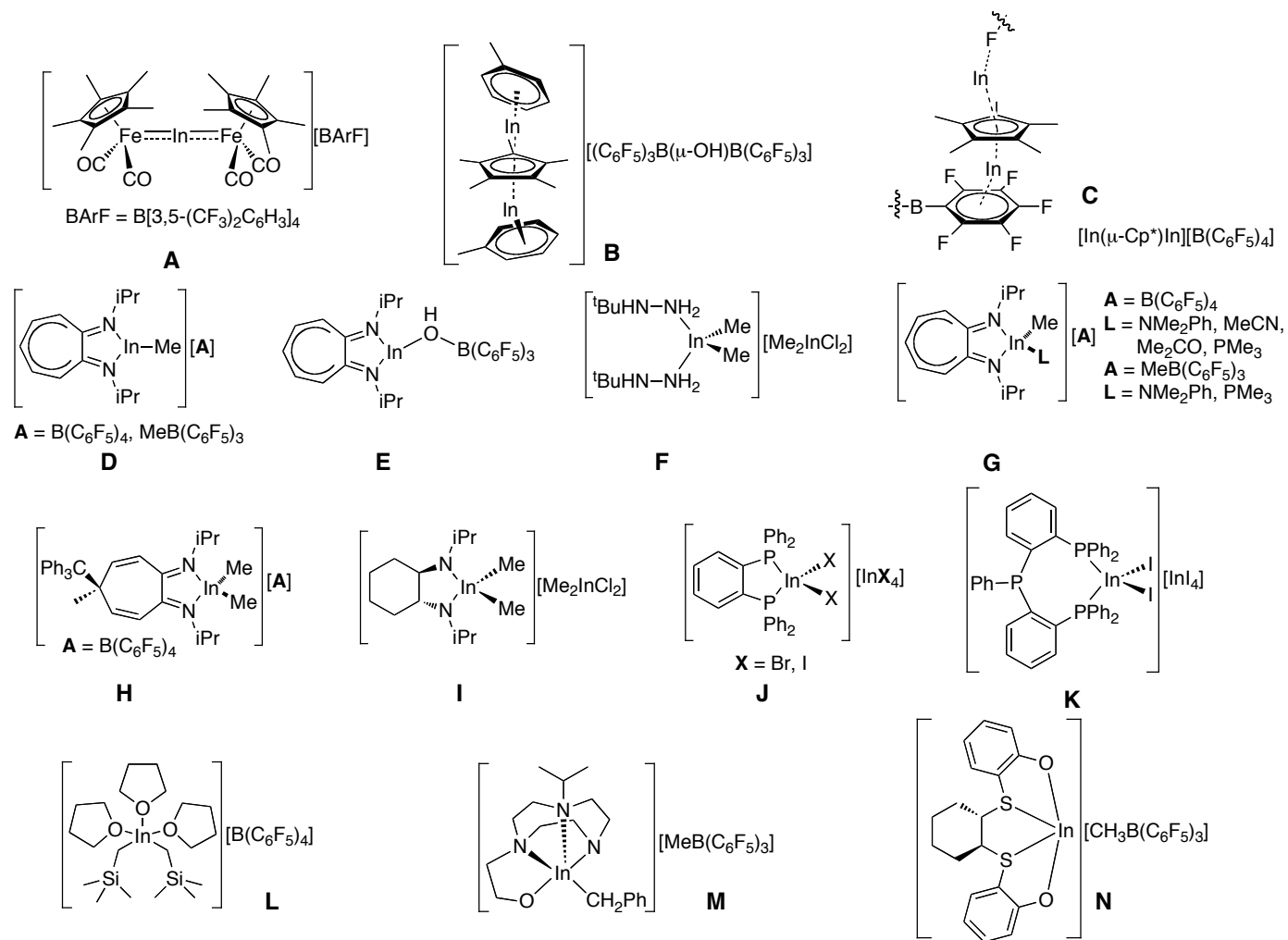


Figure 4.1. Reported cationic indium complexes. 304-306,307-314

To date, only a handful of cationic In(I) complexes **A-C**³⁰⁴⁻³⁰⁶ and In(III) complexes **D-N**³⁰⁷⁻³¹⁴ with different coordination modes have been reported in the literature (**Figure 4.1**). Group 13 cations can be generated via halide displacement and abstraction, asymmetric disproportionation, alkyl and hydride abstraction, and protonolysis reactions. The methods reported for generation of cationic indium species^{307-309,314} (**D**, **G**, **L**, **M** and **N**) are alkyl abstraction and protonolysis reactions with a strong Lewis acid, such as [HNMe₂Ph][B(C₆F₅)₃] and B(C₆F₅)₃. In particular, diaminotropolone cationic type **G**³¹⁴ complexes, which are generated via protonation reactions with anilinium salts, are isolated with dimethyl aniline coordinated to the metal center. In contrast, there are no reports of coordination of bulky “non-coordinating” counter anions, such as [B(C₆H₃(CF₃)₂)₄]⁻ (BArF) and B(C₆F₅)₄, to highly electrophilic group 13 metal centers. However, there are a few examples that show coordination between a metal and a fluorinated counter anion, such as (Cp*)₂Th(Me)(B(C₆F₅)₄), which shows two Th-F bonds bridging via the lone pairs of the fluorine atoms as seen by X-ray crystallography³¹⁵ and (Cp*)₂Zr(Me)(B(*p*-C₆H₄F)₄), which contains a single Zr-F bridge, proven by ¹⁹F NMR spectroscopy.³¹⁶

Due to the increasing use of In(III) species in catalysis,^{17-22,70-79} developing highly Lewis acid cationic In(III) complexes has become an attractive target in academia, although it has not yet become industrially relevant. To the best of our knowledge, the few of cationic indium complexes reported to date are unreactive or have not yet been reacted with potential nucleophilic substrates. The only exception is (N-isopropyl-2-(isopropylamino)troponimino) methyl indium cation **D**, which has shown trace activity for polymerization of isobutylene.³¹⁴

4.1.2 Poly(methyl methacrylate) (PMMA)

Due to its unique physical and mechanical properties, poly(methyl methacrylate) (PMMA) is used in numerous applications in the building, transportation, agricultural, textile, paper and paint industries.²⁸ In particular, the use of PMMA in biomedical applications is increasing due to its biocompatibility with no record of severe adverse effects. PMMA is routinely generated from methyl methacrylate (MMA) by radical,³¹⁷⁻³¹⁹ anionic³²⁰⁻³²² or coordination polymerization.³²³ The general method used in industry is radical

polymerization of MMA to atactic and completely amorphous PMMA.³¹⁹ However, under extremely low temperatures, highly syndiotactic PMMA can also be generated by radical polymerization, which is more desirable in most applications due to its superior mechanical properties compared to isotactic and atactic PMMA.²⁸

The most important properties of a given polymer are thermal properties, melting temperature (T_m) and glass transition temperature (T_g).^{28,324,325} T_m is a temperature where a solid turns into a liquid. Glass transition temperature (T_g), where a glassy polymer, typically hard and brittle below T_g , starts to become more comparable to rubber (described in Chapter 2). PMMA known as acrylic glass and a lightweight, shatter-resistant alternative to traditional glass is very important and attractive for some applications such as use in the optical electronic industry due to its high optical clarity, but it is not very suitable in some uses due to its brittleness.²⁸ T_g is one of the important parameters to characterize PMMA because it is influenced by the microstructure and tacticity of the polymer ($T_g = 130$ - 165 °C, 105 °C and ~ 45 °C for syndiotactic, atactic and isotactic PMMA, respectively).³²⁴ Along with the high stereoregularity of PMMA T_g increases as its molecular weight with narrow molecular weight distributions increases.³²⁴

A number of metallocene catalysts catalyze the living polymerization of MMA to high molecular weight, highly syndiotactic and isotactic PMMA.^{262,323,326-341} Polymerization of polar vinyl monomers has two requirements:³²³ that the initiator attacks the vinyl group of the monomer and attaches to the monomer at the β position of the polymer chain via conjugate Michael addition and that the catalyst is Lewis acidic enough to activate the monomer through monomer coordination to the metal center. Unlike other types of polymerization, namely free radical, cationic, and anionic polymerization,²⁸ the initiator is often not defined clearly in metal-mediated coordination polymerization as one metal center can function as both initiator and catalyst.³²³

Two major mechanistic categories exist in metal-mediated coordination polymerization of polar vinyl monomers.³²³ The first category is monometallic polymerization where one metal center acts as both initiator and catalyst (**Figure 4.2a**). Polymerization of MMA with the neutral dimeric Sm complex $[(C_5Me_5)_2SmR]_2$ ($R =$ hydride H^- or alkyl) falls into this category.³⁴² The first step is to activate the monomer via metal-monomer coordination where MMA coordinates to the highly electrophilic samarium center. Then, chain initiation

involves nucleophilic attack of the initiator (R = hydride or alkyl) on the carbonyl carbon of the activated MMA, followed by intramolecular conjugate Michael addition to form an eight-membered cyclic ester enolate chelating intermediate. Chain propagation continues through repeated conjugate Michael additions of new monomer to the enolate in the eight-membered ring propagating species (**Figure 4.2a**). The second category involves bimetallic polymerization where two metals act as initiator and catalyst, respectively (**Figure 4.2b**). One metal center (Lewis acid) is used to activate the incoming monomer via metal-monomer coordination while a second metal center acts as an initiator in a conjugate attack. In this category, a neutral zirconocene is typically paired with a cationic zirconocenium complex, as initiator and catalyst, respectively.³³⁸ Chain propagation proceeds via repeated intermolecular conjugate Michael addition of the enolate coordinated to the neutral zirconocene complex onto the monomer coordinated to the cationic zirconocene complex, forming a dinuclear ester enolate bridged zirconocene complex as an intermediate propagating species (**Figure 4.2b**).

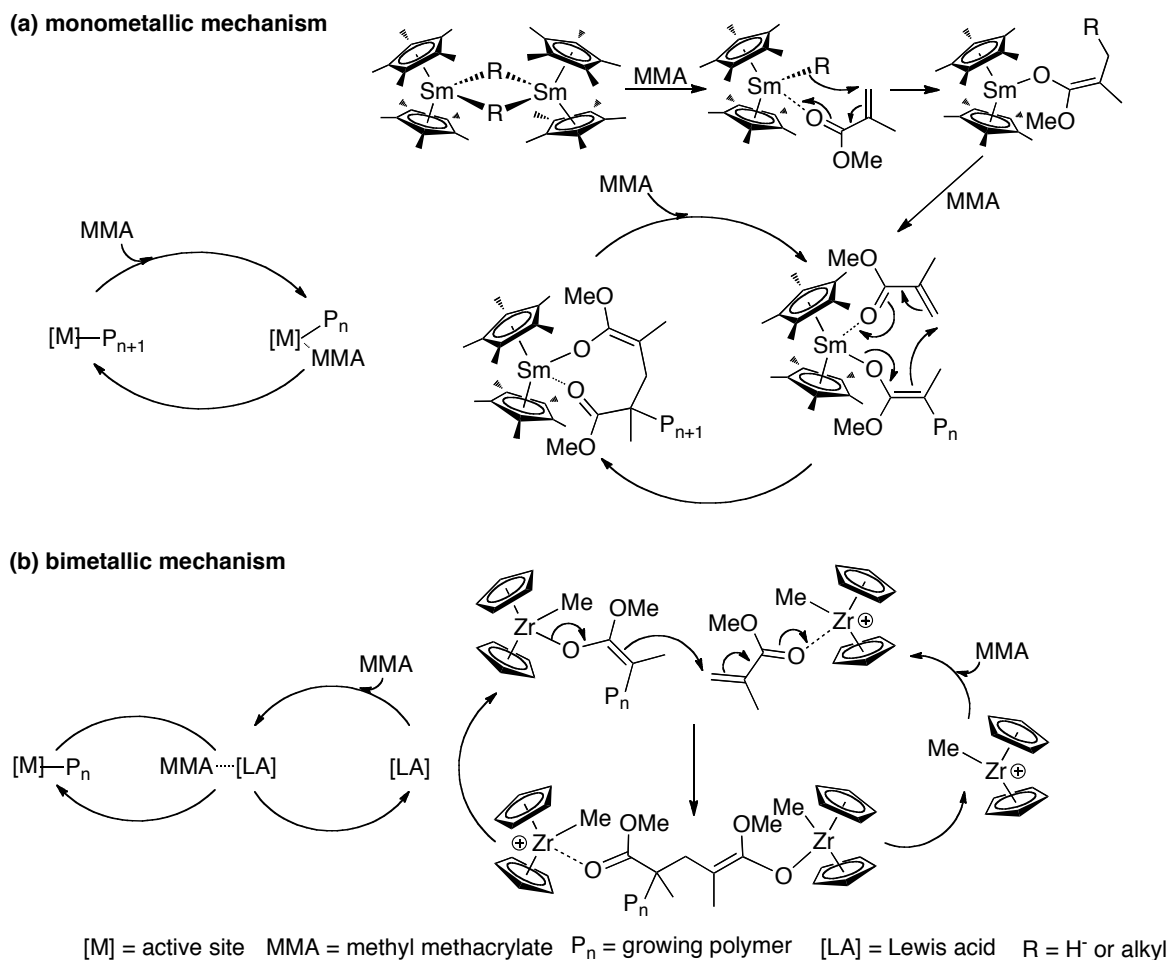


Figure 4.2. Schematic illustrations of two categories of metal-catalyzed MMA polymerization: (a) monometallic mechanism; (b) bimetallic mechanism.^{323,338,342}

Chen *et al.* reported the first example of enantiomeric site controlled polymerization of MMA.^{328,343} Their precatalyst, a neutral zirconocene mono(ester enolate) (Figure 4.3. left), was activated by a strong Lewis acid, B(C₆F₅)₃, to generate the cationic active catalyst by methide abstraction. The catalyst with the C₁-symmetric ligand has good activity (TOF (h⁻¹) = 807, 25 °C in CH₂Cl₂ or toluene) for MMA polymerization and produces highly syndioselective PMMA (rr = 94%). There is no significant change in stereoselectivity even at higher temperature (rr = 93%, 50 °C).

Furthermore, Chen's group has investigated the kinetics and mechanism of MMA polymerization in these catalytic systems and proposed a monometallic, conjugate addition mechanism.^{343,344} The propagation step proceeds via the formation of an eight-membered cationic intermediate (**III**) through an intramolecular Michael addition, and followed by

displacement of the coordinated ester group by an incoming MMA molecule to give the monomer-enolate complex (II) (Figure 4.4). The ring opening of the chelate by MMA addition is considered to be the rate-determining step while the eight-membered cationic intermediate (III) is proposed as a resting state.

Chen and coworkers were able to isolate the eight-membered cationic intermediate (active catalyst) by hydride abstraction from the bis(ester enolate) zirconocene complex using $B(C_6F_5)_3$.^{329,344} After further investigation of the correlation between the structural symmetry of the catalysts and stereoselectivity, they also reported a neutral zirconocene bis(ester enolate) with a C_2 -symmetric ligand. Recently, the Chen group has reported that cationic zirconocene catalysts polymerize renewable methylene butyrolactones (naturally produced α -methylene- γ -butyrolactone (MBL) and plant biomass-derived γ -methyl- α -methylene- γ -butyrolactone) to highly isotactic polymer (mm = >99%, 25 °C in CH_2Cl_2).^{345,346} Surprisingly, there are no reports on polymerization of vinyl monomers with metallocene catalysts in neat monomer.

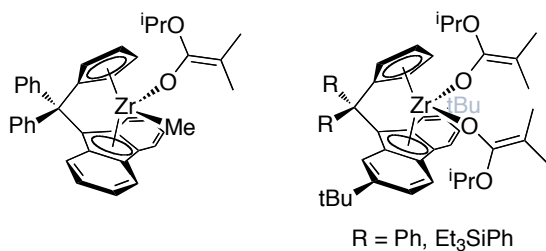


Figure 4.3. Highly stereoselective catalysts for PMMA.

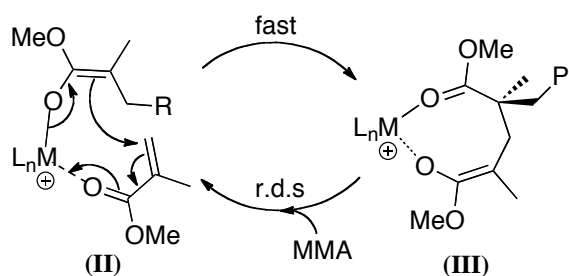


Figure 4.4. Proposed propagation cycle in the coordination-addition mechanism of MMA polymerization with zirconocene mono- and bis(ester enolate) complexes by Chen and coworkers.

There are a few examples of cationic group 13 complexes reported for polymerization of MMA yielding highly syndiotactic polymers (**Figure 4.5**).^{300,302,347,348} However, there is only one four-coordinate mononuclear aluminum complex **R** that converts MMA to syndiotactic PMMA.³⁴⁷ Although the authors stated the reactivity of this complex, there is no detailed information of polymerization conditions and molecular weights of the resulting polymer present in the literature. Surprisingly, some dinuclear aluminum species **O**, **P**, and **Q** exhibit good reactivity for MMA polymerization due to their rapid dissociation by Lewis bases such as polar vinyl monomers.^{300,302,348} This suggests dinuclear indium cationic species can be good candidates for MMA polymerization although they possess the higher tendency of aggregation compared to aluminum complexes (described in Chapter 1). Two neutral four-coordinate mononuclear aluminum complexes, **S** with a porphyrin ligand³⁴⁹ and **T** with a Schiff base ligand,³⁵⁰ show catalytic polymerization of MMA with very low activity (TOF = 8.3 h⁻¹ and 0.8 h⁻¹ for **O** and **P**, respectively). However, these neutral species become much more active with the addition of organoaluminium reagents as Lewis acid activators. For instance, the rate of MMA polymerization with the porphyrin aluminium complex **S** is greatly enhanced up to factors of tens of thousands with the addition of 3 equivalents of an aluminum phenoxide, MeAl(2,6-^tBu₂C₆H₃O)₂.^{351,352} This dramatic rate increase is due to monomer activation by the aluminum phenoxide additive, which causes the acceleration of the nucleophilic attack of the initiator from the Al center onto the activated monomer, similar to the bimetallic catalytic system described above.

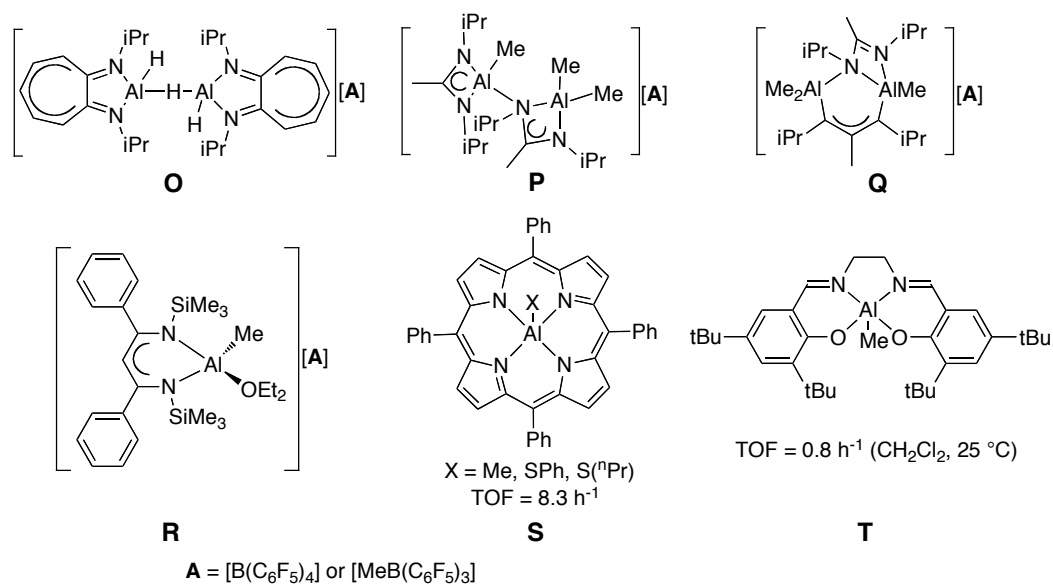
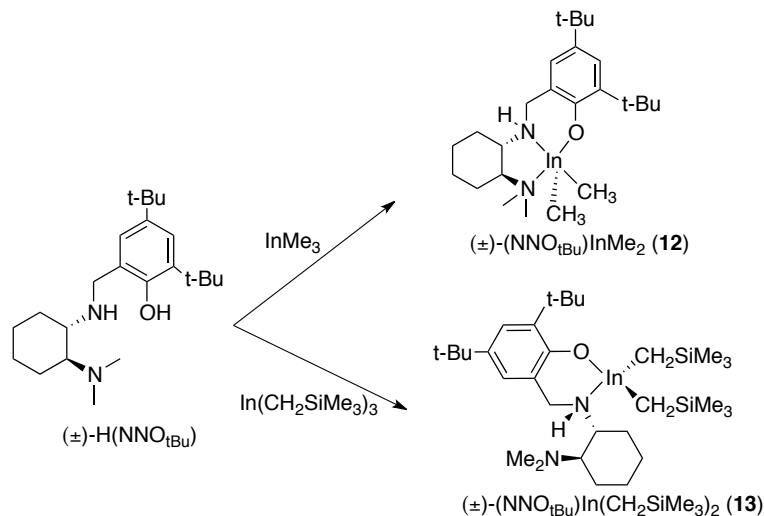


Figure 4.5. Cationic and neutral discrete mononuclear aluminum complexes for MMA polymerization.^{300,302,347-350}

In addition to the work presented in Chapter 2 of this thesis, the Mehrkhodavandi group has recently reported that neutral indium alkoxide complexes are excellent catalysts for the controlled ring opening polymerization of other cyclic esters such as caprolactone and β -butyrolactone.^{23,353} We wanted to expand the range of monomers to other polar monomers. In this chapter we discuss the synthesis and characterization of a family of cationic complexes. We also present a very rare example of catalysis by a cationic In(III) complex and show that indium cations supported by chiral diaminophenolate ligands exhibit catalytic activities for the polymerization of polar conjugated alkenes, such as methyl methacrylate (MMA).

4.2 Results and discussion

4.2.1 Synthesis and characterizations of neutral and cationic indium alkyl complexes



Scheme 4.1. Synthesis of neutral dialkyl indium complexes $(\text{NNO}_{t\text{Bu}})\text{InMe}_2$ (**12**) and $(\text{NNO}_{t\text{Bu}})\text{In}(\text{CH}_2\text{SiMe}_3)_2$ (**13**).

Neutral alkyl indium complexes were synthesized via protonolysis reactions between InR_3 (InMe_3 purchased or formed *in situ* from InCl_3 and methyl lithium,³⁵⁴ and $\text{In}(\text{CH}_2\text{SiMe}_3)_3$ generated *in situ* from InCl_3 and $(\text{Me}_3\text{SiCH}_2)\text{MgCl}$)³⁵⁵ and the racemic proligand $\text{H}(\text{NNO}_{t\text{Bu}})$ (**Scheme 4.1**). Reaction of InMe_3 with $\text{H}(\text{NNO}_{t\text{Bu}})$ yields the dimethyl species **12**, $(\text{NNO}_{t\text{Bu}})\text{InMe}_2$, in 85% purified yield. The ^1H NMR spectrum (C_6D_6) of **12** shows characteristic multiplets for the methylene backbone of the coordinated $\text{NNO}_{t\text{Bu}}$ at 4.00 and 3.08 ppm, as well as two singlets for the indium-bound methyl groups at 0.12 and -0.03 ppm (**Figure 4.7a**). Crystals of **12** suitable for X-ray diffraction were obtained from diethyl ether at -35 °C in 16 hours. The solid-state structure shows a distorted square-pyramidal geometry around the indium center with the tridentate ligand bound meridionally (**Figure 4.6**). The N1-In1 bond length (2.503(2) Å) is slightly longer than the N2-In1 distance (2.355(2) Å), likely due to the presence of the sterically hindered tertiary amine. The In-C1 and In-C2 distances, 2.161(2) and 2.150(2) Å, respectively, are similar to those of related methyl indium complexes (In-C bond length = 2.14 Å in $[(1,3\text{-dithiapropanediyl-bis}(6\text{-}t\text{-butyl-4-methyl-phenolate))\text{InMe}(\text{THF})]$;⁸⁷ In-C bond length = 2.15 Å in $(1,3\text{-diphenyltriazeno})(3,5\text{-Me}_2\text{py})\text{InMe}_2$ ³⁵⁶; In-C bond length = 2.16 Å in $\text{bis}(2\text{-}(\text{benzylamino})\text{pyridyl})\text{InMe}$ ^{87,354}).

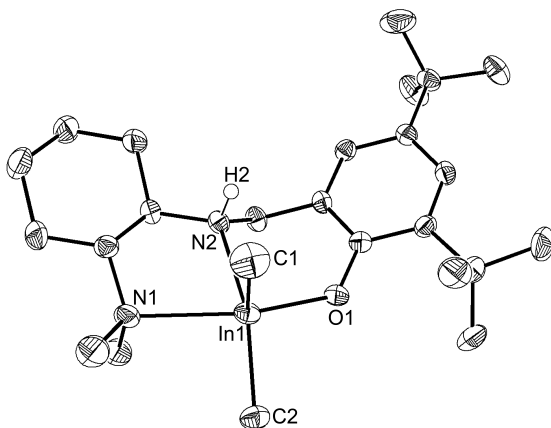


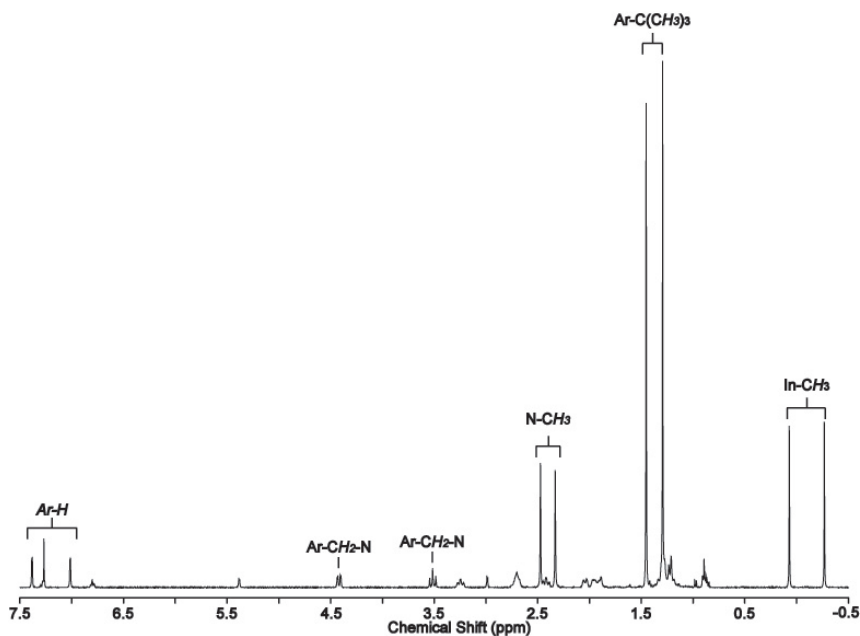
Figure 4.6. Molecular structure of **12** (depicted with thermal ellipsoids at 50% probability and most H atoms omitted for clarity).

Table 4.1. Selected distances (Å) and angles (°) for complex **12**.

12				
Bond Lengths	In1-N1	2.503(2)	In1-C2	2.150(2)
	In1-N2	2.3549(18)	In1-O1	2.1521(15)
	In1-C1	2.161(2)		
Bond Angles	N1-In1-N2	71.20(6)	N1-In1-C1	100.51(9)
	O1-In1-N2	80.66(6)	N2-In1-C1	96.17(9)
	O1-In1-C2	91.41(8)	O1-In1-C1	108.15(9)
	C2-In1-N1	91.15(8)	C1-In1-C2	127.15(10)

The dialkyl complex **13** ($\text{NNO}_{\text{tBu}}\text{In}(\text{CH}_2\text{SiMe}_3)_2$) was synthesized in a similar manner from $\text{In}(\text{CH}_2\text{SiMe}_3)_3$ and the proligand $\text{H}(\text{NNO}_{\text{tBu}})$ in diethyl ether and obtained as a white solid in a 78% crystallized yield (**Scheme 4.1**). Unlike complex **12** ($\text{NNO}_{\text{tBu}}\text{InMe}_2$), the ^1H NMR spectrum of the complex **13** (CDCl_3) shows two sets of resonance signals (**Figure 4.7b**); thus, characteristic multiplets for the methylene protons of the ancillary ligand (NNO_{tBu}) appeared in the range from 3.0 to 4.5 ppm as well as multiplet and singlet peaks for the methylene and methyl protons of a trimethylsilyl methyl group, respectively, in the range from -0.22 to 0.02 ppm. However, the interesting finding in the ^1H NMR spectrum of complex **13** is that there are only two singlets for the methyl protons on the tertiary nitrogen at 2.20 ppm and 2.23 ppm, respectively, instead of four singlets which were expected to appear, considering the existence of two singlets for complex **12** at 3.32 ppm and 3.46 ppm, respectively (**Figure 4.7**).

(a)



(b)

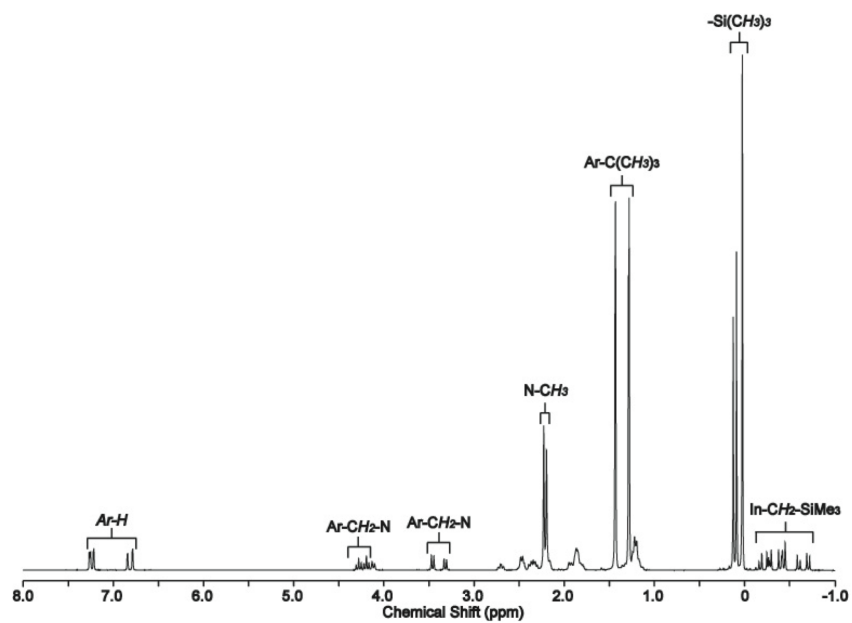


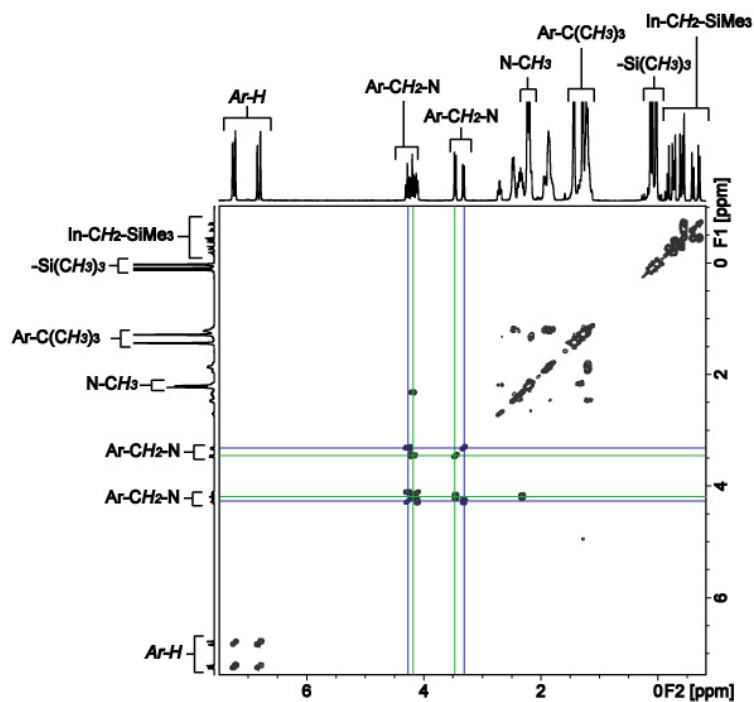
Figure 4.7. ¹H NMR spectrum of (a) (NNO_{tBu})InMe₂ (**12**) and (b) (NNO_{tBu})In(CH₂SiMe₃)₂ (**13**) (400 MHz, CDCl₃, 25 °C).

We conducted further solution studies of complex **13** (NNO_{tBu})In(CH₂SiMe₃)₂ to confirm the correlations between proton signals by 2D NMR spectroscopic experiments (¹H-¹H COSY and ¹H-¹H NOESY) (Appendix C). The 2D NMR spectroscopic studies suggest there

is a mixture of two compounds, and the resonance signals of each compound are not correlated to each other. Thus, the ^1H - ^1H COSY spectrum shows that one set of the methylene protons at 3.32 ppm and 4.31 ppm on the ancillary ligand has only one correlation between these two protons that are coupled to each other, and the ^1H - ^1H NOESY spectrum also shows the correlation between these protons through space (**Figure 4.8**). In addition, the two methyl resonance signals of the tertiary amine, with integrals of six protons respectively, are not correlated to each other in space. This suggests the tertiary amine may not be coordinated to the indium center, which causes the equivalent chemical shift of the two methyl groups due to free rotation.

All the solution analyses indicate that two inequivalent diastereomers of complex **13** are present in solution, which is in contrast to the dialkyl complex **12** (NNO_{tBu}) InMe_2 as well as the dihalide complexes (NNO_{tBu}) InX_2 ($\text{X} = \text{Cl}, \text{I}$) that show only a mixture of two enantiomers in solution, when synthesized from the racemic proligand $\text{H}(\text{NNO}_{\text{tBu}})$.

(a)



(b)

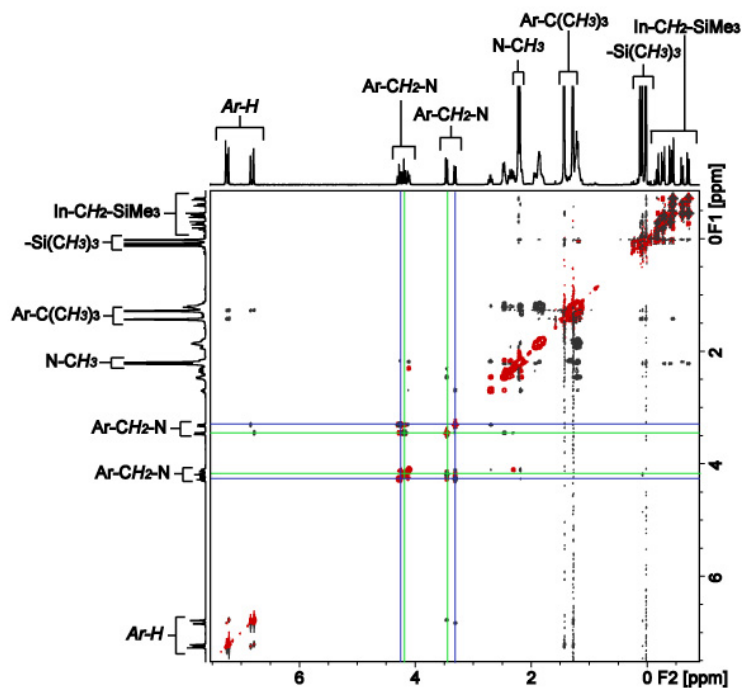


Figure 4.8. (a) ^1H - ^1H COSY and (b) ^1H - ^1H NOESY (optimized mixing time: 400 ms) spectra of $(\text{NNO}_{\text{tBu}})\text{In}(\text{CH}_2\text{SiMe}_3)_2$ (**13**) (400 MHz, CDCl_3 , 25 °C).

The solid-state structural analysis of complex **13** ($\text{NNO}_{\text{tBu}}\text{In}(\text{CH}_2\text{SiMe}_3)_2$) by single crystal X-ray diffraction revealed a distorted trigonal pyramidal indium centre with κ^2 -coordinated NNO_{tBu} , as opposed to the κ^3 -coordinated NNO_{tBu} ligand observed for complex **12**, likely due to the less bulky nature of the methyl groups in complex **12**. The different coordination of the ancillary ligand (NNO_{tBu}) to the indium center, κ^2 -coordination in complex **13** ($\text{NNO}_{\text{tBu}}\text{In}(\text{CH}_2\text{SiMe}_3)_2$) compared to κ^3 -coordination in complex **12** ($\text{NNO}_{\text{tBu}}\text{InMe}_2$) causes it to lose the enantiomeric nature of two isomers. This can explain the observation of two sets of resonances in the NMR spectra of complex **13**. In the crystal structure the two In-CR and the Ph-O atoms are in the plane of the indium atom and the central Cy-N atom is in the axial position. The average bond distance of In-CR (2.164 Å) in complex **13** is slightly shorter than that of the three-coordinate mononuclear complex $\text{In}(\text{CH}_2\text{SiMe}_3)_3$ (In-C = 2.18 Å)³⁰⁹ while the C24-In1-C28 bond angle (132.75(13)°) is larger (the average C-In-C bond angle = 118° in $\text{In}(\text{CH}_2\text{SiMe}_3)_3$)³⁰⁹ (**Figure 4.10**). There are only a few examples of neutral indium complexes with a CH_2SiMe_3 ligand as listed in **Figure 4.10**. Although those complexes have a different geometry at the indium center with different coordination environments, the In-CR bond length in complex **13** (2.164 Å) is similar to these complexes, which have In-CR bond lengths in the range of 2.12 – 2.16 Å (**Figure 4.10**).^{88,309,357}

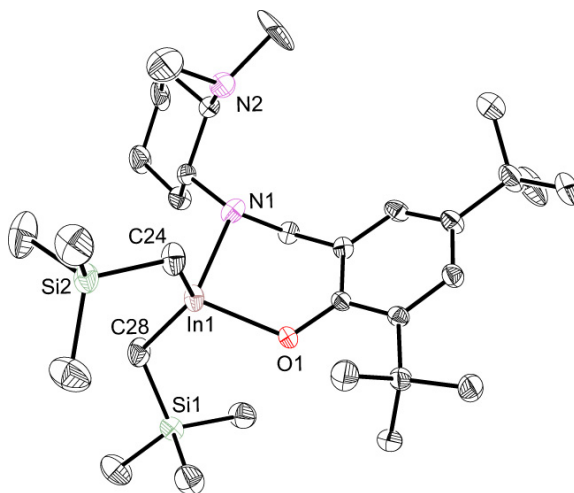
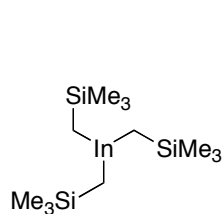


Figure 4.9. Molecular structure of complex **13** (depicted with ellipsoids at 50% probability and H atoms removed for clarity).

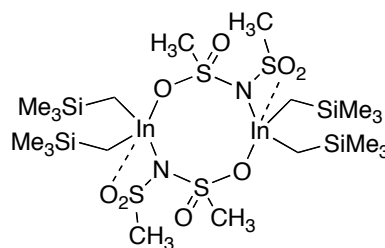
Table 4.2. Selected distances (Å) and angles (°) for complex **13**.

13				
Bond Lengths	In1-N1	2.275(3)	In1-C28	2.158(3)
	In1-C24	2.160(3)	In1-O1	2.107(2)
Bond Angles	O1-In1-C24	134.75(13)	O1-In1-N1	88.36(9)
	O1-In1-C28	106.65(11)	N1-In1-C24	101.28(11)
	C24-In1-C28	132.75(13)	N1-In1-C28	109.63(12)



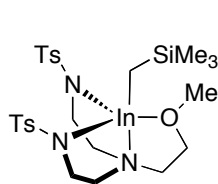
Okuda

Geometry	trigonal planar
Bond distance	In-C = 2.17-2.19 Å
Bond angle	C-In-C = 116-120 °



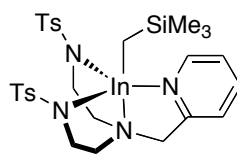
Blaschette

Geometry	distorted trigonal-bipyramidal
Bond distance	In-C = 2.12-2.13 Å
Bond angle	C-In-C = 134-150 °



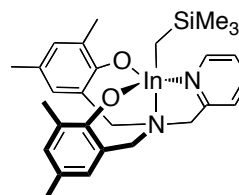
Mountford

Geometry	trigonal-bipyramidal
Bond distance	In-C = 2.13 Å
Bond angle	C-In-N _{axial} = 144 °



Mountford

Geometry	trigonal-bipyramidal
Bond distance	In-C = 2.14 Å
Bond angle	C-In-N _{axial} = 148 °



Mountford

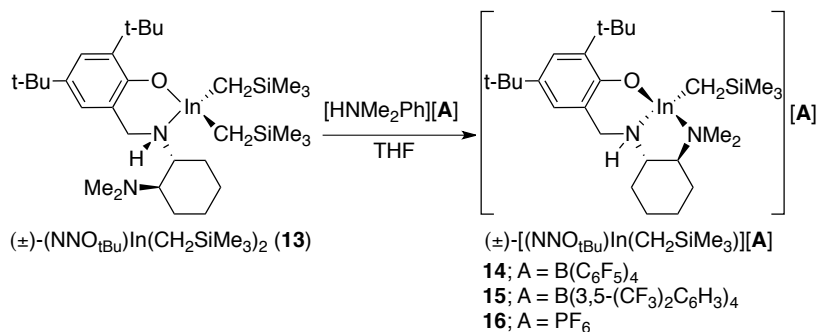
Geometry	square pyramidal
Bond distance	In-C = 2.16 Å
Bond angle	C-In-N _{axial} = 149 °

Ts = (4-methylphenyl)sulfonyl

Figure 4.10. Reported neutral alkyl indium complexes with a trimethylsilyl methyl group.^{88,309,357}

Initial attempts to generate cationic indium complexes from the dimethylindium complex **12**, (NNO_{tBu})InMe₂, with a strong Brønsted acid [HNMe₂Ph][A] (A = B(C₆F₅)₄, B(3,5-(CF₃)₂C₆H₃)₄ (BArF), PF₆) in THF were unsuccessful. This lack of reactivity may be due to steric constraints imposed by the κ^3 -coordinated geometry of **12** (NNO_{tBu})InMe₂ that does not allow the dimethylanilinium cation to come close enough to protonate the methyl group. In contrast, the κ^2 -coordinated complex **13** (NNO_{tBu})In(CH₂SiMe₃)₂ was reactive towards one

equivalent of $[\text{HNMe}_2\text{Ph}][\text{A}]$ ($\text{A} = \text{B}(\text{C}_6\text{F}_5)_4$, $\text{B}(3,5\text{-(CF}_3)_2\text{C}_6\text{H}_3)_4$ (BArF), PF_6) in THF at room temperature over 16 hours to produce the desired cationic complexes **14-16** via protonolysis of complex **13** with $[\text{HNMe}_2\text{Ph}][\text{A}]$. The ^1H NMR spectrum of a crude reaction mixture from complex **13** with $[\text{HNMe}_2\text{Ph}][\text{B}(\text{C}_6\text{F}_5)_4]$, for example, shows signals for the byproducts of the reaction, NMe_2Ph and SiMe_4 (**Figure 4.11**), suggesting the respective cationic complex **14** $[(\text{NNO}_{\text{tBu}})\text{In}(\text{CH}_2\text{SiMe}_3)][\text{B}(\text{C}_6\text{F}_5)_4]$ was formed. All the cations **14-16** were identified on the basis of ^1H , ^{13}C , ^{19}F , ^{31}P NMR spectroscopy and 2D NMR spectroscopic experiments (^1H - ^1H COSY, ^1H - ^1H NOESY at the optimized mixing time of 400 ms, ^1H - ^{13}C HMQC, ^1H - ^{13}C HMBC shown in Appendix C). The most striking finding from NMR spectroscopic analysis is that only one set of resonance signals is observed for all three cations generated from the neutral κ^2 -coordinated complex **13** $(\text{NNO}_{\text{tBu}})\text{In}(\text{CH}_2\text{SiMe}_3)_2$, which itself exhibits two sets of resonance signals in its NMR spectra, suggesting that the chemical shifts for both isomers are identical. This is consistent with the κ^3 -coordinated complex **12** $(\text{NNO}_{\text{tBu}})\text{InMe}_2$ as well as the κ^3 -coordinated dihalide indium complexes shown in Chapter 2.



Scheme 4.2. Synthesis of cationic indium complexes **14-16**.

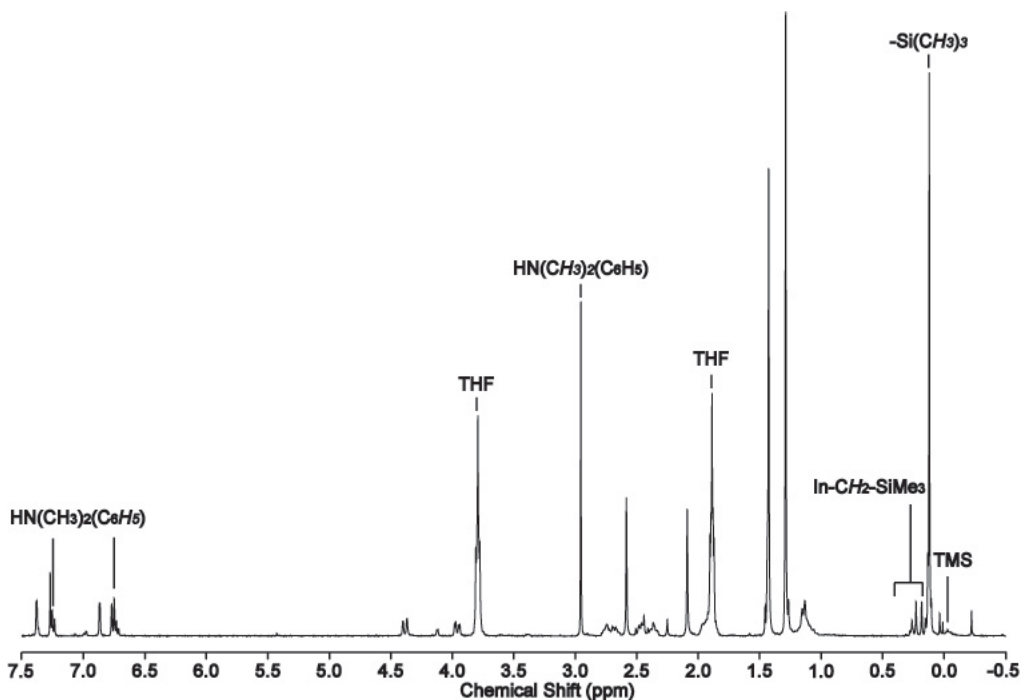


Figure 4.11. ^1H NMR spectrum of a crude product of $[(\text{NNO}_{\text{tBu}})\text{In}(\text{CH}_2\text{SiMe}_3)][\text{B}(\text{C}_6\text{F}_5)_4]$ (**14**) (CDCl_3 , $25\text{ }^\circ\text{C}$).

The ^1H NMR spectrum of complex **14** $[(\text{NNO}_{\text{tBu}})\text{In}(\text{CH}_2\text{SiMe}_3)][\text{B}(\text{C}_6\text{F}_5)_4]$ with a bulky non-coordinating anion ($\text{A} = \text{B}(\text{C}_6\text{F}_5)_4$) shows a broad singlet peak at 2.90 ppm corresponding to the NH proton while the NH resonance peak of complex **15** $[(\text{NNO}_{\text{tBu}})\text{In}(\text{CH}_2\text{SiMe}_3)][\text{BArF}]$ and complex **16** $[(\text{NNO}_{\text{tBu}})\text{In}(\text{CH}_2\text{SiMe}_3)][\text{PF}_6]$ is at 2.72 and 4.12 ppm, respectively. In addition, the protons of $\text{In-CH}_2\text{-SiMe}_3$, and $\text{Si}(\text{CH}_3)_3$ for **14** appear as multiplet peaks in the range of 0.20 to 0.26 ppm and a singlet peak at 0.17 ppm, respectively. However, the $\text{In-CH}_2\text{-Si}(\text{CH}_3)_3$ and $\text{Si}(\text{CH}_3)_3$ protons respectively appear as a singlet at 0.25 ppm and a singlet at 0.22 ppm for **15** and two doublet signals at 0.81 and 0.42 ppm and one singlet at 0.21 ppm for **16**. These results indicate that although all the anions studied in this work are considered to be weakly or non-coordinating anions, the solution structures of the cations differ significantly based on the counter anions coordinating to the highly electrophilic metal center. However, the ^{19}F NMR spectra of complexes **14-16** do not show coordination of the counter anion to the indium center. Three multiplet resonance peaks of *ortho*-, *meta*- and *para*-fluoro groups respectively at -132.7, -162.3 and -166.2 ppm for **14**, one singlet peak at -62.48 ppm for **15** and a doublet peak at -69.4 ppm ($^1J_{\text{F-P}} = 716.9$

Hz) for **16** (Figure 4.12) are seen in the ^{19}F NMR spectra, which are identical to those of reported non-coordinated anions (**A**, **G**, **H** and **L** in Figure 4.1).^{304,309,314}

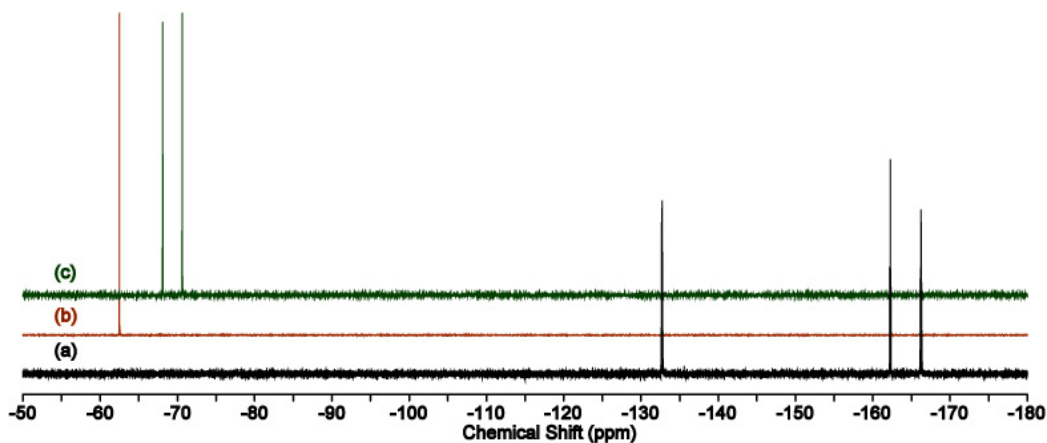


Figure 4.12. $^{19}\text{F}\{^1\text{H}\}$ NMR spectra of (a) $[(\text{NNO}_{\text{tBu}})\text{In}(\text{CH}_2\text{SiMe}_3)][\text{B}(\text{C}_6\text{F}_5)_4]$ (**14**), (b) $[(\text{NNO}_{\text{tBu}})\text{In}(\text{CH}_2\text{SiMe}_3)][\text{BArF}]$ (**15**) and (c) $[(\text{NNO}_{\text{tBu}})\text{In}(\text{CH}_2\text{SiMe}_3)][\text{PF}_6]$ (**16**) (CDCl_3 , 25 °C, neat CFCl_3 was externally referenced at 0 ppm).

Single crystals of **14** $[(\text{NNO}_{\text{tBu}})\text{In}(\text{CH}_2\text{SiMe}_3)][\text{B}(\text{C}_6\text{F}_5)_4]$ and **16** $[(\text{NNO}_{\text{tBu}})\text{In}(\text{CH}_2\text{SiMe}_3)][\text{PF}_6]$ were obtained via crystallization from a mixture of pentane and THF and a solution of diethyl ether, respectively, and the molecular structures were determined via X-ray crystallography. The solid-state structure of **14** reveals two distinct cationic species in the unit cell, both with $\kappa^3\text{-NNO}_{\text{tBu}}$ ligand coordination (Figure 4.13). One is a THF adduct, **14**•THF, with distorted trigonal bipyramidal geometry at the indium center and no interaction with $\text{B}(\text{C}_6\text{F}_5)_4$. The other is a very distorted trigonal pyramidal indium center with the closest contact to one F atom of a $\text{B}(\text{C}_6\text{F}_5)_4$ molecule at 3.5 Å (Figure 4.13). Since cationic alkyl indium complexes are rare, it is difficult to compare the solid-state structure of **14** with reported compounds. The only comparable cationic indium complex is complex **L** $[\text{In}(\text{CH}_2\text{SiMe}_3)_2(\text{THF})_3][\text{B}(\text{C}_6\text{F}_6)]$ in Figure 4.1. The molecular structure of $[\text{In}(\text{CH}_2\text{SiMe}_3)_2(\text{THF})_3][\text{B}(\text{C}_6\text{F}_6)]$ **L** shows a square pyramidal geometry with an indium center coordinated to two alkyl and three THF ligands. The In-C bond lengths of **14** ($\text{In-C}_{55} = 2.12$ Å) and **14**•THF ($\text{In1-C}_{24} = 2.14$ Å) are similar to the In-C bond of the complex **L** (2.13 Å) while the In- O_{THF} bond length in **14**•THF (2.37 Å) is within the average In- O_{THF} bond length in **L** ($\text{In-O}_{\text{eq}} = 2.44$ Å at equatorial position; $\text{In-O}_{\text{ax}} = 2.24$ Å at axial position). The closest In-F bond length to the electrophilic indium center in both of **14** and **14**•THF is

3.51 Å, which is longer than either an estimated In-F covalent bond distance (2.06 Å) or an estimated In-F van der Waals bond distance (3.40 Å). The longer distance in the crystal structure indicates no interaction between the weakly coordinating anion and the cationic metal center.

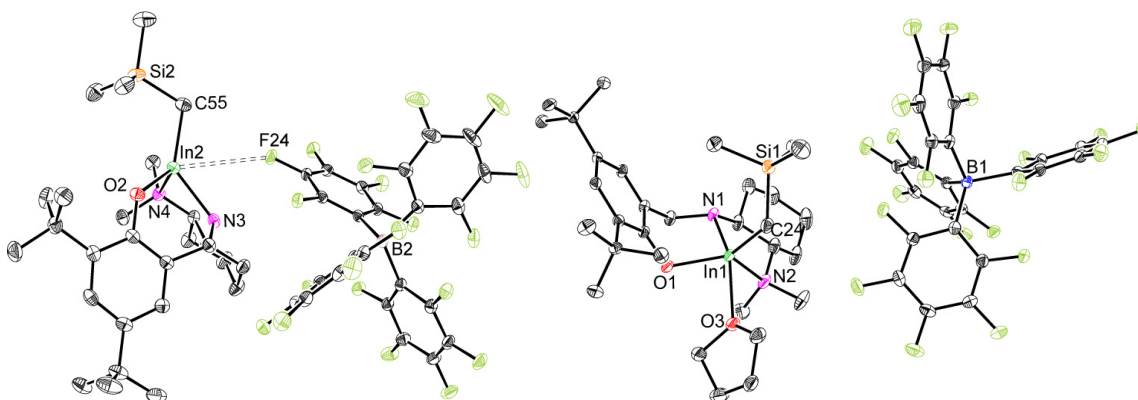


Figure 4.13. Molecular structure of **14** depicted with ellipsoids at 50% probability (H atoms and uncoordinated solvent molecules were removed for clarity). $[(\text{NNO}_{\text{tBu}})\text{In}(\text{CH}_2\text{SiMe}_3)][\text{B}(\text{C}_6\text{F}_5)_4]$ **14** (left) and **14**•THF (right) were found in the unit cell.

Table 4.3. Selected distances (Å) and angles (°) for complex [(NNO_{tBu})In(CH₂SiMe₃)] [B(C₆F₅)₄] (**14**) and **14**•THF.

14				
Bond Lengths	In2-O2	2.0355(15)	In2-C55	2.120(2)
	In2-N3	2.2129(18)	In2-F24	3.507(1)
	In2-N4	2.2757(17)		
Bond Angles	O2-In2-C55	123.47(7)	N3-In2-N4	79.84(6)
	O2-In2-N3	91.35(6)	C55-In2-N3	133.09(8)
	O2-In2-N4	108.93(6)	C55-In2-N4	111.47(8)
14 •THF				
Bond Lengths	In1-O1	2.0679(14)	In1-N2	2.3074(18)
	In1-O3	2.3687(15)	In1-C24	2.143(2)
	In1-N1	2.3254(17)		
Bond Angles	O1-In1-C24	124.80(7)	C24-In1-N2	114.74(7)
	O1-In1-N1	86.32(6)	C24-In1-O3	98.50(7)
	O1-In1-N2	119.97(6)	N1-In1-N2	76.34(6)
	O1-In1-O3	81.64(5)	N1-In1-O3	146.75(6)
	C24-In1-N1	113.72(7)	N2-In1-O3	83.10(6)

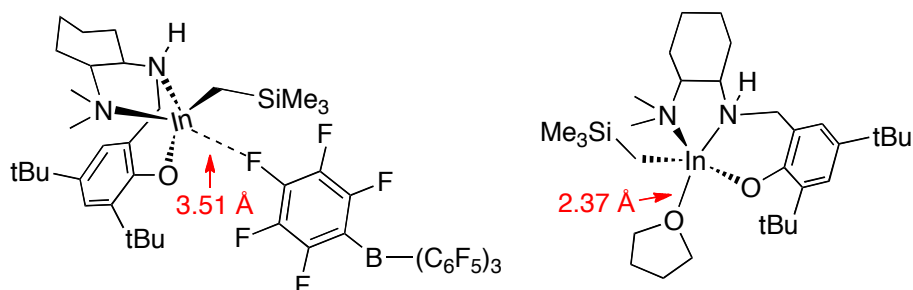


Figure 4.14. Illustrations of the molecular structures for **14** [(NNO_{tBu})In(CH₂SiMe₃)] [B(C₆F₅)₄] and **14**•THF.

The solid-state structure of complex **16** [(NNO_{tBu})In(CH₂SiMe₃)] [PF₆] shows a distorted trigonal bipyramidal indium center similar to **14**•THF with the THF molecule replaced with PF₆. Unlike **14** and **14**•THF, the In-F bond distance in **16** (2.660(1) Å) (**Figure 4.15**) is shorter than an estimated In-F van der Waals bond distance (3.40 Å) and longer than an estimated In-F covalent bond distance (2.06 Å). Although there is an interaction between the highly electrophilic indium metal center and the counter anion, the bond lengths and angles for **16** are similar to those for **14**, indicating minimal electronic impact from PF₆. This

complex is the first example among the indium cationic complexes (**Figure 4.15**) that shows a metal-counter anion interaction.

One interesting finding is that in the absence of coordinating solvents such as THF, the cations **14-16** are mononuclear both in solution and in the solid state; thus, no aggregation occurs to form five-coordinate dinuclear cationic species, which could be caused by the enhanced Lewis acidity of the metal center. This might be due to the unfavorable Coulombic interaction between two highly positive indium centers, and is consistent with other reported indium cations.

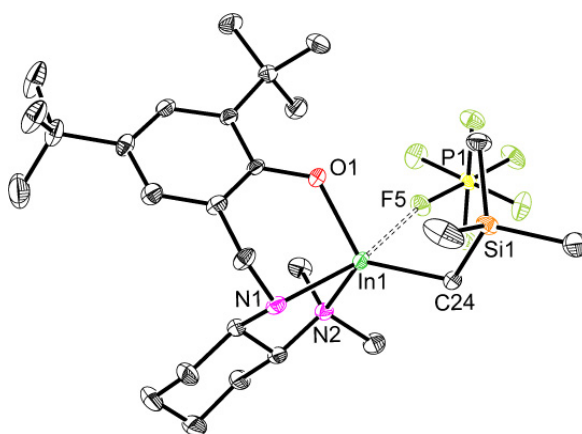


Figure 4.15. Molecular structure of complex **16** [(NNO_{tBu})In(CH₂SiMe₃)] [PF₆] depicted with ellipsoids at 50% probability (H atoms and solvent molecules removed for clarity).

Table 4.4. Selected distances (Å) and angles (°) for complex **16** [(NNO_{tBu})In(CH₂SiMe₃)] [PF₆].

16				
Bond Lengths	In1-O2	2.0450(16)	In1-C24	2.1197(19)
	In1-N1	2.2315(19)	In1-F5	2.660(1)
	In1-N2	2.2716(19)		
Bond Angles	O1-In1-C24	125.44(6)	N1-In1-N2	79.26(6)
	O1-In1-N1	88.88(5)	C24-In1-N1	121.51(6)
	O1-In1-N2	109.15(5)	C24-In1-N2	119.66(7)

4.2.2 Reactivity of cationic indium complexes with methyl methacrylate (MMA)

We tested the reactivity of the cationic compounds $[(\text{NNO}_{\text{tBu}})\text{In}(\text{CH}_2\text{SiMe}_3)][\text{A}]$ **14-16**, as well as the neutral compounds $\text{In}(\text{CH}_2\text{SiMe}_3)_3$ and $[(\text{NNO}_{\text{tBu}})\text{InCl}]_2(\mu\text{-Cl})(\mu\text{-OEt})$ **5** as catalysts for the polymerization of methyl methacrylate (MMA). Reactions showed variations in reactivity depending on the initiators and various concentrations of MMA used at 60 °C.

Polymerization of MMA with the cations **14** and **16** under identical conditions (**Table 4.5** entries 2 and 4, CH_2Cl_2 , 60 °C) shows that the catalytic activity increases, with turnover frequencies from 0.05 h^{-1} to 1.3 h^{-1} respectively, as the coordinating ability of the anions³⁵⁸ decreases ($[\text{PF}_6]^- \gg [\text{B}(\text{C}_6\text{F}_5)_4]^-$). This is surprising because the weak coordination between the fluorine atom of the anion and the indium center in complex **16**, illustrated in its solid-state structure (**Figure 4.15**), could hinder the catalytically active site and reduce the activity towards MMA. One possibility to elucidate the enhanced reactivity for the cation **16**, compared with the other cations **14** and **15**, may be a slightly reduced electrophilicity due to the $p_\pi\text{-}p_\pi$ interaction between In^{3+} and F that prevents the cation **16** from formation of a MMA adduct complex. Furthermore, the reactivity the complex with the relatively weaker coordinating anion $[\text{BArF}]^-$ (TOF = 0.13 h^{-1}) (relative coordinating ability³⁵⁸: $[\text{B}(\text{C}_6\text{F}_5)_4]^- > [\text{BArF}]^-$) towards the polymerization of MMA is slightly higher than that with $[\text{B}(\text{C}_6\text{F}_5)_4]^-$ (TOF = 0.05 h^{-1}) (**Table 4.5** entries 2 and 3, CH_2Cl_2 , 60 °C). However, it must be noted that in MMA polymerization with the zirconocenium cations as Lewis acid activators, reported by Chen and coworkers the weakly coordinating borate anion $[\text{B}(\text{C}_6\text{F}_5)_4]^-$ accelerates the rate of propagation while the rate with the moderately coordinating anion $[\text{B}(\text{C}_6\text{H}_5)]^-$ is suppressed. The rate of MMA polymerization with these indium cations appears to be much lower than those of the cationic aluminum complex **O** (**Figure 4.5**), for which further detailed polymerization data is not described in the literature.

MMA polymerization with neutral indium complexes **13** and **5** (**Table 4.5** entries 1 and 5) was conducted under the same conditions as for the cations. The catalytic activity (TOF = 2.3 h^{-1}) with complex **13** is higher than those of the cations while that of **5** (TOF = 0.09 h^{-1}) is lower than that of complex **16** with the anion $[\text{PF}_6]^-$, but similar to those of the other cations, **14** and **15**. These results suggest that the synthesis of PMMA with **5** is ineffective

because the six-coordinate indium center is too crowded to initiate the polymerization of the 1,1-disubstituted olefin MMA.

Furthermore, MMA polymerization with the neutral complex **13** and the cationic indium complex **16** with a higher concentration of MMA (2.3 M in CH₂Cl₂) and in neat MMA was conducted at 60 °C (Table 4.5 entries 7-10). Under these polymerization conditions, the reactivity of MMA with the cation **16** is enhanced, with turnover frequencies of 4.4 h⁻¹ and 7.6 h⁻¹ for the conditions with 2.3 M MMA and neat MMA respectively, while the turnover frequencies with the neutral complex **13** were decreased to 110.8 h⁻¹ and 58.8 h⁻¹ respectively. The reactivity with either the neutral or cationic complexes up to the certain high concentration of MMA (2.3 M) is much greater than with the lower MMA concentration of 0.5 M (0.5 M: TOF = 2.3 h⁻¹ for complex **13** and 1.3 h⁻¹ for complex **16**; 2.3 M: TOF = 110.8 h⁻¹ for complex **13** and 4.4 h⁻¹ for complex **16**). These results suggest that the neutral complex **13** with the κ^2 -coordination geometry in MMA polymerization exhibits much higher reactivity than the cationic complex **16** with the κ^3 -coordination geometry due to the higher Lewis acidity of the cationic indium center that causes a strong covalent bond between MMA and the metal center. In addition, complex In(CH₂SiMe₃)₃ was used to polymerize MMA with a concentration of 2.3 M in CH₂Cl₂ at 60 °C, and its activity (Table 4.5 entry 6, TOF = 15.4 h⁻¹) is lower than that of the neutral complex **13** (TOF = 110.8 h⁻¹) under identical conditions, suggesting the Schiff base ligand NNO_{tBu} influences the reactivity of the indium towards MMA polymerization.

Despite the lower activities of the cations **14-16** in MMA polymerization this is the first example of reactivity towards polar conjugated monomers with indium cations. The most significant merit with these neutral and cationic In(III) complexes for MMA polymerization compared to any known systems in the literature is that organic solvents are not necessary for polymerization; thus neat MMA can be used as both the monomer as well as a solvent.

Table 4.5. Polymerization of MMA with neutral complexes $\text{In}(\text{CH}_2\text{SiMe}_3)_3$, **13** and **5** and cationic complexes **14-16**.

Entry	Initiator	M/Cat ratio	Time (h)	Conversion (%) ^d	TOF (h^{-1}) ^e
1 ^a	13	510	168	77	2.3
2 ^a	14	510	168	2	0.05
3 ^a	15	510	168	4	0.13
4 ^a	16	510	168	42	1.3
5 ^a	5	510	168	3	0.09
6 ^b	$\text{In}(\text{CH}_2\text{SiMe}_3)_3$	1998	14	11	15.4
7 ^b	13	1998	14	78	110.8
8 ^b	16	1998	14	3	4.4
9 ^c	13	2350 (neat)	36	90	58.8
10 ^c	16	2350 (neat)	144	46	7.6

^a All reactions were carried out in CHCl_3 (4 mL) at 60 °C; initiator = 0.004 mmol, MMA = 2.04 mmol. ^b All reactions were carried out in CHCl_3 (1 mL) at 60 °C; initiator = 0.0094 mmol, MMA = 18.8 mmol (2 mL). ^c All reactions were carried out in neat MMA (3 mL) at 60 °C; initiator = 0.012 mmol, MMA = 28.2 mmol (3 mL). ^d Determined by ^1H NMR spectroscopy (CDCl_3 , 25 °C). ^e Calculated from $([\text{monomer}]_0/[\text{initiator}] \times \text{monomer conversion})/\text{Time (h)}$.

4.3 Conclusion

In this chapter, the synthesis and characterization of rare cationic indium complexes supported by a chiral tridentate ligand are described. Interestingly, these cations show catalytic activity toward the polymerization of a polar conjugated monomer, MMA, to PMMA. Surprisingly, the cationic complex **16** with the moderately coordinating anion $[\text{PF}_6]^-$ has a greater activity ($\text{TOF} = 1.3 \text{ h}^{-1}$) compared with those of the other cations with weakly coordinating anions, $[\text{B}(\text{C}_6\text{F}_5)_4]^-$ and $[\text{BArF}]^-$ ($\text{TOF} = 0.05 \text{ h}^{-1}$ for $[\text{B}(\text{C}_6\text{F}_5)_4]^-$, $\text{TOF} = 0.13 \text{ h}^{-1}$ for $[\text{BArF}]^-$) under identical conditions, suggesting the influence of the coordinating ability of the counter anion on the reactivity towards MMA polymerization.

The reactivity towards MMA polymerization with the neutral indium complexes **13** and $\text{In}(\text{CH}_2\text{SiMe}_3)_3$ ($\text{TOF} = 78 \text{ h}^{-1}$ for **13**, $\text{TOF} = 11 \text{ h}^{-1}$ for $\text{In}(\text{CH}_2\text{SiMe}_3)_3$) is much higher than that of the cations. This suggests that the highly Lewis acidic indium metal center in the cations lowers the reactivity due to a strong coordination of the Lewis basic MMA to the metal center, lowering the rate of propagation. Another important factor influencing the catalytic activity may be the geometry of the neutral metal center; **13** is a distorted trigonal pyramidal geometry with a κ^2 -coordinated NNO_{tBu} ligand, while the cations have trigonal bipyramidal geometry with a κ^3 -coordinated NNO_{tBu} ligand.

However, these cationic indium systems are much less reactive than other well-known Zr and Sm systems for polymerization of polar conjugated monomers. One hypothesis for the lower reactivity is that the cationic indium metal centers is strong coordination of the Lewis basic MMA to the highly Lewis acidic metal, reducing the rate of propagation. However, further experimental and theoretical studies are needed to confirm this hypothesis.

Although these results with very modest catalytic activity of the neutral and cationic indium complexes **14-16** for MMA polymerization are very preliminary, it is the first time reactivity of cationic In(III) complexes towards a polar conjugated vinyl monomer has been shown. This shows the potential of indium complexes as promising catalysts for polymerization of polar or nonpolar conjugated vinyl monomers. Further investigations to improve reactivity by changing the ligand electronics, to tune the Lewis acidity of the metal center, and changing the geometry of the metal center with different coordinating ligands as well as mechanistic studies of this MMA polymerization will be required in the future.

4.4 Experimental section

General Considerations. Unless otherwise indicated, all air- and/or water-sensitive reactions were carried out under dry nitrogen using either an MBraun glove box or standard Schlenk line techniques. NMR spectra were recorded on a Bruker Avance 300 MHz, 400 MHz and 600 MHz spectrometer. ^1H NMR chemical shifts are reported in ppm versus residual protons in deuterated solvents as follows: δ 7.27 CDCl_3 , $^{13}\text{C}\{^1\text{H}\}$ NMR chemical shifts are reported in ppm versus residual ^{13}C in the solvent: δ 77.2 CDCl_3 . $^{19}\text{F}\{^1\text{H}\}$ NMR chemical shifts are reported in ppm and externally referenced to neat CFCl_3 at 0 ppm. $^{31}\text{P}\{^1\text{H}\}$ NMR chemical shifts are reported in ppm and externally referenced to 85% H_3PO_4 at 0 ppm. Diffraction measurements for X-ray crystallography were made on a Bruker X8 APEX II diffraction and a Bruker APEX DUO diffraction with graphite monochromated $\text{Mo-K}\alpha$ radiation. The structures (Table C.2 in Appendix C) were solved by direct methods and refined by full-matrix least-squares using the SHELXTL crystallographic software of Bruker-AXS. Unless specified, all non-hydrogens were refined with anisotropic displacement parameters, and all hydrogen atoms were constrained to geometrically calculated positions but were not refined. EA CHN analysis was performed using a Carlo Erba EA1108 elemental analyzer. The elemental composition of unknown samples was determined by using a calibration factor. The calibration factor was determined by analyzing a suitable certified organic standard (OAS) of a known elemental composition. Molecular weights were determined by triple detection gel permeation chromatography (GPC-LLS) using a Waters liquid chromatograph equipped with a Water 515 HPLC pump, Waters 717 plus autosampler, Waters Styragel columns (4.6 \times 300 mm) HR5E, HR4 and HR2, Water 2410 differential refractometer, Wyatt tristar miniDAWN (laser light scattering detector) and a Wyatt ViscoStar viscometer. A flow rate of 0.5 mL min^{-1} was used and samples were dissolved in THF (2 mg mL^{-1}). Narrow molecular weight polystyrene standards were used for calibration purposes.

Materials. Solvents (THF, pentane, toluene, hexane and diethyl ether) were collected from a Solvent Purification System from Innovative Technology, Inc. whose columns were packed with activated alumina. CDCl_3 was dried over CaH_2 , collected by vacuum distillation and

degassed through a series of freeze-pump-thaw cycles. Dimethylanilinium tetrafluoroborate ($[\text{HNMe}_2\text{Ph}][\text{BF}_4]$), dimethylanilinium hexafluorophosphate ($[\text{HNMe}_2\text{Ph}][\text{PF}_6]$), and dimethylanilinium tetrakis[3,5-bis(trifluoromethyl)phenyl]borate ($[\text{HNMe}_2\text{Ph}][\text{BAr}^{\text{F}}_4]$) were generated by reacting dimethylanilinium chloride with the corresponding anionic metallic reagents (Na^+ or Ag^+) in THF at room temperature for 4 h. The solvent was removed under high vacuum, and addition of hexane to the residual precipitated a white solid. Each corresponding reagent was isolated as a white solid by vacuum filtration and dried *in vacuo* for 4 h. InCl_3 and InMe_3 were purchased from Strem Chemicals and used without further purification. (Trimethylsilyl)methylmagnesium chloride (1.0 M in Et_2O), dimethylanilinium tetrakis(pentafluorophenyl)borate ($[\text{HNMe}_2\text{Ph}][\text{B}(\text{C}_6\text{F}_5)_4]$), dimethylanilinium chloride ($[\text{HNMe}_2\text{Ph}]\text{Cl}$), silver hexafluorophosphate (AgPF_6), and sodium tetrakis[3,5-bis(trifluoromethyl)phenyl]borate ($\text{Na}[\text{BAr}^{\text{F}}_4]$) were purchased from Aldrich and Alfa Aesar, respectively, and used as received. Proligand $\text{H}(\text{NNO}_{\text{tBu}})^{23,125}$ and $\text{In}(\text{CH}_2\text{Si}(\text{CH}_3)_3)_3^{355}$ were synthesized according to previously reported procedures.

Synthesis of $(\text{NNO}_{\text{tBu}})\text{InMe}_2$ (12**).** A 125 mL round bottom flask was charged with InCl_3 (0.10 g, 0.45 mmol) and 15 mL of Et_2O . To this solution, MeLi in Et_2O (1.6 M, 0.85 mL, 0.45 mmol) was added dropwise and the resulting mixture was stirred at room temperature for 20 minutes. The proligand $\text{H}(\text{NNO}_{\text{tBu}})$ (0.16 g, 0.45 mmol) was added to the mixture as a solution in Et_2O (15 mL). The reaction was heated at 30 °C for 24 h, after which time it was cooled to room temperature and the solution was filtered through Celite to remove LiCl . The filtrate was concentrated to approximately 15 mL resulting in the formation of a white precipitate that was isolated by filtration, washed with pentane (3×2 mL), and dried under high vacuum to yield **12** (0.092 g, 41%). Suitable crystals for X-ray diffraction were grown from Et_2O at -35 °C.

Complex **12** can also be synthesized from isolated $\text{In}(\text{Me})_3$. A 25 mL round bottom flask was charged with $\text{In}(\text{Me})_3$ (0.071 g, 0.44 mmol) dissolved in 5 mL of Et_2O . Then a solution of the proligand (0.15 g, 0.44 mmol) in 5 mL of Et_2O was added dropwise. The reaction mixture was stirred for 30 min. After the removal of all volatiles the residue was dried *in vacuo*, to yield complex **12** as a white powder (0.188 g, 85%). ^1H NMR (400 MHz, CDCl_3): δ 7.22 (1H, d, $J=3$ Hz, *ArH*), 6.82 (1H, d, $J=3$ Hz, *ArH*), 4.31 (1H, t, $J=10$ Hz, $\text{R}_2\text{N-CH-}$

CH₂), 3.59 (1H, d, *J*=7 Hz, NH-CH₂-Ar) 2.61(1H, d, *J*=12 Hz, NH-CH₂-Ar), 2.47 (1H, m, -CH₂- of DACH), 2.21, (6H, br s, N-(CH₃)₂), 1.90 (3H, m, -CH₂- of DACH), 1.61 (1H, t, *J*=10 Hz, -CH₂- of DACH), 1.43 (9H, s, *t*-Bu), 1.28 (9H, s, *t*-Bu), 1.24 (1H, m, -CH₂- of DACH), -0.15 (3H, s, In-CH₃), -0.35 (3H, s, In-CH₃). ¹³C{¹H} NMR (75 MHz, CDCl₃): δ 163.9, 138.3, 133.0, 124.3, 123.7, 122.8, 66.8, 58.1, 53.8, 35.4, 33.9, 32.6, 32.0, 29.7, 25.2, 24.8, 21.5, -7.0, -7.2. EI-LRMS (*m/z*) 504. Elemental analysis calc. (found) for C₂₅H₄₅InN₂O: C. 59.50 (59.36), H. 8.90 (8.88), N. 5.55 (5.50).

Synthesis of (NNO_{*t*Bu})In(CH₂SiMe₃)₂ (13). A 20 mL scintillation vial was charged with proligand H(NNO_{*t*Bu}) (207 mg, 0.647 mmol) in Et₂O (5 mL). ((Trimethylsilyl)methyl)indium In(CH₂SiMe₃)₃ (243 mg, 0.647 mmol) was added to the stirring mixture dropwise. The reaction mixture was stirred for 4 h at room temperature. The solvent was removed *in vacuo* and the residue was redissolved in Et₂O or hexane (ca. 3 mL). The vial was kept in the freezer at -35 °C overnight. Colourless crystals, which were used to collect X-ray crystallographic data, were formed. The collected crystals were washed with Et₂O or hexane and dried under vacuum for several hours, yielding a white solid (320 mg, 76%). ¹H NMR (400 MHz, CDCl₃): δ 7.26 (1H, d, *J* = 2.3 Hz, Ar*H*), 7.19 - 7.24 (1H, m, Ar*H*), 6.82 - 6.86 (m, 1H, m, Ar*H*), 6.79 (1H, d, *J* = 2.0 Hz, Ar*H*), 4.23 - 4.33 (1H, m, NH-CH₂-Ar), 4.19 (1H, t, *J* = 10.9 Hz, NH-CH₂-Ar), 4.12 (1H, d, *J* = 11.0 Hz, -NH-), 3.46 (1H, d, *J* = 11.1 Hz, NH-CH₂-Ar), 3.32 (1H, d, *J* = 11.3 Hz, NH-CH₂-Ar), 2.70 (1H, td, *J* = 3.7, 10.8 Hz, -CH- of DACH), 2.42 - 2.54 (2H, m, -CH- of DACH), 2.27 - 2.42 (2H, m, -CH- of DACH, -NH-), 2.23 (6H, s, -N(CH₃)₂), 2.12 - 2.21 (7H, br. s., -N(CH₃)₂, -CH- of DACH), 1.93 (1H, m, 1H, -CH₂- of DACH), 1.73 - 1.89 (4H, m, -CH₂- of DACH), 1.43 (18H, s, Ar-(CH₃)₃), 1.34 (1H, m, -CH₂- of DACH), 1.28 (18H, m, Ar-(CH₃)₃), 0.02 - 1.26 (m, 36H, m, -Si(CH₃)₃), -0.70 - -0.22 (8H, m, In-CH₂-Si(CH₃)₃); ¹³C{¹H} NMR (101 MHz, CDCl₃) δ) δ 163.1 (Ar C), 162.4 (Ar C), 138.9 (Ar C), 138.7 (Ar C), 135.9 (Ar C), 133.8 (Ar C), 124.8 (Ar C-H), 124.4 (Ar C-H), 124.3 (Ar C-H), 124.1 (Ar C), 123.9 (Ar C-H), 123.3 (Ar C), 66.6 (-CH- of DACH), 65.4 (-CH- of DACH), 63.7 (-CH- of DACH), 58.1 (-CH- of DACH), 54.6 (HN-CH₂-Ar), 51.9 (HN-CH₂-Ar), 35.4 (-N(CH₃)₂), 35.4 (-N(CH₃)₂), 34.1 (Ar-C(CH₃)₃), 34.0 (Ar-C(CH₃)₃), 32.1 (Ar-C(CH₃)₃), 32.1 (Ar-C(CH₃)₃), 31.5 (Ar-C(CH₃)₃), 30.2 (Ar-C(CH₃)₃), 30.1 (Ar-C(CH₃)₃), 25.4 (-CH₂- of DACH), 25.1 (-CH₂- of DACH), 25.0 (-CH₂- of DACH), 21.6 (-

CH₂- of DACH), 21.1 (-CH₂- of DACH), 3.9 (-CH₂-SiMe₃), 3.0 (-Si(CH₃)₃), 2.8 (-Si(CH₃)₃), 2.6 (-Si(CH₃)₃), 2.6 (-Si(CH₃)₃), 1.8 (-CH₂-SiMe₃), 0.9 (-CH₂-SiMe₃), 0.3 (-CH₂-SiMe₃). Anal. Calcd. For C₃₁H₆₁InN₂OSi₂: C 57.39; H 9.48; N 4.32. Found: C 57.22; H 9.53; N 4.58.

Synthesis of [(NNO_{tBu})In(CH₂SiMe₃)] [B(C₆F₅)₄] (14). A 20 mL scintillation vial was charged with In(CH₂SiMe₃)₃ (68.0 mg, 0.105 mmol) in THF (3 mL). [HNMe₂Ph][B(C₆F₅)₄] (84 mg, 0.20 mmol) in THF (1 mL) was added to the stirring mixture dropwise. The reaction mixture was stirred for 16 h at room temperature. The solvent was removed *in vacuo*, and then Et₂O was added to the residue to help with THF removal. Hexane was added and evacuated repeatedly to precipitate a white solid from the solution. The white solid was washed with hexane (2 × 3 mL) and dried under high vacuum for a few hours (107.1 mg, 82%). ¹H NMR (600 MHz, CDCl₃): δ 7.39 (1H, d, *J* = 2.3 Hz, Ar*H*), 6.87 (1H, d, *J* = 2.2 Hz, Ar*H*), 4.43 (1H, d, *J* = 12.8 Hz, NH-CH₂-Ar), 3.95 (1H, dd, *J* = 3.3, 13.1 Hz, NH-CH₂-Ar), 3.82 (1H, t, *J* = 6.3 Hz, -CH₂- of THF), 2.90 (1H, br. s., -NH-), 2.65 – 2.77 (1H, m, -CH- of DACH), 2.60 (3H, s, -N(CH₃)₂), 2.41 - 2.52 (1H, m, -CH₂- of DACH), 2.31 - 2.41 (1H, m, -CH- of DACH), 2.04 (3H, s, -N(CH₃)₂), 1.81 - 1.99 (5H, m, -CH₂- of DACH and -CH₂- of THF), 1.43 (9H, s, Ar-(CH₃)₃), 1.29 (9H, s, Ar-(CH₃)₃), 1.09 – 1.24 (4H, m, CH₂- of DACH), 0.20 - 0.26 (2H, m, In-CH₂-Si(CH₃)₃) 0.17 (9H, s, -Si(CH₃)₃); ¹³C{¹H} NMR (151 MHz, CDCl₃): δ 160.0 (Ar C), 149.1 (Ar C-F), 147.6 (Ar C-F), 141.3 (Ar C), 139.2 (Ar C), 137.3 (Ar C-F), 135.7 (Ar C-F), 127.0 (Ar B-C), 126.8 (Ar C-H), 126.7 (Ar C-H), 118.3 (Ar C), 69.3 (-CH- of DACH), 68.8 (O-CH₂- of THF), 54.8 (-CH- of DACH), 50.7 (HN-CH₂-Ar), 45.9 (-N(CH₃)₂), 38.7 (-N(CH₃)₂), 35.7 (Ar-C(CH₃)₃), 34.4 (Ar-C(CH₃)₃), 31.8 (Ar-C(CH₃)₃), 30.7 (CH₂- of DACH), 29.9 (Ar-C(CH₃)₃), 25.7 (-CH₂- of THF), 24.3 (-CH₂- of DACH), 23.7 (-CH₂- of DACH), 22.9 ((-CH₂- of hexane), 21.6 (-CH₂- of DACH), 14.3 (-CH₃ of hexane), 1.7 (-Si(CH₃)₃), -1.8 (-CH₂-SiMe₃). ¹⁹F{¹H} NMR (282 MHz, CDCl₃): δ -166.2 (t, ³*J*_{F-F} = 17.3 Hz, Ar *p*-F), -162.3 (t, ³*J*_{F-F} = 21.1 Hz, Ar *m*-F), -132.7 (d, ³*J*_{F-F} = 9.0, Ar *o*-F). Anal. Calcd. For C₅₁H₅₀BF₂₀InN₂OSi•C₄H₈O: C 50.32; H 4.45; N 2.13. Found: C 50.36; H 4.46; N 2.39.

Synthesis of [(NNO_{tBu})In(CH₂SiMe₃)] [BAr^F]₄] (15). A 20 mL scintillation vial was charged with In(CH₂SiMe₃)₃ (37 mg, 0.057 mmol) in THF (5 mL). [HNMe₂Ph][BAr^F]₄] (56 mg, 0.057 mmol) in THF was added to the stirring mixture dropwise. The reaction mixture was stirred

for 16 h at room temperature. The solvent was removed *in vacuo*, and hexane was added and evacuated repeatedly to the residue to precipitate a white solid. The white solid was washed with hexane (2 × 3 mL) and dried under high vacuum for a few hours (47.1 mg, 58%). ¹H NMR (400 MHz, CDCl₃): δ 7.70 (8H, br. s., BAr^F₄ ArH), 7.55 (4H, s, BAr^F₄ ArH), 7.41 (1H, d, *J* = 2.3 Hz, ArH), 6.85 (1H, d, *J* = 2.3 Hz, ArH), 4.47 (1H, d, *J* = 13.0 Hz, NH-CH₂-Ar), 3.95 (1H, dd, *J* = 13.2 Hz, NH-CH₂-Ar), 2.72 (2H, br. s., -NH-, -CH- of DACH), 2.50 (3H, br. s., -N(CH₃)₂), 2.43 – 2.48 (1H, m, -CH₂- of DACH), 2.60 (3H, s, -N(CH₃)₂), 2.29 (1H, t, *J* = 11.4 Hz, -CH- of DACH), 1.94 (3H, s, -N(CH₃)₂), 1.78 (2H, br. m, -CH₂- of DACH), 1.42 (9H, s, Ar-(CH₃)₃), 1.28 (9H, s, Ar-(CH₃)₃), 0.96 – 1.16 (4H, m, CH₂- of DACH), 0.45 (2H, d, *J* = 2.4 Hz, In-CH₂-Si(CH₃)₃) 0.22 (9H, s, -Si(CH₃)₃); ¹³C{¹H} NMR (151 MHz, CDCl₃) δ 161.36 – 162.35 (dd, *J* = 49.94, 99.88 Hz, BAr^F₄ B-C), 159.8 (Ar C), 141.8 (Ar C), 139.4 (Ar C), 135.0 (BAr^F₄ 2C-H), 128.76 – 129.41 (m, BAr^F₄ C-(CF₃)), 127.1 (Ar 2C-H), 124.8 (d, *J* = 272.81 Hz, BAr^F₄ -CF₃), 117.8 (Ar C), 117.7 (BAr^F₄ C-H), 69.8 (-CH- of DACH), 54.8 (-CH- of DACH), 50.7 (-HN-CH₂-Ar), 46.1 (-N(CH₃)₂), 38.7 (-N(CH₃)₂), 35.7 (Ar-C(CH₃)₃), 34.4 (Ar-C(CH₃)₃), 31.7 (Ar-C(CH₃)₃), 31.4 (-CH₂- of DACH), 29.9 (Ar-C(CH₃)₃), 24.0 (-CH₂- of DACH), 23.7 (-CH₂- of DACH), 21.4 (-CH₂- of DACH), 1.9 (-Si(CH₃)₃), -0.6 (-CH₂-SiMe₃). ¹⁹F{¹H} NMR (282 MHz, CDCl₃): δ -62.5. Anal. Calcd. For C₅₉H₆₂BF₂₄InN₂OSi: C 49.74; H 4.39; N 1.97. Found: C 50.01; H 4.37; N 1.94.

Synthesis of [(NNO_{IBu})In(CH₂SiMe₃)] [PF₆] (16). A 20 mL scintillation vial was charged with In(CH₂SiMe₃)₃ (136 mg, 0.210 mmol) in THF (5 mL). [HNMe₂Ph][PF₆] (56 mg, 0.21 mmol) was added to the stirring mixture dropwise. The reaction mixture was stirred for 16 h at room temperature. The solvent was removed *in vacuo*, and then Et₂O was added and removed under vacuum. Hexane (5 mL) was added to the residue to precipitate a white solid. The precipitate was filtered through a fine frit. The white solid was washed with hexane (2 × 3 mL) and dried under high vacuum for a few hours (126.6 mg, 85%). ¹H NMR (400 MHz, CDCl₃): δ 7.34 (1H, d, *J* = 2.3 Hz, ArH), 6.84 (1H, d, *J* = 2.3 Hz, ArH), 4.52 (1H, d, *J* = 13.2 Hz, NH-CH₂-Ar), 4.12 (1H, d, *J* = 9.1 Hz, -NH-), 3.93 (1H, dd, *J* = 3.0, 13.3 Hz, NH-CH₂-Ar), 3.49 (2H, q, *J* = 7.0 Hz, O-CH₂-CH₃ of Et₂O), 2.90 (1H, td, *J* = 3.5, 11.5 Hz, -CH- of DACH), 2.65 (3H, s, -N(CH₃)₂) 2.49 – 2.61 (1H, m, -CH- of DACH), 2.34 – 2.44 (1H, m, -CH₂- of DACH), 2.09 (3H, s, -N(CH₃)₂), 1.78 - 1.98 (3H, m, -CH₂- of DACH), 1.32 - 1.56 (11H, m, -CH₂- of DACH and Ar-(CH₃)₃), 1.29 (9H, s, Ar-(CH₃)₃), 1.22 (3H, t, O-CH₂-CH₃

of Et₂O), 0.97 - 1.15 (2H, m, -CH₂- of DACH), 0.81 (1H, d, *J* = 13.0 Hz, In-CH₂-Si(CH₃)₃), 0.42 (1H, *J* = 12.9 Hz, In-CH₂-Si(CH₃)₃), 0.21 (9H, s, .43 (9H, s, -Si(CH₃)₃); ¹³C{¹H} NMR (101 MHz, CDCl₃): δ 160.4 (Ar C), 139.5 (Ar C), 138.7 (Ar C), 126.7 (Ar C-H), 125.7 (Ar C-H), 118.4 (Ar C), 66.8 (-CH- of DACH), 66.1 (O-CH₂- of Et₂O), 54.0 (HN-CH₂-Ar), 49.9 (-CH- of DACH), 45.6 (-N(CH₃)₂), 38.9 (-N(CH₃)₂), 35.6 (Ar-C(CH₃)₃), 34.2 (Ar-C(CH₃)₃), 31.9 (Ar-C(CH₃)₃), 30.1 (Ar-C(CH₃)₃), 29.2 (CH₂- of DACH), 24.4 (-CH₂- of DACH), 24.0 (-CH₂- of DACH), 21.9 (-CH₂- of DACH), 15.5 (-CH₃ of Et₂O), 2.0 (-Si(CH₃)₃), 0.1 (-CH₂-SiMe₃). ¹⁹F{¹H} NMR (282 MHz, CDCl₃): δ -69.4 (d, ¹J_{F-P} = 716.9 Hz). ³¹P{¹H} NMR (121 MHz, CDCl₃): δ -143.3 (sept, ¹J_{P-F} = 717.3 Hz). Anal. Calcd. For C₂₇H₅₀F₆InN₂OPSi•C₄H₁₀O: C 47.69; H 7.75; N 3.59. Found: C 47.69; H 7.45; N 4.59.

Representative large-scale polymerization of methyl methacrylate (MMA) with complex **13 in solution.** A Schlenk flask was charged with a solution of **13** (6.5 mg, 0.0092 mmol) in 1 mL CHCl₃. 2 mL of MMA (2 mL, 0.019 mol) was added directly to the flask by a syringe. The mixture was stirred at 60 °C for 14 h. The resulting clear solution was cooled down to room temperature. Some of the solution was dissolved in CDCl₃ to be analyzed by ¹H NMR spectroscopy to determine conversion. The remaining polymeric material was dissolved in CHCl₃ (100 mL) and added to cold wet methanol (0 °C, 7 mL). The polymer precipitated from solution and was isolated by centrifugation. The supernatant was decanted and the polymer was dried under high vacuum for 2 h prior to analysis.

Chapter 5: Template Synthesis of Functionalized Carbenes on Iron Complexes⁴

5.1 Introduction

5.1.1 History of singlet carbenes

A carbene is a neutral divalent carbon atom with two nonbonding electrons and two electrons involved in sigma bonds with neighboring atoms. Carbenes can be categorized into two classes depending on the ground state spin multiplicity of the non-bonding electrons: singlet carbenes and triplet carbenes (**Figure 5.1**).^{40,359-361} My research was exclusively focused on exploring the reactivity and electronic properties, influenced by various substituents, of the metal-bound carbenic carbon of singlet or Fischer type carbenes.

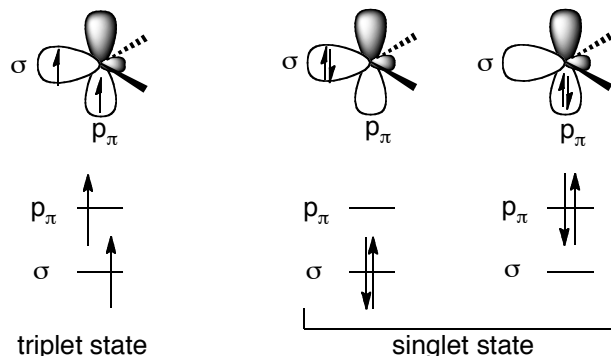
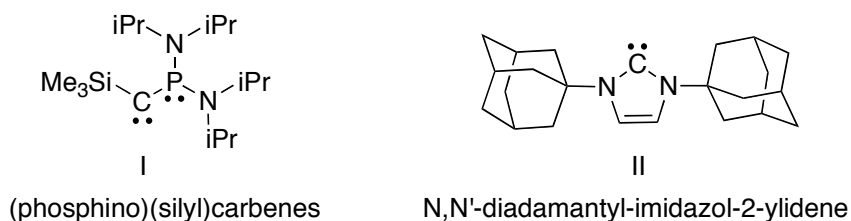


Figure 5.1. Ground state spin multiplicity and electronic configurations of triplet and singlet carbenes.^{40,359-361}

Although Doering introduced singlet carbenes as transient intermediates in organic chemistry,³⁶² and Breslow proposed an unusually stable singlet carbene, thiozol-2-ylidene, as an intermediate in the catalytic cycle of thiamine (vitamin B₁) in the 1950s,³⁶³ carbene species were considered inaccessible compounds due to their high reactivity and short lifetime (**Figure 5.1**).

⁴ Chapter 4 has been published in *Organometallics* in 2009⁴ and 2010.⁵



In 1970 N-heterocycliccarbenes (NHCs), which are singlet carbenes containing a carbenic carbon directly connected to at least one nitrogen atom within the heterocycle, were first reported *in situ* by Wanzlick and Schonher by deprotonation of an imidazolium salt.³⁶⁴ Landmark breakthroughs in carbene chemistry were the discovery of the first isolable, stable (phosphino)(silyl)carbene (I) as a red oil by Bertrand *et al.*³⁶⁵ and the first stable crystalline carbene, N,N'-diadamantyl-imidazol-2-ylidene (II), by Arduengo *et al.*³⁶⁶, obtained by deprotonation of its corresponding salt with a strong base (NaH). Since this discovery, NHCs have been studied extensively, in particular as strong donor ligands for transition metals²⁹⁻³¹ in catalysis and lately as organocatalysts.³⁶ The use of NHCs as ligands has prompted a massive effort to modify their electronic and steric properties by varying the carbene-bound substituents and developing multidentate donor-functionalized analogues.³²⁻³⁵ Although the major focus in the literature has been on ligands based on two donors to stabilize the carbene (“push-push” carbenes), early work on acyclic carbenes³⁶ and recent expansion toward stable cyclic (alkyl)(amino)carbenes^{41, 42} has reinforced the importance of investigating new families of carbene ligands.

5.1.2 Transition metal carbene complexes

Carbene-metal complexes are classified into two categories based on the nature of their carbon-metal bonding: Fischer carbene and Schrock carbene complexes.^{367,368} The first recognized metal-carbene complex was synthesized and characterized by Fischer, who reported methoxyphenylmethylene tungsten (0) pentacarbonyl in 1964.³⁶⁹ Fischer carbenes consist of an electron rich late transition metal and a singlet carbene fragment supported by a heteroatom such as nitrogen or oxygen.⁴⁰ The heteroatom substituent of the Fischer carbene ligand helps to stabilize the empty *p* orbital on the carbenic carbon by π donation from one of the lone pairs on the oxygen (resonance structures shown in **Figure 5.2a**).^{369,370} Fischer-type carbenes have a bent geometry with a small valence angle at the central carbon of the

carbene,³⁷¹⁻³⁷⁴ and this allows strong binding to a metal fragment. A resonance structure of a Fischer carbene shows a partial positive charge on the carbene carbon and explains the electrophilicity of these species (**Figure 5.2a**).^{39,370,375} The Fischer-type carbene is a σ -donor via the lone pair, but the empty p orbital on the carbon is also a weak acceptor for π -back donation from the metal d -orbital.³⁷⁰

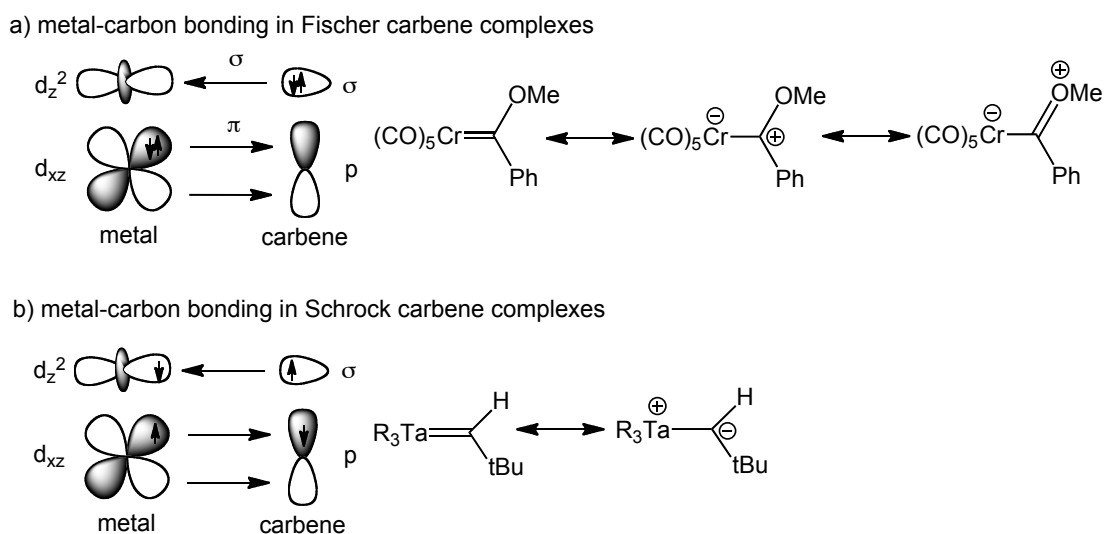


Figure 5.2. Representations of metal-carbon bonding in a) Fischer carbene complexes³⁶⁹ and b) Schrock carbene complexes.³⁷⁶

In contrast to Fischer carbenes, Schrock carbene complexes have their central metal in a high oxidation state (usually an early transition metal)^{367,368,370} and contain C or H substituents at the carbon atom such dialkylcarbenes or alkylcarbenes. The metal-carbon double bond in Schrock carbene complexes is generated from covalent interactions involving electrons in the metal molecular orbitals and two unpaired electrons in a σ and π orbital of the carbene carbon.^{367,368,370} As shown in **Figure 5.2b**,³⁷⁶ the carbenic carbon is more electronegative than the metal, which leads to a net negative charge on the (nucleophilic)carbon.^{367,368,377} Schrock type carbenes are poorly stabilized due to a small gap between their singlet and triplet ground states.^{367,368,39}

Fischer carbenes can be excellent supports for metal complexes.^{34,378} Strategies for forming metal carbene complexes can be classified into two major categories. The first category involves ligand substitution using persistent carbenes or their masked forms such as imidazolium salts.²⁹ The second category encompasses techniques that involve modification

of an existing metal-C(ligand) function. In the first category, the most well-known example is the formation of the Grubbs' second generation NHC-ruthenium catalyst.²⁹ The second category, template synthesis of metal carbene fragments, is the focus of my work.³⁷⁹

One attractive and commonly used route for the template synthesis of carbenes is rapid, spontaneous nucleophilic attack on the coordinated carbon of isocyanide complexes.³⁷⁹⁻³⁸² This affords aminocarbene metal complexes when the metal center is sufficiently acidic. The metal complexes react with protic nucleophiles such as primary and secondary amines or alcohols to yield acyclic diamino- and (alkoxy)(amino)carbene complexes.^{380,383,384} They also afford NHC complexes (cyclic diamino-, (oxy)(amino)- and (thio)(amino)carbenes) by spontaneous, base-promoted, 1,3-dipolarophile-promoted and 1,3-dipole-promoted cyclization^{381,382, 385-387} Complexes with benzannulated carbenes (benzoxazolylienes and benzimidazolinylienes) can be formed from 2-hydroxyaryl isocyanide and 2-aminoarylisocyanide precursors by spontaneous cyclization, though they need to be protected before their metalation.^{388,389} The N,N-dialkylated analogues can be generated via deprotonation of the cyclic NH,NH-carbene ligands followed by N,N-dialkylation with two equivalents of allyl bromide.³⁸⁸ Asymmetrical N,N'-substituted ligands are afforded by deprotonation of 1,3-H,H-NHC ligands followed by alkylation.³⁸⁸ They can also lead to high-oxidation-state-metal complexes coordinated with 4 or 7 carbenes on the central metal.^{390,391} However, these modified N,N'-substituted carbene complexes have not significantly improved catalytic activity due to the limited possible modifications of the carbene ligands.³⁸⁸

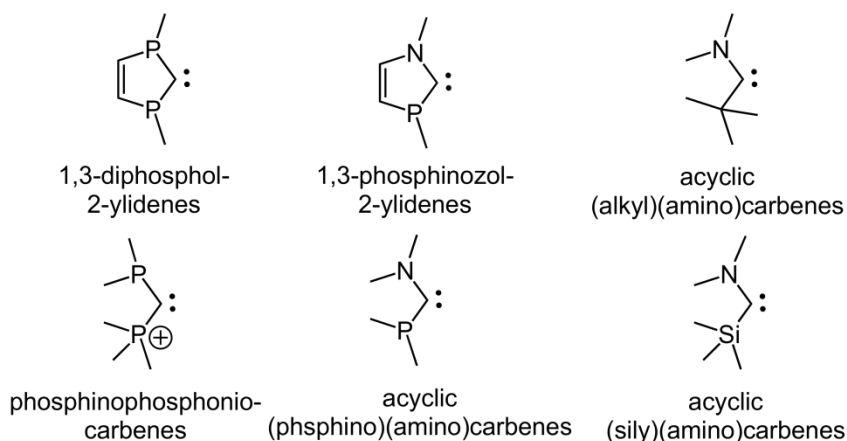


Figure 5.3. Illustration of Bertrand carbenes.^{50,51,392-396}

Use of heteroatoms other than S, O or N in Fischer carbenes is rare. Bertrand and co-workers have shown the enhancement of the electron donating ability of carbenes that contain a phosphino, alkyl (or aryl), or silyl group and an amino group instead of two amino groups at the carbene carbon (**Figure 5.3**).^{50,51,392-396} These can be divided into different categories based on the electronic nature of the substituents. “Push-pull” carbenes, such as (phosphino)(silyl)- and (phosphanyl)carbenes, both bearing a π -donating and a π -withdrawing group. “Push-push” carbenes, such as NHC carbenes, acyclic diaminocarbenes, (oxy)- and (thio)(amino)carbenes, have two π -withdrawing groups, but the amino and alkoxy groups also act as strong σ -electron withdrawing groups (**Figure 5.4**).³⁹ A third category comprises (aryl)(amino)- and (aryl)(phosphino)carbenes which feature one substituent that acts as both a π -donor and σ -attractor (an amino group) or a π - and σ -donor (a phosphino group) and the other substituent acts as a spectator.³⁹

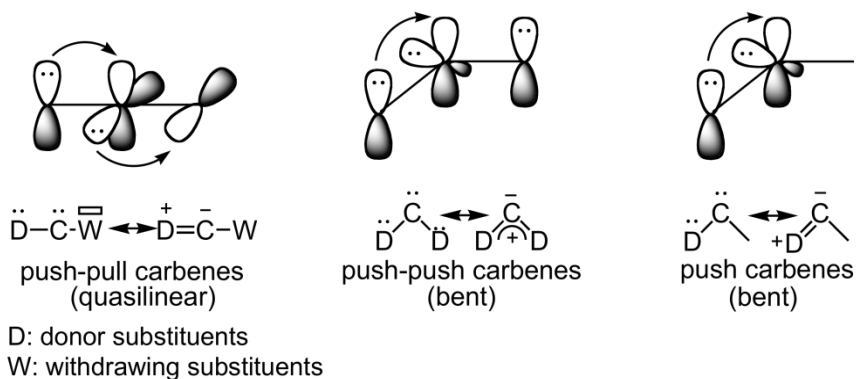


Figure 5.4. Different modes of stabilization of the carbene center with different types of substituents.⁵⁰

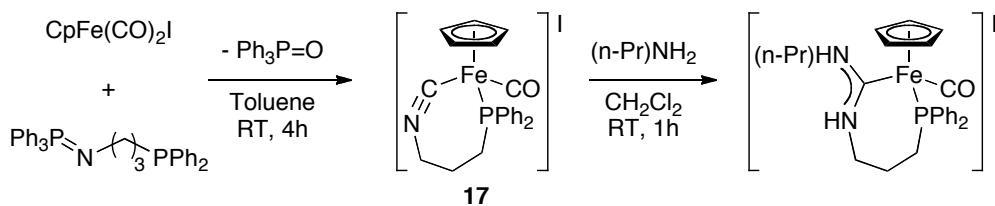
These types of isolated carbenes can be modified in numerous ways to tune their catalytic reactivity and allow for chirality at the α position. The first example of α -arylation of an aldehyde with an aryl chloride has been demonstrated with cyclic (alkyl)(amino)carbene palladium complexes with no evidence of the competing aldol condensation because of the unique steric and electronic properties of the carbene ligand.⁴¹ These open carbenes should induce higher chiral effects compared with either modification of 4 and/or 5 positions or simple attachment of chiral substituents at the amine.

Despite their promise in catalysis, carbenes with P or Si substituents remain largely unexplored because the synthesis of the free carbenes is complicated, and, most importantly, the isolated carbenes are difficult to study and apply to catalysis due to their instability to temperature and/or moisture and their sensitivity to air. Therefore, the synthesis of these carbene metal complexes is very limited. Prior to my work there was only one example of an acyclic (silyl)(amino)carbene complex reported in the literature,⁵⁰ and no examples of monodentate (phosphino)(amino)carbenes (only two examples of side-on coordinated acyclic (phosphino)(amino)carbene complexes (η^2 -complexes) are known).⁴⁸ The only known methodology for formation of these carbene complexes is formation of the free carbene followed by ligand substitution, as described above.

5.2 Results and discussion

In 1995, Liu and co-workers³⁹⁷ reported the synthesis of an acyclic diamino carbene iron(II) complex from the reaction of phosphino-isocyanide chelated iron(II) complex **17** with *n*-propylamine. Complex **17**, a piano stool iron(II) complex bearing a chelating isocyanide-phosphine ligand, is generated by reacting a phosphinimine-phosphine compound with $\text{CpFe}(\text{CO})_2\text{I}$ (Cp = cyclopentadienyl) and forming phosphine oxide as by-product (**Scheme 5.1**).

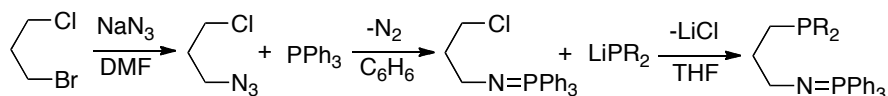
Herein, I have used Liu's complex, **17**, as a starting scaffold for developing a synthetic methodology towards a family of acyclic and cyclic tethered carbene transition metal complexes. Their electronic properties and reactivity have been systematically studied and DFT calculations, in collaboration with Prof. P. Diaconescu, have been used to understand the trends observed.



Scheme 5.1. Synthesis of phosphine-tethered diaminocarbene complexes from **17**.³⁹⁷

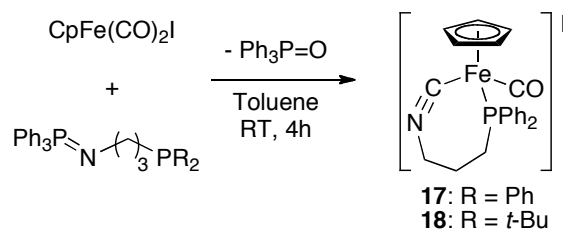
5.2.1 Synthesis of the iron isocyanide template

We began our work by generating the iron isocyanide scaffold developed by Liu et al., complex **17**, via modified procedures (**Scheme 5.1**).³⁹⁷ The phosphinimine-phosphine proligand is generated by treating 3-bromopropylazide with triphenylphosphine to generate the iminophosphorane⁶⁴ followed by reaction of this fragment with lithium phosphide. (**Scheme 5.2**). Although Liu only reported the triphenylphosphine analogue of the compound, we have also prepared the di-*t*-butylphosphine analogue of this proligand. The ³¹P{¹H} NMR spectra of the phosphino-phosphinimine ligand Ph₃P=N(CH₂)₃PR₂ (R = *t*-Bu) shows two singlets at 28.5 and 3.8 ppm for the phosphino and iminophosphorane moieties (For R = Ph there are singlets at -15.0 and 4.8 ppm).



Scheme 5.2. Synthesis of phosphinimine phosphine proligands (R = Ph, *t*-Bu).^{397, 64}

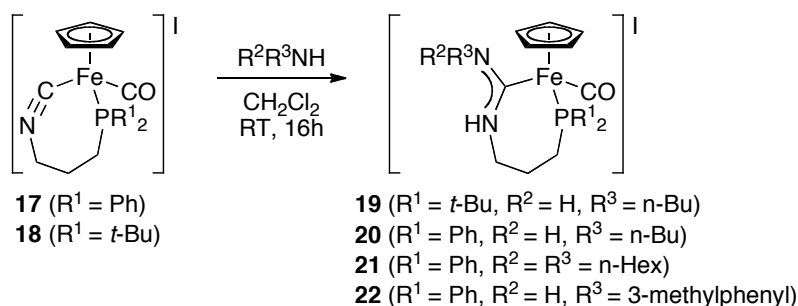
Reaction of Ph₃P=N(CH₂)₃P(*t*-Bu)₂ with CpFe(CO)I₂ formed the (*t*-butyl)phosphine functionalized isocyanide complex **18** (**Scheme 5.3**).³⁹⁷ The IR spectrum of **18** shows peaks corresponding to the isocyanide ($\nu_{\text{CN}} = 2089 \text{ cm}^{-1}$) and carbonyl ($\nu_{\text{CO}} = 1999 \text{ cm}^{-1}$) moieties. The ¹³C{¹H} NMR spectrum of **18** shows signals for the isocyanide and carbonyl carbons at 183.1 and 214.2 ppm, respectively. These data confirm the formation of the isocyanide complex **18** and Ph₃P=O which suggests a nucleophilic attack of the iminophosphorane at the carbonyl ligand. The ³¹P{¹H} NMR spectrum of the reaction mixture containing **18** shows a signal at 29.9 ppm for Ph₃P=O as well as a signal at 53.8 ppm, which indicates the formation of a phosphino moiety coordinated to the metal center (87.7 ppm for **18**).



Scheme 5.3. Synthesis of the phosphino-isocyanide iron (II) complexes, **17** and **18**.³⁹⁷

5.2.2 Acyclic diaminocarbene complexes

Reactions of complexes **17** and **18** with excess *n*-butyl-, di-hexyl-, or 3-methylphenylamine at room temperature in CH₂Cl₂ yield acyclic, diaminocarbene complexes **19-22** in greater than 70% yield (**Scheme 5.4**). The characteristic features of **19** are two singlets in the ¹H NMR spectrum at 5.96 and 7.97 ppm, corresponding to the **19** N-*H* protons, an upfield shifted ³¹P{¹H} NMR signal at 77.9 ppm, and a significantly downfield shifted ¹³C{¹H} NMR signal at 221 ppm. The NMR spectral features of carbene complexes **20-22** are similar to those of **19**; complex **21**, which was formed from a secondary amine, shows only one singlet for the N-*H* proton, at 7.75 ppm. The average ν_{CO} and ν_{CN} stretching frequencies for **19-22** are 1950 and 1541 cm⁻¹, respectively, indicating minimal electronic changes with ligand substitution. Although it is possible to form orthometallated aminocarbene complexes of electron poor metals substituted with a phenyl group,³⁹⁸ orthometallation is not observed with complex **22** due to the electronically saturated iron center.



Scheme 5.4. Synthesis of acyclic diaminocarbene complexes **19-22**.

The molecular structures of **19** and **21** were determined by single-crystal X-ray diffraction and show piano-stool iron centers with a distorted octahedral geometry coordinated to planar carbenes (**Figure 5.5**). The Fe-C_{carbene} (**19**, 1.958 Å; **21**, 1.992 Å), C_{carbene}-N1 (**19**, 1.332 Å; **21**, 1.345 Å) and C_{carbene}-N2 (**19**, 1.342 Å; **21**, 1.356 Å) distances are longer than those of the parent isocyanide complex **1** (Fe-C_{isocyanide}, 1.77 Å and C_{isocyanide}-N, 1.20 Å).³⁹⁷ The Fe-C_{carbene}-N1 angles (~120°) are more acute than the Fe-C-N angle in **17** (169°). The N1-C_{carbene}-N2 angles (**19**, 115.1°; **21**, 113.6°) are intermediate between free acyclic diaminocarbenes (121°)^{399,400} and NHCs (104.7 and 102.2°)^{366,401} but larger than reported for half-sandwich iron(II) NHC complexes likely due to their acyclic nature.⁴⁰² These results indicate that there

are no significant differences between secondary and tertiary amino substituents on the carbene carbon and the coordinated carbene has the resonance form $-\text{N}=\text{C}=\text{N}-$, with very weak electron back donation from the metal center to the carbene carbon (more below).

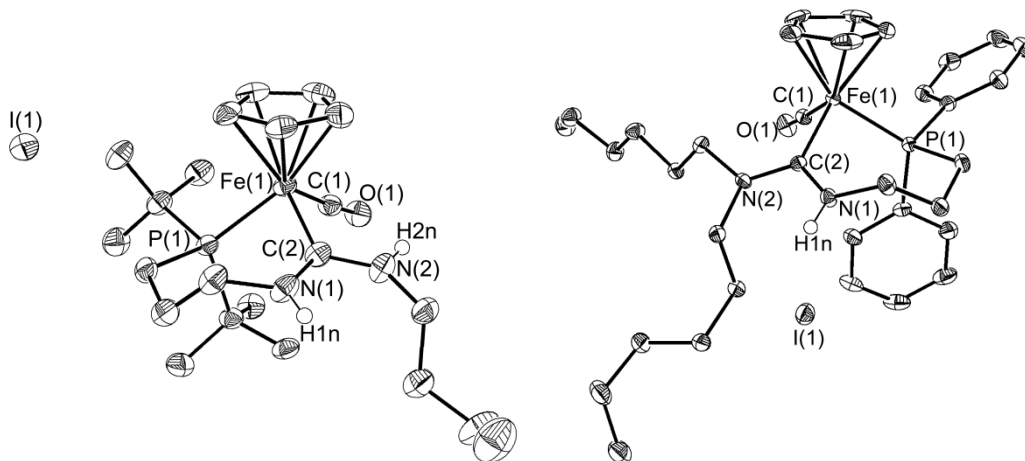


Figure 5.5. Molecular structures of complexes **19** (left) and **21** (right) (depicted with thermal ellipsoids at 50% probability and most H atoms omitted for clarity).

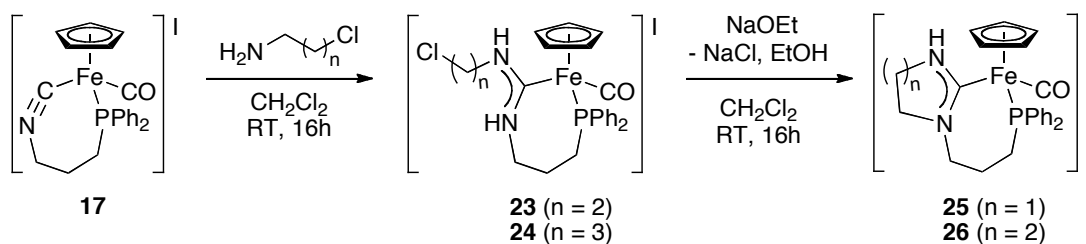
Table 5.1. Selected distances (Å) and angles (°) for **19** and **21**.

Complex 19				
Bond Lengths	C1-Fe1	1.742(3)	C1-O1	1.152(3)
	C2-Fe1	1.958(3)	C2-N1	1.332(4)
	P1-Fe1	2.287(9)	C2-N2	1.342(4)
Bond Angles	N1-C2-N2	115.1(3)	Cl-Fe1-C2	95.93(12)
	N1-C2-Fe1	126.7(2)	C1-Fe1-P1	89.58(10)
	N2-C2-Fe1	117.9(2)	C2-Fe1-P1	94.55(9)
	Fe1-C1-O1	175.8(2)		
Complex 21				
Bond Lengths	C1-Fe1	1.749(3)	C1-O1	1.151(3)
	C2-Fe1	1.992(3)	C2-N1	1.345(3)
	P1-Fe1	2.2029(8)	C2-N2	1.356(3)
Bond Angles	N1-C2-N2	113.6(2)	C1-Fe1-P1	89.00(10)
	N1-C2-Fe1	122.7(2)	C2-Fe1-P1	95.03(8).
	N2-C2-Fe1	123.6(2)	C2-N1-C10	128.1
	Fe1-C1-O1	175.6(3)	C2-N2-C23	124.1(2)
	Cl-Fe1-C2	95.23(12)		

The above electronic interpretation based on structural characteristics is supported by the results of DFT calculations performed by Prof. P. Diaconescu on the cations of **19**, **20**, and **21**.⁵

5.2.3 Cyclic diaminocarbene complexes

Analogous tethered N-heterocyclic carbene complexes are generated via a two-step route (**Scheme 5.5**). Reactions of **17** with 4 equivalents of 2-chloroethylamine or 3-chloropropylamine afford the corresponding acyclic diaminocarbene complexes **23** and **24** in greater than 90% yield. Subsequent dehydrohalogenations of **23** and **24** by excess NaOEt yield the air-stable, 5- and 6-membered, cyclic diaminocarbene complexes **25** and **26** in greater than 80% yield. Transformation of the acyclic diaminocarbene **23** to the 5-membered cyclic diaminocarbene **25** is readily monitored by ¹H NMR spectroscopy: the two broad singlets for the N-H protons at 6.69 ppm and 8.84 ppm of **23** are replaced by one broad resonance at 8.31 ppm for the **25** NH proton (**Figure 5.6a**). Similar results are observed for the transformation of **24** to **26** (**Figure 5.6b**).



Scheme 5.5. Synthesis of cyclic diaminocarbene complexes **25** and **26**.

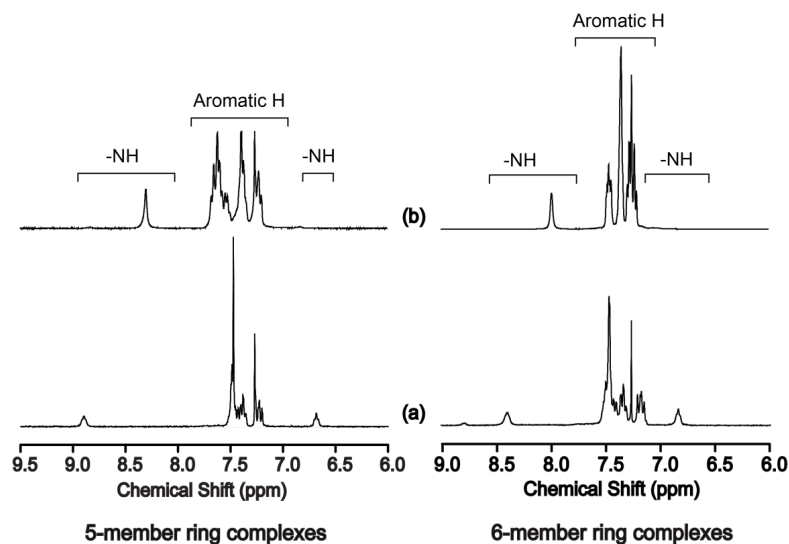


Figure 5.6. ^1H NMR spectra of (a) the acyclic diaminocarbene complexes, **23** (left), **24** (right), and (b) the 5- and 6-membered cyclic diaminocarbene complex, **25** (left), **26** (right) (400 MHz, CDCl_3 , 25 $^\circ\text{C}$).

The molecular structures of **23** and **26** were determined by single-crystal X-ray diffraction and show similar octahedral piano-stool iron centers consistent with those of the acyclic diaminocarbene complexes **19** and **21** (**Figure 5.7** and **Figure 5.8**). The carbonyl stretching frequencies of the acyclic ($\nu_{\text{CO}} = 1948\text{--}1959 \text{ cm}^{-1}$) and cyclic ($\nu_{\text{CO}} = 1949\text{--}1952 \text{ cm}^{-1}$) diaminocarbene fragments are also similar, indicating very little electronic difference between the species. More distinct differences in CO frequencies are reported between acyclic (ν_{CO} avg. of 2021 cm^{-1}) and saturated cyclic (ν_{CO} avg. of 2038 cm^{-1}) square planar carbene complexes such as *cis*-(CO) $_2$ Rh(carbene)Cl.⁴⁰³

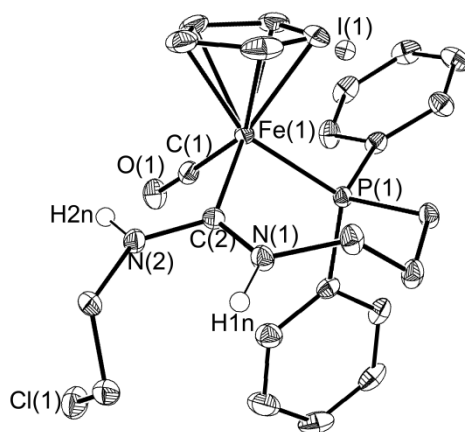


Figure 5.7. Molecular structure of complex **23** (depicted with thermal ellipsoids at 50% probability and most H atoms omitted for clarity).

Table 5.2. Selected distances (Å) and angles (°) for **23**.

Complex 23				
Bond Lengths	C1-Fe1	1.744(3)	C1-O1	1.147(4)
	C2-Fe1	1.949(3)	C2-N1	1.330(4)
	P1-Fe1	2.192(8)	C2-N2	1.344(4)
Bond Angles	N1-C2-N2	115.7(3)	Cl-Fe1-C2	93.38(13)
	N1-C2-Fe1	127.2(2)	C1-Fe1-P1	89.66(10)
	N2-C2-Fe1	117.1(2)	C2-Fe1-P1	95.23(9)
	Fe1-C1-O1	177.5(3)	C2-N1-C10	127.2(2)

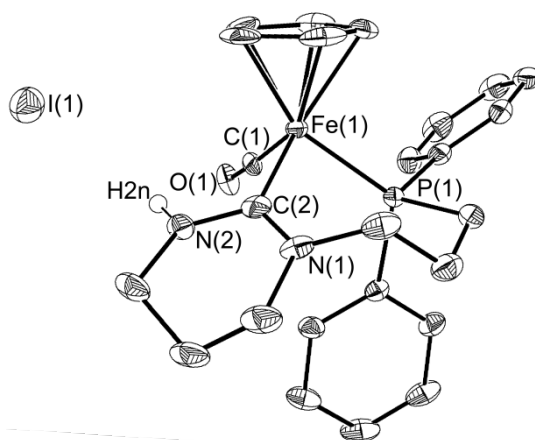
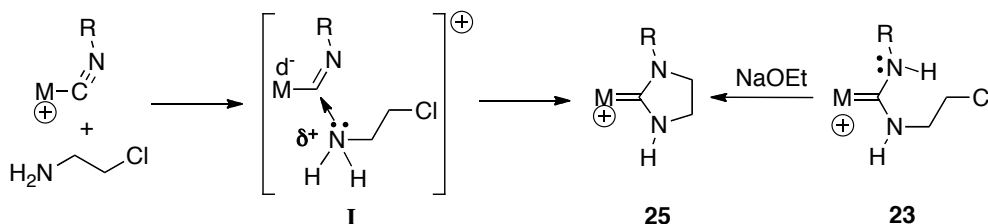


Figure 5.8. Molecular structure of complex **26** (depicted with thermal ellipsoids at 50% probability and most H atoms as well as solvent molecules omitted for clarity).

Table 5.3. Selected distances (Å) and angles (°) for **26**.

Complex 26				
Bond Lengths	C1-Fe1	1.751(7)	C1-O1	1.137(9)
	C2-Fe1	1.972(7)	C2-N1	1.336(9)
	P1-Fe1	2.1958(19)	C2-N2	1.336(10)
Bond Angles	N1-C2-N2	116.7(6)	Cl-Fe1-C2	96.5(3)
	N1-C2-Fe1	127.2(6)	C1-Fe1-P1	88.5(2)
	N2-C2-Fe1	116.1(5)	C2-Fe1-P1	93.4(2)
	Fe1-C1-O1	172.9(6)	C2-N1-C5	123.7(6)

The electronic similarity between **23** and **25** and between **25** and **26** determined from structural characteristics is supported by the results of DFT calculations performed on the cations for the three complexes. The comparison between the three complexes indicates that all the electronic parameters investigated are similar to each other and to those for complexes **19-21**.⁵

**Scheme 5.6.** The two proposed mechanisms for the formation of **25**.

Formation of the intermediate species **23** and **24** suggests a mechanism different from that proposed for the reaction of haloamines with isocyanide complexes.³⁷⁹ In one case, the formation of the cyclic diaminocarbene palladium complexes is proposed to occur by initial nucleophilic attack by the bromoethylamine on the palladium-bound isocyanide carbon to yield an imino intermediate (**I**) with subsequent deprotonation and ring closure in the presence of a second molecule of 2-bromoethylamine (**Scheme 5.6**). However, intermediate **I** was not detected in this and other similar systems.⁴⁰⁴⁻⁴⁰⁶ We propose a similar first step; however, in our system this is followed by proton transfer in intermediate **I** from the amine to the imido to give the acyclic diaminocarbene complex **23**, which is not observed nor proposed in the case of the palladium complexes.³⁷⁹ The NOE spectrum of **23**, in which we selectively saturated the N2-*H* signal, shows that N1-*H* (6.69 ppm) and N2-*H* (8.84 ppm) are not close enough to have dipole-dipole coupling. In addition, the four methylene protons of

the chloroethyl functionality are close enough to have a through-space interaction with the saturated N2-*H* resonance (**Figure 5.9**). Deprotonation of **23** by the addition of NaOEt results in a spontaneous intramolecular cyclization to yield complex **25**.

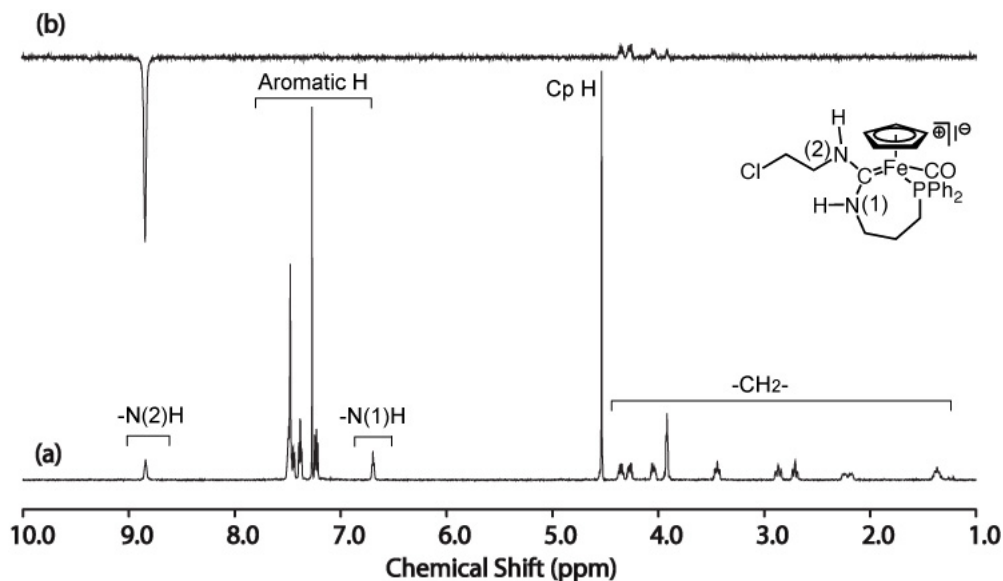
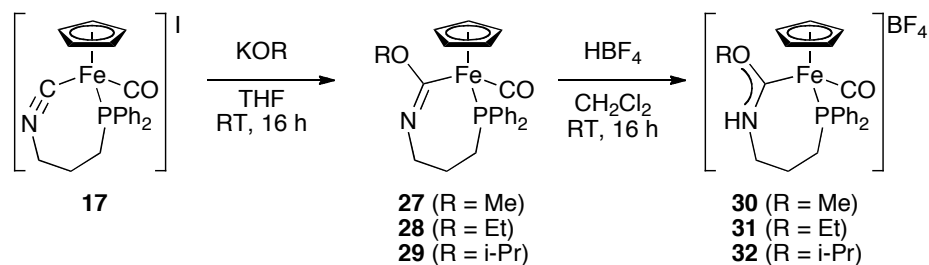


Figure 5.9. (a) ^1H NMR spectrum and (b) the nuclear Overhauser effect (NOE) spectrum of complex **23** saturating the N2-*H* signal at 8.84 ppm (600 MHz, CDCl_3 , 25 °C).

5.2.4 (Oxy)(amino)carbene complexes

The chemistry of the diamino carbenes can be expanded to (oxy)(amino)carbenes. Literature reports show that the reaction of metal-activated isocyanide ligands with alcohols can form cyclic and acyclic (oxy)(amino)carbenes in one step.³⁷⁹ However, the lack of a reaction between the coordinated isocyanide in **17** and protic alcohols prompted us to use a two-step route comprised of direct nucleophilic attack on the isocyanide by an alkoxide, followed by protonation of the resulting ylide to form carbene complexes (**Scheme 5.7**).⁴



Scheme 5.7. Synthesis of acyclic (oxy)(amino)carbanion and carbene complexes, **27-29** and **30-32**, respectively.

Reactions of complex **17** with KOR (R = Me, Et, *i*-Pr) form ylidene complexes **27-29** in quantitative yield. These complexes lead to acyclic (oxy)(amino)carbene complexes **30-32** in 90% isolated yield upon subsequent protonations of the imido nitrogen with HBF₄ (**Scheme 5.7**). The carbonyl stretching frequencies of the ylidene complexes are approximately 20 cm⁻¹ lower than those of the carbene complexes, indicating a more electron rich iron center with the formally anionic ylidene carbon ligand. The respective average C=N stretching frequencies of complexes **27-29** (~1560 cm⁻¹) and **30-32** (1550 cm⁻¹) suggest greater electronic communication through the carbene carbon and the lone pair on the neighboring oxygen. DFT calculations performed on the ylidene complex **27** and the cation of **30** also indicate that there are larger electronic differences between these two complexes than between any other pair/series previously calculated.⁵

The ¹H NMR spectra of the ylidene complexes **27-29** show characteristic resonances for the methyl and methine groups of the alkoxide substituents at high fields. The spectra of the corresponding carbene complexes **30-32** show one additional broad singlet for the N-H resonance at ~8.7 ppm. The ¹³C NMR spectra of **30-32** show signals that are ~40 ppm downfield of **27-29**, signifying a slight difference in electron density between the carbene and ylidene carbons. The molecular structure of **27** was determined by X-ray crystallography (**Figure 5.10**). The C_{ylidene}-Fe distance in **27** (1.965 Å) is similar to that of **19** (1.958 Å) and about 0.19 Å greater than that of isocyanide complex **17** (1.77 Å).³⁹⁷

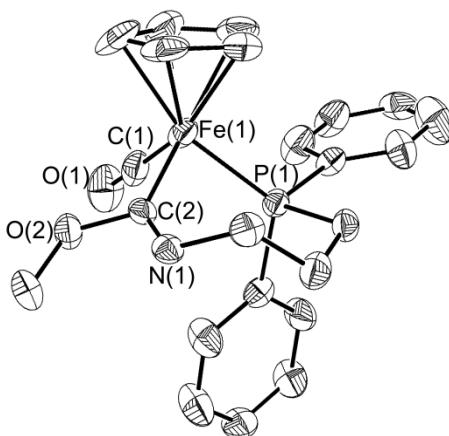
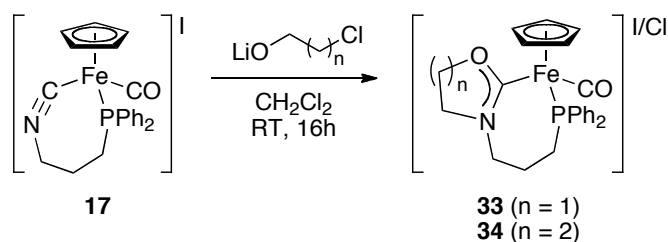


Figure 5.10. Molecular structure of complex **27** (depicted with thermal ellipsoids at 50% probability and all H atoms as well as solvent molecules omitted for clarity).

Table 5.4. Selected distances (Å) and angles (°) for **27**.

Complex 27				
Bond Lengths	C1-Fe1	1.744(6)	C1-O1	1.160(7)
	C2-Fe1	1.965(6)	C2-N1	1.260(6)
	P1-Fe1	2.263(5)	C2-O2	1.403(6)
Bond Angles	O2-C2-N1	114.9(5)	Cl-Fe1-C2	92.4(2)
	O2-C2-Fe1	174.41(1)	C1-Fe1-P1	90.96(18)
	N1-C2-Fe1	134.8(4)	C2-Fe1-P1	90.48(16)
	C2-N1-C8	120.2(4)	C2-O2-C11	116.09(7)

Five- and six-membered cyclic (oxy)(amino)carbene complexes, **33** and **34**, were synthesized by the reaction of lithium 2-chloroethoxide or 3-chloropropanoxide with complex **17** in CH_2Cl_2 at room temperature (**Scheme 5.8**). The ^1H NMR spectrum of each complex shows new methine resonances, while the $^{13}\text{C}\{^1\text{H}\}$ NMR spectra show downfield shifted carbene carbon signals, 229.0 and 231.3 ppm for **33** and **34**, respectively. The IR spectra of **33** and **34** show $\text{C}=\text{N}$ absorptions at 1529 cm^{-1} for both complexes, a $\sim 34\text{ cm}^{-1}$ decrease in ν_{CO} compared to **17**. The carbonyl stretch in **34** (1966 cm^{-1}) is similar to that in the acyclic analogues **30-32** and higher than in the ylidene complex **27** (1937 cm^{-1}), suggesting a more electron rich iron center in the latter compounds. These results also suggest that, as with the cyclic diaminocarbene complexes, the change in ring size does not have a significant effect on the electronic properties of the complexes.



Scheme 5.8. Synthesis of 5- and 6- membered cyclic (oxy)(amino)carbene complexes, **33-34**.

The molecular structure of **34** was determined by X-ray crystallography (**Figure 5.11**). The Fe-C_{carbene} distance (1.976 Å) is slightly longer than the analogous distance in the ylidene complex **27** (1.965 Å), but the difference is within experimental error. As with previously discussed complexes, the C_{carbene}-N1 distance of **34** (1.322 Å) is longer than that of the acyclic (oxy)(amino) ylidene complex **27** (1.260 Å) and that of the isocyanide complex **17** (1.20 Å). The C_{carbene}-O2 distance of **34** (1.330 Å) is shorter than that of complex **27** (1.403 Å). Interestingly, the C_{carbene}-N1 (1.332 Å) and C_{carbene}-O2 (1.330 Å) distances are similar. DFT calculations on the full cation of **34** agree with the crystallographic observations.⁵

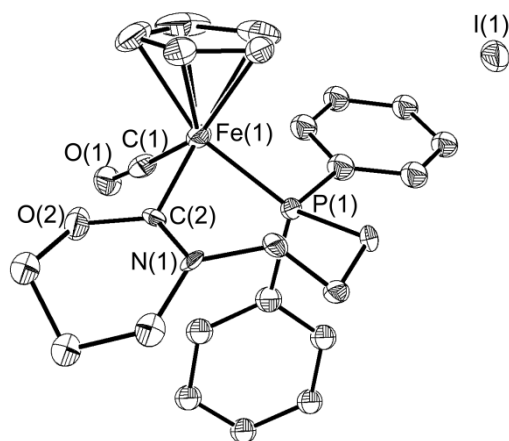


Figure 5.11. Molecular structure of complex **34** (depicted with thermal ellipsoids at 50% probability and all H atoms omitted for clarity).

Table 5.5. Selected distances (Å) and angles (°) for **34**.

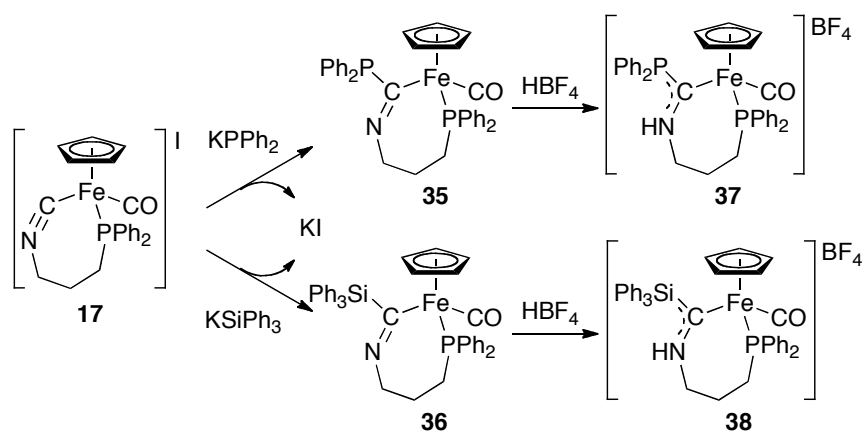
Complex 34				
Bond Lengths	C1-Fe1	1.742(4)	C1-O1	1.146(5)
	C2-Fe1	1.976(5)	C2-N1	1.322(9)
	P1-Fe1	2.185(7)	C2-O2	1.330(11)
Bond Angles	N1-C2-O2	122.8(7)	C2-N1-C23	122.5(9)
	N1-C2-Fe1	127.6(5)	C10-N1-C23	113.8(9)
	O2-C2-Fe1	109.5(5)	C1-Fe1-C2	92.0(2)
	Fe1-C1-O1	176.9(3)	C1-Fe1-P1	93.27(19)
	C2-N1-C10	123.6(8)	C2-Fe1-P1	93.5(3).

5.2.5 Acyclic (silyl) and (phosphino)(amino)carbene complexes

Recent expansion of the carbene field to stable cyclic (alkyl)(amino)carbenes (CAACs)⁴¹ has demonstrated that “push-spectator” carbenes (NX-carbenes; X = C, P, Si) can be stronger donors than NHCs (“push-push” carbenes) and, with a judicious choice of alkyl substituents, can lead to efficient catalysis.⁴²

P- or Si-functionalized carbenes remain largely unexplored as ligands,^{36,39,43,44} although rare examples were shown to be excellent ligands for rhodium.⁴⁵⁻⁵¹ Challenges in the synthesis of the free carbenes and in the formation of complexes via ligand substitution pathways have severely limited the utility of these species as ligands. Donor-functionalized analogues of these carbenes are hitherto unknown.

We used a similar two step template methodology as outlined above to generate donor-functionalized (phosphino)(amino)- and (silyl)(amino)carbenes.^{407,408} To our knowledge this strategy has not been used for P- or Si-substituted carbenes previously. Our general methodology, which was used to generate acyclic (oxy)(amino)carbene complexes **30-32**, involves nucleophilic attack on a chelating isocyanide-triphenylphosphine ligand coordinated to a CpFe(CO) fragment, complex **17**, to form ylidene complexes followed by protonation of the resulting imine to yield the desired carbene complexes (**Scheme 5.9**).^{48,49}



Scheme 5.9. Methodology for the template synthesis of donor-functionalized NX-Carbenes (X = P, Si).

The reaction of the iron isocyanide complex **17**^{397,409} with one equivalent of KPPH₂ or KSiPh₃ in THF at $-78\text{ }^{\circ}\text{C}$ affords the corresponding iron ylidene complexes **35** and **36**, respectively. However, complex **36** was obtained in 28% isolated yield along with an unidentified byproduct (10% isolated yield). The molecular structures of **35** and **36** were determined by single-crystal X-ray crystallography and show octahedral piano-stool iron centers similar to that of the reported isocyanide complex **17** (Figure 5.12).^{397,409} The metal-bound carbon atoms in **35** and **36** are planar. The Fe-C_{ylidene} distances in **35** and **36** of 2.005(3) and 1.997(3) are significantly longer than the Fe-C_{isocyanide} distance reported for **17** (1.77 Å) indicating that the latter has a greater bond order than the Fe-C_{ylidene} bonds. In contrast to the sole reported Rh-NPC complex^{48,49} the ylidene-bound phosphorous atom in **35** is not coordinated to the metal. In this case η^2 coordination is not expected because complex **35** features a coordinatively saturated iron center.⁴¹⁰

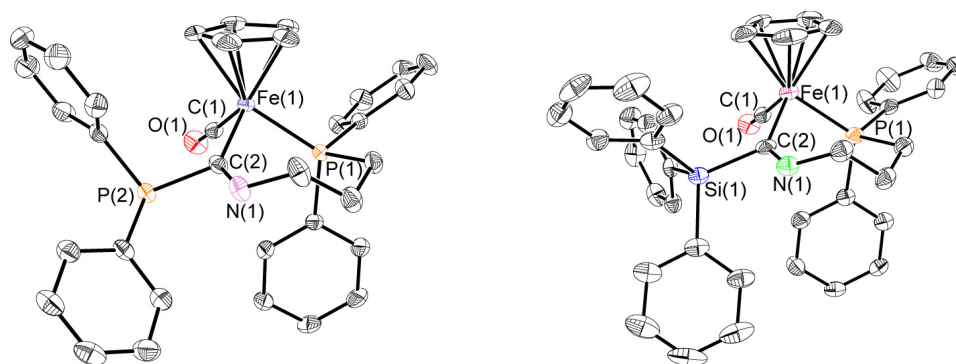


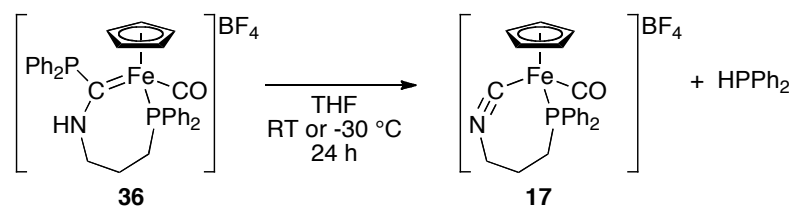
Figure 5.12. Molecular structures of **35** (left) and **36** (right) (thermal ellipsoids at 35% probability).⁴

Table 5.6. Selected distances (Å) and angles (°) for **35** and **36**.

Complex 35				
Bond Lengths	C1-Fe1	1.7325(19)	C1-O1	1.158(2)
	C2-Fe1	1.9973(18)	C2-N1	1.262(2)
	P1-Fe1	2.1735(6)	C2-P2	1.8852(18)
Bond Angles	N1-C2-P2	115.28(13)	C1-Fe1-C2	96.01(8)
	N1-C2-Fe1	132.94(14)	C1-Fe1-P1	92.34(6)
	P2-C2-Fe1	111.78(9)	C2-Fe1-P1	89.85(5)
	Fe1-C1-O1	172.82(16)	P2-C2-Fe1	111.78(9)
Complex 36				
Bond Lengths	C1-Fe1	1.741(3)	C1-O1	1.163(3)
	C2-Fe1	2.005(3)	C2-N1	1.289(4)
	P1-Fe1	2.1868(9)	C2-Si1	1.913(3)
Bond Angles	N1-C2-Si1	106.3(2)	C1-Fe1-C2	98.98(15)
	N1-C2-Fe1	130.4(2)	C1-Fe1-P1	88.49(12)
	Si1-C2-Fe1	122.68(16)	C2-Fe1-P1	89.97(9)
	Fe1-C1-O1	170.9(4)	Si1-C2-Fe1	122.6(8)

The reaction of the ylidene complexes **35** and **36** with an equimolar amount of HBF_4 in CHCl_3 at $-35\text{ }^\circ\text{C}$ forms the corresponding carbene complexes **37** and **38** (Scheme 5.9). The (silyl)(amino)carbene complex **38** was obtained in 97% isolated yield; however, although the analogous (phosphino)(amino)carbene complex **37** is formed quantitatively, it decomposes in solution and more slowly in the solid state (see below). The characteristic downfield N-H ^1H NMR resonances at 9.64 and 10.62 ppm confirm the formation of the carbene complexes **37** and **38**, respectively; the resonance for the related diaminocarbene iron complex appears at

7.97 ppm.³⁹⁷ The $^{13}\text{C}\{^1\text{H}\}$ NMR spectra for **37** and **38** show significantly deshielded Fe- C_{carbene} signals at 276.4 and 299.4 ppm. These downfield signals are indicative of push-spectator carbenes;³⁹⁷ the ^{13}C NMR signals for reported complexes of push-push carbenes are significantly more upfield.^{48,49} The (silyl)(amino)carbene fragment does not behave as a push-pull carbene and is instead analogous to aryl- or alkylamino carbenes.⁵⁰



Scheme 5.10. Conversion of carbene complex **37** to **17** and HPPPh₂.

A THF solution of the (phosphino)(amino)carbene complex **37** reverts to the isocyanide complex **17** and diphenylphosphine in a few hours, although traces of **17** are evident after only a few minutes at room temperature (**Scheme 5.10**). This decomposition process occurs at room temperature as well as at -35°C over several hours. The phosphine release from **37** and formation of **17** was monitored by $^{31}\text{P}\{^1\text{H}\}$ NMR spectroscopy (**Figure 5.13**). The direct reaction of isocyanide complex **17** with HPPPh₂ does not result in the formation of carbene complex **37**. The $^{31}\text{P}\{^1\text{H}\}$ NMR spectrum of **37** shows two sets of doublets at 38.1 and 51.0 ppm for the Fe- and carbene-bound phosphines, respectively ($^3J_{\text{P-P}} = 12$ Hz). Over time, these signals disappear and new signals for Fe-*P* in **17** (54.4 ppm) and diphenylphosphine (−40 ppm) appear. Furthermore, a number of different decomposed products were observed after 24h. The reaction likely occurs via intramolecular deprotonation of the cyclic amine by the carbene-bound diphenylphosphine, followed by phosphine elimination.⁴⁸ This indicates that unlike the amino functionality there is no π contribution from the phosphino-moiety which retains its lone pair and is able to deprotonate the amine.

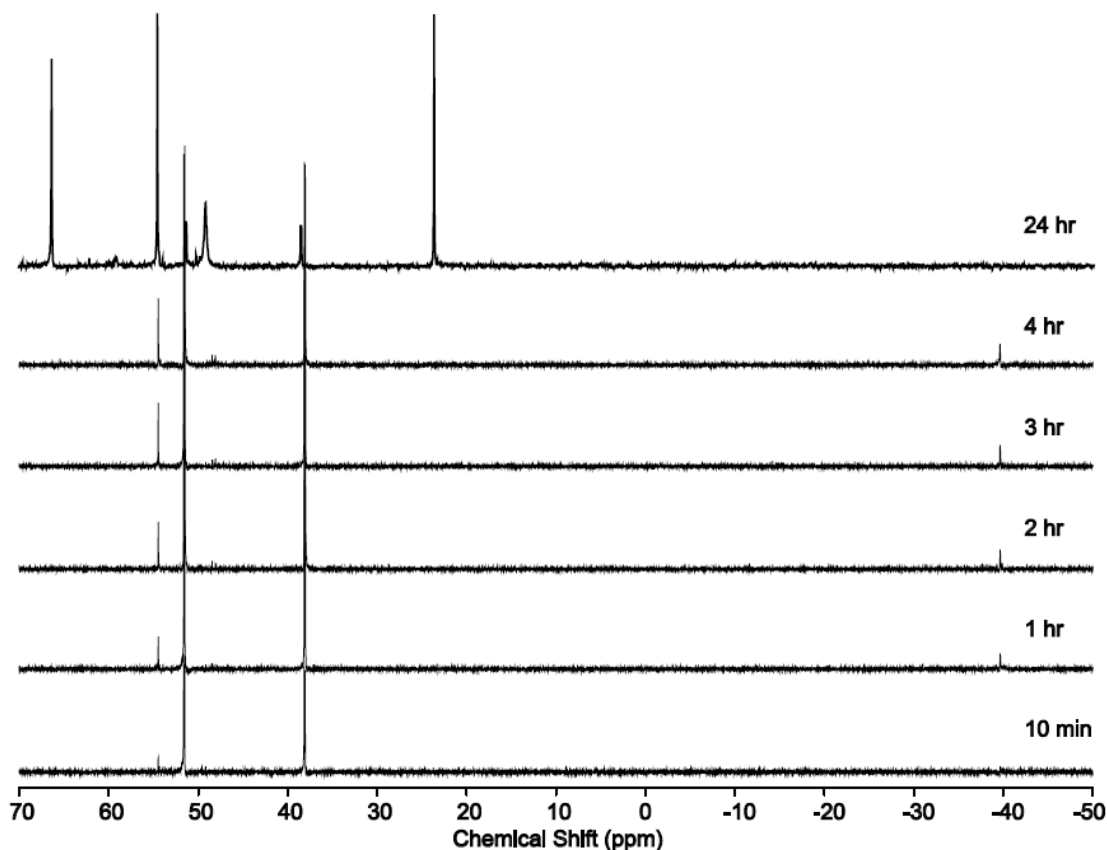


Figure 5.13. $^{31}\text{P}\{^1\text{H}\}$ NMR spectra of the (phosphino)(amino)carbene complex **37** monitored at different time periods at room temperature.

The carbonyl stretching frequencies of complexes **35–38** were used to gauge the electronic differences between the ligands. The ylidene complexes **35** and **36** had ν_{CO} stretches at 1912 and 1915 cm^{-1} respectively, while the carbene complexes **37** and **38** had stretches at 1956 and 1959 cm^{-1} . The ylidene complexes **35** and **36** are neutral while the carbene complexes **37** and **38** are cationic. Therefore, a direct comparison between them is not meaningful. However, the progressive increase in the stretching frequencies of the latter suggests decreased electron density on the metal which corresponds to the decrease in π electron contribution to the carbene center as substituents are changed from N (ν_{CO} 1949 cm^{-1}) to P to Si.

The molecular structure of **38** has been elucidated by X-ray crystallography and shows a distorted-octahedral iron center similar to that of **36** (**Figure 5.14**). The Fe- $\text{C}_{\text{carbene}}$ distance (1.943 Å) of **38** is shorter than that of **36** (2.005 Å), in agreement with the ionic nature of **38**. The $\text{C}_{\text{carbene}}\text{-N1}$ distance (1.302 Å) of the (silyl)(amino)carbene complex **38** is longer than that

of the ylidene complex **36** (1.289 Å). The C_{carbene}-Si distance (1.933 Å) in **38** is shorter than that of complex **36** (1.913 Å). The distances and angles of **38** are consistent with those in the only other reported (silyl)(amino)carbene complex, (COD)(Cl)Rh=C(NMe₂)(SiMePh₂) (C-N 1.316 Å, C-Si 1.927 Å, C-Rh 1.993 Å).⁵⁰ The structural data support the fact that the Si substituent acts as a spectator, as observed previously.

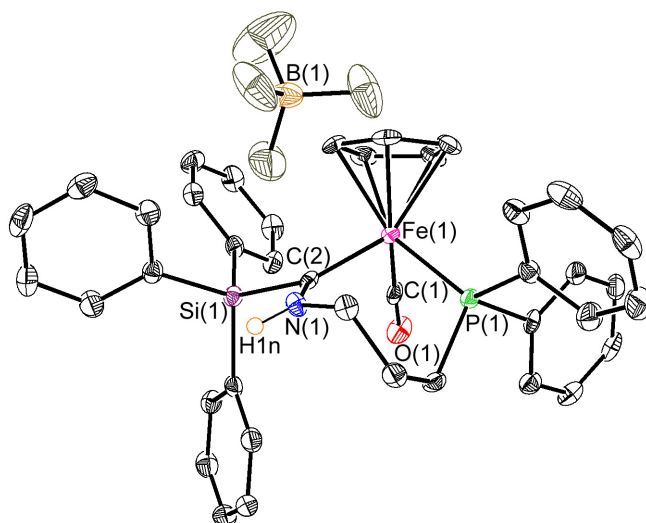


Figure 5.14. Molecular structure of complex **38** (depicted with thermal ellipsoids at 50% probability and most H atoms omitted for clarity).

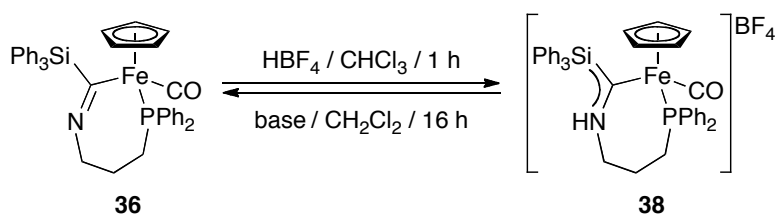
Table 5.7. Selected distances (Å) and angles (°) for **38**.

Complex 38				
Bond Lengths	C1-Fe1	1.750(3)	C1-O1	1.149(4)
	C2-Fe1	1.943(3)	C2-N1	1.302(4)
	P1-Fe1	2.2094(9)	C2-Si1	1.933(3)
Bond Angles	Si1-C2-N1	110.6(2)	Fe1-C1-O1	178.1(3)
	N1-C2-Fe1	127.5(2)	C2-N1-C10	127.7(3)
	Si1-C2-Fe1	121.90(16)		

The above interpretation is supported by the results of DFT calculations performed on the full molecule of **36** and the cation of **38**.⁵ These results are also compared to those obtained from a geometry optimization on the full molecule (COD)(Cl)Rh=C(NMe₂)(SiMePh₂).⁵⁰

5.2.6 Reactivity of acyclic (silyl)(amino) carbene with an unconventional base

The (silyl)(amino)carbene complex **38** can be converted back to the ylidene complex **36** via reaction with 6 equivalents of sodium triacetoxyborohydride ($\text{NaHB}(\text{OAc})_3$) in CH_2Cl_2 , at room temperature under static vacuum overnight. The conversion was monitored by $^{31}\text{P}\{^1\text{H}\}$ NMR spectroscopy (**Figure 5.15**). The reaction is slow; about 30% of complex **38** is converted to **36** in one day without any further decomposition. The full conversion of **38** to **36** requires four evacuations of the reaction mixture in four days. A more reactive hydride source such as LiAlH_4 reacts rapidly (1 hour) at room temperature, and even at $-35\text{ }^\circ\text{C}$; however, many byproducts are observed along with the desired product **36**.



Scheme 5.11. Reversible reaction of acyclic (silyl)(amino) ylidene (**36**) and carbene (**38**) complexes.

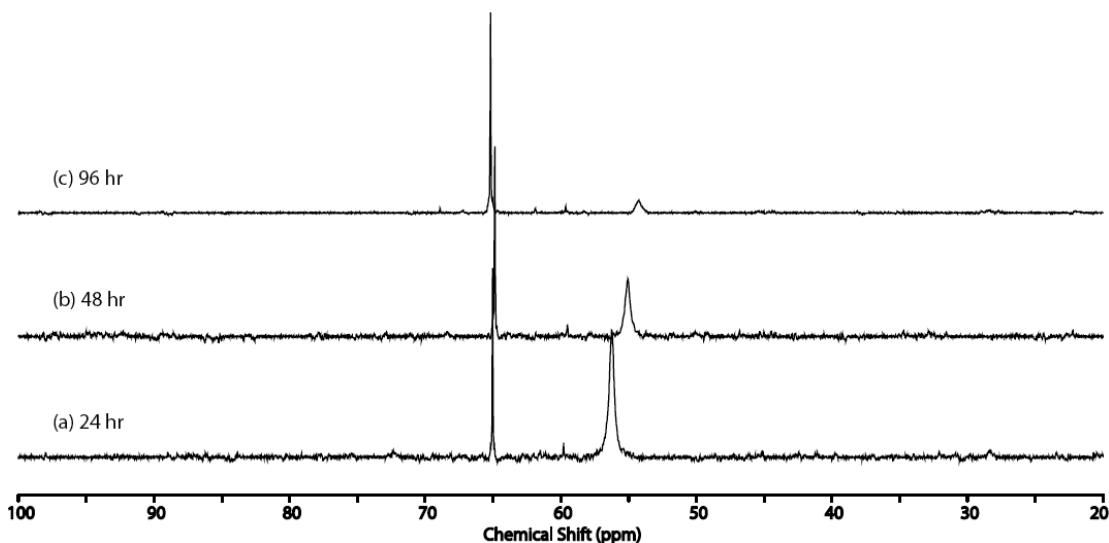


Figure 5.15. $^{31}\text{P}\{^1\text{H}\}$ NMR spectra for conversion of complex **38** to complex **36** by reacting with (a) 6 equivalents, (b) 12 equivalents, and (c) 24 equivalents of $\text{NaHB}(\text{OAc})_3$.

5.3 Conclusion

Herein we described the synthesis and characterization of a family of phosphine-tethered ylidene and carbene complexes of iron(II) using template synthesis from a half-sandwich complex bearing a chelating isocyanide-phosphine ligand.

The acyclic diamino carbene complexes are prepared by the reaction of the isocyanide iron(II) complex with primary and secondary amines, while the 5- and 6-membered cyclic analogues are synthesized using routes reported in the literature, via spontaneous cyclization and base-promoted cyclization, respectively. A new mechanism for the formation of cyclic diaminocarbene complexes is proposed based on in situ observation and crystallographic identification of intermediates.

Direct reaction of alcohols, phosphines, and silanes with the isocyanide iron(II) complex does not form XCN carbene complexes ($X = O, P, \text{ or } Si$). These complexes may be generated, however, via a two-step procedure involving the synthesis of ylidene complexes via nucleophilic attack on the iron-bound isocyanide carbon followed by protonation of the resulting cyclic imine to form the carbene complexes.

Diagnostic $^{13}C\{^1H\}$ NMR data for the resulting carbenes show a distinct trend with the nature of the substituent: $C_{\text{carbene}}\text{-N}$ (~ 219 ppm) $< C_{\text{carbene}}\text{-O}$ (~ 230 ppm) $< C_{\text{carbene}}\text{-P}$ (~ 276 ppm)⁷² $< C_{\text{carbene}}\text{-Si}$ (~ 299 ppm). The shifts correlate well with the donor-acceptor properties of the substituent X in XCN carbene complexes. The greater degree of $C_{\text{carbene}}\text{-X}$ π -bonding, where $X = N$ rather than $X = O, P, \text{ and } Si$, is reflected in the greater shielding of C_{carbene} in aminocarbene complexes. IR spectroscopic data on these octahedral iron complexes are not as diagnostic for determining the different electronic properties of the carbene complexes. DFT calculations were used to support the electronic interpretations based on crystallographic and NMR spectroscopic data. For a series of complexes with different C_{carbene} substituents, the Fe- C_{carbene} Mayer bond order increases from **20** (0.90) to **30** (0.95), and to **38** (1.03).

This work contributes two major findings to the field of metal-carbene chemistry. We have reported the first examples of donor-functionalized NX-carbenes ($X = P, Si$) generated via a two-step template synthesis on a piano-stool iron(II) complex. Spectroscopic evaluation of these complexes indicates that although they are both “push-spectator” carbenes they are nevertheless electronically distinct. This work opens up avenues for

template synthesis of currently inaccessible acyclic and cyclic carbenes. In addition, we were able to systematically study the impact on electronic properties of functionalized aminocarbene complexes by changing different neighboring heteroatoms starting from a single complex, **17**.

5.4 Experimental section

General methods: Unless otherwise specified all procedures were carried out using standard Schlenk techniques or in an MBraun glovebox. A Bruker Avance 300 MHz spectrometer and Bruker Avance 400dir MHz spectrometer were used to record the ^1H NMR, $^{13}\text{C}\{^1\text{H}\}$ NMR, and $^{31}\text{P}\{^1\text{H}\}$ NMR spectra. ^1H NMR chemical shifts are given in ppm versus residual protons in deuterated solvents as follows: δ 5.32 for CD_2Cl_2 , and δ 7.27 for CDCl_3 . $^{13}\text{C}\{^1\text{H}\}$ NMR chemical shifts are given in ppm versus residual ^{13}C in solvents as follows: δ 54.00 for CD_2Cl_2 , and δ 77.23 for CDCl_3 . $^{31}\text{P}\{^1\text{H}\}$ NMR chemical shifts are given in ppm versus 85% H_3PO_4 set at 0.00 ppm. A Waters/Micromass LCT mass spectrometer equipped with an electrospray (ESI) ion source and a Kratos-50 mass spectrometer equipped with an electron impact ionization (EI) source were used to record low-resolution and high-resolution spectra. IR spectra were obtained on a Thermo Scientific FT-IR spectrometer (Nicolet 4700). Diffraction measurements for X-ray crystallography were made on a Bruker X8 APEX II diffraction with graphite monochromated Mo-K α radiation. The structures were solved by direct methods and refined by full-matrix least-squares using the SHELXTL crystallographic software of the Bruker-AXS. Unless specified, all non-hydrogens were refined with anisotropic displacement parameters, and all hydrogen atoms were constrained to geometrically calculated positions but were not refined. ESI mass spectra were obtained on a Waters/Micromass LCT time-of-flight (TOF) mass spectrometer equipped with an electrospray ion source. CHN analysis was performed using Carlo Erba EA1108 elemental analyzer. The elemental composition of an unknown sample is determined by using a calibration factor. The calibration factor is determined by analyzing a suitable certified organic standard (OAS) of a known elemental composition.

All solvents were degassed and dried using 3 Å molecular sieves in an MBraun Solvent Purification System. THF, Et_2O , and C_6H_6 (C_6D_6) were further dried over Na/benzophenone and distilled under N_2 . CH_3CN (CD_3CN), CH_2Cl_2 (CD_2Cl_2), and CHCl_3 (CDCl_3) were dried

over CaH_2 and vacuum-transferred to a Strauss flask and then degassed through a series of freeze-pump-thaw cycles. Deuterium-labeled NMR solvents were purchased from Cambridge Isotope Laboratory. Other chemicals and solvents were purchased from Aldrich, Fisher, Alfa Aesar, or STREM and were used without further purification. 1-azido-3-chloropropane,⁴¹¹ N-(3-chloropropyl)triphenylphosphinimine,³⁹⁷ N-(3-(Diphenylphosphino)propyl)triphenylphosphinimine,³⁹⁷ $\text{CpFe}(\text{CO})_2\text{I}$, KPh_2 ,⁴¹² and KSiPh_3 ^{413,413} were prepared according to literature procedures.

Synthesis of 1-azido-3-chloropropane. Sodium azide, NaN_3 (10.0 g, 63.5 mmol) was added to a solution of 1-bromo-3chloropropane (4.05 g, 63.5 mmol) in DMF (200 ml) at room temperature. The reaction mixture was stirred overnight. Water (200 ml) and ether (100 ml) were added to the reaction mixture, which was partitioned between aqueous and organic layers. The organic layer was washed with water three times and then saturated NaCl solution (50 mL) was added to the organic layer. The collected organic layer was dried over MgSO_4 and concentrated to obtain the desired product (6.54 g, 86%) as colorless oil. ^1H NMR (300 MHz, CDCl_3) δ 2.063 (m, 2H), 3.51 (t, 2H), 3.64 (t, 2H).

Synthesis of N-(3-chloropropyl)triphenylphosphinimine. A 25 ml ether solution of triphenylphosphine (6.05 g, 23.1 mmol) was added to a solution of 1 (2.97 g, 24.8 mmol) in ether (25 ml). The reaction solution was stirred overnight, and the solvent was removed under reduced pressure. A white solid 2 (8.01 g, 98%) was obtained. ^1H NMR (300 MHz, CDCl_3) δ 1.98 (m, 2H), 3.22 (dt, 2H), 3.69 (t, 2H), 7.71 - 7.27 (m, 15H); $^{31}\text{P}\{^1\text{H}\}$ NMR (300 MHz, CDCl_3) δ 6.6 ppm.

Synthesis of N-(3-(Diphenylphosphino)propyl)triphenylphosphinimine. A solution of diphenylphosphine was prepared by addition of a 1.6 M hexane solution of n-butyllithium (4.3 ml, 6.93 mmol) to a solution of diphenylphosphine (1.28 g, 6.89 mmol) in THF (20 ml). The mixture was stirred for 1 hour, then added to a solution of N-(3-chloropropyl)triphenylphosphinimine (2.57 g, 7.25 mmol) in THF (20 ml), and the resulting solution was then stirred overnight at room temperature. The THF solvent was completely removed under reduced pressure, and the residue was dissolved in benzene and filtered through Celite to remove a white precipitate of LiCl. The filtrate was concentrated and

recrystallized from acetonitrile to obtain the desired product (3.29 g, 94%) as a white solid, which is moisture, but not air, sensitive. ^1H NMR (300 MHz, C_6D_6) δ 12.18 (m, 2H), 2.54 (m, 2H), 3.62 (m, 2H), 7.17 (s, 4H), 7.64 (m, 4H), 7.84 (m, 7H); $^{13}\text{C}\{^1\text{H}\}$ NMR (300 MHz, C_6D_6) δ 26.25 (d, 1C), 32.49 (dd, - CPh_2), 46.62 (dd, -CN-), 130.84-133.94 (m, 12C), 140.61 (d, 1C); $^{31}\text{P}\{^1\text{H}\}$ NMR (300 MHz, C_6D_6) δ -14.37 (s, - CPh_2), 5.72 (s, - N=PPh_3).

Synthesis of N-(3-(Di(t-butyl)phosphino)propyl)triphenylphosphinimine. The synthesis was carried out in the same manner as the phenyl analogue (see above). (3.09 g, 92%) ^1H NMR (300 MHz, C_6D_6) δ 1.16 (d, $J=10.4$, 18 H), 1.74 (m, 2H), 2.20 (m, 2H), 3.57 (dt, $J=13.1$, 6.3 Hz, 2H), 7.08 - 7.76 (m, 15H); $^{31}\text{P}\{^1\text{H}\}$ NMR (300 MHz, C_6D_6) δ 28.5 (s, - CPh_2), 3.8 (s, - N=PPh_3).

Synthesis of $\text{CpFe}(\text{CO})_2\text{I}$. A solution of iodine (1.45 g, 5.72 mmol) in 60 ml DCM was added dropwise to a solution of bis(cyclopentadienyl)tetracarbonyldiiron, $\text{Cp}_2\text{Fe}_2(\text{CO})_4$, (2.02 g, 5.72 mmol) in 100 ml DCM at room temperature. The reaction mixture was stirred for 2 hours, and then the solvent was removed under vacuum to obtain a brown solid. The residue was dissolved in benzene and filtered through Celite. The filtrate was dried completely under vacuum, then pentane was added, and the brown solid was collected on a frit by washing with a minimum amount of pentane. (3.50 g, 90%) IR (CDCl_3) 2040 cm^{-1} , 2000 cm^{-1} (ν_{CO}); ^1H NMR (300 MHz, CDCl_3) δ 5.10 (s, 5H).

Synthesis of complex 17. The preparation of complex **17** is a modification of a literature procedure.³⁹⁷ A solution of N-(3-(diphenylphosphino)propyl)triphenylphosphinimine (2.52 g, 5.01 mmol) and $\text{CpFe}(\text{CO})_2\text{I}$ (1.52 g, 5.01 mmol) in toluene (200 mL) was stirred at room temperature overnight. A yellow precipitate was collected on a fine frit. The yellow solid was washed with toluene and THF to remove triphenylphosphine oxide completely and then dried under vacuum to yield **17** as a yellow solid (2.44 g, 92% yield). IR (CDCl_3) 2089 cm^{-1} (ν_{CN}) and 1999 cm^{-1} (ν_{CO}). ^1H NMR (300 MHz, CDCl_3) δ 1.90 - 2.18 (m, - CH_2 -, 1H), 2.18 - 2.47 (m, - CH_2 -, 1H), 2.73 (td, $J=13.42$, 9.25 Hz, - CH_2 -, 1H), 3.39 (ddd, $J=14.50$, 4.45, 4.34 Hz, - CH_2 -, 1H), 3.78 - 3.98 (m, - CH_2 -, 1H), 4.80 (ddd, $J=14.90$, 8.74, 4.23 Hz, - CH_2 -, 1H), 5.02 (d, $J=1.14$ Hz, Cp H, 5H), 7.42 - 7.79 (m, Aryl H, 10H); $^{13}\text{C}\{^1\text{H}\}$ NMR (75.44 MHz, CDCl_3) δ 28.45 (d, $J=6.13$ Hz, - CH_2 , 1C), 31.66 (d, $J=32.20$ Hz, - CH_2 , 1C), 48.76 (s, - CH_2 ,

1C), 85.90 (s, Cp C, 5C), 123.44, 134.95 (m, Aryl C, 12C), 183.58 (d, $J=35.27$ Hz, $C_{isocyanide}$), 212.51 (d, $J=23.00$ Hz, $C_{carbonyl}$); $^{31}\text{P}\{^1\text{H}\}$ NMR (121.44 MHz, CDCl_3) δ 53.8.

Synthesis of complex 18. The preparation of complex **18** followed the same procedure as complex **17** with the corresponding proligand N-(3-(di(*tert*-butyl)phosphino)propyl)triphenylphosphinimine (0.92 g, 2.0 mmol). Complex **18** was obtained as a yellow solid (0.56 g, 73%). IR (CDCl_3) 2090 cm^{-1} (ν_{CN}) and 2001 cm^{-1} (ν_{CO}); ^1H NMR (300 MHz, CDCl_3) δ 1.28 (d, $J=13.9$ Hz, $-\text{CH}_3$, 9H), 1.49 (d, $J=13.7$ Hz, $-\text{CH}_3$, 9H), 1.69 - 1.83 (m, $-\text{CH}_2$, 1H), 2.60 - 2.86 (m, $-\text{CH}_3$, 3H), 3.51 (dd, $J=15.1, 4.6$ Hz, $-\text{CH}_2$, 1H), 4.04 - 4.14 (m, $-\text{CH}_2$, 1H), 5.16 (s, Cp H, 5H); $^{13}\text{C}\{^1\text{H}\}$ NMR (75.44 MHz, CDCl_3) δ 26.50 (d, $J=22.41$ Hz, $-\text{CH}_2$, 1C), 29.54 (d, $J=5.17$ Hz, $-\text{CH}_2$, 1C), 29.69 (d, $J=2.30$ Hz, $-\text{CH}_3$, 3C), 31.02 (br s, $-\text{CH}_3$, 3C), 39.06 (d, $J=10.92$ Hz, $-\text{CH}_2$, 1C), 40.57 (d, $J=12.64$ Hz, $-\text{C}(\text{CH}_3)_3$, 1C), 48.78 (s, $-\text{C}(\text{CH}_3)_3$, 1C), 84.03 (s, Cp C, 5C), 183.14 (d, $J=29.88$ Hz, $C_{isocyanide}$), 214.18 (d, $J=19.54$ Hz, $C_{carbonyl}$); $^{31}\text{P}\{^1\text{H}\}$ NMR (121.44 MHz, CDCl_3) δ 87.74. Anal. Calc. for **18** ($\text{C}_{18}\text{H}_{29}\text{FeINOP}$), N, 2.86; C, 44.20; H, 5.98. Obtained: N, 3.13; C, 44.37; H, 5.86.

Synthesis of complex 19. An excess amount of n-butyl amine (5 mL, 0.05 mol) was added to a solution of complex **18** (500 mg, 0.9 mmol) in CH_2Cl_2 (20 mL) at room temperature. The reaction mixture was stirred overnight, then concentrated *in vacuo*. Et_2O (10 mL) was added to precipitate the yellow solid, complex **19**. Complex **19** was collected on a fine frit and dried *in vacuo* (0.423 g, 89%). IR (CDCl_3) 19450 cm^{-1} (ν_{CO}); ^1H NMR (400 MHz, CDCl_3) δ 1.17 (d, $J=12.46$ Hz, $-\text{CH}_3$, 9H), 1.24 (d, $J=12.12$ Hz, $-\text{CH}_3$, 9H), 1.29-1.49 (m, $-\text{CH}_3$, 3H), 1.54 (br s., $-\text{CH}_2$, 2H), 1.79 (br s., $-\text{CH}_2$, 3H), 1.97 (br s., $-\text{CH}_2$, 1H), 2.10 - 2.31 (m, $-\text{CH}_2$, 1H), 2.48 - 2.65 (m, $-\text{CH}_2$, 1H), 3.22 (br s., $-\text{CH}_2$, 1H), 3.27 - 3.48 (m, $-\text{CH}_2$, 2H), 3.98 - 4.13 (m, $-\text{CH}_2$, 1H), 4.75 (s, Cp C, 5H), 5.96 (br s., $-\text{NH}$, 1H), 7.97 (br s., $-\text{NH}$, 1H); $^{13}\text{C}\{^1\text{H}\}$ NMR (100.58 MHz, CDCl_3) δ 13.48 (s, $-\text{CH}_3$, 1C), 19.84 (s, $-\text{CH}_2$, 1C), 25.67 (s, $-\text{CH}_2$, 1C), 28.90 (d, $J=9.69$ Hz, $-\text{CH}_2$, 1C), 29.60 (br s., $-\text{CH}_3$, 3C), 29.81 (br s., $-\text{CH}_3$, 3C), 30.25 (s, $-\text{CH}_2$, 1C), 37.52 (d, $J=17.99$ Hz, $-\text{CH}_2$, 1C), 38.40 (d, $J=17.99$ Hz, $-\text{CH}_2$, 1C), 45.94 (s, $-\text{C}(\text{CH}_3)_3$, 1C), 46.78 (s, $-\text{C}(\text{CH}_3)_3$, 1C), 84.30 (s, Cp C, 5C), 210.71 (d, $C_{carbonyl}$, 1C), 221.00 (d, $J=31.83$ Hz, $C_{carbene}$, 1C); $^{31}\text{P}\{^1\text{H}\}$ NMR (121.44 MHz, CDCl_3) δ 77.88. Anal. Calc. for **18** ($\text{C}_{22}\text{H}_{41}\text{FeIN}_2\text{OP}$), N, 4.97; C, 46.91; H, 7.34. Obtained: N, 5.48; C, 46.54; H, 7.19.

Synthesis of complex 19. An excess amount of *n*-butyl amine (5 mL, 0.05 mol) was added to a solution of complex **17** (500 mg, 0.9 mmol) in CH₂Cl₂ (20 mL) at room temperature. The reaction mixture was stirred overnight, and the solution was concentrated *in vacuo*. Et₂O (10 mL) was added to precipitate a yellow solid, which was dried *in vacuo* to obtain complex **19** (0.524 g, 92%). IR (CDCl₃) 1948.91 cm⁻¹ (ν_{CO}); ¹H NMR (400 MHz, CDCl₃) δ 0.98 (t, *J* = 7.31 Hz, -CH₃, 3H), 1.16 - 1.39 (m, -CH₂, 2H), 1.42 - 1.64 (m, -CH₂, 2H), 1.64 - 1.85 (m, -CH₂, 2H), 2.09 - 2.31 (m, -CH₂, 1H), 2.68 - 2.85 (m, -CH₂, 1H), 3.45 - 3.72 (m, -CH₂, 3H), 4.13 - 4.36 (m, -CH₂, 1H), 4.54 (s, *Cp H*, 5H), 6.50 (br s., -NH, 1H), 7.10 - 7.58 (m, *Aryl H*, 10H), 8.15 (br s., -NH, 1H); ¹³C{¹H} NMR (100.58 MHz, CDCl₃) δ 13.54 (d, *J*=8.30 Hz, -CH₃, 1C), 19.91 (s, -CH₂, 1C), 24.68 (s, -CH₂, 1C), 30.44 (s, -CH₂, 1C), 35.35 (m, *J*=22.14 Hz, -CH₂, 1C), 41.80 (s, -CH₂, 1C) 45.68 (s, -CH₂, 1C), 46.07 (s, -CH₂, 1C), 84.76 (s, *Cp C*, 5C), 128.07 (d, *J*=9.69 Hz, *Aryl C*, 2C), 128.61 (d, *J*=9.69 Hz, *Aryl C*, 2C), 129.68 (d, *J*=8.30 Hz, *Aryl C*, 2C), 131.82 (d, *J* = 11.07 Hz, *Aryl C*, 2C) 132.43 (d, *J* = 8.30 Hz, *Aryl C*, 2C) 132.83 (s, *Aryl C*, 1C), 138.75 (m, *J* = 48.44 Hz, *Aryl C*, 1C), 209.61 (d, *J* = 24.91 Hz, *C_{carbonyl}*, 1C), 218.05 (d, *J*=31.83 Hz, *C_{carbene}*, 1C); ³¹P{¹H} NMR (121.44 MHz, CDCl₃) δ 56.70. Anal. Calc. for **19** (C₂₆H₃₂FeIN₂OP), N, 4.65; C, 51.85; H, 5.36. Obtained: N, 5.38; C, 51.64; H, 5.80.

Synthesis of complex 21. The preparation of complex **5** followed the same procedure as complex **20** with the corresponding amine (5 mL, 0.002 mol). Complex **21** was obtained as a yellow solid (0.628 g, 93 %). IR (CDCl₃) 1947.76 cm⁻¹ (ν_{CO}); ¹H NMR (400 MHz, CDCl₃) δ 0.82-0.91 (m, -CH₃, 6H), 1.30 (d, *J*=3.58 Hz, -CH₂, 9H), 1.43 - 1.60 (m, -CH₂, 2H), 1.60-1.86 (m, -CH₂, 3H), 1.93 (br s., -CH₂, 1H), 2.11-2.33 (m, -CH₂, 1H), 2.60-2.72 (m, -CH₂, 1H), 2.82-2.91 (m, -CH₂, 1H), 3.08-3.20 (m, -CH₂, 1H), 3.43 (dt, *J*=13.61, 6.76 Hz, -CH₂, 1H), 3.64-3.81 (m, -CH₂, 2H), 3.95-4.06 (m, -CH₂, 1H), 4.29-4.43 (m, -CH₂, 2H), 4.50 (s, *Cp H*, 5H), 4.78 (br s., *Aryl H*, 2H), 7.03-7.11 (m, *Aryl H*, 2H), 7.18-7.25 (m, *Aryl H*, 2H), 7.32-7.44 (m, *Aryl H*, 2H), 7.47-7.56 (m, *Aryl H*, 2H), 7.75 (br s., -NH, 1H); ¹³C{¹H} NMR (100.58 MHz, CDCl₃) δ; 13.82 (d, *J*=13.56 Hz, -CH₃, 2C), 22.24 (s, -CH₂, 1C), 22.35 (s, -CH₂, 2C), 24.51 (s, -CH₂, 1C), 26.41 (s, -CH₂, 1C), 26.70 (s, -CH₂, 1C), 26.94 (s, -CH₂, 1C), 28.97 (s, -CH₂, 1C), 31.41 (d, *J*=3.70 Hz, -CH₂, 2C), 35.11 (d, -CH₂, 1C), 49.90 (s, -CH₂, 1C), 59.78 (s, -CH₂, 1C), 85.21 (s, *Cp C*, 5C), 128.00 (d, *J*=9.86 Hz, *Aryl C*, 2C), 128.80 (d,

$J=9.86$ Hz, *Aryl C*, 2C), 129.72 (d, $J=8.63$ Hz, *Aryl C*, 2C), 129.95 (s, *Aryl C*, 1C), 130.82 (s, *Aryl C*, 1C), 132.47 (d, $J=46.86$ Hz, *Aryl C*, 1C), 133.29 (d, $J=9.86$ Hz, *Aryl C*, 2C), 139.28 (d, $J=51.79$ Hz, *Aryl C*, 1C), 210.00 (d, $J=20.96$ Hz, C_{carbonyl} , 1C), 219.16 (d, $J=36.99$ Hz, C_{carbene} , 1C); $^{31}\text{P}\{^1\text{H}\}$ NMR (121.44 MHz, CDCl_3) δ 55.87; Anal. Calc. for **21** ($\text{C}_{34}\text{H}_{48}\text{FeIN}_2\text{OP}$), N, 3.92; C, 57.16; H, 6.77. Obtained: N, 4.12; C, 57.72; H, 7.33.

Synthesis of complex 22. The preparation of complex **22** followed the same procedure as complex **20** with the corresponding amine (0.409 g, 3.82 mmol) and complex **1** (0.505 g, 0.96 mmol). Complex **22** was obtained as a yellow solid (0.550 g, 90 %). IR (CDCl_3) 1954.00 cm^{-1} (ν_{CO}); ^1H NMR (400 MHz, CDCl_3) δ 1.01 (br s., $-\text{CH}_2$, 1H), 1.95-2.19 (m, $-\text{CH}_2$, 1H), 2.23 (s, $-\text{CH}_3$, 3H), 2.70 (t, $J=15.19$ Hz, $-\text{CH}_2$, 1H), 3.04 (br s., $-\text{CH}_2$, 1H), 3.38 (dd, $J=13.83, 6.83$ Hz, $-\text{CH}_2$, 1H), 3.59-3.77 (m, $-\text{CH}_2$, 1H), 4.43 (br s., $-\text{CH}_2$, 1H), 4.64 (br s., *Cp H*, 5H), 7.11 (br s., $-\text{NH}$, 1H), 7.19-7.26 (m, *Aryl H*, 6H), 7.33 (br s., *Aryl H*, 6H), 7.45 (br s., *Aryl H*, 2H), 9.38 (br s., $-\text{NH}$, 1H); $^{13}\text{C}\{^1\text{H}\}$ NMR (100.58 MHz, CDCl_3) δ 21.77 (br s., $-\text{CH}_3$, 1C), 24.15 (br s., $-\text{CH}_2$, 1C), 34.55 (d, $J=25.89$ Hz, $-\text{CH}_2$, 1C), 45.17 (br s., $-\text{CH}_2$, 1C), 73.52 (br s., *Aryl H*, 2C), 85.60 (br s., *Cp C*, 5C), 127.63-135.68 (m, *Aryl H*, 16C), 217.92 (d, $J=28.36$ Hz, C_{carbonyl} , 1C), 234.63 (d, $J=25.89$ Hz, C_{carbene} , 1C); $^{31}\text{P}\{^1\text{H}\}$ NMR (121.44 MHz, CDCl_3) δ 57.90. Anal. Calc. for **22** ($\text{C}_{29}\text{H}_{30}\text{FeIN}_2\text{OP}$), N, 4.40; C, 54.74; H, 4.75. Obtained: N, 4.26; C, 54.99; H, 4.84.

Synthesis of complex 23. A solution of 2-chloroethylamine hydrochloride (0.70 g, 6.05 mmol), $[\text{Cl}(\text{CH}_2)_2\text{NH}_3]\text{Cl}$, was treated with a solution of an equimolar amount of NaOEt (0.41 g, 6.0 mmol) in EtOH (2 mL) at room temperature. The reaction mixture was continuously stirred for 10 minutes to complete the formation of 2-chloroethylamine as well as NaCl salt. The amine solution was filtered through a glass fiber filter and added dropwise to a solution of complex **17** (0.80 g, 1.5 mmol) in CH_2Cl_2 (10 mL) at room temperature. The mixture was stirred overnight. A yellow precipitate was collected, washed with Et_2O (2×10 mL) and dried under vacuum. Complex **23** was obtained as a yellow solid (0.85g, 93 %). IR (CDCl_3) 1958.83 cm^{-1} (ν_{CO}); ^1H NMR (600 MHz, CDCl_3) δ 11.32-1.42 (m, $-\text{CH}_2$, 1H), 2.14-2.29 (m, $-\text{CH}_2$, 1H), 2.67-2.75 (m, $-\text{CH}_2$, 1H), 2.82-2.92 (m, $-\text{CH}_2$, 1H), 3.44 (ddd, $J=14.63, 9.76, 5.06$ Hz, $-\text{CH}_2$, 1H), 3.88-3.96 (m, $-\text{CH}_2$, 2H), 4.01-4.09 (m, $-\text{CH}_2$, 1H), 4.24-4.31 (m, $-\text{CH}_2$, 1H), 4.35 (ddd, $J=14.59, 7.23, 7.10$ Hz, $-\text{CH}_2$, 1H), 4.50-4.57 (m, *Cp H*, 5H), 6.69 (t,

$J=5.57$ Hz, $-NH$, 1H), 7.23 (dd, $J=10.63$, 7.68 Hz, *Aryl H*, 2H), 7.38 (td, $J=7.68$, 1.92 Hz, *Aryl H*, 2H), 7.42-7.53 (m, *Aryl H*, 6H), 8.84 (br s., $-NH$, 1H); $^{13}C\{^1H\}$ NMR (100.58 MHz, $CDCl_3$) δ 24.71 (s, $-CH_2$, 1C), 35.56 (d, $J=22.19$ Hz, $-CH_2$, 1C), 43.99 (s, $-CH_2$, 1C), 45.50 (br s., $-CH_2$, 1C), 47.52 (s, $-CH_2$, 1C), 84.67 (s, *Cp C*, 5C), 128.92 (d, $J=9.86$ Hz, *Aryl C*, 2C), 129.16 (d, $J=8.63$ Hz, *Aryl C*, 2C), 129.93 (d, $J=8.63$ Hz, *Aryl C*, 2C), 130.39 (d, $J=2.46$ Hz, *Aryl C*, 1C), 131.33 (d, $J=2.47$ Hz, *Aryl C*, 1C), 132.59 (s, *Aryl C*, 1C), 132.91 (d, $J=9.87$ Hz, *Aryl C*, 1C), 138.33 (d, $J=49.31$ Hz, *Aryl C*, 1C), 211.35 (d, $J=28.36$ Hz, C_{carbonyl} , 1C), 218.11 (d, $J=32.06$ Hz, C_{carbene} , 1C); $^{31}P\{^1H\}$ NMR (121.44 MHz, $CDCl_3$) δ 56.44. Anal. Calc. for **23** ($C_{24}H_{27}ClFeIN_2OP$), N, 4.60; C, 47.36; H, 4.47. Obtained: N, 4.66; C, 47.58; H, 4.52.

Synthesis of complex 24. A solution of 3-chloropropylamine hydrochloride (0.79 g, 6.1 mmol), $[Cl(CH_2)_3NH_3]Cl$, was treated with a solution of an equimolar amount of NaOEt (0.41 g, 6.0 mmol) in EtOH (2mL) at room temperature. The reaction mixture was continuously stirred for 10 minutes to complete the formation of 2-chloropropylamine as well as NaCl salt. The amine solution was filtered through a glass fiber filter and added dropwise to a solution of complex **17** (0.80 mg, 1.51 mmol) in CH_2Cl_2 (10 mL) at room temperature, and then the mixture was stirred overnight. The reaction mixture was then concentrated under vacuum. Et_2O (10 mL) was added to the residual and a yellow solid precipitated, which was collected on a frit, washed with pentane (2×5 mL), and pumped to dryness under vacuum to yield complex **24** as a yellow solid (0.89 g, 95 %). IR ($CDCl_3$) 1952.12 cm^{-1} (ν_{CO}); 1H NMR (300 MHz, $CDCl_3$) δ 1.27 - 1.51 (m, $-CH_2$, 1H), 2.08 - 2.47 (m, $-CH_2$, 3H) 2.64 - 2.96 (m, $-CH_2$, 2H) 3.38 - 3.59 (m, $-CH_2$, 1H), 3.66 - 4.05 (m, $-CH_2$, 4H), 4.14 - 4.39 (m, $-CH_2$, 1H), 4.56 (d, $J=1.37$ Hz, *Cp H*, 5H), 6.84 (br s., $-NH$, 1H), 7.18 (dd, $J=10.62$, 7.42 Hz, *Aryl H*, 2H), 7.30 - 7.38 (m, *Aryl H*, 2H), 7.39 - 7.56 (m, *Aryl H*, 6H), 8.41 (br s., $-NH$, 1H); $^{13}C\{^1H\}$ NMR (100.58 MHz, $CDCl_3$) δ 24.74 (s, $-CH_2$, 1C), 31.17 (s, $-CH_2$, 1C), 35.34 (d, $J=22.20$ Hz, $-CH_2$, 1C), 43.11 (s, $-CH_2$, 2C), 45.56 (d, $J=2.47$ Hz, $-CH_2$, 1C), 84.83 (s, *Cp C*, 5C), 128.44 (d, $J=9.86$ Hz, *Aryl C*, 2C), 128.87 (d, $J=8.63$ Hz, *Aryl C*, 2C), 129.80-130.15 (m, *Aryl C*, 3C), 130.77 (s, *Aryl C*, 1C), 132.73 (d, $J=9.86$ Hz, *Aryl C*, 2C), 133.15 (s, *Aryl C*, 1C), 138.99 (d, $J=49.32$ Hz, *Aryl C*, 1C), 211.04 (d, $J=24.66$ Hz, C_{carbonyl} , 1C), 218.16 (d, $J=32.06$ Hz, C_{carbene} , 1C); $^{31}P\{^1H\}$ NMR (121.44 MHz, $CDCl_3$) δ 56.45. Anal. Calc. for **24** ($C_{25}H_{29}ClFeIN_2OP$), N, 4.50; C, 48.22; H, 4.69. Obtained: N, 4.43; C, 48.14; H, 4.67.

Synthesis of complex 25. A suspension of complex **23** (200 mg, 0.3 mmol) in CH₂Cl₂ (10 mL) was reacted with a 5 mL EtOH solution of four equimolar amounts of NaOEt (89.3 mg, 1.31 mmol) at room temperature. After stirring overnight, the mixture was pumped to dryness and the residue was dissolved in a minimum amount of CH₂Cl₂ (3 mL). The solution was filtered through Celite for removal of NaCl salt and excess NaOEt. The filtrate was concentrated and Et₂O (10 mL) was added to filter the solution and obtain a yellow precipitate, **25** (0.156 g, 83%). IR (CDCl₃) 1948.77 cm⁻¹ (ν_{CO}); ¹H NMR (400 MHz, CDCl₃) δ 1.51 (br s., -CH₂, 1H), 1.79 (br s., -CH₂, 1H), 2.64-2.80 (m, -CH₂, 1H), 2.87-3.04 (m, -CH₂, 1H), 3.37-3.57 (m, -CH₂, 2H), 3.57-3.73 (m, -CH₂, 4H), 4.75 (s, Cp H, 5H), 7.13-7.23 (m, Aryl H, 2H), 7.28-7.41 (m, Aryl H, 3H), 7.42-7.48 (m, Aryl H, 1H), 7.51 (t, J=6.49 Hz, Aryl H, 2H), 7.55 - 7.63 (m, Aryl H, 2H), 8.31 (br s., -NH, 1H); ¹³C{¹H} NMR (100.58 MHz, CDCl₃) 23.04 (s, -CH₂, 1C), 34.24 (d, J=24.54 Hz, -CH₂, 1C), 44.75 (s, -CH₂, 1C), 48.39 (s, -CH₂, 1C), 52.31 (s, -CH₂, 1C), 85.47 (s, Cp C, 5C), 128.61 (d, J=10.73 Hz, Aryl C, 2C), 129.23 (d, J=9.20 Hz, Aryl C, 2C), 130.43 (s, Aryl C, 1C), 130.74 (s, Aryl C, 1C), 131.22 (d, J=9.20 Hz, Aryl C, 2C), 131.54 (d, J=9.20 Hz, Aryl C, 2C), 211.54 (d, J=27.60 Hz, C_{carbonyl}, 1C), 218.81 (d, J=29.14 Hz, C_{carbene}, 1C); ³¹P{¹H} NMR (121.44 MHz, CDCl₃) δ 56.95. Anal. Calc. for **25** (C₂₄H₂₆FeIN₂OP), N, 4.90; C, 50.38; H, 4.58. Obtained: N, 5.38; C, 50.08; H, 4.91.

Synthesis of complex 26. A suspension of complex **24** (200 mg, 0.3 mmol) in CH₂Cl₂ (10 mL) was reacted with a 5 mL EtOH solution of four equimolar amounts of NaOEt (87.4 mg, 1.28 mmol) at room temperature. After stirring overnight, the mixture was pumped to dryness and the residue was dissolved in a minimum amount of CH₂Cl₂ (3 mL). The solution was filtered through Celite for removal of NaCl and excess NaOEt. The filtrate was concentrated and Et₂O (10 mL) was added to filter the solution and obtain a yellow precipitate, **26** (0.152 g, 81%). IR (CDCl₃) 1952.24 cm⁻¹ (ν_{CO}); ¹H NMR (400 MHz, CDCl₃) δ 1.02-1.20 (m, -CH₂, 1H), 1.78-1.94 (m, -CH₂, 1H), 1.96-2.09 (m, -CH₂, 1H), 2.09-2.32 (m, -CH₂, 1H), 2.61-2.77 (m, -CH₂, 1H), 2.94-3.06 (m, -CH₂, 1H), 3.11 (d, J=12.63 Hz, -CH₂, 1H), 3.26-3.53 (m, -CH₂, 4H), 4.26 (dd, J=14.59, 9.47 Hz, -CH₂, 1H), 4.67 (s, Cp H, 5H), 7.20-7.33 (m, Aryl H, 4H), 7.36 (br s., Aryl H, 4H), 7.43-7.53 (m, Aryl H, 2H), 8.00 (br s., -NH, 1H); ¹³C{¹H} NMR (100.58 MHz, CDCl₃) δ 20.87 (s, -CH₂, 1C), 22.02 (s, -CH₂, 1C),

34.26 (d, $J=22.14$ Hz, $-\text{CH}_2$, 1C), 41.17 (s, $-\text{CH}_2$, 1 C), 49.42 (s, $-\text{CH}_2$, 1C), 56.29 (br s., $-\text{CH}_2$, 1C) 84.84 (s, C_p C, 5C), 128.32 (d, $J=11.07$ Hz, $Aryl$ C, 2C), 128.80 (d, $J=8.30$ Hz, $Aryl$ C, 2C), 129.87 (d, $J=8.30$ Hz, $Aryl$ C, 2C), 130.74 (s, $Aryl$ C, 2C), 132.87 (d, $J=8.30$ Hz, $Aryl$ C, 2C), 133.38 (s, $Aryl$ C, 1C), 139.22 (d, $J=47.06$ Hz, $Aryl$ C, 1C), 205.75 (d, $J=24.91$ Hz, C_{carbonyl} , 1C), 218.25 (d, $J=33.22$ Hz, C_{carbene} , 1C); $^{31}\text{P}\{^1\text{H}\}$ NMR (121.44 MHz, CDCl_3) δ 56.21. Anal. Calc. for **26** ($\text{C}_{25}\text{H}_{28}\text{FeIN}_2\text{OP}\cdot\text{CH}_2\text{Cl}_2$), N, 4.46; C, 48.72; H, 4.65. Obtained: N, 4.38; C, 48.38; H, 4.74.

Synthesis of complex 27. A solution of potassium *tert*-butoxide, KO^tBu (0.22 g, 2.0 mmol) in methanol (MeOH) (5 mL) was added to a solution of complex **17** (1.01 g, 1.91 mmol) in THF (10 mL) at room temperature. The mixture was stirred overnight after which the solvent was removed completely *in vacuo* and the remaining residue was dissolved in benzene. The solution was filtered through Celite to remove KI. The filtrate was evaporated *in vacuo* to obtain the desired product **27** as a yellow solid (0.745 g, 90%). IR (CDCl_3) 1936.99 cm^{-1} (ν_{CO}); ^1H NMR (400 MHz, CDCl_3) δ 1.33-1.49 (m, $-\text{CH}_2$, 1H), 1.83-2.01 (m, $-\text{CH}_2$, 1H), 2.52-2.64 (m, $-\text{CH}_2$, 1H), 2.73-2.85 (m, $-\text{CH}_2$, 1H), 3.54 (dd, $J=12.46, 9.73$ Hz, $-\text{CH}_2$, 1H), 3.72 (s, $-\text{CH}_3$, 3H), 3.81 (dd, $J=12.29, 7.17$ Hz, $-\text{CH}_2$, 1H), 4.46 (d, $J=1.37$ Hz, C_p H, 5H), 7.26-7.34 (m, $Aryl$ H, 3H), 7.36-7.44 (m, $Aryl$ H, 5H), 7.51-7.58 (m, $Aryl$ H, 2H); $^{13}\text{C}\{^1\text{H}\}$ NMR (100.58 MHz, CDCl_3) δ 24.75 (s, $-\text{CH}_2$, 1C), 35.71 (d, $J=22.14$ Hz, $-\text{CH}_2$, 1C), 49.99 (d, $J=4.15$ Hz, $-\text{CH}_2$, 1C), 53.76 (s, $-\text{CH}_3$, 1C), 83.27 (s, C_p C, 5C), 127.91 (d, $J=9.69$ Hz, $Aryl$ C, 2C), 128.30 (d, $J=8.30$ Hz, $Aryl$ C, 2C), 129.26 (s, $Aryl$ C, 1C), 129.66 (s, $Aryl$ C, 1C), 130.63 (d, $J=9.69$ Hz, $Aryl$ C, 2C), 132.90 (d, $J=9.69$ Hz, $Aryl$ C, 2C), 136.04 (d, $J=45.67$ Hz, $Aryl$ C, 1C), 140.36 (d, $J=41.52$ Hz, $Aryl$ C, 1C), 198.03 (d, $J=33.22$ Hz, C_{ylidene} , 1C), 221.08 (d, $J=31.83$ Hz, C_{carbonyl} , 1C); $^{31}\text{P}\{^1\text{H}\}$ NMR (121.44, CDCl_3) δ 60.55. Anal. Calc. for **11** ($\text{C}_{23}\text{H}_{24}\text{FeNO}_2\text{P}$), N, 3.23; C, 63.76; H, 5.58. Obtained: N, 3.32; C, 64.11; H, 5.67.

Synthesis of complex 28. The preparation of complex **28** followed the same procedure as complex **27** with KO^tBu (0.22 g, 2.0 mmol) in ethanol (EtOH) (5 mL) and complex **17** (1.01 g, 1.91 mmol) in THF (10 mL). Complex **28** was obtained as a yellow solid (0.760 g, 89%). IR (CDCl_3) 1937.11 cm^{-1} (ν_{CO}); ^1H NMR (400 MHz, CDCl_3) δ 1.30 (t, $-\text{CH}_3$, $J=7.08$ Hz, 3H), 1.34-1.52 (m, $-\text{CH}_2$, 1H), 1.73-1.96 (m, $-\text{CH}_2$, 1H), 2.48-2.64 (m, $-\text{CH}_2$, 1H), 2.74 (m, $J=13.46, 13.46, 6.36, 3.41$ Hz, $-\text{CH}_2$, 1H), 3.43-3.59 (m, $-\text{CH}_2$, 1H), 3.74 (dd, $J=12.37, 7.77$

Hz, -CH₂, 1H), 4.02 (dq, *J*=10.37, 7.01 Hz, -CH₂, 1H), 4.17 (dq, *J*=10.39, 7.06 Hz, -CH₂, 1H), 4.43 (d, *J*=1.02 Hz, *Cp H*, 5H), 7.22-7.33 (m, *Aryl H*, 2H), 7.33-7.43 (m, *Aryl H*, 5H), 7.48-7.61 (m, *Aryl H*, 3H); ¹³C{¹H} NMR (100.58 MHz, CDCl₃) δ 14.99 (s, -CH₃, 1C), 24.78 (s, -CH₂, 1C), 35.38 (d, *J*=22.19 Hz, -CH₂, 1C), 49.94 (br s., -CH₂, 1C), 61.14 (s, -CH₂, 1C), 83.46 (s, *Cp C*, 5C), 127.76 (d, *J*=9.86 Hz, *Aryl C*, 2C), 128.19 (d, *J*=8.63 Hz, *Aryl C*, 2C), 129.26 (s, *Aryl C*, 1C), 129.49 (s, *Aryl C*, 1C), 130.84 (d, *J*=8.63 Hz, 2C), 132.61 (d, *J*=8.63 Hz, 2C), 133.56 (d, *J*=17.26 Hz, 1C), 136.67 (d, 1C), 197.64 (d, *J*=30.83 Hz, 1C, *C_{ylidene}*), 221.22 (d, *J*=32.06 Hz, 1C, *C_{carbonyl}*); ³¹P{¹H} NMR (121.44 MHz, CDCl₃) δ 61.09. Anal. Calc. for **28** (C₂₄H₂₆FeNO₂P), N, 3.13; C, 64.44; H, 5.86. Obtained: N, 3.12; C, 64.47; H, 5.90.

Synthesis of complex 29. The preparation of complex **29** followed the same procedure as complex **27** with KO^tBu (0.22 g, 2.0 mmol) in *iso*-propanol (*i*PrOH) (5 mL) and complex **17** (1.01 g, 1.91 mmol) in THF (10 mL). Complex **29** was obtained as a yellow solid (0.819 g, 93%). IR (CDCl₃) 1935.67 cm⁻¹ (*ν*_{CO}); ¹H NMR (400 MHz, CDCl₃) δ 1.20 (d, *J*=6.14 Hz, -CH₃, 3H), 1.30 (d, *J*=6.14 Hz, -CH₃, 3H), 1.35-1.52 (m, -CH₂, 1H), 1.75-1.93 (m, -CH₂, 1H), 2.48-2.61 (m, -CH₂, 1H), 2.72 (m, *J*=13.48, 13.48, 6.32, 3.41 Hz, -CH₂, 1H), 3.52 (dd, *J*=12.37, 9.47 Hz, -CH₂, 1H), 3.69-3.81 (m, -CH₂, 1H), 4.40 (s, *Cp H*, 5H), 5.24 (spt, *J*=6.17 Hz, -CH, 1H), 7.27-7.33 (m, *Aryl H*, 3H) 7.39-7.47 (m, *Aryl H*, 5H), 7.52-7.65 (m, *Aryl H*, 2H); ¹³C{¹H} NMR (100.58 MHz, CDCl₃) δ 22.49 (s, -CH₃, 1C), 22.80 (s, -CH₃, 1C), 24.77 (s, -CH₂, 1C), 35.45 (d, *J*=22.57 Hz, -CH₂, 1C), 50.19 (d, *J*=5.37 Hz, -CH₂, 1C), 65.27 (s, -CH, 1C), 83.52 (s, *Cp C*, 5C), 127.71 (d, *J*=9.67 Hz, *Aryl C*, 2C), 128.22 (d, *J*=9.67 Hz, *Aryl C*, 2C), 129.24 (s, *Aryl C*, 1C), 129.47 (s, *Aryl C*, 1C), 130.95 (d, *J*=8.60 Hz, *Aryl C*, 2C), 132.86 (d, *J*=9.67 Hz, *Aryl C*, 2C), 136.79 (d, *J*=45.13 Hz, *Aryl C*, 1C), 140.00 (d, *J*=39.76 Hz, *Aryl C*, 1C), 196.27 (d, *J*=33.31 Hz, *C_{ylidene}*, 1C) 221.37 (d, *J*=33.31 Hz, *C_{carbonyl}*, 1C); ³¹P{¹H} NMR (121.44 MHz, CDCl₃) δ 61.28. Anal. Calc. for **29** (C₂₅H₂₈FeNO₂P), N, 3.04; C, 65.09; H, 6.12. Obtained: N, 3.00; C, 64.91; H, 6.07.

Synthesis of complex 30. An equimolar amount of 6.2 M HBF₄ (0.12 mL, 0.74 mmol) in Et₂O was added dropwise to a solution of complex **27** (0.304 g, 0.702 mmol) in CH₂Cl₂ (10 mL) at room temperature. The reaction was stirred overnight, then the solution was concentrated *in vacuo*. Complex **30** was precipitated as a yellow solid by addition of diethyl

ether to the residue and collected on a fine frit (0.340 g, 93%). IR (CDCl₃) 1960.15 cm⁻¹ (ν_{CO}); ¹H NMR (400 MHz, CDCl₃) δ 1.67 (br s., -CH₂, 1H), 1.89 (br s., -CH₂, 1H), 2.88 (br s., -CH₂, 2H), 3.87 (br s., -CH₂, 2H), 4.02 (br s., -CH₃, 3H), 4.59 (br s., Cp H, 5H), 7.10 - 7.26 (m, Aryl H, 2H), 7.32 - 7.47 (m, Aryl H, 3H), 7.52 (br s., Aryl H, 5H), 8.81 (br s., -NH, 1H); ¹³C{¹H} NMR (100.58 MHz, CDCl₃) δ 24.28 (s, -CH₃, 1C), 34.63 (d, $J=27.60$ Hz, -CH₂, 1C), 45.10 (s, -CH₂, 1C), 57.50 (s, -CH₂, 1C), 85.56 (s, Cp C, 5C), 128.17 - 130.00 (m, Aryl C, 5C), 130.30 - 132.20 (m, Aryl C, 7C), 218.25 (d, $J=27.60$ Hz, C_{carbonyl}, 1C) 237.08 (d, $J=27.60$ Hz, C_{carbene}, 1C); ³¹P{¹H} NMR (121.44 MHz, CDCl₃) δ 55.59. Anal. Calc. for **30** (C₂₃H₂₅BF₄FeNO₂P), N, 2.69; C, 53.01; H, 4.84. Obtained: N, 2.63; C, 52.74; H, 4.98.

Synthesis of complex 31. The preparation of complex **31** followed the same procedure as complex **30** with 6.2 M HBF₄ (0.11 mL, 0.68 mmol) in Et₂O and complex **28** (0.298 g, 0.666 mmol) in CH₂Cl₂ (10 mL). Complex **31** was obtained as a yellow solid (0.324 g, 91%). IR (CDCl₃) 1958.49 cm⁻¹ (ν_{CO}); ¹H NMR (400 MHz, CDCl₃) δ 1.51 (br s., -CH₃, 3H), 1.71 (br s., -CH₂, 1H), 1.90 (br s., -CH₂, 1H), 2.87 (br s., -CH₂, 2H), 3.86 (br s., -CH₂, 2H), 4.25 (br s., -CH₂, 2H), 4.58 (br s., Cp H, 5H), 7.16 - 7.26 (m, Aryl H, 1H), 7.33 - 7.47 (m, Aryl H, 3H), 7.53 (br s., Aryl H, 6H), 8.73 (br s., -NH, 1H); ¹³C{¹H} NMR (100.58 MHz, CDCl₃) δ 13.88 (br s., -CH₃, 1C), 24.15 (br s., -CH₂, 1C), 34.22 (d, $J=24.66$ Hz, -CH₂, 1C), 44.83 (br s., -CH₂, 1C), 66.22 (br s., -CH₂, 1C), 85.43 (br s., Cp C, 5C), 127.98-129.44 (m, Aryl C, 4 C), 130.17-132.12 (m, Aryl C, 5C), 132.25-135.96 (m, Aryl C, 3C), 218.09 (d, $J=27.13$ Hz, C_{carbonyl}, 1C), 236.34 (d, $J=29.59$ Hz, C_{carbene}, 1C); ³¹P{¹H} NMR (121.44 MHz, CDCl₃) δ 55.60. Anal. Calc. for **31** (C₂₄H₂₇BF₄FeNO₂P), N, 2.62; C, 53.87; H, 5.09. Obtained: N, 2.49; C, 54.14; H, 5.22.

Synthesis of complex 32. The preparation of complex **32** followed the same procedure as complex **30** with 6.2 M HBF₄ (0.11 mL, 0.68 mmol) in Et₂O and complex **29** (0.299 g, 0.648 mmol) in CH₂Cl₂ (10 mL). Complex **32** (0.310 g, 87%) was obtained as a yellow solid. IR (CDCl₃) 1958.91cm⁻¹ (ν_{CO}); ¹H NMR (400 MHz, CDCl₃) δ 1.46 (d, $J=25.13$ Hz, -CH₃, 6H), 1.67 (br s., -CH₂, 1H), 1.97 (br s., 1H), 2.86 (br s., -CH₂, 2H), 3.89 (br s., -CH₂, 2H), 4.54 (br s., Cp H, 5H), 5.02 (br s., -CH, 1H), 7.24 (br s., Aryl H, 1H), 7.31-7.47 (m, Aryl H, 3H), 7.52 (br s., Aryl H, 6 H), 8.55 (br s., -NH, 1H); ¹³C{¹H} NMR (100.58 MHz, CDCl₃) δ 21.77 (br s., -CH₃, 1C) 21.97 (br s., -CH₃, 1C) 24.15 (br s., -CH₂, 1C) 34.55 (d, $J=25.89$ Hz, -CH₂, 1C)

45.17 (br s., -CH₂, 1C) 73.52 (br s., -CH, 1C) 85.60 (br s., Cp C, 5C) 127.63 - 135.68 (m, Aryl C, 12C) 217.92 (d, *J*=28.36 Hz, C_{carbonyl}, 1C) 234.63 (d, *J*=25.89 Hz, C_{carbene}, 1C); ³¹P{¹H} NMR (121.44 MHz, CDCl₃) δ 56.02. Anal. Calc. for **32** (C₂₅H₂₉BF₄FeNO₂P), N, 2.55; C, 54.68; H, 5.32. Obtained: N, 2.49; C, 54.20; H, 5.27.

Synthesis of complex 33. To a solution of 2-chloroethanol (0.3 mL, 4 mmol) in THF (3 mL) at room temperature was added 1.6 M *n*-BuLi in *n*-hexane (1 mL, 1.6 mmol), followed by complex **17** (800 mg, 1 mmol) in CH₂Cl₂ (10 mL) and the reaction mixture was stirred overnight. The mixture was dried *in vacuo*, and the resulting yellow solid was dissolved in a minimum amount of CH₂Cl₂ (3 mL). The solution was then filtered through Celite to remove salt and then the solvent was removed *in vacuo*. Et₂O (10 mL) was added to the residue, and a yellow solid was precipitated and collected on a fine frit, washed with pentane (5 mL) and dried *in vacuo* to yield complex **33** (0.788 g, 91%). IR (CDCl₃) 1963.60 cm⁻¹ (ν_{CO}); ¹H NMR (300 MHz, CDCl₃) δ 1.78 (br s., -CH₂, 1H) 1.85 (br s., -CH₂, 1H) 2.78 - 2.94 (m, -CH₂, 1H) 3.03 - 3.23 (m, -CH₂, 1H) 3.83 - 4.14 (m, -CH₂, 4H), 4.66 (t, -CH₂, *J*=9.71 Hz, 2H), 4.73 (d, *J*=1.14 Hz, Cp H, 5H) 7.22 - 7.33 (m, Aryl H, 2H) 7.38 - 7.50 (m, Aryl H, 3H) 7.57 (d, *J*=5.48 Hz, Aryl H, 5H); ¹³C{¹H} NMR (100.58 MHz, CDCl₃) δ 22.35 (s, -CH₂, 1C), 33.75 (d, *J*=27.58 Hz, -CH₂, 1C), 47.15 (s, -CH₂, 1C), 52.27 (s, -CH₂, 1C), 70.04 (s, -CH₂, 1C), 85.78 (s, Cp C, 5C), 128.56 (d, *J*=10.11 Hz, Aryl C, 2C), 128.94 (d, *J*=10.11 Hz, Aryl C, 2C), 130.07 (d, *J*=9.19 Hz, Aryl C, 2C), 130.34 (s, Aryl C, 1C), 131.12 (s, Aryl C, 1C), 131.67 (d, *J*=10.11 Hz, Aryl C, 2C), 135.35 (d, *J*=46.88 Hz, Aryl C, 2C), 217.62 (d, *J*=26.66 Hz, C_{carbonyl}, 1C), 229.00 (d, *J*=28.50 Hz, C_{carbene}, 1C); ³¹P{¹H} NMR (121.44 MHz, CDCl₃) δ 55.79. Anal. Calc. for **33** (C₂₄H₂₅FeINO₂P), N, 2.44; C, 50.29; H, 4.40. Obtained: N, 2.58; C, 50.56; H, 4.92.

Synthesis of complex 34. To a solution of 3-chloropropanol (0.3 mL, 4 mmol) in THF (3 mL) at room temperature were added 1.6 M *n*-BuLi in *n*-hexane (1 mL, 1.6 mmol), followed by complex **17** (800 mg, 2 mmol) in CH₂Cl₂ (10 mL) and the reaction mixture was stirred overnight. The mixture was dried *in vacuo* and the resulting yellow solid was dissolved in a minimum amount of CH₂Cl₂ (3 mL). The solution was then filtered through Celite to remove salt and then the solvent was removed *in vacuo*. Et₂O (10 mL) was added to the residue, and a yellow solid was precipitated and collected on a fine frit, washed with pentane (5 mL), and

dried *in vacuo* to yield complex **34** as a yellow powder (0.798 g, 90%). IR (CDCl₃) 1966.33 cm⁻¹ (ν_{CO}); ¹H NMR (300 MHz, CDCl₃) δ 1.33 (br s., -CH₂, 1H), 1.95-2.15 (m, -CH₂, 1H), 2.15-2.30 (m, -CH₂, 2H), 2.73-2.93 (m, -CH₂, 1H), 3.07-3.31 (m, -CH₂, 2H), 3.73-3.97 (m, -CH₂, 2H), 4.32-4.50 (m, -CH₂, 2H), 4.50-4.62 (m, -CH₂, 1H), 4.76 (s, Cp H, 5H), 7.24-7.58 (m, Aryl H, 10H); ¹³C{¹H} NMR (100.58 MHz, CDCl₃) δ 20.93 (s, -CH₂, 1C), 21.31 (s, -CH₂, 1C), 33.77 (d, $J=24.91$ Hz, -CH₂, 1C), 48.50 (s, -CH₂, 1C), 66.99 (s, -CH₂, 1C), 84.78 (br s., Cp C, 5C), 128.28 (d, $J=9.69$ Hz, Aryl C, 2C), 128.65 (d, $J=9.69$ Hz, Aryl C, 2C), 129.92 (br s., Aryl C, 3C), 130.60 (s, Aryl C, 1C), 131.91 (d, $J=8.30$ Hz, Aryl C, 2C), 133.02 (d, $J=48.44$ Hz, Aryl C, 1C), 137.19 (s, Aryl C, 1C), 217.97 (d, $J=29.06$ Hz, C_{carbonyl}, 1C), 231.32 (d, $J=29.06$ Hz, C_{carbene}, 1C); ³¹P{¹H} NMR (121.44 MHz, CDCl₃) δ 56.30. Anal. Calc. for **34** (C₂₅H₂₇FeINO₂P), N, 2.39; C, 51.13; H, 4.63. Obtained: N, 2.50; C, 51.66; H, 4.69.

Synthesis of complex 35. A solution of KPPH₂ was prepared by adding a THF solution (10 mL) of diphenylphosphine (0.70 g, 3.8 mmol) to potassium metal (0.18 g, 4.62 mg/atom) in THF (10 mL) dropwise at -78 °C, and the resulting solution was stirred at -78 °C for 12 h. The solution of KPPH₂ was filtered at room temperature through Celite to remove the excess potassium metal. The filtered solution was added dropwise to a suspension of complex **17** (2.00 g, 3.78 mmol) in THF (30 mL) at -78 °C, and the reaction mixture was stirred at room temperature overnight. Half of the solvent (ca. 15 mL) was removed *in vacuo*. The resulting yellow suspension was filtered, and the collected precipitate was washed twice with a minimal amount of THF. The yellow precipitate was redissolved in benzene and the solution was filtered through Celite to remove KI. The solvent was removed *in vacuo* to yield complex **35** as a yellow powder (1.78 g, 80%). X-ray quality yellow needles were grown in CDCl₃ at room temperature. IR (CDCl₃) 1912 cm⁻¹ (ν_{CO}); ¹H NMR (300 MHz, CDCl₃) δ 1.52 (m, 1 H), 2.00 - 2.25 (m, 1 H), 2.73 (td, $J = 12.97, 2.88$ Hz, 1 H), 3.02 - 3.17 (m, 1 H), 3.63 (t, $J = 10.51$ Hz, 1 H), 3.91 (d, $J = 1.37$ Hz, 5 H), 4.57 (dd, $J = 10.43, 7.96$ Hz, 1H), 7.10 - 7.23 (m, 5 H), 7.32 - 7.43 (m, 6 H), 7.44 - 7.54 (m, 5H) 7.79(m, 2H), 7.86 - 7.98 (m, 2H); ¹³C{¹H} NMR (100.58 MHz, CDCl₃) δ 23.04 (s, 1 C), 36.97 (d, $J=20.08$ Hz, 1 C), 56.05 (d, $J=19.64$, 1 C), 84.00 (s, 5C), 126.64 - 143.15 (m, 24 C), 214.30 (dd, $J=70.57, 23.96$ Hz, -C=N-), 221.04 (dd, $J=16.91, 20.42$ Hz, -CO); ³¹P{¹H} NMR (121.44 MHz, CDCl₃) δ 31.51 (d, $J=23.76$ Hz, -C-PPh₂), 57.28 (d, $J=23.76$ Hz, Fe-PPh₂-). MS (ESI, m/z): calc. mass

588.1309, obs. mass 588.1319 (M⁺). (This compound slowly decomposes in the solid state at -35 °C, EA was not possible.)

Synthesis of complex 36. Triphenylsilylpotassium (KSiPh₃) was obtained as a yellow precipitate by reacting a solution of hexaphenyldisilane (0.40 g, 0.76 mmol) in Et₂O (10 mL) with potassium metal (0.12 g, 3.04 mg/atom) at 35 °C under static vacuum for 48 h. The solvent was removed *in vacuo* and the yellow residue was dissolved in THF (20 mL). This solution was filtered and added dropwise to a suspension of complex **17** (0.79 g, 1.5 mmol) in THF (50 mL) at -78 °C, and the reaction mixture was warmed to room temperature with stirring overnight. The solvent was removed *in vacuo*, the residue redissolved in benzene, and the solution filtered through Celite to remove KI. The solvent was again removed under vacuum to collect a dark yellow precipitate. In order to fully separate the product from the major byproduct, the precipitate was left as a suspension in Et₂O (20 mL) at room temperature overnight and then filtered. The filtrate, containing a major amount of the byproduct and a small amount of complex **36**, was collected as a brown solution. These steps were repeated 4 times until the byproduct was removed and complex **36**, the residue from the Et₂O washings, was isolated as a yellow solid (0.282 g, 28%). X-ray quality orange prisms of complex **36** were grown in CDCl₃ at -35 °C. IR (CDCl₃) 1915.17 cm⁻¹ (ν_{CO}); ¹H NMR (400 Hz, CDCl₃) δ 1.75 - 2.09 (m, 2 H), 2.57 - 2.80 (m, 2 H), 4.03 (t, *J*=10.28 Hz, 1 H), 4.22 (s, 5H), 5.02-5.14 (m, 1H), 7.11 - 7.23 (m, 4 H), 7.29-7.40 (m, 13 H), 7.41-7.55 (m, 2 H), 7.67-7.79 (m, 5H); ¹³C{¹H} NMR (100.58 MHz, CDCl₃) δ 22.64 (s, 1C), 34.52 (d, *J*=20.99 Hz, 1C), 59.57 (d, *J*=5.65 Hz, 1C), 83.40 (s, 5C), 127.22 - 140.44 (m, 30C), 219.49 (d, *J*=36.33 Hz, -CO), 234.38 (d, *J*=16.15 Hz, -C=N-); ³¹P{¹H} NMR (121.44 MHz, CDCl₃) δ 58.37 (s, 1P). MS (ESI, *m/z*): calc. mass 662.1731, obs. mass 662.1736 (M⁺). Anal. Calc. for 3 ([C₄₀H₃₆FeNOPSi]·1/2[CHCl₃]) N, 1.94; C, 67.44; H, 5.10. Obtained N, 2.54; C, 67.34; H, 5.29.

Byproduct. The purified byproduct was obtained by silica flash chromatography of the brown solution through a column and removal of the Et₂O *in vacuo* to yield a yellow solid (0.028 g, 10%). IR (CDCl₃) 1945.18cm⁻¹ (ν_{CN}), 1884.44cm⁻¹ (ν_{CO}); ¹H NMR (400 MHz, CDCl₃) δ 1.76 (m, 2H), 2.08 (br. s., 1H), 2.32 - 2.50 (m, 1H), 2.51-2.59 (m, 1H) 2.80 (br. s., 1H), 3.04 - 3.25 (m, 2H), 3.27 (d, *J*=4.80 Hz, 1H), 4.78 (br. s., 1H), 5.34 (br. s., 1H), 7.30 (d,

$J=7.41$ Hz, 6H), 7.34 - 7.58 (m, 22H); $^{13}\text{C}\{^1\text{H}\}$ NMR (100.58 MHz, CDCl_3) δ 22.64 (s, 1C), 34.52 (d, $J=20.99$ Hz, 1C), 59.57 (d, $J=5.65$ Hz, 1C), 83.40 (s, 5C), 127.22 - 140.44 (m, 30C), 218.34 (d, $J=26.44$ Hz, -CN-), 223.16 (br. s., -CO); $^{31}\text{P}\{^1\text{H}\}$ NMR (121.44 MHz, CDCl_3) δ 57.80 (s, 1P). MS (ESI, m/z): calc. mass 659.1524, obs. mass 659.1497 (M+). Anal. Calc. for byproduct ($\text{C}_{40}\text{H}_{32}\text{FeNOPSi}$) N, 2.12; C, 72.83; H, 5.20. Obtained N, 2.28; C, 72.24; H, 5.75.

Synthesis of complex 37. A solution of complex 2 (0.61 g, 1.0 mmol) in CHCl_3 (10 mL) was cooled to -35 °C, and an equimolar solution of 6.2 M HBF_4 (0.17 mL, 1.0 mmol) in diethyl ether was added dropwise using a micro syringe. The reaction solution was warmed up to room temperature for 5 min. After removal of the solvent *in vacuo* a yellow solid of complex 4 was collected. In order to remove decomposition byproducts (an iron(II) isocyanide-phosphine complex and diphenylphosphine) from the desired complex 4, the product was suspended in THF overnight at room temperature. The suspension was filtered through a frit to collect the product **37** (0.208 g, 30%). IR (CDCl_3) 1955.87 cm^{-1} (ν_{CO}); ^1H NMR (400 MHz, CDCl_3) δ 1.37 (br. s., 1 H), 2.20 - 2.48 (m, 1 H), 3.10 - 3.41 (m, 2 H), 4.17 (s, 6 H), 4.29 (br. s., 1 H), 7.22 (br. s., 2 H), 7.31 - 7.39 (m, 4 H), 7.43 - 7.55 (m, 6 H), 7.60 (d, $J=6.04$ Hz, 3 H), 7.70 (d, $J=9.06$ Hz, 2 H), 7.87 (t, $J=7.00$ Hz, 2 H), 9.64 (br. s., 1 H); $^{13}\text{C}\{^1\text{H}\}$ NMR (100.58 MHz, CDCl_3) δ 23.68 (br. s., 1 C), 34.94 (d, $J=24.48$ Hz, 1 C), 51.47 (br. s., 1 C), 85.93 (s, 5C), 128.62 - 139.56 (m, 24 C), 217.17 (dd, $J=19.58, 8.97$ Hz, -CO), 276.39 (dd, $J=61.20, 23.66$ Hz, =C-NH-); $^{31}\text{P}\{^1\text{H}\}$ NMR (121.44, CDCl_3) δ 38.05 (d, $J=11.88$ Hz, -C-PPh₂), 50.98 (d, $J=11.88$ Hz, Fe-PPh₂-). MS (ESI, m/z): calc. mass 588.1309, obs. mass 588.1298 (M+). This compound slowly decomposes in the solid state at -35 °C and in solution therefore EA was not possible.

Synthesis of complex 38. A solution of HBF_4 (6.2 M, 0.012 mL, 0.074 mmol) in Et_2O was added to a solution of complex 3 (0.05 g, 0.08 mmol) in CHCl_3 (5 mL) at -35 °C. The reaction mixture was stirred at room temperature for 1 h. The solvent was then removed *in vacuo*. Et_2O was added to the residue to precipitate out complex 5 as a yellow solid (0.058 g, 97%). IR (CDCl_3) 1958.83 cm^{-1} (ν_{CO}); ^1H NMR (400 MHz, CDCl_3) δ 1.46 (br. s., 1 H), 2.23-2.53 (m, 1 H), 2.90 (t, $J=12.91$, 1H), 3.25-3.45 (m, 1H), 4.40 (br. s., 6 H), 4.50 (br. s., 1H), 6.95-7.14 (m, 3H), 7.26-7.77 (m, 22H), 10.62 (br. s., 1 H); $^{13}\text{C}\{^1\text{H}\}$ NMR (100.58 MHz,

CDCl₃) δ 23.09 (s, 1C), 34.99 (d, $J=22.61$ Hz, 1C), 54.28 (br. s., 1C), 85.80 (s, 5C), 127.86 - 138.89 (m, 30C), 216.45 (d, $J=32.29$ Hz, -CO), 299.38 (br. s., =C-NH-); ³¹P{¹H} NMR (121.44 MHz, CDCl₃) δ 55.42. MS (ESI, m/z): calc. mass 662.1732, obs. mass 662.1747 (M⁺). Anal. Calc. for **38** (C₄₀H₃₇BF₄FeNOPSi), N, 1.87; C, 64.11; H, 4.98. Obtained: N, 2.17; C, 64.24; H, 5.21.

Reversible reaction of acyclic (silyl)(amino) carbene (38) to an ylidene (37) complex. A suspension of NaHB(OAc)₃ (0.015 g, 0.40 mmol) in CH₂Cl₂ (2 mL) was added to a solution of complex **38** (0.05 g, 0.07 mmol) in CH₂Cl₂ (5 mL) at room temperature and was kept *under static vacuum* overnight. This step was repeated over four days to complete the conversion from complex **38** to complex **37**, while adding more equivalents of the reducing reagent each day. The solution was concentrated *in vacuo* for an NMR sample.

Chapter 6: General Conclusion and Future Directions

The aim of my Ph.D. research has been the design and fine tuning of ancillary ligands for metal catalysts in order to: (1) investigate the mechanism of the chiral dinuclear In(III) catalysts for the highly controlled nature of the ring opening polymerization of lactide, reported first by the Mehrkhodavandi group, (2) develop chiral neutral and cationic alkyl In(III) catalysts for controlled polymerization of polar vinyl monomers and (3) study the synthesis and reactivity of the cyclic and acyclic donor functionalized carbene Fe(II) complexes.

Chapter 2 showed that indium alkoxide complexes in this family are invariably dinuclear in the solid state as well as in solution, as confirmed by a variety of NMR spectroscopic techniques and X-ray crystallography. There are two significant pieces of evidence to confirm that dinuclear alkoxy-bridged indium complexes are thermodynamically favored in these systems: (1) although the dissociation of the dinuclear complexes in solution occurred with added donors / dihalide indium complexes the major products in all irreversible reactions are the dinuclear complexes, and (2) the 50:50 mixture of enantiopure bis-ethoxy bridged dinuclear complexes, (*R,R/R,R*)- and (*S,S/S,S*)-[(NNO_R)In(I)(OEt)]₂ in the noncentrosymmetric geometry center, is converted to the meso bis-ethoxy bridged dinuclear complex, (meso)-[(NNO_R)In(I)(OEt)]₂ in the centrosymmetric geometry.

The mechanistic studies of polymerization conducted with the racemic and enantiopure mono- and bis-alkoxy bridged In(III) catalysts in Chapter 3 elucidate the significant role of the chiral alkoxy-bridged dinuclear species in the polymerization behavior and selectivity for the ring opening polymerization of lactide. Due to the stable dinuclear polymeryl-bridged complex as a steady state, the highly controlled polymerization is possible without chain termination. Further computational work is required to examine the stability of the monoalkoxy- and bisalkoxy-bridged dinuclear indium catalysts in the presence of polar solvents or monomers. In addition, it will be very interesting to compute the first insertion pathway with (*R,R/R,R*)-**5** and rac LA which will prove the non-linear relationship between the observed rate constant and percent (*R,R/R,R*)-**5**.

The studies will influence the design of future indium-based complexes in catalysis. We are interested in developing a family of dinuclear indium complexes where two indium metal

centers are bridged through alkyl or benzyl alkoxy linkages on the ancillary ligand such as (NNONN)-type ligands.

Additionally, we show in Chapter 4 that changing the Lewis acidities and structural geometries at neutral and cationic In(III) centers influences the catalytic reactivity of MMA polymerization. The reactivity toward MMA polymerization with the neutral indium complexes with a κ^2 -coordinated NNO_{tBu} ligand is higher than that of the cations with a κ^3 -coordinated NNO_{tBu} ligand. Importantly, the counter anions in the cationic complexes greatly influence the reactivity of the polymerization. This study shows the potential of the neutral and cationic indium complexes as promising catalysts for polymerization of polar or nonpolar conjugated vinyl monomers through modification of ligands to tune the Lewis acidities of the indium center and modify the coordination environment around the center in the future.

However, modifications of the ligand (bidentate ligand with a hemilabile arm or with softer L donors) and the initiator on the metal center as well as the polymerization conditions will be required to enhance their catalytic reactivity. In addition, the stereoselectivity and the mechanism of polymerization of MMA with the current neutral and cationic indium systems must be investigated. We will also extend our work to polymerization of renewable methylene butyrolactones, including naturally occurring α -methylene- γ -butyrolactone (MBL) and plant biomass-derived γ -methyl- α -methylene- γ -butyrolactone.

Finally, this work demonstrates the electronic properties of an iron complex are influenced by the nature of the various donor functionalized carbene ligands as explored in Chapter 5. This study shows that the electronic properties of the XCN carbene ligands to the iron center can be tuned by changing different neighboring heteroatoms X; thus, the greater degree of $\text{C}_{\text{carbene}}\text{-X}$ π -bonding, where X = N rather than X = O, P, and Si, is reflected in the greater shielding of $\text{C}_{\text{carbene}}$ in XCN carbene complexes. This work also demonstrates that template synthesis can be a fantastic methodology to provide currently inaccessible acyclic and cyclic carbenes. This systematic study of the template synthesis of acyclic and cyclic carbenes on a model system has enabled us to investigate the synthesis and reactivity of potentially catalytic ruthenium, rhodium, and palladium analogues.

Future investigations in this area will involve the synthesis and characterization of phosphino-isocyanide proligands and ruthenium complexes without a Cp ligand. A family of

phosphino-isocynide proligands containing various backbones such as alkyl or aromatic functionalities can be synthesized using known literature procedures.^{414,415} Reaction of ruthenium starting materials and the phosphino-isocynide proligands via ligand substitution will yield the desired phosphino-isocynide coordinated ruthenium scaffold. The ruthenium-bound ligand scaffold can be further modified to generate acyclic and cyclic fragments via nucleophilic attack on the isocynide by nucleophiles such as amines, alcohols and alkoxides.

These studies will inspire the following graduate students to develop the next generation of catalysts by designing new ligands for their aiming catalysis.

References

- (1) Yu, I.; Acosta-Ramirez, A.; Mehrkhodavandi, P. *J. Am. Chem. Soc.* **2012**, *134*, 12758.
- (2) Osten, K.; Yu, I.; Duffy, I. R.; Lagaditis, P. V. O.; Yu, C.-C.; Wallis, C. J.; Mehrkhodavandi, P. *Dalton Trans.* **2012**, DOI: 10.1039/c2dt30148b.
- (3) Acosta-Ramirez, A.; Douglas, A. F.; Yu, I.; Patrick, B. O.; Diaconescu, P. L.; Mehrkhodavandi, P. *Inorg. Chem.* **2010**, *49*, 5444.
- (4) Yu, I.; Wallis, C. J.; Patrick, B. O.; Mehrkhodavandi, P. *Organometallics* **2009**, *28*, 6370.
- (5) Yu, I.; Wallis, C. J.; Patrick, B. O.; Diaconescu, P. L.; Mehrkhodavandi, P. *Organometallics* **2010**, *29*, 6065.
- (6) Press Release: The Nobel Prize in Chemistry 2005. http://nobelprize.org/nobel_prizes/chemistry/laureates/2005/press.html. [Online Early Access].
- (7) Wastes - Resource Conservation - Common Wastes & Materials. <http://www.epa.gov/osw/conserve/materials/plastics.htm> [Online Early Access].
- (8) Auras, R.; Harte, B.; Selke, S. *Macromol. Biosci.* **2004**, *4*, 835.
- (9) Johansson, C.; Bras, J.; Mondragon, I.; Nechita, P.; Plackett, D.; Simon, P.; Svetec, D. G.; Virtanen, S.; Baschetti, M. G.; Breen, C.; Clegg, F.; Aucejo, S. *Bioresources* **2012**, *7*, 2506.
- (10) Marsh, K.; Bugusu, B. *J. Food Sci.* **2007**, *72*, R39.
- (11) Kricheldorf, H. R.; Kreiseraunders, I.; Boettcher, C. *Polymer* **1995**, *36*, 1253.
- (12) Filachione, E. M.; Fisher, C. H. *Ind. Eng. Chem.* **1944**, *36*, 223.
- (13) Dorgan, J. R.; Lehermeier, H.; Mang, M. *J. Polym. Environ.* **2000**, *8*, 1.
- (14) Othman, N.; Xu, C.; Mehrkhodavandi, P.; Hatzikiriakos, S. G. *Polym. J.* **2012**, DOI 10.1016/j.polymer.2012.03.068.
- (15) Othman, N.; Acosta-Ramirez, A.; Mehrkhodavandi, P.; Dorgan, J. R.; Hatzikiriakos, S. G. *J. Rheol.* **2011**, *55*, 987.
- (16) Drumright, R. E.; Gruber, P. R.; Henton, D. E. *Adv. Mater.* **2000**, *12*, 1841.
- (17) Loh, T. P.; Chua, G. L. *Chem. Commun. (Cambridge, U. K.)* **2006**, 2739.
- (18) Frost, C. G.; Hartley, J. P. *Mini-Rev. Org. Chem.* **2004**, *1*, 1.
- (19) Fringuelli, F.; Piermatti, O.; Pizzo, F.; Vaccaro, L. *Curr. Org. Chem.* **2003**, *7*, 1661.
- (20) Chauhan, K. K.; Frost, C. G. *J. Chem. Soc.-Perkin Transactions 1* **2000**, 3015.
- (21) Li, C. J.; Chan, T. H. *Tetrahedron* **1999**, *55*, 11149.
- (22) Cintas, P. *Synlett* **1995**, 1087.
- (23) Douglas, A. F.; Patrick, B. O.; Mehrkhodavandi, P. *Angew. Chem. Int. Ed.* **2008**, *47*, 2290.
- (24) Atwood, D. A. *Coord. Chem. Rev.* **1998**, *176*, 407.
- (25) Dagorne, S.; Atwood, D. A. *Chem. Rev.* **2008**, *108*, 4037.
- (26) Aida, T.; Inoue, S. *Acc. Chem. Res.* **1996**, *29*, 39.
- (27) Aida, T.; Mizuta, R.; Yoshida, Y.; Inoue, S. *Makromol. Chem. Macromol. Chem. Phys.* **1981**, *182*, 1073.
- (28) Stickler, M.; Rhein, T. *Polymethacrylates*; VHS: New York, 1992; Vol. 421.
- (29) Scholl, M.; Ding, S.; Lee, C. W.; Grubbs, R. H. *Org. Lett.* **1999**, *1*, 953.
- (30) Scholl, M.; Trnka, T. M.; Morgan, J. P.; Grubbs, R. H. *Tetrahedron Lett.* **1999**, *40*, 2247.

- (31) Huang, J. K.; Stevens, E. D.; Nolan, S. P.; Petersen, J. L. *J. Am. Chem. Soc.* **1999**, *121*, 2674.
- (32) de Frémont, P.; Marion, N.; Nolan, S. P. *Coord. Chem. Rev.* **2009**, *253*, 862.
- (33) Jacobsen, H.; Correa, A.; Poater, A.; Costabile, C.; Cavallo, L. *Coord. Chem. Rev.* **2009**, *253*, 687.
- (34) Hahn, F. E.; Jahnke, M. C. *Angew. Chem.-Int. Edit.* **2008**, *47*, 3122.
- (35) Herrmann, W. A. *Angew. Chem. Int. Ed. Engl.* **2002**, *41*, 1290.
- (36) Vignolle, J.; Cattoen, X.; Bourissou, D. *Chem. Rev.* **2009**, *109*, 3333.
- (37) Arnold, P. L.; Pearson, S. *Coord. Chem. Rev.* **2007**, *251*, 596.
- (38) Jones, N. D.; Cavell, R. G. *J. Organomet. Chem.* **2005**, *690*, 5485.
- (39) Canac, Y.; Soleilhavoup, M.; Conejero, S.; Bertrand, G. *J. Organomet. Chem.* **2004**, *689*, 3857.
- (40) Bourissou, D.; Guerret, O.; Gabbai, F. P.; Bertrand, G. *Chem. Rev.* **2000**, *100*, 39.
- (41) Lavallo, V.; Canac, Y.; Prasang, C.; Donnadiou, B.; Bertrand, G. *Angew. Chem. Int. Ed.* **2005**, *44*, 5705.
- (42) Anderson, D. R.; Lavallo, V.; O'Leary, D. J.; Bertrand, G.; Grubbs, R. H. *Angew. Chem. Int. Ed.* **2007**, *46*, 7262.
- (43) Cantat, T.; Mezailles, N.; Maignot, N.; Ricard, L.; Le Floch, P. *Chem. Commun.* **2004**, 1274.
- (44) Ruiz, J.; Mosquera, M. E. G.; Garcia, G.; Patron, E.; Riera, V.; Garcia-Granda, S.; Van der Maelen, F. *Angew. Chem. Int. Ed.* **2003**, *42*, 4767.
- (45) Asay, M.; Kato, T.; Saffon-Merceron, N.; Cossio, F. P.; Baceiredo, A.; Bertrand, G. *Angew. Chem. Int. Ed.* **2008**, *47*, 7530.
- (46) Masuda, J. D.; Martin, D.; Lyon-Saunier, C.; Baceiredo, A.; Gornitzka, H.; Donnadiou, B.; Bertrand, G. *Chemistry-an Asian Journal* **2007**, *2*, 178.
- (47) Martin, D.; Baceiredo, A.; Gornitzka, H.; Schoeller, W. W.; Bertrand, G. *Angew. Chem. Int. Ed.* **2005**, *44*, 1700.
- (48) Merceron-Saffon, N.; Gornitzka, H.; Baceiredo, A.; Bertrand, G. *J. Organomet. Chem.* **2004**, *689*, 1431.
- (49) Teuma, E.; Lyon-Saunier, C.; Gornitzka, H.; Mignani, G.; Baceiredo, A.; Bertrand, G. *J. Organomet. Chem.* **2005**, *690*, 5541.
- (50) Canac, Y.; Conejero, S.; Donnadiou, B.; Schoeller, W. W.; Bertrand, G. *J. Am. Chem. Soc.* **2005**, *127*, 7312.
- (51) Merceon, N.; Miqueu, K.; Baceiredo, A.; Bertrand, G. *J. Am. Chem. Soc.* **2002**, *124*, 6806.
- (52) Ruiz, J.; Garcia, G.; Mosquera, M. E. G.; Perandones, B. F.; Gonzalo, M. P.; Vivanco, M. *J. Am. Chem. Soc.* **2005**, *127*, 8584.
- (53) Ruiz, J.; Perandones, B. F.; Garcia, G.; Mosquera, M. E. G. *Organometallics* **2007**, *26*, 5687.
- (54) Hahn, F. E.; Langenhahn, V.; Pape, T. *Chem Commun* **2005**, 5390.
- (55) Hahn, F. E.; Langenhahn, V.; Lugger, T.; Pape, T.; Le Van, D. *Angew. Chem. Int. Ed. Engl.* **2005**, *44*, 3759.
- (56) Kaufhold, O.; Stasch, A.; Pape, T.; Hepp, A.; Edwards, P. G.; Newman, P. D.; Hahn, E. *J. Am. Chem. Soc.* **2009**, *131*, 306.
- (57) Buffet, J.-C.; Okuda, J.; Arnold, P. L. *Inorg. Chem.* **2010**, *49*, 419.

- (58) Schumann, H.; Kaufmann, J.; Wassermann, B. C.; Girgsdies, F.; Jaber, N.; Blum, J. Z. *Anorg. Allg. Chem.* **2002**, 628, 971.
- (59) Schumann, H.; Kaufmann, J.; Dechert, S. *Z. Anorg. Allg. Chem.* **2004**, 630, 1999.
- (60) Gao, Q.; Jiang, F. L.; Wu, M. Y.; Huang, Y. G.; Chen, L.; Wei, W.; Hong, M. C. *J. Solid State Chem.* **2009**, 182, 1499.
- (61) Yuan, F.; Zhu, C. J.; Sun, J. T.; Liu, Y. J.; Pan, Y. *J. Organomet. Chem.* **2003**, 682, 102.
- (62) Chitsaz, S.; Neumuller, B. *Organometallics* **2001**, 20, 2338.
- (63) Pauls, J.; Chitsaz, S.; Neumuller, B. *Z. Anorg. Allg. Chem.* **2000**, 626, 2028.
- (64) Ziemkowska, W.; Anulewicz-Ostrowska, R. *J. Organomet. Chem.* **2004**, 689, 2056.
- (65) Ziemkowska, W.; Kucharski, S.; Kolodziej, A.; Anulewicz-Ostrowska, R. *J. Organomet. Chem.* **2004**, 689, 2930.
- (66) Ziemkowska, W.; Stella, P.; Anulewicz-Ostrowska, R. *J. Organomet. Chem.* **2005**, 690, 722.
- (67) Ullrich, M.; Mitzel, N. W.; Bergander, K.; Frohlich, R. *Dalton Trans.* **2006**, 714.
- (68) Ziemkowska, W.; Cyranski, M. K. *Organometallics* **2009**, 28, 5593.
- (69) Bösing, P.; Mitzel, N. W. *Dalton Trans.* **2010**, 39, 66.
- (70) Lu, J.; Hong, M. L.; Ji, S. J.; Loh, T. P. *Chem. Commun.* **2005**, 1010.
- (71) Lu, J.; Hong, M. L.; Ji, S. J.; Teo, Y. C.; Loh, T. P. *Chem. Commun.* **2005**, 4217.
- (72) Lu, J.; Ji, S. J.; Loh, T. P. *Chem. Commun.* **2005**, 2345.
- (73) Teo, Y. C.; Tan, K. T.; Loh, T. P. *Chem. Commun.* **2005**, 1318.
- (74) Lu, J.; Ji, S. J.; Teo, Y. C.; Loh, T. P. *Org. Lett.* **2005**, 7, 159.
- (75) Teo, Y. C.; Goh, J. D.; Loh, T. P. *Org. Lett.* **2005**, 7, 2743.
- (76) Zhang, X.; Chen, D. H.; Liu, X. H.; Feng, X. M. *J. Org. Chem.* **2007**, 72, 5227.
- (77) Fu, F.; Teo, Y. C.; Loh, T. P. *Org. Lett.* **2006**, 8, 5999.
- (78) Teo, Y. C.; Loh, T. P. *Org. Lett.* **2005**, 7, 2539.
- (79) Zhao, J. F.; Tsui, H. Y.; Wu, P. J.; Lu, J.; Loh, T. P. *J. Am. Chem. Soc.* **2008**, 130, 16492.
- (80) Broderick, E. M.; Guo, N.; Wu, T. P.; Vogel, C. S.; Xu, C. L.; Sutter, J.; Miller, J. T.; Meyer, K.; Cantat, T.; Diaconescu, P. L. *Chem. Commun.* **2011**, 47, 9897.
- (81) Ul-haq, M. I.; Acosta-Ramirez, A.; Mehrkhodavandi, P.; Signorell, R. *J. Supercrit. Fluids* **2010**, 51, 376.
- (82) Broderick, E. M.; Guo, N.; Vogel, C. S.; Xu, C.; Sutter, J.; Miller, J. T.; Meyer, K.; Mehrkhodavandi, P.; Diaconescu, P. L. *J. Am. Chem. Soc.* **2011**, 133, 9278.
- (83) Othman, N.; Jazrawi, B.; Mehrkhodavandi, P.; Hatzikiriakos, S. G. *Rheol. Acta* **2012**, 51, 357.
- (84) Hsieh, I. P.; Huang, C. H.; Lee, H. M.; Kuo, P. C.; Huang, J. H.; Lee, H. I.; Cheng, J. T.; Lee, G. H. *Inorg. Chim. Acta* **2006**, 359, 497.
- (85) Hu, M. G.; Wang, M.; Zhang, P. L.; Wang, L.; Zhu, F. J.; Sun, L. C. *Inorg. Chem. Commun.* **2010**, 13, 968.
- (86) Normand, M.; Kirillov, E.; Roisnel, T.; Carpentier, J. F. *Organometallics* **2012**, 31, 1448–1457.
- (87) Peckermann, I.; Kapelski, A.; Spaniol, T. P.; Okuda, J. *Inorg. Chem.* **2009**, 48, 5526.
- (88) Blake, M. P.; Schwarz, A. D.; Mountford, P. *Organometallics* **2011**, 30, 1202.
- (89) Pietrangelo, A.; Hillmyer, M. A.; Tolman, W. B. *Chem. Commun.* **2009**, 2736.

- (90) Pietrangelo, A.; Knight, S. C.; Gupta, A. K.; Yao, L. J.; Hillmyer, M. A.; Tolman, W. B. *J. Am. Chem. Soc.* **2010**, *132*, 11649.
- (91) Aluthge, D. C.; Patrick, B. O.; Mehrkhodavandi, P. *Chem. Commun.* **2013**, Invited article in the "Emerging Investigators" issue. .
- (92) Spassky, N.; Wisniewski, M.; Pluta, C.; LeBorgne, A. *Macromol. Chem. Phys.* **1996**, *197*, 2627.
- (93) Ovitt, T. M.; Coates, G. W. *J. Am. Chem. Soc.* **1999**, *121*, 4072.
- (94) Zhong, Z. Y.; Dijkstra, P. J.; Feijen, J. *Angew. Chem. Int. Ed.* **2002**, *41*, 4510.
- (95) Zhong, Z. Y.; Dijkstra, P. J.; Feijen, J. *J. Am. Chem. Soc.* **2003**, *125*, 11291.
- (96) Zhong, Z. Y.; Dijkstra, P. J.; Feijen, J. *J. Biomater. Sci., Polym. Ed.* **2004**, *15*, 929.
- (97) Nomura, N.; Ishii, R.; Akakura, M.; Aoi, K. *J. Am. Chem. Soc.* **2002**, *124*, 5938.
- (98) Le Borgne, A.; Vincens, V.; Jouglard, M.; Spassky, N. *Makromol. Chem., Macromol. Symp.* **1993**, *73*, 37.
- (99) Le Borgne, A.; Wisniewski, M.; Spassky, N. *Polym. Prepr. (Am. Chem. Soc., Div. Polym. Chem.)* **1995**, *36*, 217.
- (100) Wisniewski, M.; LeBorgne, A.; Spassky, N. *Macromol. Chem. Phys.* **1997**, *198*, 1227.
- (101) Bhaw-Luximon, A.; Jhurry, D.; Spassky, N. *Polym. Bull.* **2000**, *44*, 31.
- (102) Jhurry, D.; Bhaw-Luximon, A.; Spassky, N. *Macromol. Symp.* **2001**, *175*, 67.
- (103) Hormnirun, P.; Marshall, E. L.; Gibson, V. C.; White, A. J. P.; Williams, D. J. *J. Am. Chem. Soc.* **2004**, *126*, 2688.
- (104) Ma, H. Y.; Melillo, G.; Oliva, L.; Spaniol, T. P.; Englert, U.; Okuda, J. *Dalton Trans.* **2005**, 721.
- (105) Ovitt, T. M.; Coates, G. W. *J. Polym. Sci. A Polym. Chem.* **2000**, *38*, 4686.
- (106) Shannon, R. D. *Acta Crystallogr., Sect. A* **1976**, *32*, 751.
- (107) Downs, A. J.; Himmel, H.-J. *New light on the chemistry of the group 13 metals*; John Wiley & Sons, Ltd: Chichester, West Sussex, 2011.
- (108) Lappert, M. F. *J. Chem. Soc.* **1962**, 542.
- (109) Branch, C. S.; Bott, S. G.; Barron, A. R. *J. Organomet. Chem.* **2003**, *666*, 23.
- (110) Williams, C. K.; Breyfogle, L. E.; Choi, S. K.; Nam, W.; Young, V. G.; Hillmyer, M. A.; Tolman, W. B. *J. Am. Chem. Soc.* **2003**, *125*, 11350.
- (111) Geldbach, T. J.; Pregosin, P. S.; Bassetti, M. *Organometallics* **2001**, *20*, 2990.
- (112) Valentini, M.; Pregosin, P. S.; Ruegger, H. *Organometallics* **2000**, *19*, 2551.
- (113) Jiang, Q. Z.; Ruegger, H.; Venanzi, L. M. *Inorg. Chim. Acta* **1999**, *290*, 64.
- (114) Pichota, A.; Pregosin, P. S.; Valentini, M.; Worle, M.; Seebach, D. *Angew. Chem. Int. Ed.* **2000**, *39*, 153.
- (115) Colton, R.; Dagostino, A.; Traeger, J. C. *Mass Spectrom. Rev.* **1995**, *14*, 79.
- (116) Makhouloufi, R.; Mansot, J. L.; Hirsch, E.; Wery, J.; Candau, S. J.; Thomas, D.; Rolland, J. P. *Colloid Polym. Sci.* **1995**, *273*, 242.
- (117) Beyer, G. L. *Physical Methods of chemistry*; Wiley-Interscience: New York, 1971; Vol. 1.
- (118) Guerin, G.; Raez, J.; Manners, I.; Winnik, M. A. *Macromolecules* **2005**, *38*, 7819.
- (119) Kriesel, J. W.; Konig, S.; Freitas, M. A.; Marshall, A. G.; Leary, J. A.; Tilley, T. D. *J. Am. Chem. Soc.* **1998**, *120*, 12207.
- (120) Macchioni, A.; Ciancaleoni, G.; Zuccaccia, C.; Zuccaccia, D. *Chem. Soc. Rev.* **2008**, *37*, 479.
- (121) Valentini, M.; Pregosin, P. S.; Ruegger, H. *J. Chem. Soc., Dalton Trans.* **2000**, 4507.

- (122) Selvakumar, K.; Valentini, M.; Pregosin, P. S.; Albinati, A.; Eisentrager, F. *Organometallics* **2000**, *19*, 1299.
- (123) Price, W. S. *Concept. Magnetic Res.* **1997**, *9*, 299.
- (124) Edward, J. T. *J. Chem. Educ.* **1970**, *47*, 261.
- (125) Mitchell, J. M.; Finney, N. S. *Tetrahedron Lett.* **2000**, *41*, 8431.
- (126) Larrow, J. F.; Jacobsen, E. N.; Gao, Y.; Hong, Y. P.; Nie, X. Y.; Zepp, C. M. *J. Org. Chem.* **1994**, *59*, 1939.
- (127) Carothers, W. H.; Dorough, G. L.; van Natta, F. J. *J. Am. Chem. Soc.* **1983**, *54*, 761.
- (128) Gupta, A. P.; Kumar, V. *Eur. Polym. J.* **2007**, *43*, 4053.
- (129) Gupta, B.; Revagade, N.; Hilborn, J. *Prog. Polym. Sci.* **2007**, *32*, 455.
- (130) Williams, C. K.; Hillmyer, M. A. *Polym. Rev.* **2008**, *48*, 1.
- (131) Thomas, C. M.; Lutz, J.-F. *Angew. Chem. Int. Ed.* **2011**, *50*, 9244
- (132) Nakamura, L. K. *Int. J. Sys Bacteriol.* **1981**, *31*, 56.
- (133) Akerberg, C.; Hofvendahl, K.; Zacchi, G.; Hahn-Hagerdal, B. *Appl. Microbiol. Biotechnol.* **1998**, *49*, 682.
- (134) Hofvendahl, K.; Hahn-Hagerdal, B. *Enzyme Microb. Technol.* **2000**, *26*, 87.
- (135) Datta, R.; Tsai, S. P.; Bonsignore, P.; Moon, S. H.; Frank, J. R. *FEMS Microbiol. Rev.* **1995**, *16*, 221.
- (136) Hofvendahl, K.; Akerberg, C.; Zacchi, G.; Hahn-Hagerdal, B. *Appl. Microbiol. Biotechnol.* **1999**, *52*, 163.
- (137) Vijayakumar, J.; Aravindan, R.; Viruthagiri, T. *Chem. Biochem. Eng. Q.* **2008**, *22*, 245.
- (138) Yin, P. M.; Nishina, N.; Kosakai, Y.; Yahiro, K.; Park, Y.; Okabe, M. *J. Ferment. Bioeng.* **1997**, *84*, 249.
- (139) BP Statistical Review of World Energy. [Online Early Access]. Published Online: 2012.
- (140) Vanhummel, G. J.; Harkema, S.; Kohn, F. E.; Feijen, J. *Acta Crystallogr., Sect. B: Struct. Sci.* **1982**, *38*, 1679.
- (141) Jungfleisch, E.; Godchot, M. *Compt. Rend. Hebd. Seances Acad. Sci.* **1906**, *142*, 637.
- (142) Mecking, S. *Angew. Chem. Int. Ed.* **2004**, *43*, 1078.
- (143) Thakur, K. A. M.; Kean, R. T.; Hall, E. S.; Kolstad, J. J.; Munson, E. J. *Macromolecules* **1998**, *31*, 1487.
- (144) Thakur, K. A. M.; Kean, R. T.; Hall, E. S.; Kolstad, J. J.; Lindgren, T. A.; Doscotch, M. A.; Siepmann, J. I.; Munson, E. J. *Macromolecules* **1997**, *30*, 2422.
- (145) Thakur, K. A. M.; Kean, R. T.; Zell, M. T.; Padden, B. E.; Munson, E. J. *Chem. Commun.* **1998**, 1913.
- (146) Dechy-Cabaret, O.; Martin-Vaca, B.; Bourissou, D. *Chem. Rev.* **2004**, *104*, 6147.
- (147) Ovitt, T. M.; Coates, G. W. *J. Am. Chem. Soc.* **2002**, *124*, 1316.
- (148) Zell, M. T.; Padden, B. E.; Paterick, A. J.; Thakur, K. A. M.; Kean, R. T.; Hillmyer, M. A.; Munson, E. J. *Macromolecules* **2002**, *35*, 7700.
- (149) Chabot, F.; Vert, M.; Chapelle, S.; Granger, P. *Polymer* **1983**, *24*, 53.
- (150) Castillo, J. A.; Borchmann, D. E.; Cheng, A. Y.; Wang, Y. F.; Hu, C.; Garcia, A. J.; Weck, M. *Macromolecules* **2012**, *45*, 62.
- (151) Coulembier, O.; Lemaury, V.; Josse, T.; Minoia, A.; Cornil, J.; Dubois, P. *Chem. Sci.* **2012**, *3*, 723.
- (152) Culkin, D. A.; Jeong, W. H.; Csihony, S.; Gomez, E. D.; Balsara, N. R.; Hedrick, J. L.; Waymouth, R. M. *Angew. Chem. Int. Ed.* **2007**, *46*, 2627.

- (153) Dove, A. P.; Li, H. B.; Pratt, R. C.; Lohmeijer, B. G. G.; Culkin, D. A.; Waymouth, R. M.; Hedrick, J. L. *Chem. Commun.* **2006**, 2881.
- (154) Kakuchi, R.; Tsuji, Y.; Chiba, K.; Fuchise, K.; Sakai, R.; Satoh, T.; Kakuchi, T. *Macromolecules* **2010**, *43*, 7090.
- (155) Kakwere, H.; Perrier, S. *J. Polym. Sci. A Polym. Chem.* **2009**, *47*, 6396.
- (156) Kamber, N. E.; Jeong, W.; Waymouth, R. M.; Pratt, R. C.; Lohmeijer, B. G. G.; Hedrick, J. L. *Chem. Rev.* **2007**, *107*, 5813.
- (157) Koeller, S.; Kadota, J.; Deffieux, A.; Peruch, F.; Massip, S.; Leger, J. M.; Desvergne, J. P.; Bibal, B. *J. Am. Chem. Soc.* **2009**, *131*, 15088.
- (158) Makiguchi, K.; Satoh, T.; Kakuchi, T. *J. Polym. Sci. A Polym. Chem.* **2011**, *49*, 3769.
- (159) Makiguchi, K.; Satoh, T.; Kakuchi, T. *Macromolecules* **2011**, *44*, 1999.
- (160) Miyake, G. M.; Chen, E. Y. X. *Macromolecules* **2011**, *44*, 4116.
- (161) Pratt, R. C.; Lohmeijer, B. G. G.; Long, D. A.; Lundberg, P. N. P.; Dove, A. P.; Li, H. B.; Wade, C. G.; Waymouth, R. M.; Hedrick, J. L. *Macromolecules* **2006**, *39*, 7863.
- (162) Pratt, R. C.; Lohmeijer, B. G. G.; Long, D. A.; Waymouth, R. M.; Hedrick, J. L. *J. Am. Chem. Soc.* **2006**, *128*, 4556.
- (163) Qian, H. T.; Wohl, A. R.; Crow, J. T.; Macosko, C. W.; Hoye, T. R. *Macromolecules* **2011**, *44*, 7132.
- (164) Sen, T. K.; Sau, S. C.; Mukherjee, A.; Modak, A.; Mandal, S. K.; Koley, D. *Chem. Commun.* **2011**, *47*, 11972.
- (165) Zhang, L.; Nederberg, F.; Pratt, R. C.; Waymouth, R. M.; Hedrick, J. L.; Wade, C. G. *Macromolecules* **2007**, *40*, 4154.
- (166) Chivers, T.; Konu, J. *Comments Inorg. Chem.* **2009**, *30*, 131.
- (167) Williams, C. K. *Chem. Soc. Rev.* **2007**, *36*, 1573.
- (168) Hoogenboom, R.; Schubert, U. S. *Chem. Soc. Rev.* **2006**, *35*, 622.
- (169) Dijkstra, P. J.; Du, H. Z.; Feijen, J. *Polym. Chem.* **2011**, *2*, 520.
- (170) Buffet, J. C.; Okuda, J. *Polym. Chem.* **2011**, *2*, 2758.
- (171) Thomas, C. M. *Chem. Soc. Rev.* **2010**, *39*, 165.
- (172) Stanford, M. J.; Dove, A. P. *Chem. Soc. Rev.* **2010**, *39*, 486.
- (173) O'Keefe, B. J.; Hillmyer, M. A.; Tolman, W. B. *J. Chem. Soc., Dalton Tras.* **2001**, 2215.
- (174) Sutar, A. K.; Maharana, T.; Dutta, S.; Chen, C. T.; Lin, C. C. *Chem. Soc. Rev.* **2010**, *39*, 1724.
- (175) Lu, W. Y.; Hsiao, M. W.; Hsu, S. C. N.; Peng, W. T.; Chang, Y. J.; Tsou, Y. C.; Wu, T. Y.; Lai, Y. C.; Chen, Y.; Chen, H. Y. *Dalton Trans.* **2012**, *41*, 3659.
- (176) Huang, Y.; Tsai, Y. H.; Hung, W. C.; Lin, C. S.; Wang, W.; Huang, J. H.; Dutta, S.; Lin, C. C. *Inorg. Chem.* **2010**, *49*, 9416.
- (177) Yu, T. L.; Huang, B. H.; Hung, W. C.; Lin, C. C.; Wang, T. C.; Ho, R. M. *Polymer* **2007**, *48*, 4401.
- (178) Huang, C. A.; Chen, C. T. *Dalton Trans.* **2007**, 5561.
- (179) Hsueh, M. L.; Huang, B. H.; Wu, J. C.; Lin, C. C. *Macromolecules* **2005**, *38*, 9482.
- (180) Ko, B. T.; Lin, C. C. *J. Am. Chem. Soc.* **2001**, *123*, 7973.
- (181) Cushion, M. G.; Mountford, P. *Chem. Commun.* **2011**, *47*, 2276.
- (182) Sarazin, Y.; Liu, B.; Roisnel, T.; Maron, L.; Carpentier, J. F. *J. Am. Chem. Soc.* **2011**, *133*, 9069.
- (183) Wheaton, C. A.; Hayes, P. G. *Catal. Sci. Tech.* **2012**, *2*, 125.

- (184) Sung, C. Y.; Li, C. Y.; Su, J. K.; Chen, T. Y.; Lin, C. H.; Ko, B. T. *Dalton Trans.* **2012**, 41, 953.
- (185) Song, S. D.; Zhang, X. Y.; Ma, H. Y.; Yang, Y. *Dalton Trans.* **2012**, 41, 3266.
- (186) Sun, H. S.; Ritch, J. S.; Hayes, P. G. *Inorg. Chem.* **2011**, 50, 8063.
- (187) Ma, W. A.; Wang, Z. X. *Organometallics* **2011**, 30, 4364.
- (188) Grala, A.; Ejfler, J.; Jerzykiewicz, L. B.; Sobota, P. *Dalton Trans.* **2011**, 40, 4042.
- (189) Chuang, H. J.; Weng, S. F.; Chang, C. C.; Lin, C. C.; Chen, H. Y. *Dalton Trans.* **2011**, 40, 9601.
- (190) Chen, H. Y.; Peng, Y. L.; Huang, T. H.; Sutar, A. K.; Miller, S. A.; Lin, C. C. *J. Mol. Catal. A: Chem.* **2011**, 339, 61.
- (191) Borner, J.; Vieira, I. D.; Pawlis, A.; Doring, A.; Kuckling, D.; Herres-Pawlis, S. *Chem. Eur. J.* **2011**, 17, 4507.
- (192) Wheaton, C. A.; Hayes, P. G. *Chem. Commun.* **2010**, 46, 8404.
- (193) Wang, L. Y.; Ma, H. Y. *Dalton Trans.* **2010**, 39, 7897.
- (194) Wang, L. Y.; Ma, H. Y. *Macromolecules* **2010**, 43, 6535.
- (195) Ng, J. J.; Durr, C. B.; Lance, J. M.; Bunge, S. D. *Eur. J. Inorg. Chem.* **2010**, 1424.
- (196) Liu, Z. Z.; Gao, W.; Zhang, J. S.; Cui, D. M.; Wu, Q. L.; Mu, Y. *Organometallics* **2010**, 29, 5783.
- (197) Drouin, F.; Oguadinma, P. O.; Whitehorne, T. J. J.; Prud'homme, R. E.; Schaper, F. *Organometallics* **2010**, 29, 2139.
- (198) Di Iulio, C.; Jones, M. D.; Mahon, M. F.; Apperley, D. C. *Inorg. Chem.* **2010**, 49, 10232.
- (199) Darensbourg, D. J.; Karroonnirun, O. *Macromolecules* **2010**, 43, 8880.
- (200) Wheaton, C. A.; Ireland, B. J.; Hayes, P. G. *Organometallics* **2009**, 28, 1282.
- (201) Tsai, Y. H.; Lin, C. H.; Lin, C. C.; Ko, B. T. *J. Polym. Sci. A Polym. Chem.* **2009**, 47, 4927.
- (202) Shen, M. Y.; Peng, Y. L.; Hung, W. C.; Lin, C. C. *Dalton Trans.* **2009**, 9906.
- (203) Labourdette, G.; Lee, D. J.; Patrick, B. O.; Ezhova, M. B.; Mehrkhodavandi, P. *Organometallics* **2009**, 28, 1309.
- (204) Grunova, E.; Roisnel, T.; Carpentier, J. F. *Dalton Trans.* **2009**, 9010.
- (205) Chen, M. T.; Chang, P. J.; Huang, C. A.; Peng, K. F.; Chen, C. T. *Dalton Trans.* **2009**, 9068.
- (206) Arnold, P. L.; Casely, I. J.; Turner, Z. R.; Bellabarba, R.; Tooze, R. B. *Dalton Trans.* **2009**, 7236.
- (207) Wu, J. C.; Chen, Y. Z.; Hung, W. C.; Lin, C. C. *Organometallics* **2008**, 27, 4970.
- (208) Ejfler, J.; Szafert, S.; Mierzwicki, K.; Jerzykiewicz, L. B.; Sobota, P. *Dalton Trans.* **2008**, 6556.
- (209) Tang, H. Y.; Chen, H. Y.; Huang, J. H.; Lin, C. C. *Macromolecules* **2007**, 40, 8855.
- (210) Lian, B.; Thomas, C. M.; Casagrande, O. L.; Lehmann, C. W.; Roisnel, T.; Carpentier, J. F. *Inorg. Chem.* **2007**, 46, 328.
- (211) Chisholm, M. H.; Gallucci, J. C.; Phomphrai, K. *Inorg. Chem.* **2005**, 44, 8004.
- (212) Chisholm, M. H.; Lin, C. C.; Gallucci, J. C.; Ko, B. T. *Dalton Trans.* **2003**, 406.
- (213) Chisholm, M. H.; Gallucci, J.; Phomphrai, K. *Chem. Commun.* **2003**, 48.
- (214) Chamberlain, B. M.; Cheng, M.; Moore, D. R.; Ovitt, T. M.; Lobkovsky, E. B.; Coates, G. W. *J. Am. Chem. Soc.* **2001**, 123, 3229.

- (215) Matsubara, K.; Terata, C.; Sekine, H.; Yamatani, K.; Harada, T.; Eda, K.; Dan, M.; Koga, Y.; Yasuniwa, M. *J. Polym. Sci. A Polym. Chem.* **2012**, *50*, 957.
- (216) Chen, H. L.; Dutta, S.; Huang, P. Y.; Lin, C. C. *Organometallics* **2012**, *31*, 2016.
- (217) Whitelaw, E. L.; Loraine, G.; Mahon, M. F.; Jones, M. D. *Dalton Trans.* **2011**, *40*, 11469.
- (218) Qian, F.; Liu, K. Y.; Ma, H. Y. *Chin. J. Catal.* **2011**, *32*, 189.
- (219) Otero, A.; Lara-Sanchez, A.; Fernandez-Baeza, J.; Alonso-Moreno, C.; Castro-Osma, J. A.; Marquez-Segovia, I.; Sanchez-Barba, L. F.; Rodriguez, A. M.; Garcia-Martinez, J. C. *Organometallics* **2011**, *30*, 1507.
- (220) Li, C. Y.; Tsai, C. Y.; Lin, C. H.; Ko, B. T. *Dalton Trans.* **2011**, *40*, 1880.
- (221) Darensbourg, D. J.; Karroonnirun, O.; Wilson, S. J. *Inorg. Chem.* **2011**, *50*, 6775.
- (222) Thibault, M. H.; Fontaine, F. G. *Dalton Trans.* **2010**, *39*, 5688.
- (223) Silvestri, A.; Grisi, F.; Milione, S. *J. Polym. Sci. A Polym. Chem.* **2010**, *48*, 3632.
- (224) Schwarz, A. D.; Chu, Z. Y.; Mountford, P. *Organometallics* **2010**, *29*, 1246.
- (225) Qian, F.; Liu, K. Y.; Ma, H. Y. *Dalton Trans.* **2010**, *39*, 8071.
- (226) Phomphrai, K.; Chumsaeng, P.; Sangtrirutnugul, P.; Kongsaree, P.; Pohmakotr, M. *Dalton Trans.* **2010**, *39*, 1865.
- (227) Hild, F.; Haquette, P.; Brelot, L.; Dagorne, S. *Dalton Trans.* **2010**, *39*, 533.
- (228) Bouyahyi, M.; Roisnel, T.; Carpentier, J. F. *Organometallics* **2010**, *29*, 491.
- (229) Du, H. Z.; Velders, A. H.; Dijkstra, P. J.; Sun, J. R.; Zhong, Z. Y.; Chen, X. S.; Feijen, J. *Chem. Eur. J.* **2009**, *15*, 9836.
- (230) Chisholm, M. H.; Gallucci, J. C.; Quisenberry, K. T.; Zhou, Z. P. *Inorg. Chem.* **2008**, *47*, 2613.
- (231) Bouyahyi, M.; Grunova, E.; Marquet, N.; Kirillov, E.; Thomas, C. M.; Roisnel, T.; Carpentier, J. F. *Organometallics* **2008**, *27*, 5815.
- (232) Nomura, N.; Ishii, R.; Yamamoto, Y.; Kondo, T. *Chem. Eur. J.* **2007**, *13*, 4433.
- (233) Du, H. Z.; Pang, X.; Yu, H. Y.; Zhuang, X. L.; Chen, X. S.; Cui, D. M.; Wang, X. H.; Jing, X. B. *Macromolecules* **2007**, *40*, 1904.
- (234) Chisholm, M. H.; Patmore, N. J.; Zhou, Z. P. *Chem. Commun.* **2005**, 127.
- (235) Amgoune, A.; Lavanant, L.; Thomas, C. M.; Chi, Y.; Welter, R.; Dagorne, S.; Carpentier, J. F. *Organometallics* **2005**, *24*, 6279.
- (236) Tang, Z. H.; Chen, X. S.; Yang, Y. K.; Pang, X.; Sun, J. R.; Zhang, X. F.; Jing, X. B. *J. Polym. Sci. A Polym. Chem.* **2004**, *42*, 5974.
- (237) Ishii, R.; Nomura, N.; Kondo, T. *Polym. J.* **2004**, *36*, 261.
- (238) Horeglad, P.; Kruk, P.; Pecaut, J. *Organometallics* **2010**, *29*, 3729.
- (239) Chmura, A. J.; Chuck, C. J.; Davidson, M. G.; Jones, M. D.; Lunn, M. D.; Bull, S. D.; Mahon, M. F. *Angew. Chem. Int. Ed.* **2007**, *46*, 2280.
- (240) Nimitsiriwat, N.; Gibson, V. C.; Marshall, E. L.; Elsegood, M. R. J. *Dalton Trans.* **2009**, 3710.
- (241) Nimitsiriwat, N.; Gibson, V. C.; Marshall, E. L.; Elsegood, M. R. J. *Inorg. Chem.* **2008**, *47*, 5417.
- (242) Dove, A. P.; Gibson, V. C.; Marshall, E. L.; Rzepa, H. S.; White, A. J. P.; Williams, D. J. *J. Am. Chem. Soc.* **2006**, *128*, 9834.
- (243) Kowalski, A.; Libiszowski, J.; Biela, T.; Cypriak, M.; Duda, A.; Penczek, S. *Macromolecules* **2005**, *38*, 8170.

- (244) Nimitsiriwat, N.; Marshall, E. L.; Gibson, V. C.; Elsegood, M. R. J.; Dale, S. H. *J. Am. Chem. Soc.* **2004**, *126*, 13598.
- (245) Lahcini, M.; Castro, P. M.; Kalmi, M.; Leskela, M.; Repo, T. *Organometallics* **2004**, *23*, 4547.
- (246) Chisholm, M. H.; Delbridge, E. E.; Gallucci, J. C. *New J. Chem.* **2004**, *28*, 145.
- (247) Dove, A. P.; Gibson, V. C.; Marshall, E. L.; White, A. J. P.; Williams, D. J. *Chem. Commun.* **2001**, 283.
- (248) Kricheldorf, H. R. *Chem. Rev.* **2009**, *109*, 5579.
- (249) Gorczynski, J. L.; Chen, J. B.; Fraser, C. L. *J. Am. Chem. Soc.* **2005**, *127*, 14956.
- (250) McGuinness, D. S.; Marshall, E. L.; Gibson, V. C.; Steed, J. W. *J. Polym. Sci. A Polym. Chem.* **2003**, *41*, 3798.
- (251) O'Keefe, B. J.; Breyfogle, L. E.; Hillmyer, M. A.; Tolman, W. B. *J. Am. Chem. Soc.* **2002**, *124*, 4384.
- (252) Gibson, V. C.; Marshall, E. L.; Navarro-Llobet, D.; White, A. J. P.; Williams, D. J. *J. Chem. Soc., Dalton Tras.* **2002**, 4321.
- (253) Dobrzynski, P.; Kasperczyk, J.; Janeczek, H.; Bero, M. *Polymer* **2002**, *43*, 2595.
- (254) Stolt, M.; Sodergard, A. *Macromolecules* **1999**, *32*, 6412.
- (255) Stopper, A.; Okuda, J.; Kol, M. *Macromolecules* **2012**, *45*, 698.
- (256) Jeffery, B. J.; Whitelaw, E. L.; Garcia-Vivo, D.; Stewart, J. A.; Mahon, M. F.; Davidson, M. G.; Jones, M. D. *Chem. Commun.* **2011**, *47*, 12328.
- (257) Buffet, J.-C.; Okuda, J. *Chem. Commun.* **2011**, *47*, 4796.
- (258) Whitelaw, E. L.; Jones, M. D.; Mahon, M. F. *Inorg. Chem.* **2010**, *49*, 7176.
- (259) Schwarz, A. D.; Herbert, K. R.; Paniagua, C.; Mountford, P. *Organometallics* **2010**, *29*, 4171.
- (260) Saha, T. K.; Rajashekhar, B.; Gowda, R. R.; Ramkumar, V.; Chakraborty, D. *Dalton Trans.* **2010**, *39*, 5091.
- (261) Zelikoff, A. L.; Kopilov, J.; Goldberg, I.; Coates, G. W.; Kol, M. *Chem. Commun.* **2009**, 6804.
- (262) Ning, Y.; Zhang, Y.; Rodriguez-Delgado, A.; Chen, E. Y. X. *Organometallics* **2008**, *27*, 5632.
- (263) Chmura, A. J.; Davidson, M. G.; Frankis, C. J.; Jones, M. D.; Lunn, M. D. *Chem. Commun.* **2008**, 6611.
- (264) Chmura, A. J.; Davidson, M. G.; Frankis, C. J.; Jones, M. D.; Lunn, M. D. *Chem. Commun.* **2008**, 1293.
- (265) Gornshtein, F.; Kapon, M.; Botoshansky, M.; Eisen, M. S. *Organometallics* **2007**, *26*, 497.
- (266) Atkinson, R. C. J.; Gerry, K.; Gibson, V. C.; Long, N. J.; Marshall, E. L.; West, L. J. *Organometallics* **2007**, *26*, 316.
- (267) Chmura, A. J.; Davidson, M. G.; Jones, M. D.; Lunn, M. D.; Mahon, M. F.; Johnson, A. F.; Khunkamchoo, P.; Roberts, S. L.; Wong, S. S. F. *Macromolecules* **2006**, *39*, 7250.
- (268) Amgoune, A.; Thomas, C. M.; Roisnel, T.; Carpentier, J. F. *Chem. Eur. J.* **2006**, *12*, 169.
- (269) Otero, A.; Fernandez-Baeza, J.; Lara-Sanchez, A.; Alonso-Moreno, C.; Marquez-Segovia, I.; Sanchez-Barba, L. F.; Rodriguez, A. M. *Angew. Chem. Int. Ed.* **2009**, *48*, 2176.

- (270) Platel, R. H.; White, A. J. P.; Williams, C. K. *Inorg. Chem.* **2011**, *50*, 7718.
- (271) Wong, A. W.; Miller, K. L.; Diaconescu, P. L. *Dalton Trans.* **2010**, *39*, 6726.
- (272) Diaconescu, P. L. *Comments Inorg. Chem.* **2010**, *31*, 196.
- (273) Platel, R. H.; White, A. J. P.; Williams, C. K. *Chem. Commun.* **2009**, 4115.
- (274) Stanlake, L. J. E.; Beard, J. D.; Schafer, L. L. *Inorg. Chem.* **2008**, *47*, 8062.
- (275) Platel, R. H.; White, A. J. P.; Williams, C. K. *Inorg. Chem.* **2008**, *47*, 6840.
- (276) Hodgson, L. M.; Platel, R. H.; White, A. J. P.; Williams, C. K. *Macromolecules* **2008**, *41*, 8603.
- (277) Carver, C. T.; Monreal, M. J.; Diaconescu, P. L. *Organometallics* **2008**, *27*, 363.
- (278) Platel, R. H.; Hodgson, L. M.; White, A. J. P.; Williams, C. K. *Organometallics* **2007**, *26*, 4955.
- (279) Wheaton, C. A.; Hayes, P. G.; Ireland, B. J. *Dalton Trans.* **2009**, 4832.
- (280) Kohn, F. E.; Vanommen, J. G.; Feijen, J. *Eur. Polym. J.* **1983**, *19*, 1081.
- (281) Kricheldorf, H. R.; Berl, M.; Scharnagl, N. *Macromolecules* **1988**, *21*, 286.
- (282) Dubois, P.; Jacobs, C.; Jerome, R.; Teyssie, P. *Macromolecules* **1991**, *24*, 2266.
- (283) O'Keefe, B. J.; Monnier, S. M.; Hillmyer, M. A.; Tolman, W. B. *J. Am. Chem. Soc.* **2001**, *123*, 339.
- (284) Williams, C. K.; Brooks, N. R.; Hillmyer, M. A.; Tolman, W. B. *Chem. Commun.* **2002**, 2132.
- (285) Ma, H. Y.; Spaniol, T. P.; Okuda, J. *Angew. Chem. Int. Ed.* **2006**, *45*, 7818.
- (286) Duda, A.; Penczek, S. *Makromol. Chem., Macromol. Symp.* **1991**, *47*, 127.
- (287) Ma, H. Y.; Okuda, J. *Macromolecules* **2005**, *38*, 2665.
- (288) Hormnirun, P.; Marshall, E. L.; Gibson, V. C.; Pugh, R. I.; White, A. J. P. *Proc. Natl. Acad. Sci. U. S. A.* **2006**, *103*, 15343.
- (289) Natta, G.; Pino, P.; Corradini, P.; Danusso, F.; Mantica, E.; Mazzanti, G.; Moraglio, G. *J. Am. Chem. Soc.* **1955**, *77*, 1708.
- (290) Bovey, F. A.; Mirau, P. A. *NMR of polymers*; Academic Press, Inc.: San Diego, 1996.
- (291) footnote LA activation parameters with k vs. kobs.
- (292) Girard, C.; Kagan, H. B. *Angew. Chem. Int. Ed.* **1998**, *37*, 2923.
- (293) footnote Provisional patent.
- (294) Bochmann, M.; Dawson, D. M. *Angew. Chem. Int. Ed. Engl.* **1996**, *35*, 2226.
- (295) Coles, M. P.; Jordan, R. F. *J. Am. Chem. Soc.* **1997**, *119*, 8125.
- (296) Bruce, M.; Gibson, V. C.; Redshaw, C.; Solan, G. A.; White, A. J. P.; Williams, D. J. *Chem. Commun.* **1998**, 2523.
- (297) Atwood, D. A.; Jegier, J. A.; Rutherford, D. *J. Am. Chem. Soc.* **1995**, *117*, 6779.
- (298) Jegier, J. A.; Atwood, D. A. *Inorg. Chem.* **1997**, *36*, 2034.
- (299) Emig, N.; Nguyen, H.; Krautscheid, H.; Reau, R.; Cazaux, J. B.; Bertrand, G. *Organometallics* **1998**, *17*, 3599.
- (300) Korolev, A. V.; Ihara, E.; Guzei, I. A.; Young, V. G.; Jordan, R. F. *J. Am. Chem. Soc.* **2001**, *123*, 8291.
- (301) Korolev, A. V.; Guzei, I. A.; Jordan, R. F. *J. Am. Chem. Soc.* **1999**, *121*, 11605.
- (302) Baugh, L. S.; Sissano, J. A. *J. Polym. Sci. A Polym. Chem.* **2002**, *40*, 1633.
- (303) Dagonne, S.; Lavanant, L.; Welter, R.; Chassenieux, C.; Haquette, P.; Jaouen, G. *Organometallics* **2003**, *22*, 3732.
- (304) Bunn, N. R.; Aldridge, S.; Kays, D. L.; Coombs, N. D.; Rossin, A.; Willock, D. J.; Day, J. K.; Jones, C.; Ooi, L. L. *Organometallics* **2005**, *24*, 5891.

- (305) Cowley, A. H.; Macdonald, C. L. B.; Silverman, J. S.; Gorden, J. D.; Voigt, A. *Chem. Commun.* **2001**, 175.
- (306) Jones, J. N.; Macdonald, C. L. B.; Gorden, J. D.; Cowley, A. H. *J. Organomet. Chem.* **2003**, 666, 3.
- (307) Peckermann, I.; Dols, T. S.; Spaniol, T. P.; Okuda, J. *J. Organomet. Chem.* **2010**, 695, 2325.
- (308) Robson, D. A.; Bylikin, S. Y.; Cantuel, M.; Male, N. A. H.; Rees, L. H.; Mountford, P.; Schroder, M. *J. Chem. Soc., Dalton Tras.* **2001**, 157.
- (309) Peckermann, I.; Robert, D.; Englert, U.; Spaniol, T. P.; Okuda, J. *Organometallics* **2008**, 27, 4817.
- (310) Sigl, M.; Schier, A.; Schmidbaur, H. *Eur. J. Inorg. Chem.* **1998**, 203.
- (311) Chamazi, N. N.; Heravi, M. M.; Breyhan, T.; Neumuller, B. *Z. Anorg. Allg. Chem.* **2007**, 633, 1243.
- (312) Guzei, I. A.; Dagorne, S.; Jordan, R. F. *Acta Crystallogr., Sect. C, Cryst. Struct. Commun.* **2001**, 57, 143.
- (313) Uhl, W.; Emden, C. H.; Geiseler, G.; Harms, K. *Z. Anorg. Allg. Chem.* **2003**, 629, 2157.
- (314) Delpech, F.; Guzei, I. A.; Jordan, R. F. *Organometallics* **2002**, 21, 1167.
- (315) Yang, X. M.; Stern, C. L.; Marks, T. J. *Organometallics* **1991**, 10, 840.
- (316) Horton, A. D.; Orpen, A. G. *Organometallics* **1991**, 10, 3910.
- (317) Kamigaito, M.; Satoh, K. *Macromolecules* **2008**, 41, 269.
- (318) Matyjaszewski, K. *Isr. J. Chem.*, 52, 206.
- (319) Tsarevsky, N. V.; Braunecker, W. A.; Matyjaszewski, K. *J. Organomet. Chem.* **2007**, 692, 3212.
- (320) Hu, Y. J.; Gustafson, L. O.; Zhu, H. P.; Chen, E. Y. X. *J. Polym. Sci. A Polym. Chem.*, 49, 2008.
- (321) Lu, J. M.; Huang, Z. B.; Han, B. Y.; Wu, Y. X.; Yang, W. T. *J. Appl. Polym. Sci.*, 125, 2085.
- (322) Vlcek, P.; Cadova, E.; Kriz, J.; Latalova, P.; Janata, M.; Toman, L.; Masar, B. *Polymer* **2005**, 46, 4991.
- (323) Chen, E. Y. X. *Chem. Rev.* **2009**, 109, 5157.
- (324) Ute, K.; Miyatake, N.; Hatada, K. *Polymer* **1995**, 36, 1415.
- (325) Ute, K.; Yamasaki, Y.; Naito, M.; Miyatake, N.; Hatada, K. *Polym. J.* **1995**, 27, 951.
- (326) Jin, J. Z.; Mariott, W. R.; Chen, E. Y. X. *J. Polym. Sci. A Polym. Chem.* **2003**, 41, 3132.
- (327) Escude, N. C.; Chen, E. Y. X. *Chem. Mater.* **2009**, 21, 5743.
- (328) Ning, Y.; Chen, E. Y. X. *J. Am. Chem. Soc.* **2008**, 130, 2463.
- (329) Ning, Y. L.; Chen, E. Y. X. *Macromolecules* **2006**, 39, 7204.
- (330) Ning, Y. L.; Cooney, M. J.; Chen, E. Y. X. *J. Organomet. Chem.* **2005**, 690, 6263.
- (331) Yasuda, H. *J. Polym. Sci. A Polym. Chem.* **2001**, 39, 1955.
- (332) Chen, Y. X.; Metz, M. V.; Li, L. T.; Stern, C. L.; Marks, T. J. *J. Am. Chem. Soc.* **1998**, 120, 6287.
- (333) Bolig, A. D.; Chen, E. Y. X. *J. Am. Chem. Soc.* **2001**, 123, 7943.
- (334) Frauenrath, H.; Keul, H.; Hocker, H. *Macromolecules* **2001**, 34, 14.
- (335) Bandermann, F.; Ferenz, M.; Sustmann, R.; Sicking, W. *Macromol. Symp.* **2001**, 174, 247.

- (336) Cameron, P. A.; Gibson, V. C.; Graham, A. J. *Macromolecules* **2000**, *33*, 4329.
- (337) Nguyen, H.; Jarvis, A. P.; Lesley, M. J. G.; Kelly, W. M.; Reddy, S. S.; Taylor, N. J.; Collins, S. *Macromolecules* **2000**, *33*, 1508.
- (338) Li, Y. F.; Ward, D. G.; Reddy, S. S.; Collins, S. *Macromolecules* **1997**, *30*, 1875.
- (339) Deng, H.; Shiono, T.; Soga, K. *Macromolecules* **1995**, *28*, 3067.
- (340) Collins, S.; Ward, D. G. *J. Am. Chem. Soc.* **1992**, *114*, 5460.
- (341) Collins, S.; Ward, D. G.; Suddaby, K. H. *Macromolecules* **1994**, *27*, 7222.
- (342) Yasuda, H.; Yamamoto, H.; Yokota, K.; Miyake, S.; Nakamura, A. *J. Am. Chem. Soc.* **1992**, *114*, 4908.
- (343) Bolig, A. D.; Chen, E. Y. X. *J. Am. Chem. Soc.* **2004**, *126*, 4897.
- (344) Rodriguez-Delgado, A.; Chen, E. Y. X. *Macromolecules* **2005**, *38*, 2587.
- (345) Chen, X.; Caporaso, L.; Cavallo, L.; Chen, E. Y. X. *J. Am. Chem. Soc.*, *134*, 7278.
- (346) Hu, Y. J.; Miyake, G. M.; Wang, B. L.; Cui, D. M.; Chen, E. Y. X. *Chem. Eur. J.*, *18*, 3345.
- (347) Cosledan, F.; Hitchcock, P. B.; Lappert, M. F. *Chem. Commun.* **1999**, 705.
- (348) Dagorne, S.; Guzei, I. A.; Coles, M. P.; Jordan, R. F. *J. Am. Chem. Soc.* **2000**, *122*, 274.
- (349) Kuroki, M.; Aida, T.; Inoue, S. *J. Am. Chem. Soc.* **1987**, *109*, 4737.
- (350) Cameron, P. A.; Gibson, V. C.; Irvine, D. J. *Angew. Chem. Int. Ed.* **2000**, *39*, 2141.
- (351) Kuroki, M.; Watanabe, T.; Aida, T.; Inoue, S. *J. Am. Chem. Soc.* **1991**, *113*, 5903.
- (352) Sugimoto, H.; Kuroki, M.; Watanabe, T.; Kawamura, C.; Aida, T.; Inoue, S. *Macromolecules* **1993**, *26*, 3403.
- (353) Zhou, Y. L.; Richeson, D. S. *Organometallics* **1995**, *14*, 3558.
- (354) Beachley, O. T.; Rusinko, R. N. *Inorg. Chem.* **1979**, *18*, 1966.
- (355) Leman, J. T.; Roman, H. A.; Barron, A. R. *Organometallics* **1993**, *12*, 2986.
- (356) Blaschette, A.; Michalides, A.; Jones, P. G. *J. Organomet. Chem.* **1991**, *411*, 57.
- (357) Strauss, S. H. *Chem. Rev.* **1993**, *93*, 927.
- (358) Hirai, K.; Itoh, T.; Tomioka, H. *Chem. Rev.* **2009**, *109*, 3275.
- (359) Kirmse, W. *Angew. Chem. Int. Ed.* **2003**, *42*, 2117.
- (360) Tomioka, H. *Acc. Chem. Res.* **1997**, *30*, 315.
- (361) Doering, W. V.; Hoffmann, A. K. *J. Am. Chem. Soc.* **1954**, *76*, 6162.
- (362) Breslow, R. *J. Am. Chem. Soc.* **1958**, *80*, 3719.
- (363) Schonher, H. j.; Wanzlick, H. W. *Liebigs Ann. Chem.* **1970**, *731*, 176.
- (364) Igau, A.; Grutzmacher, H.; Baceiredo, A.; Bertrand, G. *J. Am. Chem. Soc.* **1988**, *110*, 6463.
- (365) Arduengo, A. J.; Harlow, R. L.; Kline, M. *J. Am. Chem. Soc.* **1991**, *113*, 361.
- (366) Vyboishchikov, S. E.; Frenking, G. *Chem. Eur. J.* **1998**, *4*, 1439.
- (367) Vyboishchikov, S. F.; Frenking, G. *Chem. Eur. J.* **1998**, *4*, 1428.
- (368) Fischer, E. O.; Maasbol, A. *Angew. Chem. Int. Ed.* **1964**, *3*, 580.
- (369) Taylor, T. E.; Hall, M. B. *J. Am. Chem. Soc.* **1984**, *106*, 1576.
- (370) Harrison, J. F. *J. Am. Chem. Soc.* **1971**, *93*, 4112.
- (371) Harrison, J. F.; Liedtke, R. C.; Liebman, J. F. *J. Am. Chem. Soc.* **1979**, *101*, 7162.
- (372) Pauling, L. *J. Chem. Soc., Chem. Commun.* **1980**, 688.
- (373) Irikura, K. K.; Goddard, W. A.; Beauchamp, J. L. *J. Am. Chem. Soc.* **1992**, *114*, 48.
- (374) Schoeller, W. W.; Eisner, D.; Grigoleit, S.; Rozhenko, A. B.; Alijah, A. *J. Am. Chem. Soc.* **2000**, *122*, 10115.

- (375) Schrock, R. R. *J. Am. Chem. Soc.* **1974**, *96*, 6796.
- (376) Schrock, R. R. *Acc. Chem. Res.* **1979**, *12*, 98.
- (377) Herrmann, W. A.; Ofele, K.; von Preysing, D.; Herdtweck, E. In *J Organomet Chem* 2003; Vol. 684, p 235.
- (378) Michelin, R. A.; Pombeiro, A. J. L.; Fatima, M.; da Silva, C. G. *Coord. Chem. Rev.* **2001**, *218*, 75.
- (379) Miller, J.; Balch, A. L.; Enemark, J. H. *J. Am. Chem. Soc.* **1971**, *93*, 4613.
- (380) Michelin, R. A.; Zanotto, L.; Braga, D.; Sabatino, P.; Angelici, R. J. *Inorg. Chem.* **1988**, *27*, 85.
- (381) Michelin, R. A.; Zanotto, L.; Braga, D.; Sabatino, P.; Angelici, R. J. *Inorg. Chem.* **1988**, *27*, 93.
- (382) Bonati, F.; Minghetti, G. *J. Organomet. Chem.* **1970**, *24*, 251.
- (383) Minghetti, G.; Bonati, F. *J. Organomet. Chem.* **1973**, *54*, C62.
- (384) Liu, C. Y.; Chen, D. Y.; Lee, G. H.; Peng, S. M.; Liu, S. T. *Organometallics* **1996**, *15*, 1055.
- (385) Wehlan, M.; Thiel, R.; Fuchs, J.; Beck, W.; Fehlhammer, W. P. *J. Organomet. Chem.* **2000**, *613*, 159.
- (386) Langenhahn, V.; Beck, G.; Zinner, G.; Lentz, D.; Herrschaft, B.; Fehlhammer, W. P. *J. Organomet. Chem.* **2007**, *692*, 2936.
- (387) Hahn, F. E.; Langenhahn, V.; Meier, N.; Lugger, T.; Fehlhammer, W. P. *Chem. Eur. J.* **2003**, *9*, 704.
- (388) Hahn, F. E.; Plumed, C. G.; Munder, M.; Lugger, T. *Chem. Eur. J.* **2004**, *10*, 6285.
- (389) Plaia, U.; Stolzenberg, H.; Fehlhammer, W. P. *J. Am. Chem. Soc.* **1985**, *107*, 2171.
- (390) Frankel, R.; Kernbach, U.; Bakola-Christianopoulou, M.; Plaia, U.; Suter, M.; Ponikwar, W.; Noth, H.; Moinet, C.; Fehlhammer, W. P. *J. Organomet. Chem.* **2001**, *617*, 530.
- (391) Castan, F.; Baceiredo, A.; Fischer, J.; Decian, A.; Commenges, G.; Bertrand, G. *J. Am. Chem. Soc.* **1991**, *113*, 8160.
- (392) Soleilhavoup, M.; Baceiredo, A.; Treutler, O.; Ahlrichs, R.; Nieger, M.; Bertrand, G. *J. Am. Chem. Soc.* **1992**, *114*, 10959.
- (393) Marrot, S.; Kato, T.; Cossio, F. P.; Gornitzka, H.; Baceiredo, A. *Angew. Chem. Int. Ed.* **2006**, *45*, 7447.
- (394) Frey, G. D.; Song, M.; Bourg, J.-B.; Donnadiou, B.; Soleilhavoup, M.; Bertrand, G. *Chem. Commun.* **2008**, 4711.
- (395) Sole, S.; Gornitzka, H.; Schoeller, W. W.; Bourissou, D.; Bertrand, G. *Science* **2001**, *292*, 1901.
- (396) Liu, C. Y.; Chen, D. Y.; Cheng, M. C.; Peng, S. M.; Liu, S. T. *Organometallics* **1995**, *14*, 1983.
- (397) Amgoune, A.; Thomas, C. M.; Carpentier, J. F. *Pure Appl. Chem.* **2007**, *79*, 2013.
- (398) Yam, V. W. W.; Chu, B. W. K.; Cheung, K. K. *Chem. Commun.* **1998**, 2261.
- (399) Alder, R. W.; Allen, P. R.; Murray, M.; Orpen, A. G. *Angew. Chem. Int. Ed. Engl.* **1996**, *35*, 1121.
- (400) Alder, R. W.; Blake, M. E. *Chem. Commun.* **1997**, 1513.
- (401) Arduengo, A. J.; Goerlich, J. R.; Marshall, W. J. *J. Am. Chem. Soc.* **1995**, *117*, 11027.
- (402) Ohki, Y.; Hatanaka, T.; Tatsumi, K. *J. Am. Chem. Soc.* **2008**, *130*, 17174.

- (403) Herrmann, W. A.; Ofele, K.; von Preysing, D.; Herdtweck, E. *J. Organomet. Chem.* **2003**, *684*, 235.
- (404) Motschi, H.; Angelici, R. *J. Organometallics* **1982**, *1*, 343.
- (405) Belluco, U.; Crociani, B.; Michelin, R.; Uguagliati, P. *Pure Appl. Chem.* **1983**, *55*, 47.
- (406) Belluco, U.; Michelin, R. A.; Uguagliati, P. *J. Organomet. Chem.* **1983**, *250*, 565.
- (407) Vignolle, J.; Donnadiou, B.; Bourissou, D.; Soleilhavoup, M.; Bertrand, G. *J. Am. Chem. Soc.* **2006**, *128*, 14810.
- (408) Schwarz, M.; Kickelbick, G.; Schubert, U. *Eur. J. Inorg. Chem.* **2000**, 1811.
- (409) Ku, R. Z.; Chen, D. Y.; Lee, G. H.; Peng, S. M.; Liu, S. T. *Angew. Chem. Int. Ed.* **1997**, *36*, 2631.
- (410) Despagnet, E.; Miqueu, K.; Gornitzka, H.; Dyer, P. W.; Bourissou, D.; Bertrand, G. *J. Am. Chem. Soc.* **2002**, *124*, 11834.
- (411) Yao, L.; Smith, B. T.; Aube, J. *J. Org. Chem.* **2004**, *69*, 1720.
- (412) Ashby, E. C.; Park, B.; Patil, G. S.; Gadru, K.; Gurumurthy, R. *J. Org. Chem.* **1993**, *58*, 424.
- (413) Gilman, H.; Wu, T. C. *J. Org. Chem.* **1953**, *18*, 753.
- (414) Jacobsen, E. J.; Stelzer, L. S.; Belonga, K. L.; Carter, D. B.; Im, W. B.; Sethy, V. H.; Tang, A. H.; VonVoigtlander, P. F.; Petke, J. D. *J. Med. Chem.* **1996**, *39*, 3820.
- (415) Li, Y. Z.; Li, Z. M.; Li, F.; Wang, Q. R.; Tao, F. G. *Tetrahedron Lett.* **2005**, *46*, 6159.

Appendices

Appendix A

A.1 Characterization of indium complexes

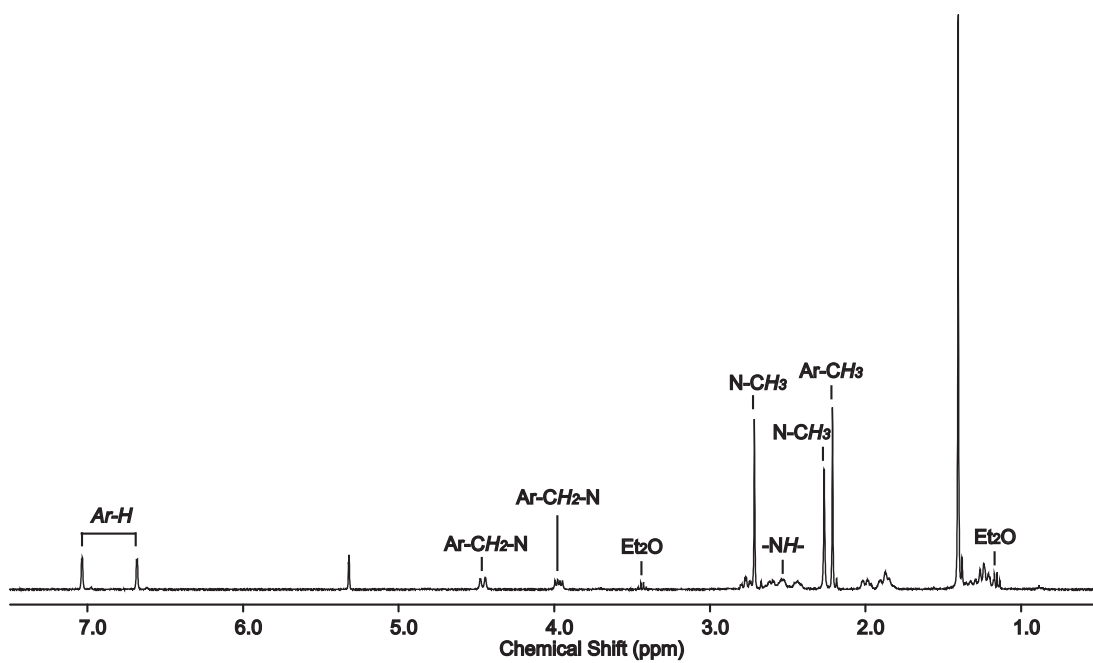


Figure A-1. ^1H NMR spectrum (400 MHz, CD_2Cl_2 , 25 °C) of $(\text{NNO}_{\text{Me}})\text{InCl}_2$ (**3**).

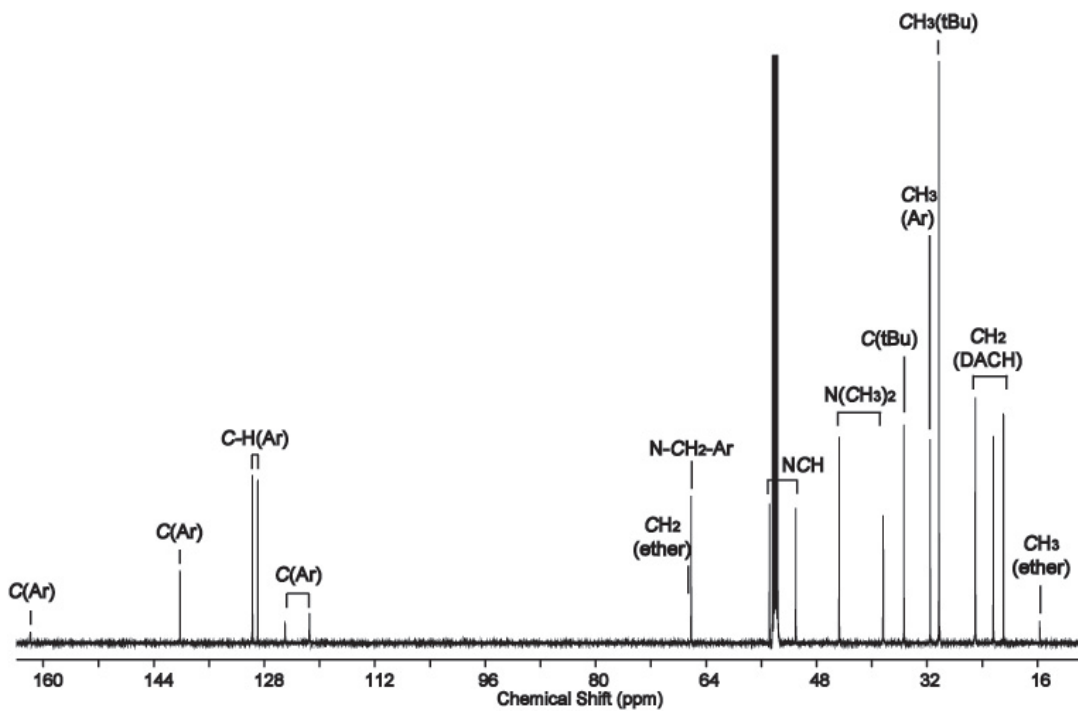


Figure A-2. $^{13}\text{C}\{^1\text{H}\}$ NMR spectrum (151 MHz, CD_2Cl_2 , 25 °C) of $(\text{NNO}_{\text{Me}})\text{InCl}_2$ (**3**).

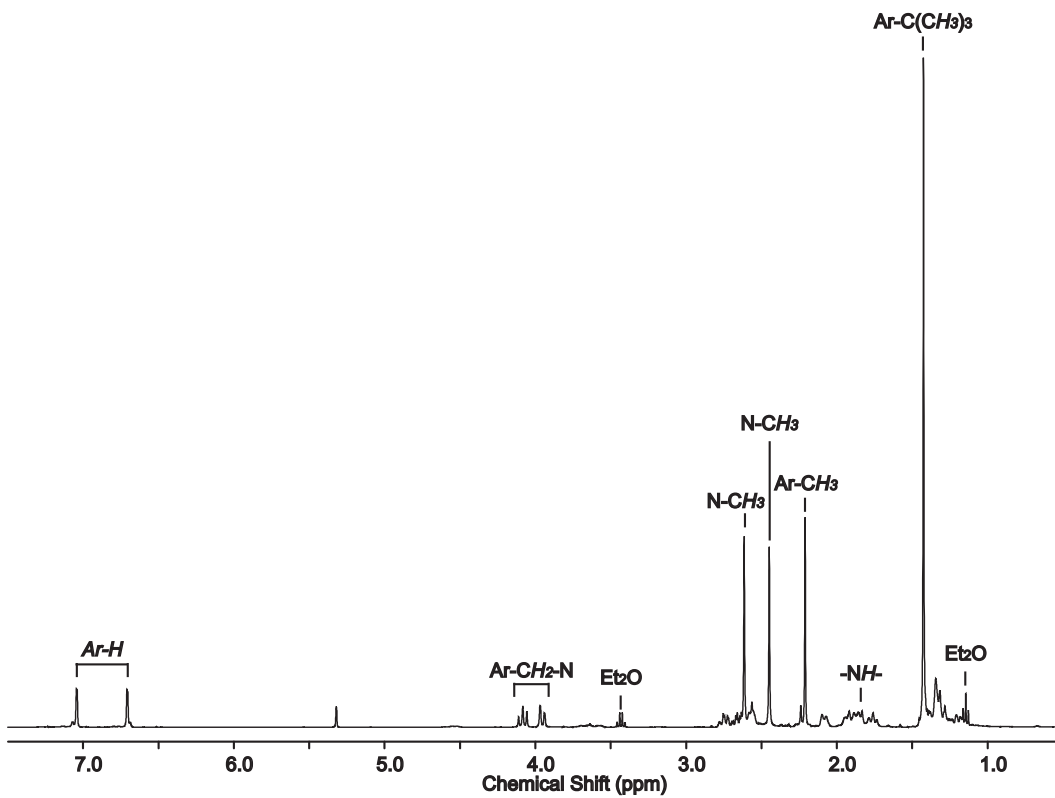


Figure A-3. ^1H NMR spectrum (400 MHz, CD_2Cl_2 , 25 °C) of $(\text{NNO}_{\text{Me}})\text{InI}_2$ (**4**).

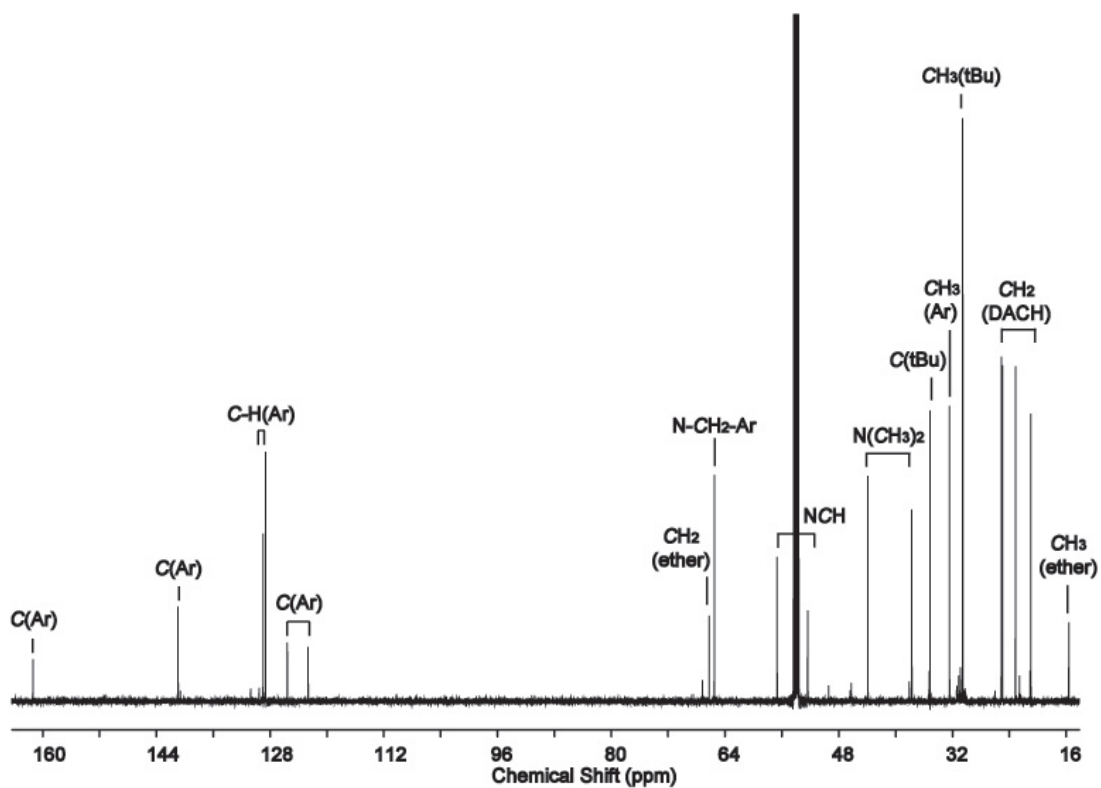


Figure A-4. $^{13}\text{C}\{^1\text{H}\}$ NMR spectrum (151 MHz, CD_2Cl_2 , 25 °C) of $(\text{NNO}_{\text{Me}})\text{InI}_2$ (**4**).

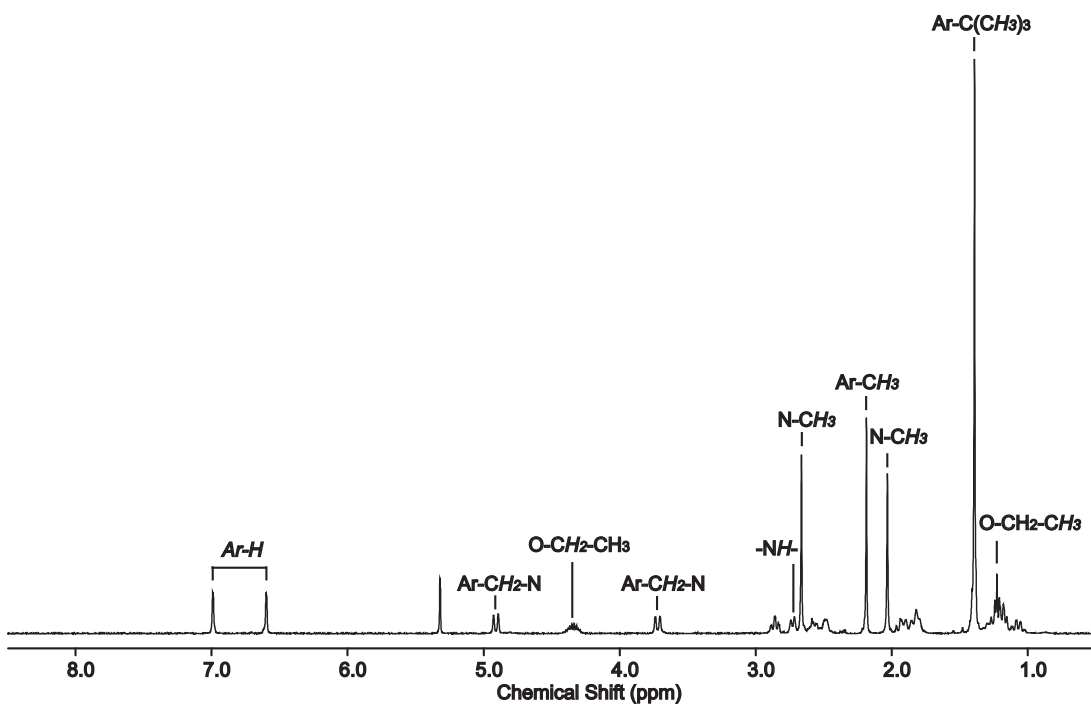


Figure A-5. ^1H NMR spectrum (400 MHz, CD_2Cl_2 , 25 $^\circ\text{C}$) of $[(\text{NNO}_{\text{Me}})\text{InCl}]_2(\mu\text{-Cl})(\mu\text{-OEt})$ (**6**).

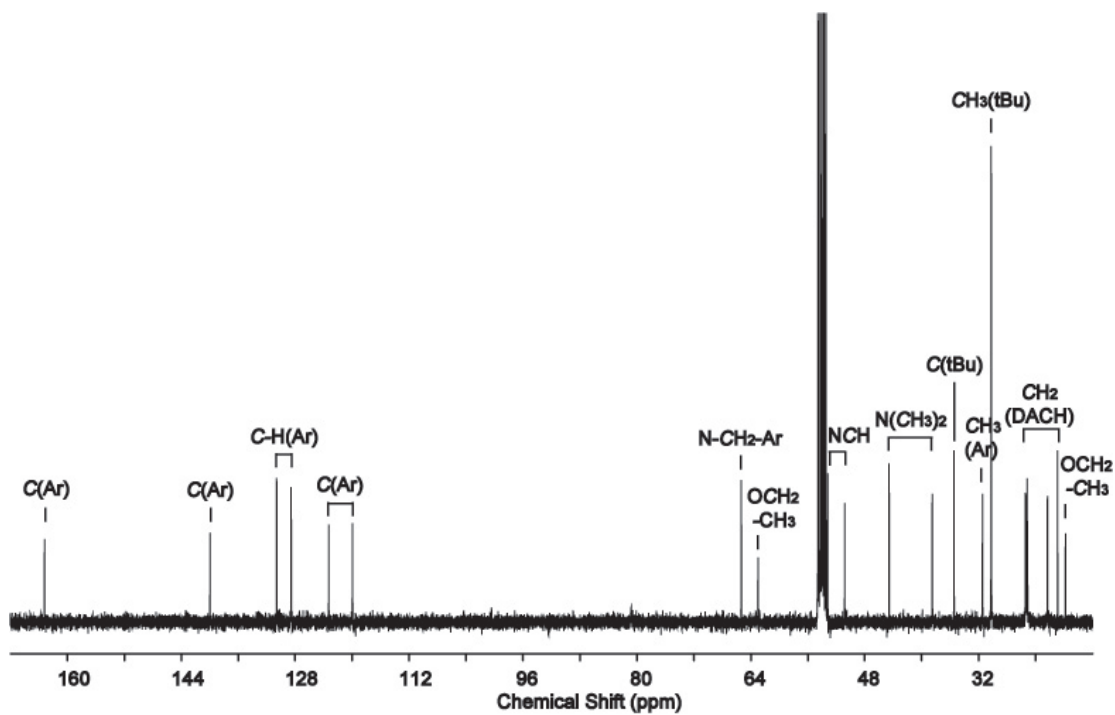


Figure A-6. $^{13}\text{C}\{^1\text{H}\}$ NMR spectrum (101 MHz, CD_2Cl_2 , 25 $^\circ\text{C}$) of $[(\text{NNO}_{\text{Me}})\text{InCl}]_2(\mu\text{-Cl})(\mu\text{-OEt})$ (**6**).

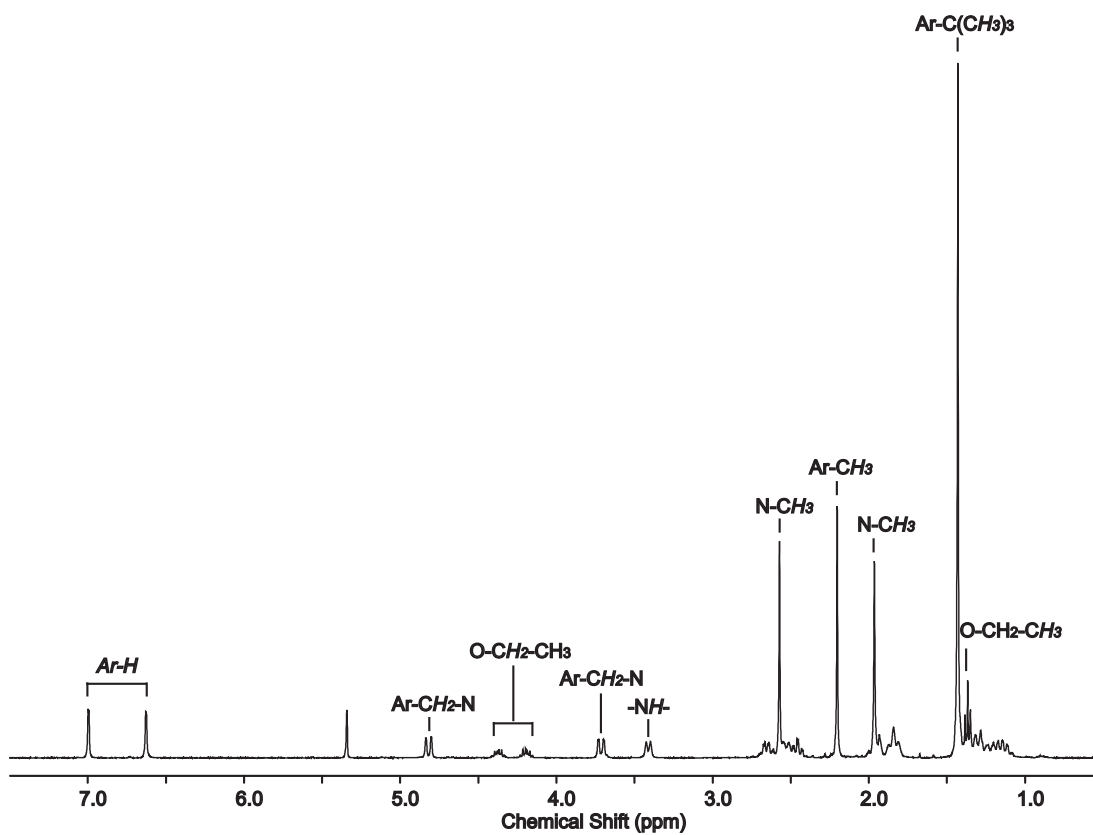


Figure A-7. ^1H NMR spectrum (400 MHz, CD_2Cl_2 , 25 $^\circ\text{C}$) of $[(\text{NNO}_{\text{Me}})\text{InI}]_2(\mu\text{-I})(\mu\text{-OEt})$ (7).

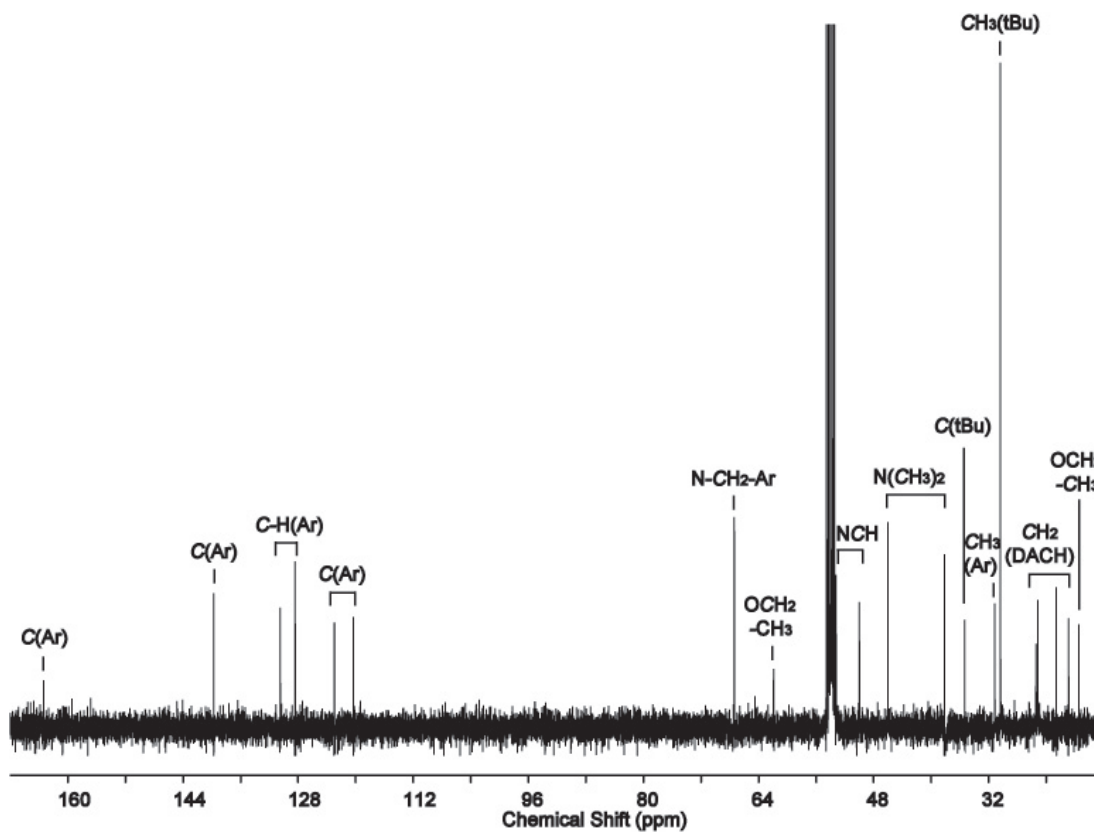


Figure A-8. $^{13}\text{C}\{^1\text{H}\}$ NMR spectrum (101 MHz, CD_2Cl_2 , 25 °C) of $[(\text{NNO}_{\text{Me}})\text{InI}_2(\mu\text{-I})(\mu\text{-OEt})]$ (7).

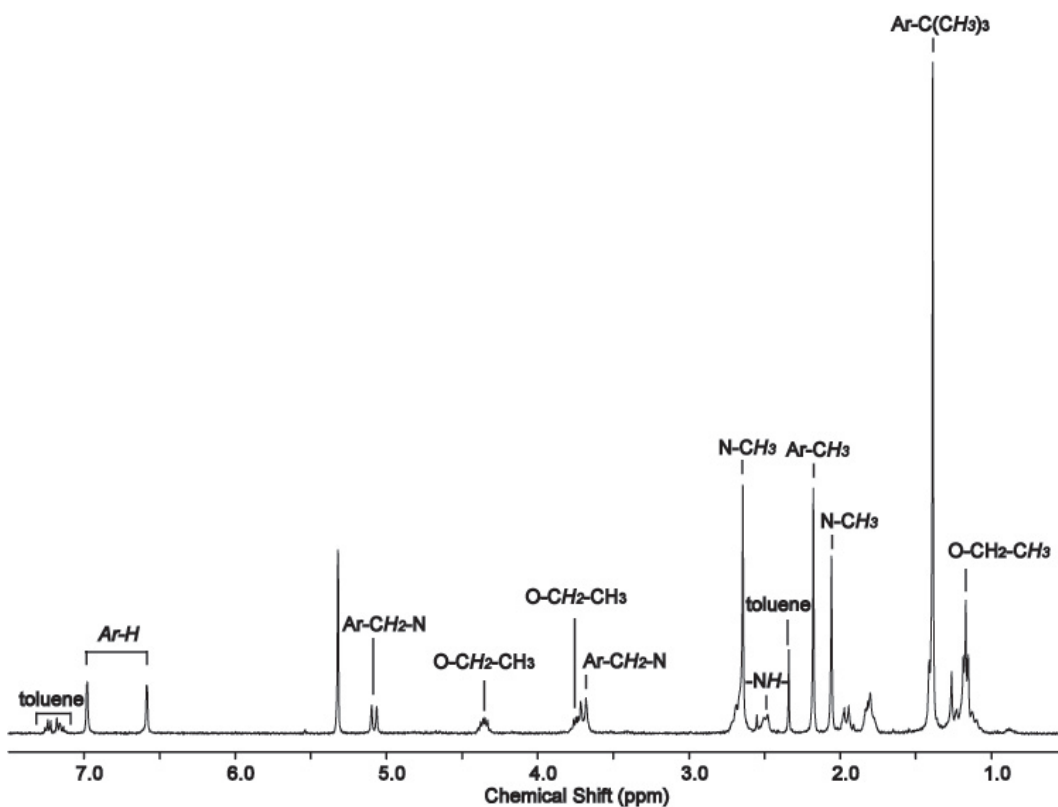


Figure A-9. ^1H NMR spectrum (400 MHz, CD_2Cl_2 , 25 °C) of meso- $[(\text{NNO}_{\text{Me}})\text{In}(\text{I})(\mu\text{-OEt})]_2$ (meso-8).

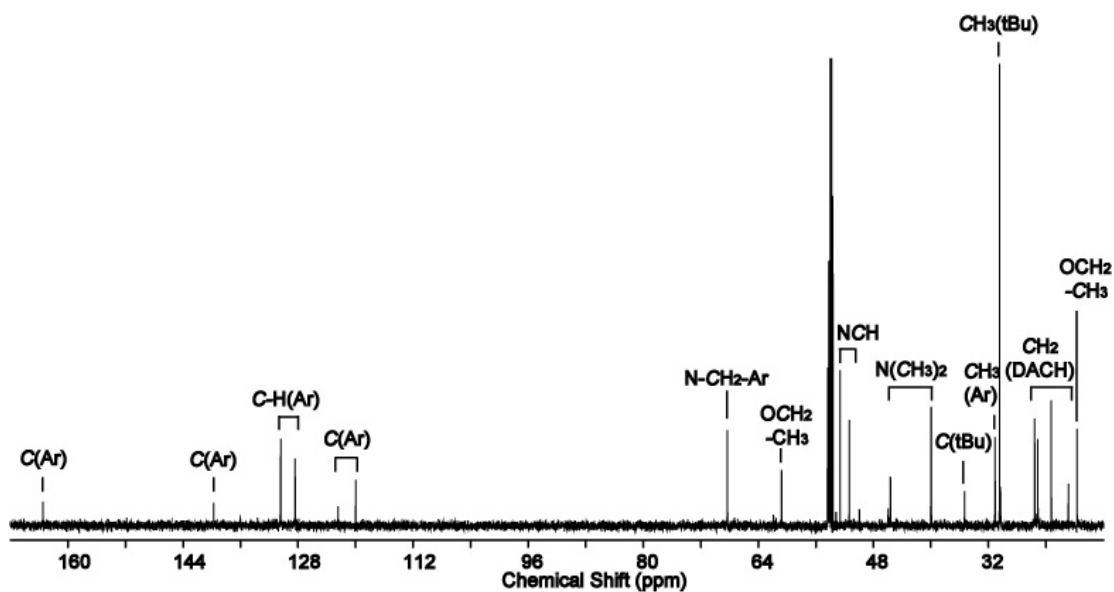


Figure A-10. $^{13}\text{C}\{^1\text{H}\}$ NMR spectrum (151 MHz, CD_2Cl_2 , 25 °C) of meso- $[(\text{NNO}_{\text{Me}})\text{In}(\text{I})(\mu\text{-OEt})]_2$ (meso-8).

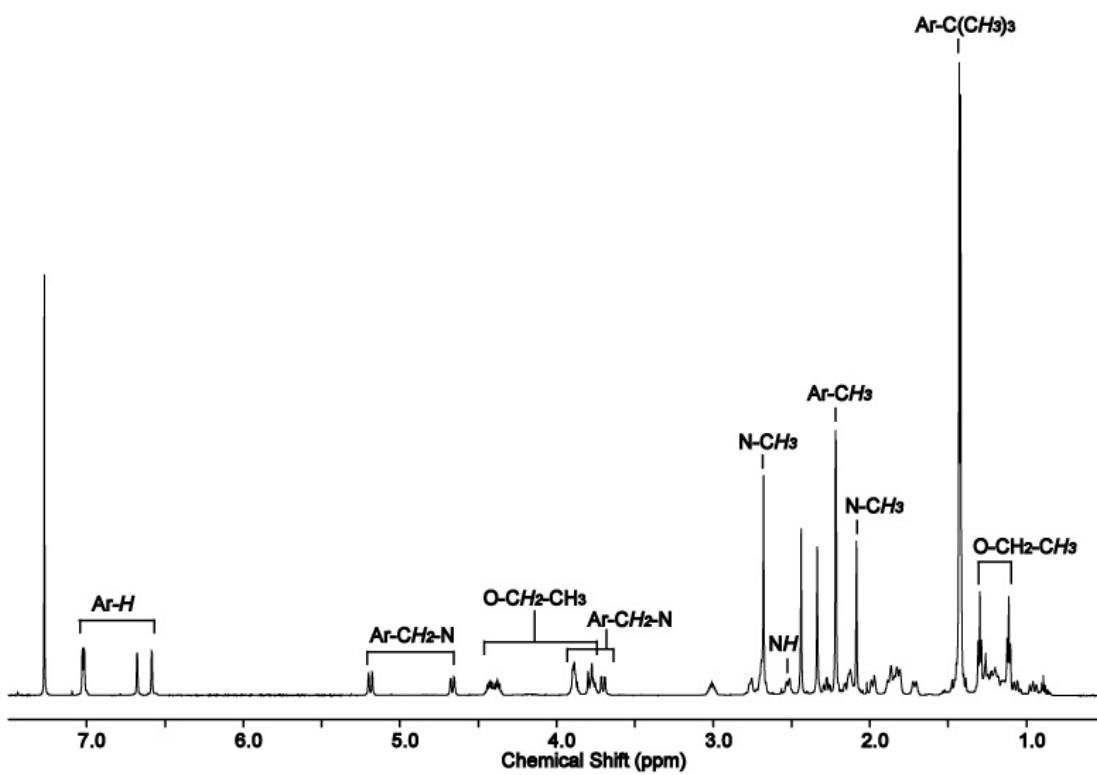
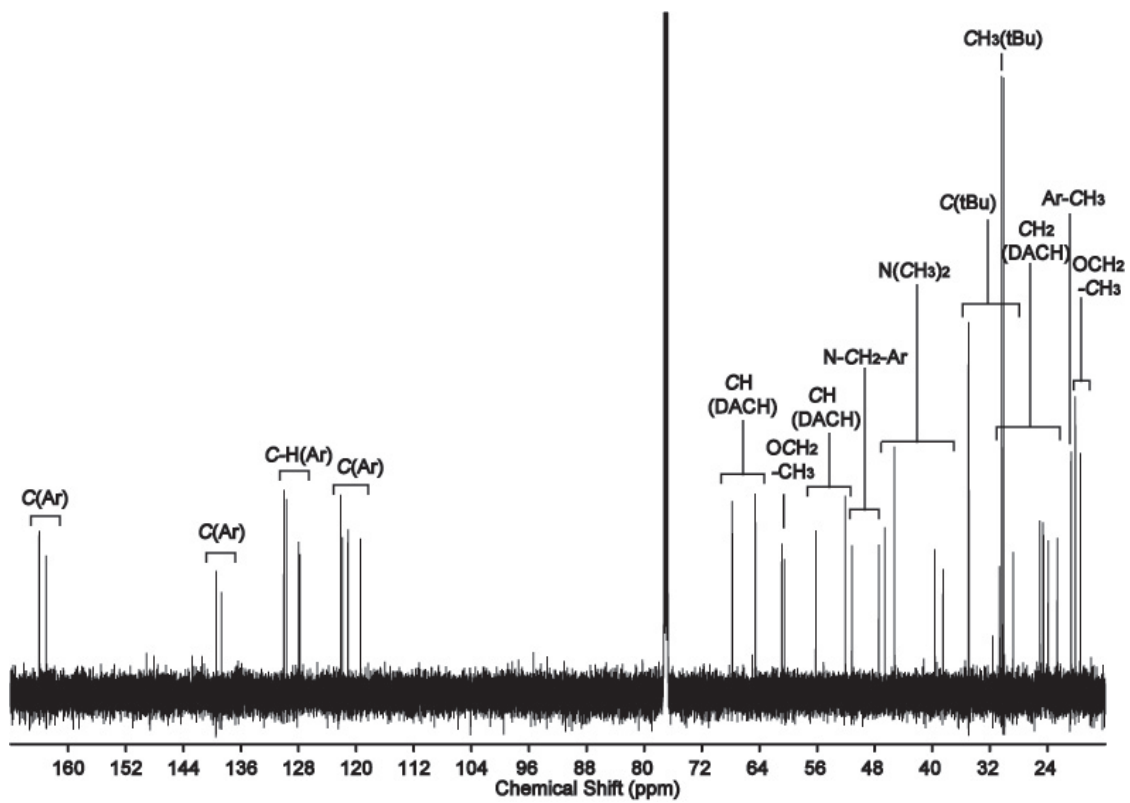
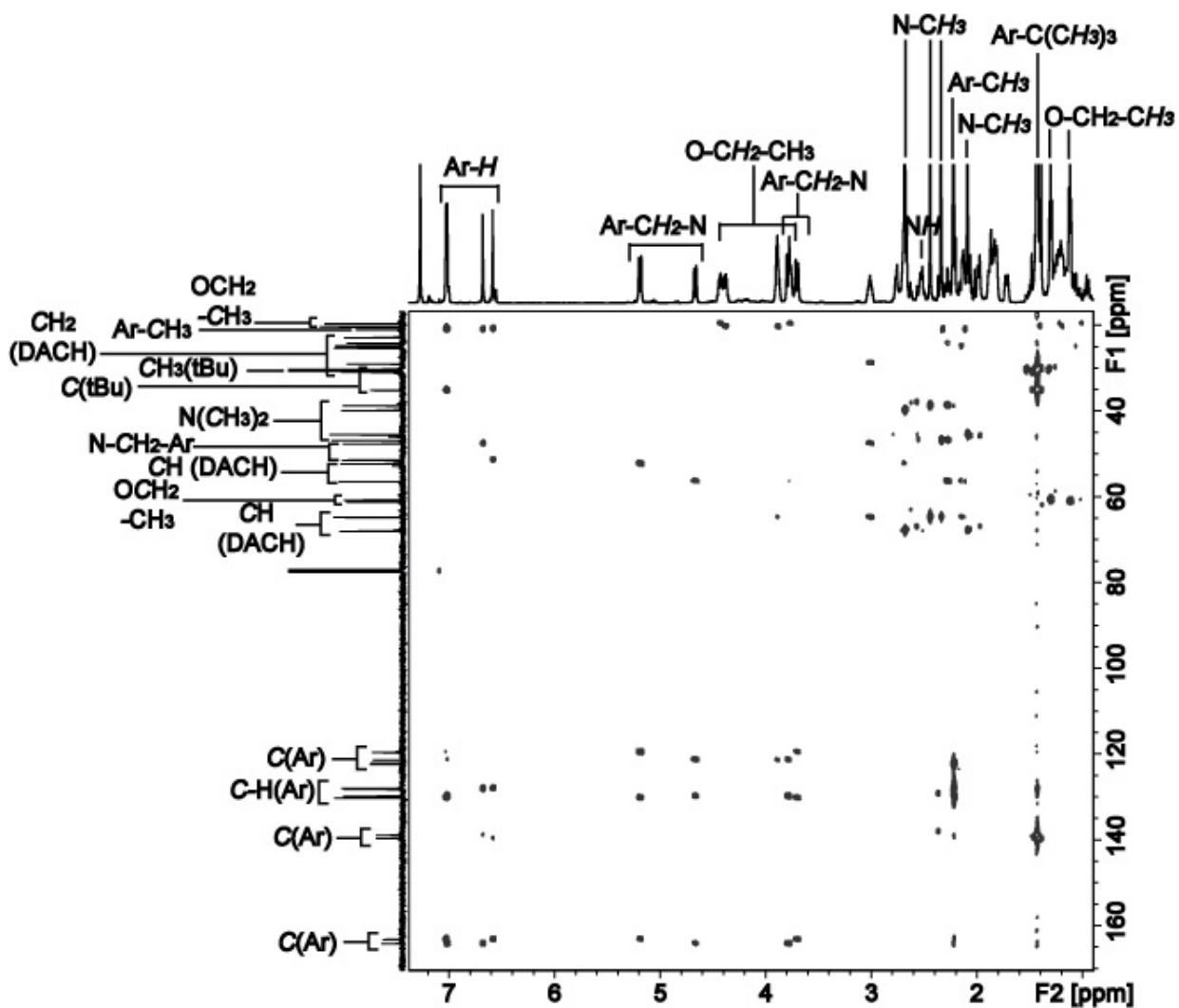


Figure A-11. ¹H NMR spectrum (600 MHz, CDCl₃, 25 °C) of (*R,R/R,R*)- or (*S,S/S,S*)-[(NNO_{Me})In(I)(μ-OEt)]₂ (**8**).

(a)



(b)



(c)

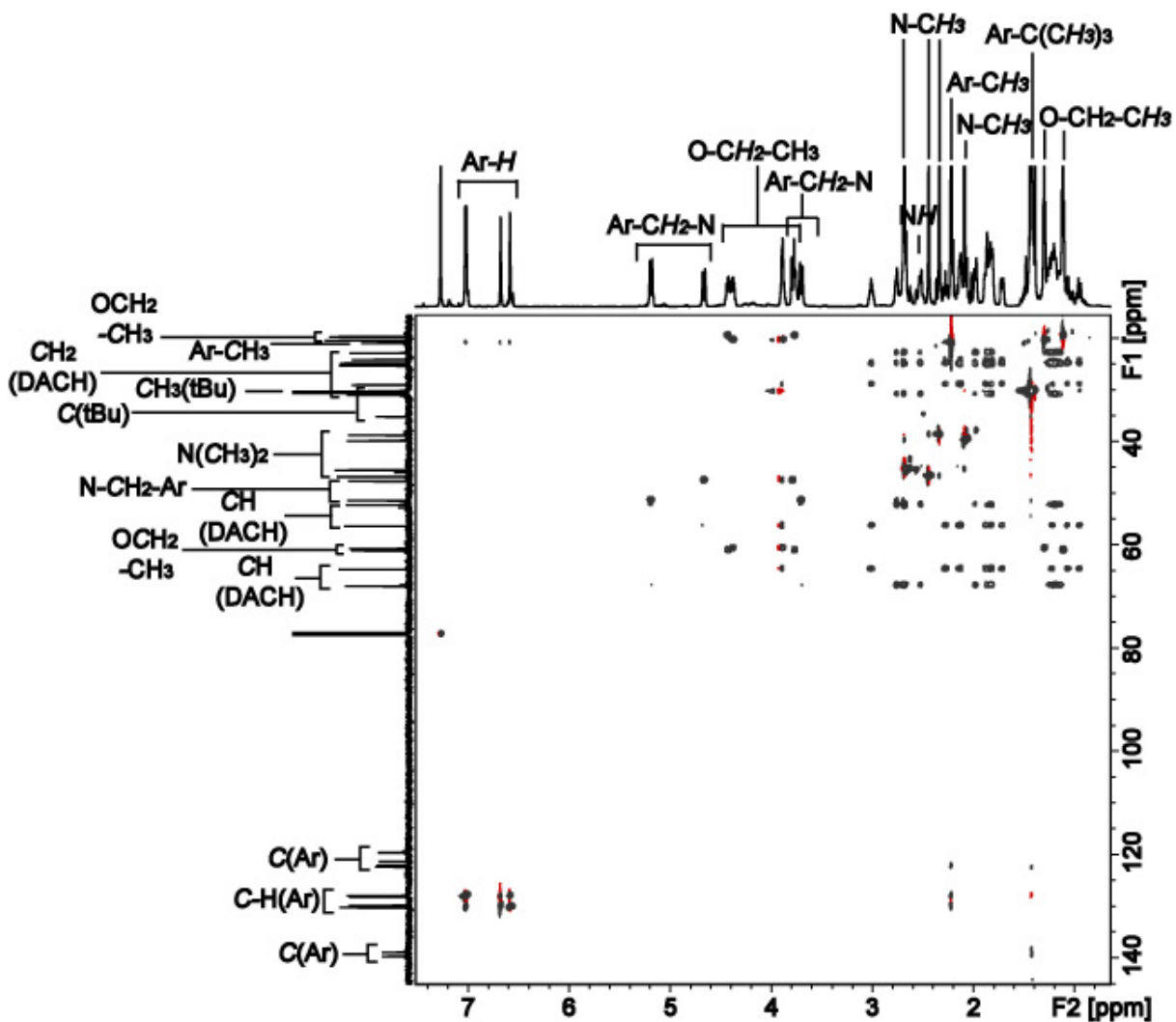


Figure A-12. (a) $^{13}\text{C}\{^1\text{H}\}$ NMR spectrum (151 MHz, CDCl_3 , 25 °C) (b) ^1H - ^{13}C HMBC spectrum and (c) ^1H - ^{13}C HSQCTOCSY spectrum of (*R,R,R,R*)- or (*S,S,S,S*)-[(NNO_{Me})In(I)(μ -OEt)₂] (**8**).

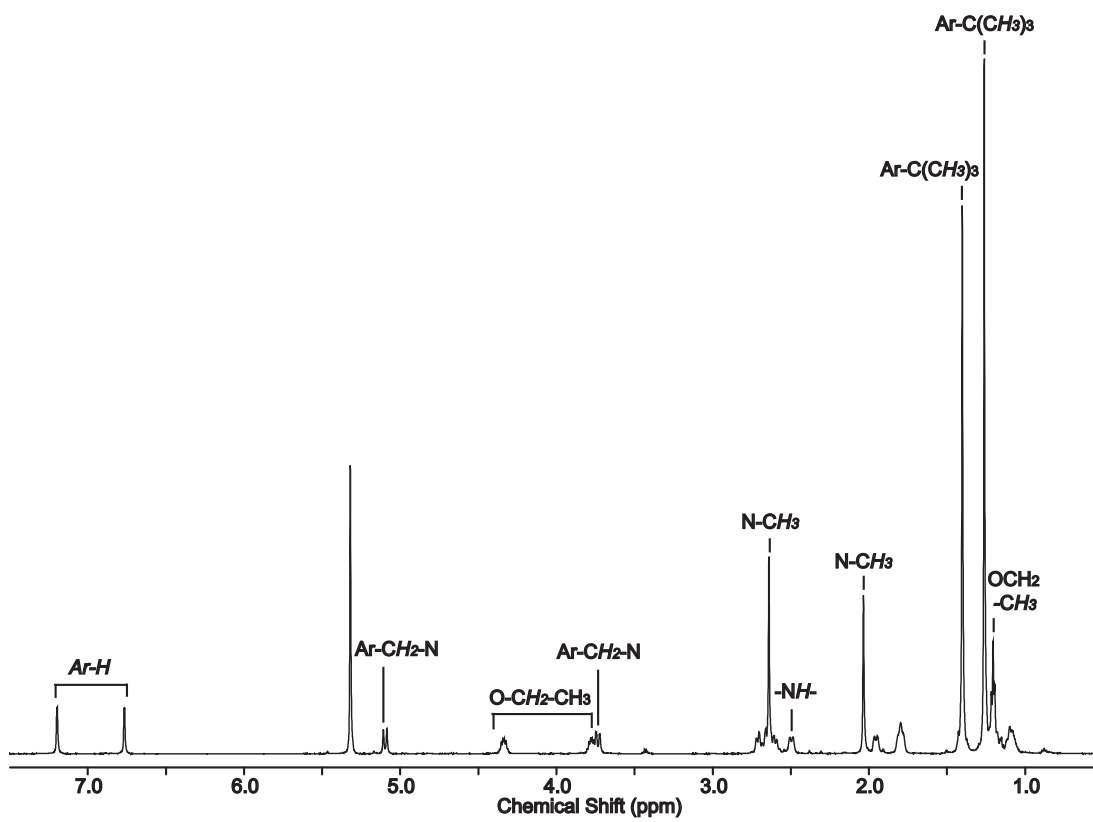


Figure A-13. ^1H NMR spectrum (400 MHz, CD_2Cl_2 , 25 $^\circ\text{C}$) of meso- $[(\text{NNO}_{\text{tBu}})\text{In}(\text{I})(\mu\text{-OEt})_2]_2$ (meso-9).

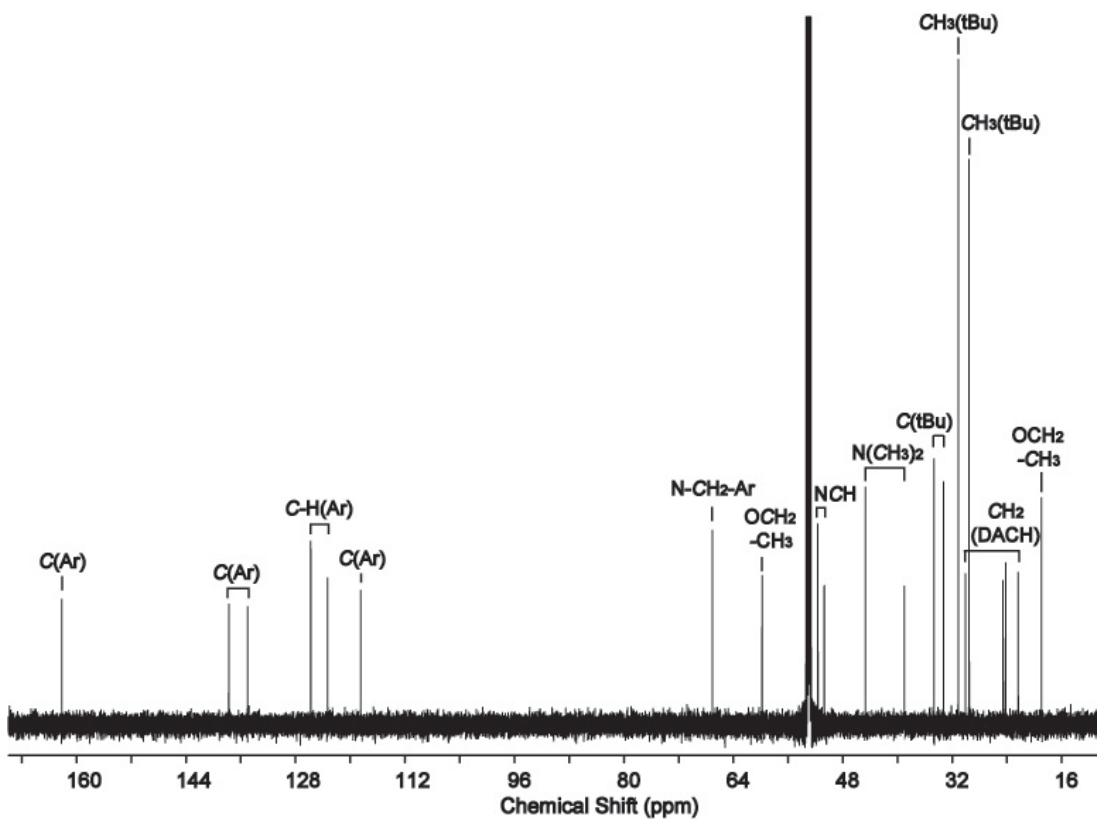


Figure A-14. $^{13}\text{C}\{^1\text{H}\}$ NMR spectrum (151 MHz, CD_2Cl_2 , 25 °C) of meso-[(NNO_{tBu})In(I)(μ -OEt)]₂ (meso-9).

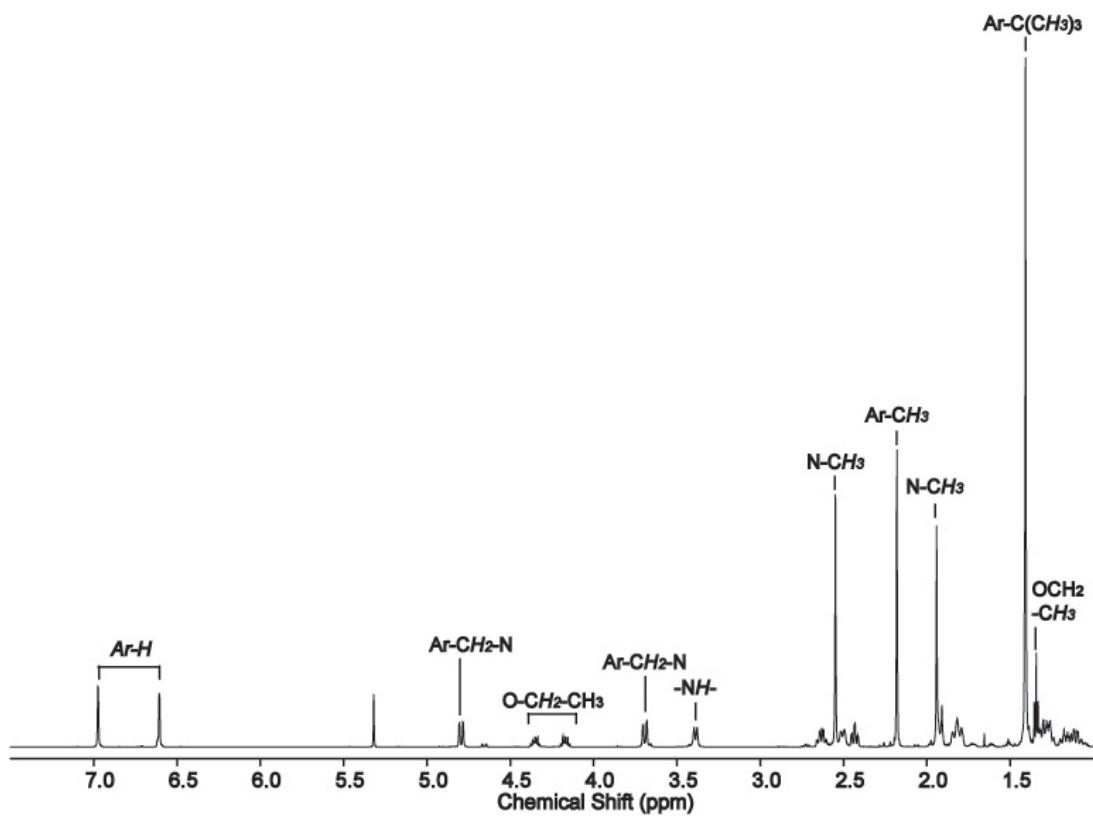


Figure A-15. ^1H NMR spectrum (600 MHz, CD_2Cl_2 , 25 $^\circ\text{C}$) of $[(\text{NNO}_{\text{Me}})\text{InI}]_2(\mu\text{-OH})(\mu\text{-OEt})$ (**10**).

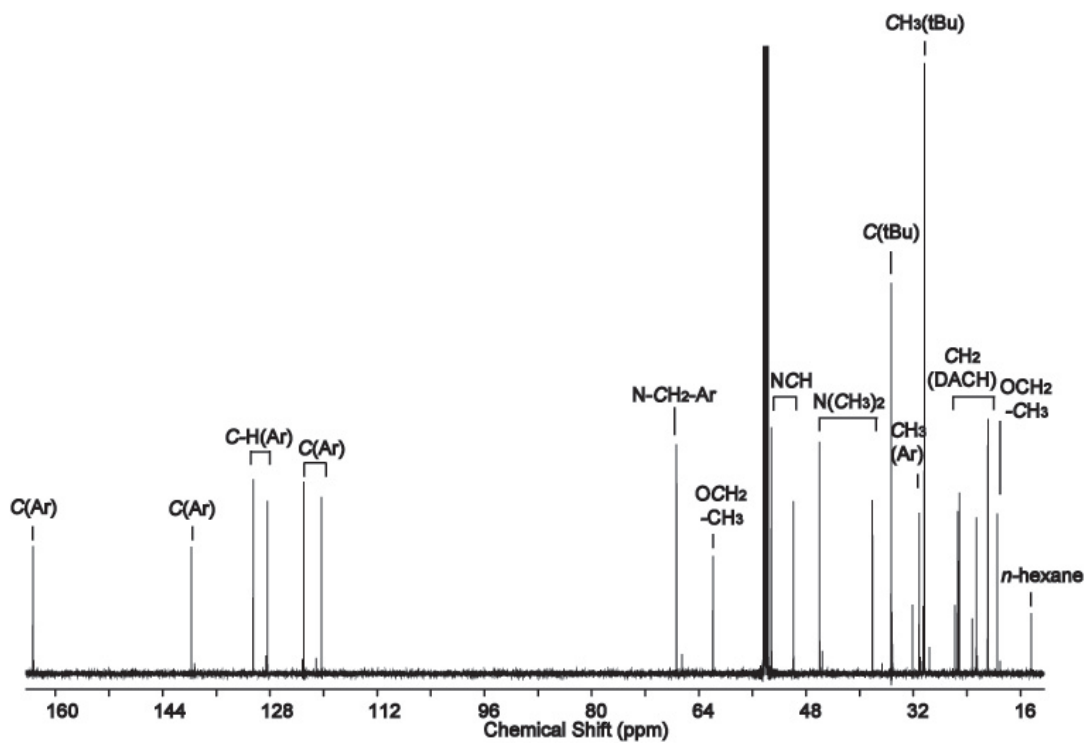


Figure A-16. $^{13}\text{C}\{^1\text{H}\}$ NMR spectrum (101 MHz, CD_2Cl_2 , 25 °C) of $[(\text{NNO}_{\text{Me}})\text{InI}]_2(\mu\text{-OH})(\mu\text{-OEt})$ (**10**).

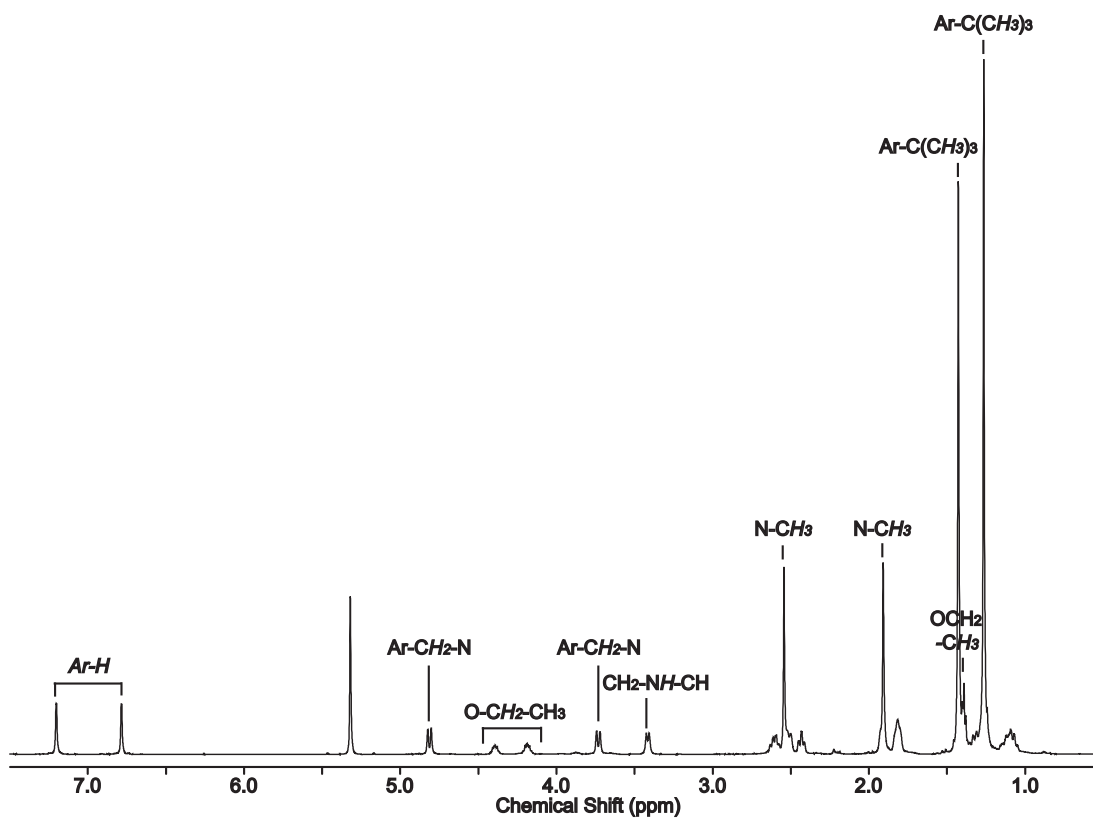


Figure A-17. ^1H NMR spectrum (600 MHz, CD_2Cl_2 , 25 $^\circ\text{C}$) of $[(\text{NNO}_{\text{tBu}})\text{InI}]_2(\mu\text{-OH})(\mu\text{-OEt})$ (**11**).

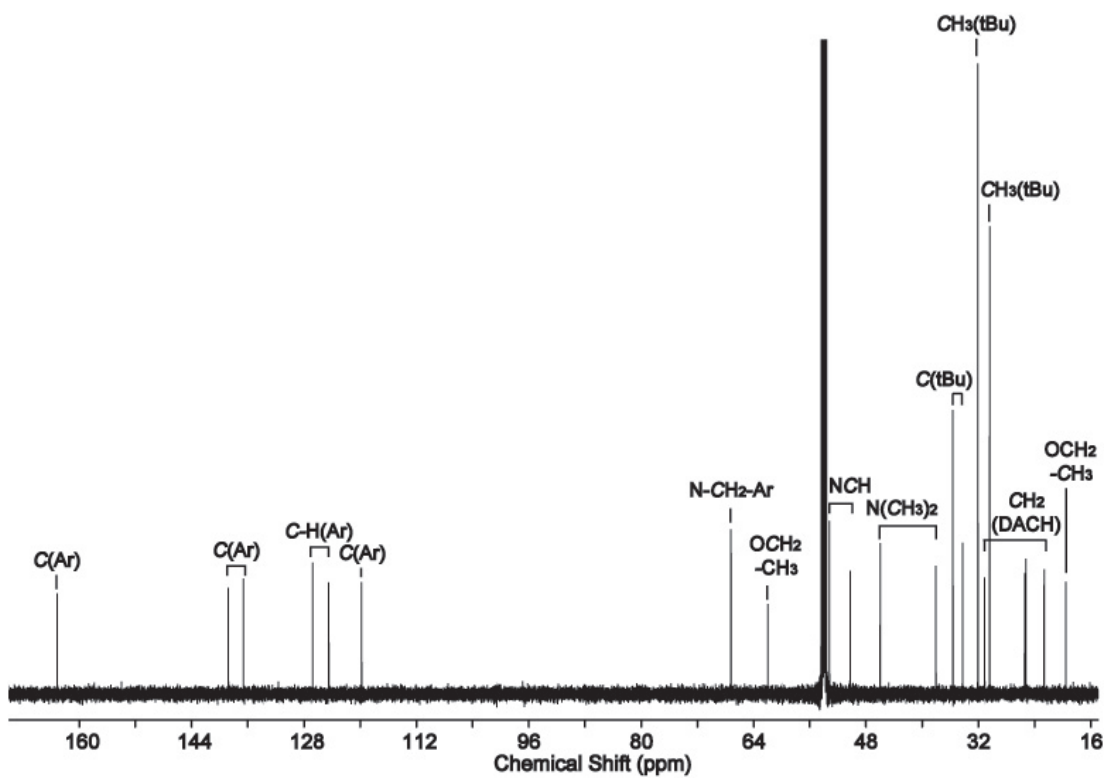


Figure A-18. $^{13}\text{C}\{^1\text{H}\}$ NMR spectrum (151 MHz, CD_2Cl_2 , 25 °C) of $[(\text{NNO}_{\text{tBu}})\text{InI}]_2(\mu\text{-OH})(\mu\text{-OEt})$ (**11**).

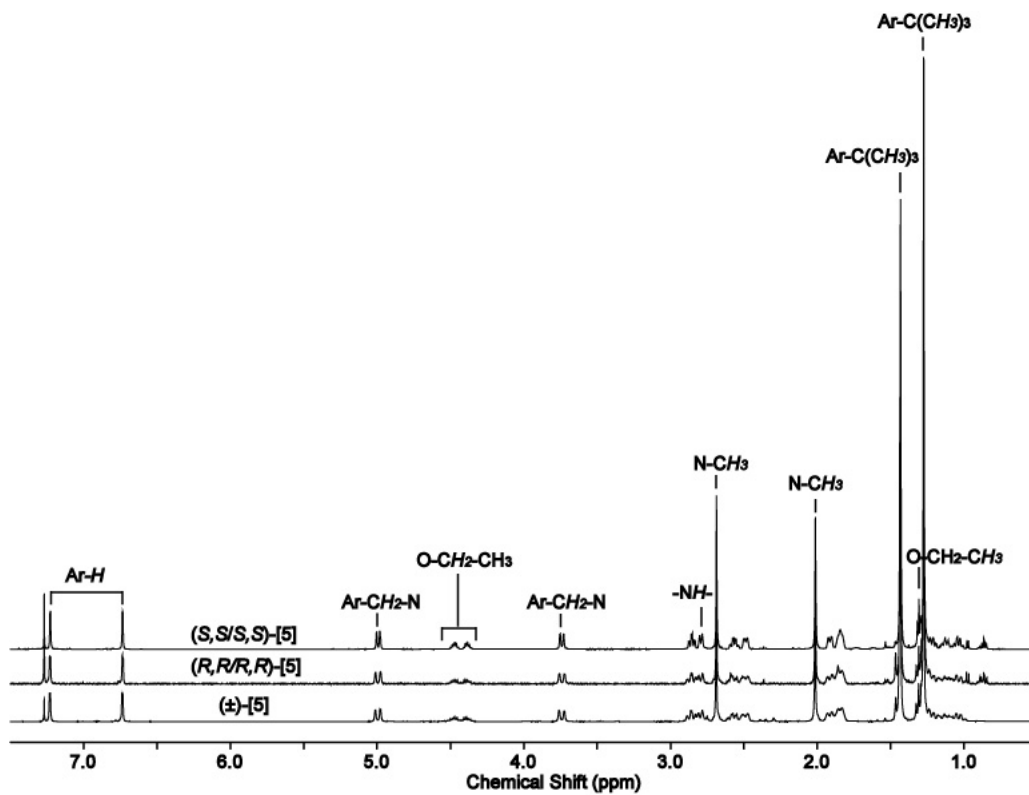


Figure A-19. ¹H spectra (400 MHz, CDCl₃, 25 °C) of (±)-, (R,R/R,R)-, and (S,S/S,S)-5.

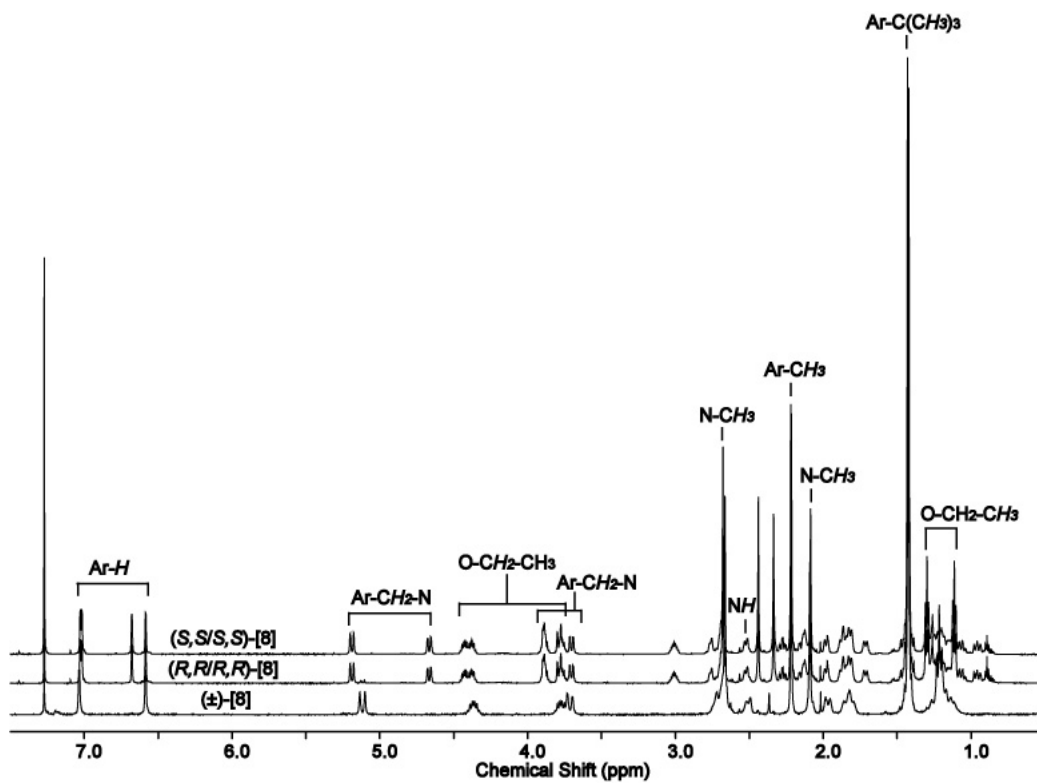


Figure A-20. ¹H spectra (400 MHz, CDCl₃, 25 °C) of meso-, (R,R/R,R)-, and (S,S/S,S)-8.

A.2 Selective crystal data for (±)-3, (S,S)-4, (S,S/S,S)-8, meso-9, (±)-11, and (R,R/R,R)-[(NNO_{Me})In(I)(μ-OH)]₂.

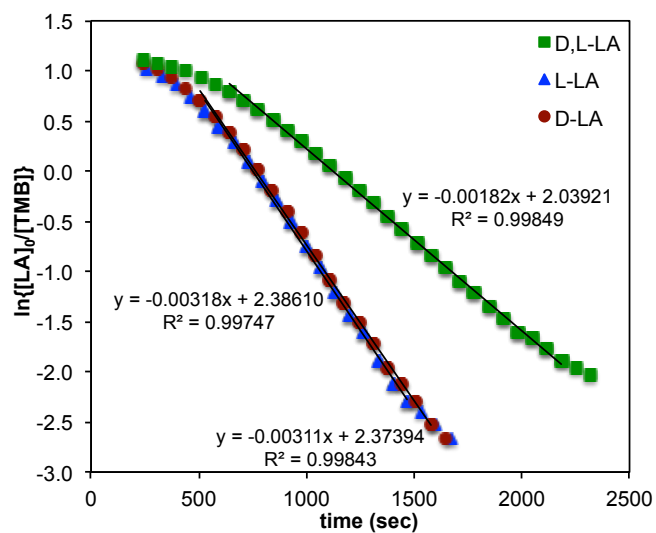
	(±)-3	(S,S)-4	(S,S/S,S)-8	Meso-9	(±)-11	(R,R/R,R)- [(NNO _{Me})In(I)(μ-OH)] ₂
empirical formula	C ₂₀ H ₃₃ Cl ₂ InN ₂ O	C ₂₂ H ₃₆ I ₂ InN ₃ O	C ₄₈ H ₈₄ Cl ₈ I ₂ In ₂ N ₄ O ₄	C ₂₅ H ₄₄ IIInN ₂ O ₂	C ₄₈ H ₈₃ I ₂ In ₂ N ₄ O ₄	C ₅₆ H ₁₀₀ I ₂ In ₂ N ₄ O ₈
fw	503.2	727.16	1548.23	646.34	1263.62	1440.84
<i>T</i> (K)	173	173	100	173	173	173
<i>a</i> (Å)	13.9254(9)	8.2900(3)	9.3280(6)	10.4732(6)	10.5934(2)	10.3684(8)
<i>b</i> (Å)	16.6104(10)	12.3742(5)	11.9779(9)	10.9899(6)	17.4212(4)	11.1950(8)
<i>c</i> (Å)	9.7594(7)	12.9732(5)	14.8126(9)	11.9172(7)	15.6610(3)	14.5462(11)
<i>α</i> (deg)	90	90	81.227(4)	84.305(3)	90	102.916(4)
<i>β</i> (deg)	90	98.477(2)	84.778(4)	86.763(3)	102.1280(10)	102.609(4)
<i>γ</i> (deg)	90	90	69.172(4)	79.914(3)	90	101.865(4)
volume (Å ³)	2257.4(3)	1316.28(9)	1527.55(18)	1342.73(13)	2825.73(10)	1547.5(2)
<i>Z</i>	4	2	1	2	2	1
cryst syst	orthorhombic	monoclinic	triclinic	triclinic	monoclinic	triclinic
space group	<i>P na</i> 2 ₁	<i>P</i> 2 ₁	<i>P</i> 1	<i>P</i> -1	<i>P</i> 2 ₁	<i>P</i> 1
<i>d</i> _{calc} (g/cm ³)	1.481	1.835	1.683	1.599	1.949	1.546
<i>μ</i> (Mo Kα) (cm ⁻¹)	12.95	32.6	21.57	20.52	19.49	17.94
2θ _{max} (deg)	57.8	56.4	60.2	55.1	45	57.4
absor corr (<i>T</i> _{min} , <i>T</i> _{max})	0.765, 0.878	0.850, 0.729	0.804, 0.937	0.802, 0.902	0.600, 0.746	0.735, 0.914
total no. of rflns	27 260	34 097	67 425	27 585	35 657	64 151
no. of indep rflns (<i>R</i> _{int})	5 920 (0.020)	6 467 (0.039)	17 790 (0.0391)	6 135 (0.033)	7358 (0.039)	15 160 (0.0375)
residuals (refined on <i>F</i> ²): <i>R</i> ₁ ; <i>wR</i> ₂	0.018, 0.043	0.031, 0.064	0.045, 0.060	0.045, 0.060	0.029, 0.060	0.039, 0.086
GOF	1.057	1.095	1.016	1.028	1.046	1.076
no. obsrvns [<i>I</i> > 2σ(<i>I</i>)]	5670	9888	9647	4764	6914	9722
residuals (refined on <i>F</i> ²): <i>R</i> ₁ ^a ; <i>wR</i> ₂ ^b)	0.017, 0.042	0.028, 0.063	0.030, 0.055	0.026, 0.053	0.026, 0.058	0.033, 0.079

$$^a R_1 = \sum ||F_o| - |F_c|| / \sum |F_o|. \quad ^b wR_2 = [\sum (w (F_o^2 - F_c^2)^2) / \sum w(F_o^2)_2]^{1/2}$$

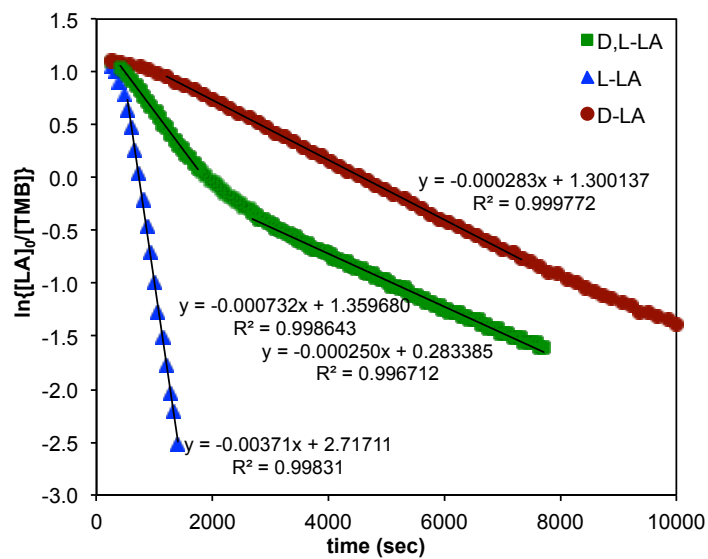
Appendix B

B.1 Stereoselectivity

(a) Rates of polymerization with (\pm)-5



(b) Rates of polymerization with (*R,R/R,R*)-5



(c) Rates of polymerization with (S,S/S,S)-**5**

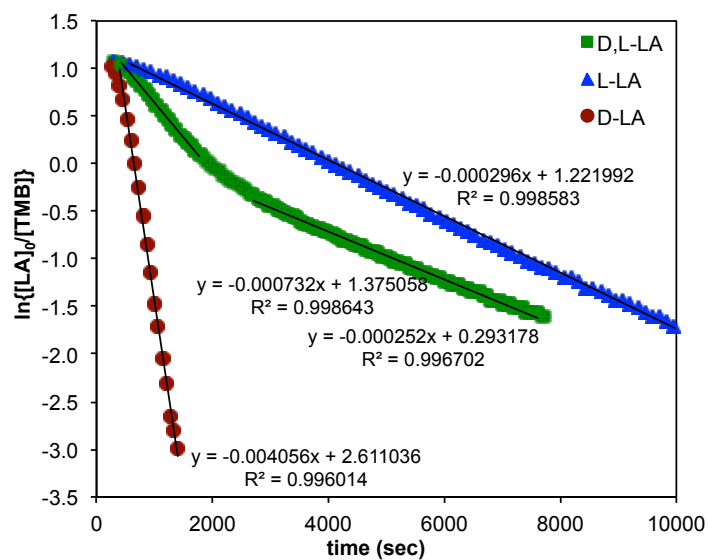
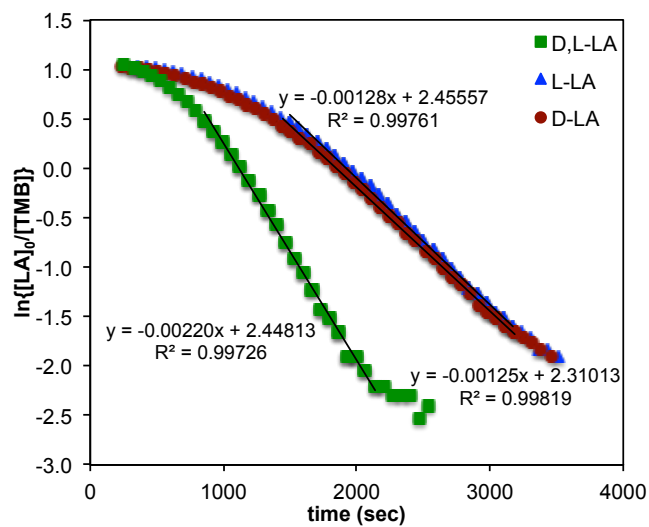
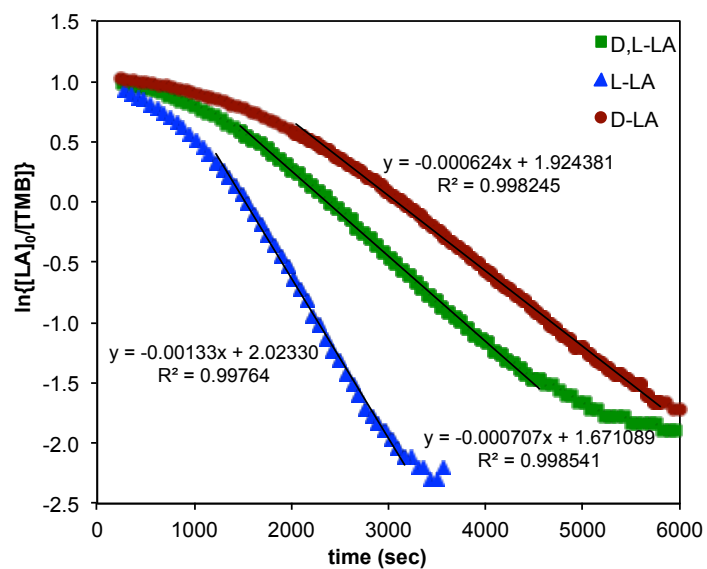


Figure B-1. Kinetic data for polymerization of D,L-LA, L-LA, and D-LA by (a) (±)-**5**, (b) (R,R/R,R)-**5**, (c) (S,S/S,S)-**5**. $[LA]_0 = 0.45$ M, $[5] = 0.0023$ M, $[LA]_0/[5] = 198$ for R,R/R,R and S,S/S,S-**5** ($CDCl_3$, 25 °C).

(a) Rates of polymerization with (\pm)-**8**



(b) Rates of polymerization with (*R,R/R,R*)-**8**



(c) Rates of polymerization with (*S,S/S,S,S*)-**8**

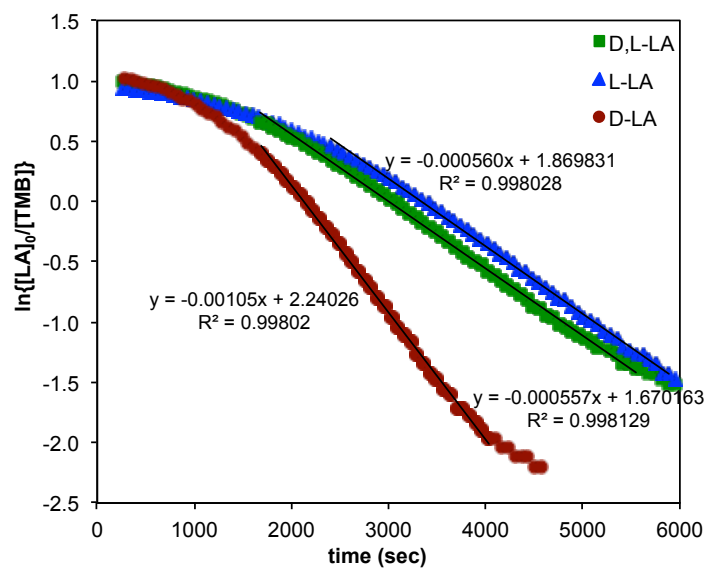


Figure B-2. Kinetic data for polymerization of D,L-LA, L-LA, and D-LA by (a) (\pm)-**8**, (b) (*R,R/R,R*)-**8**, and (c) (*S,S/S,S,S*)-**8**. $[LA]_0 = 0.114$ M, $[8] = 0.00052$ M, $[LA]_0/[8] = 220$ for *R,R/R,R*- and *S,S/S,S,S*-**8** (400 MHz, $CDCl_3$, 25 °C).

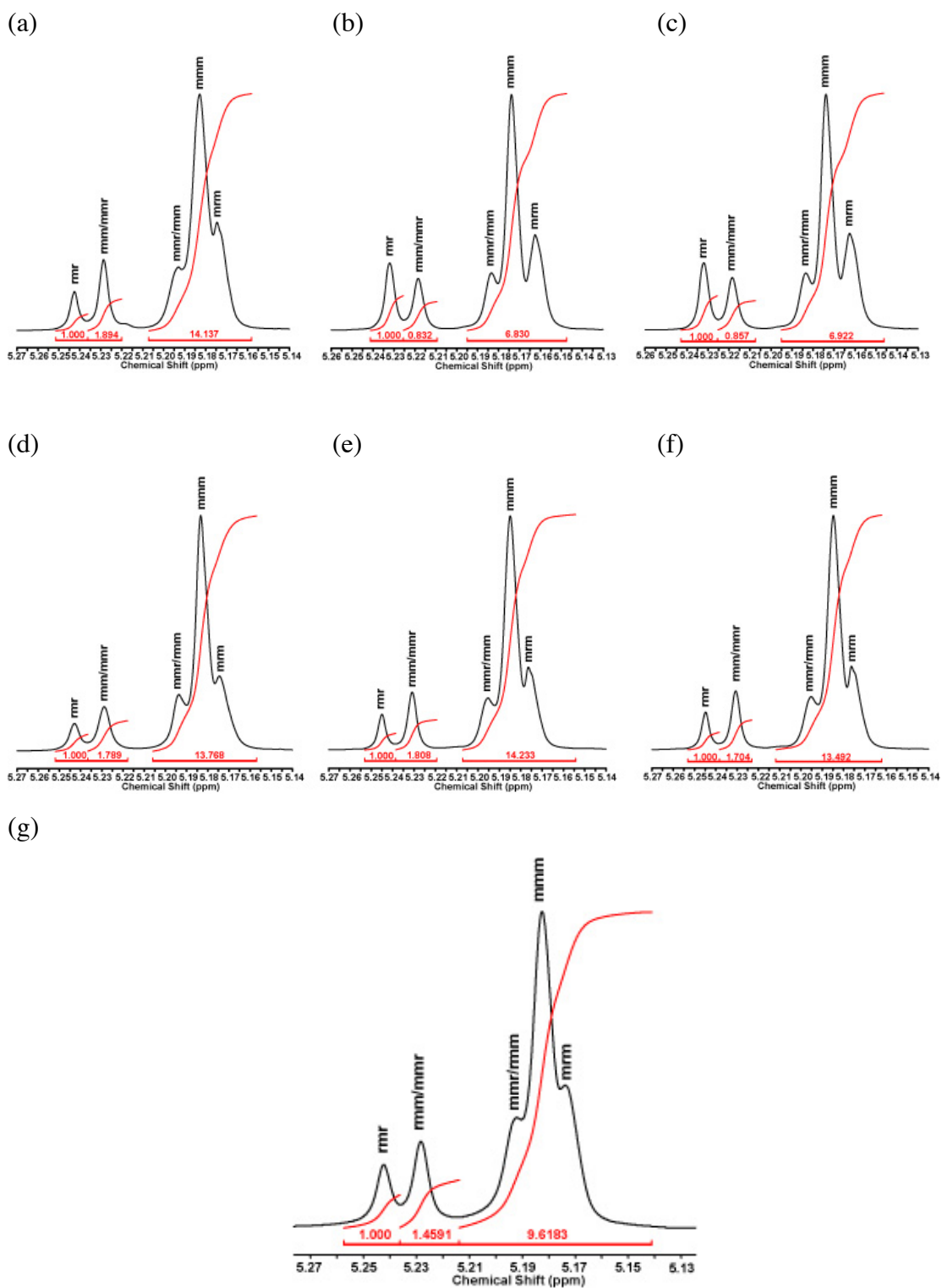
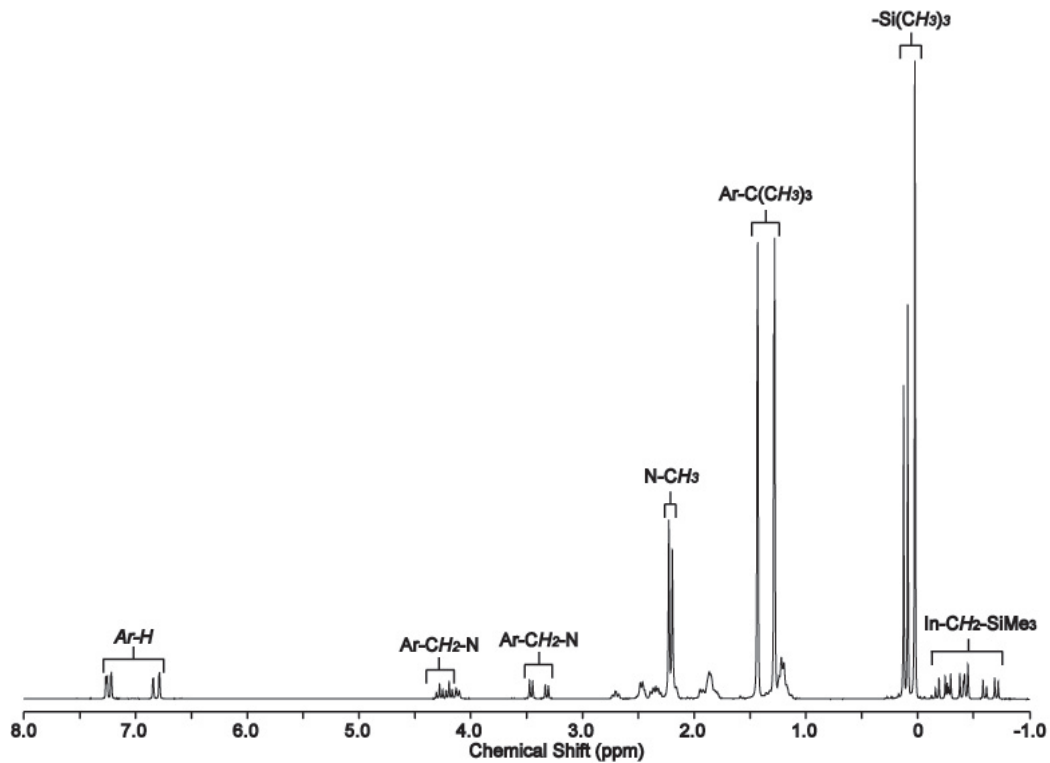


Figure B-3. $^1\text{H}\{^1\text{H}\}$ NMR spectra (600 MHz, CDCl_3 , 25 °C) of PLA obtained from ROP of D,L-LA with a) (\pm) -5, (b) (R,R/R,R)-5, (c) (S,S/S,S)-5, (d) (\pm) -8, (e) (R,R/R,R)-8, (f) (S,S/S,S)-8, and (g) (\pm) -7 ($P_m = 0.59$).

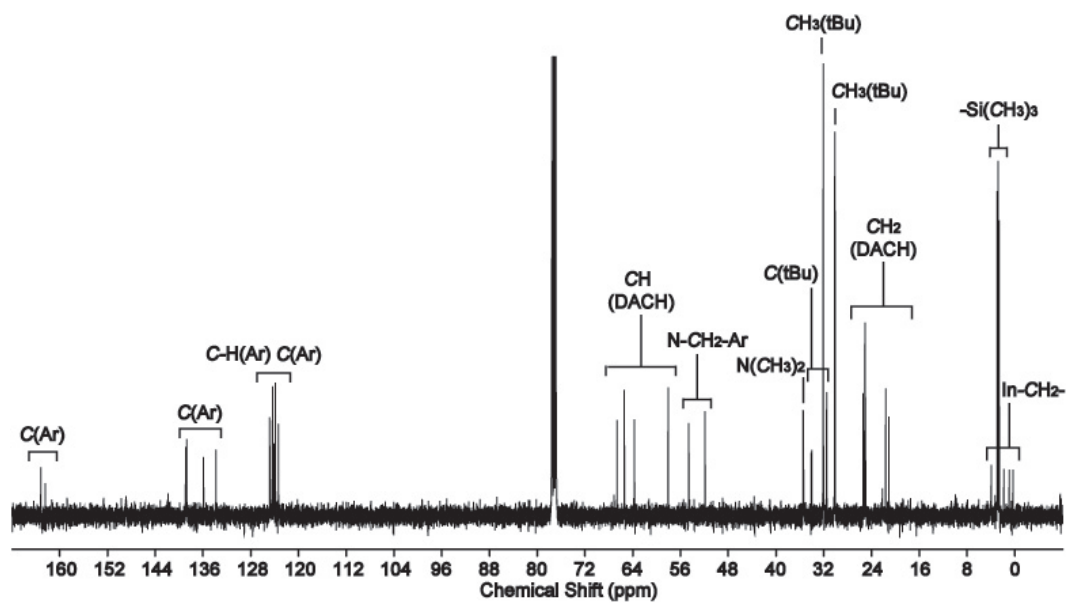
Appendix C

C.1 Characterization of neutral and cationic indium complexes

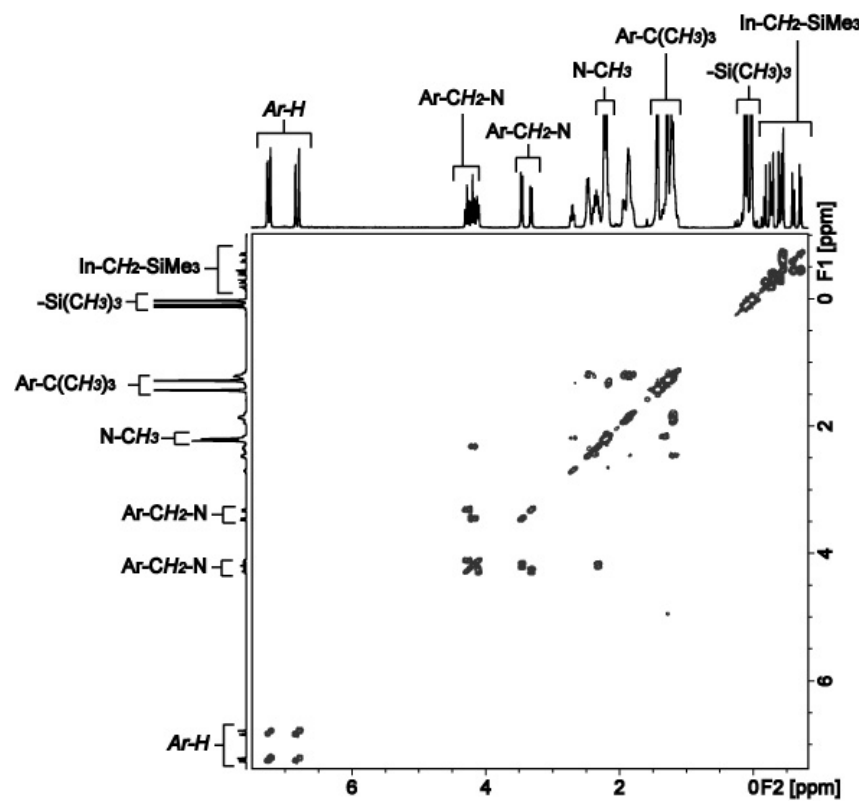
(a)



(b)



(c)



(e)

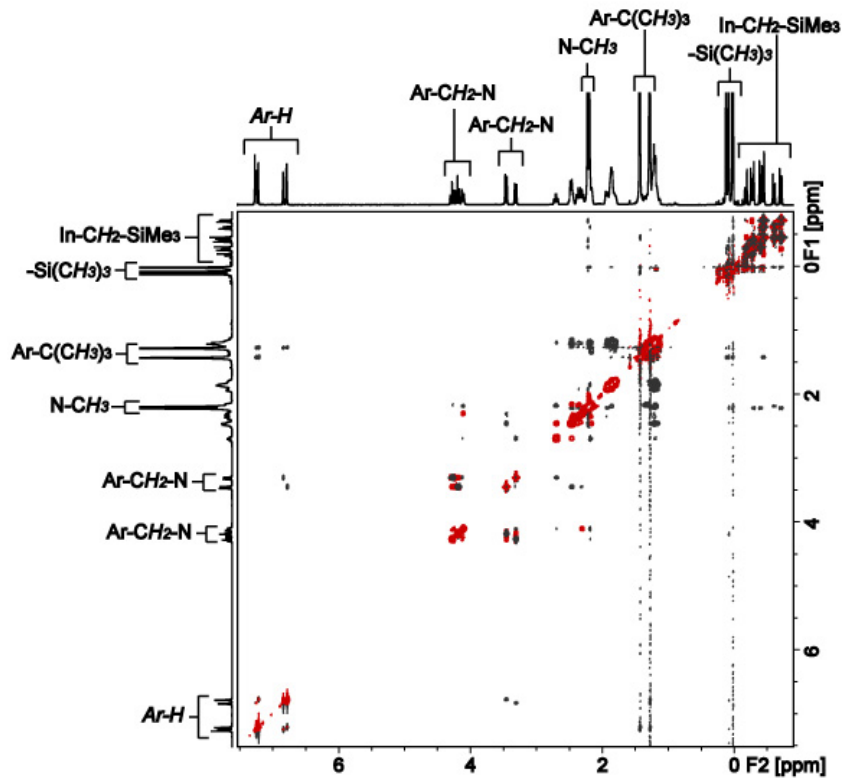
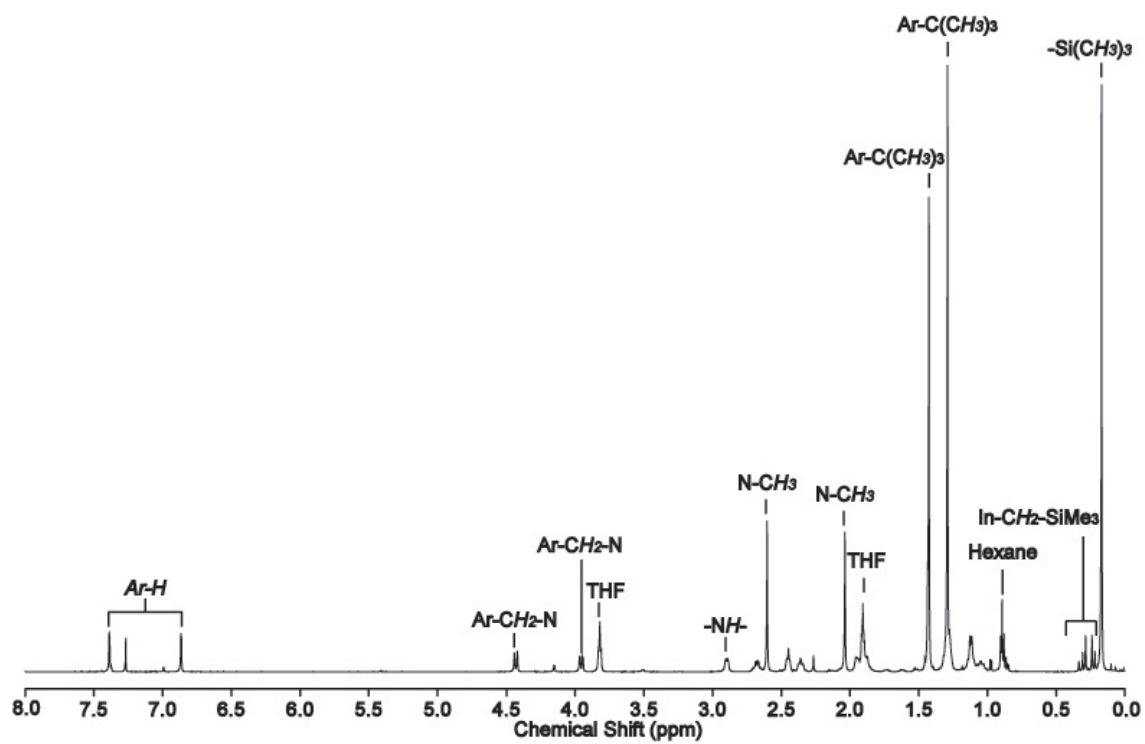
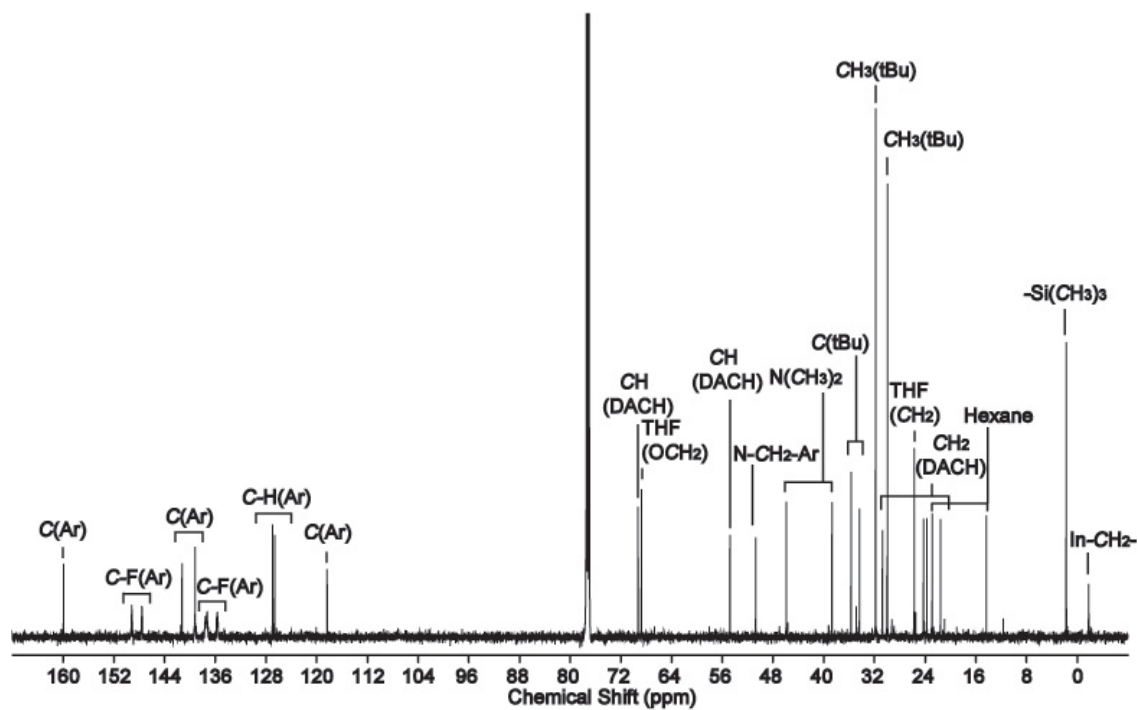


Figure C-1. (a) ^1H NMR, (b) $^{13}\text{C}\{^1\text{H}\}$ NMR, (c) ^1H - ^1H COSY and (e) ^1H - ^1H NOESY (optimized mixing time: 400 ms) spectrum of **13** (NNO_{tBu}) $\text{In}(\text{CH}_2\text{SiMe}_3)_2$ (**1**) (400 MHz, CDCl_3 , 25 °C).

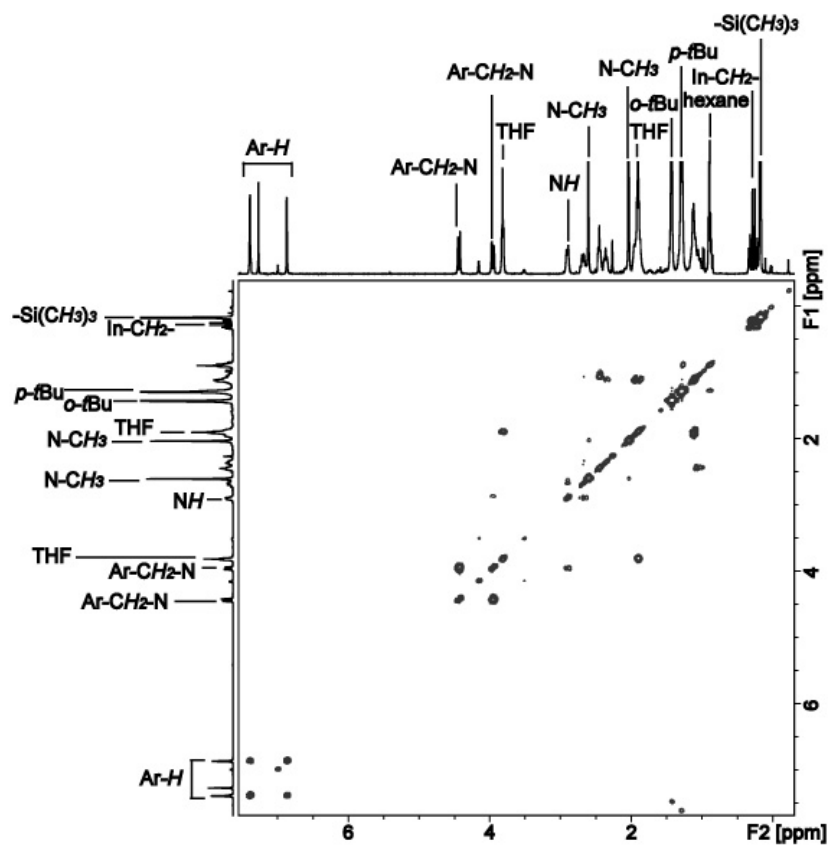
(a)



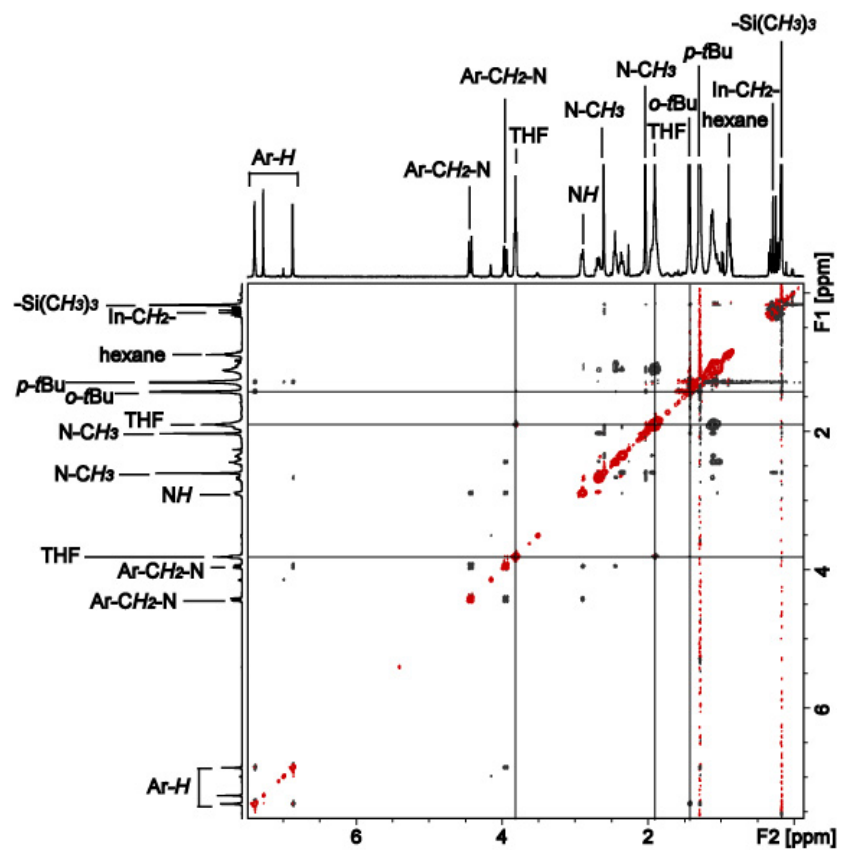
(b)



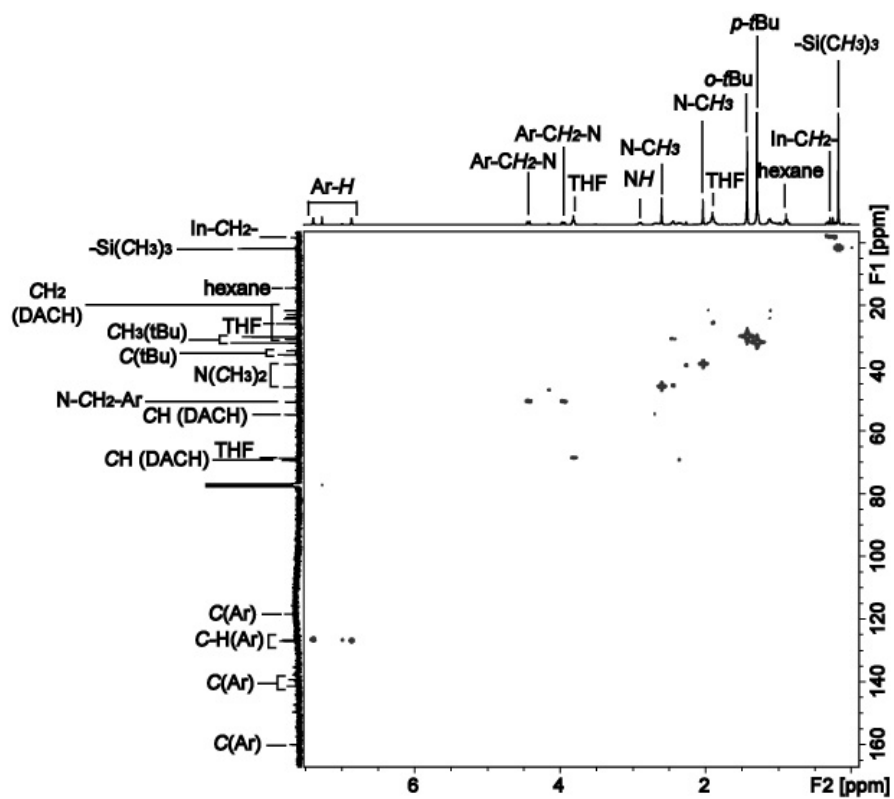
(c)



(d)



(e)



(f)

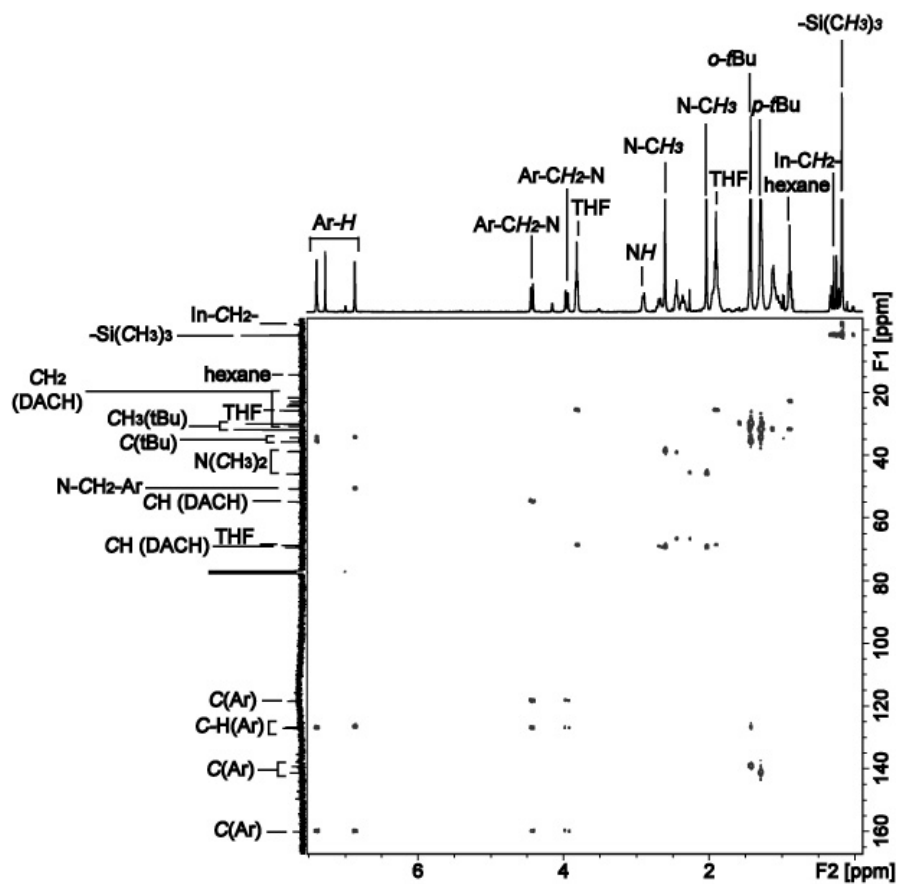
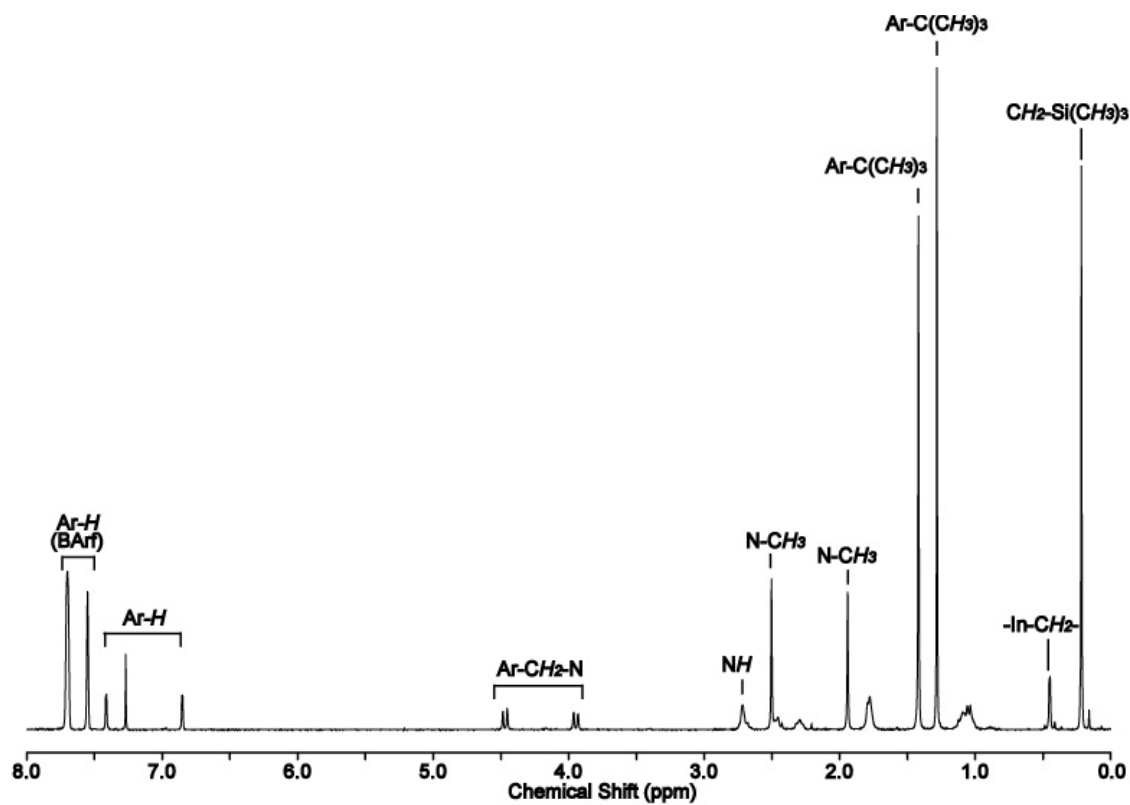
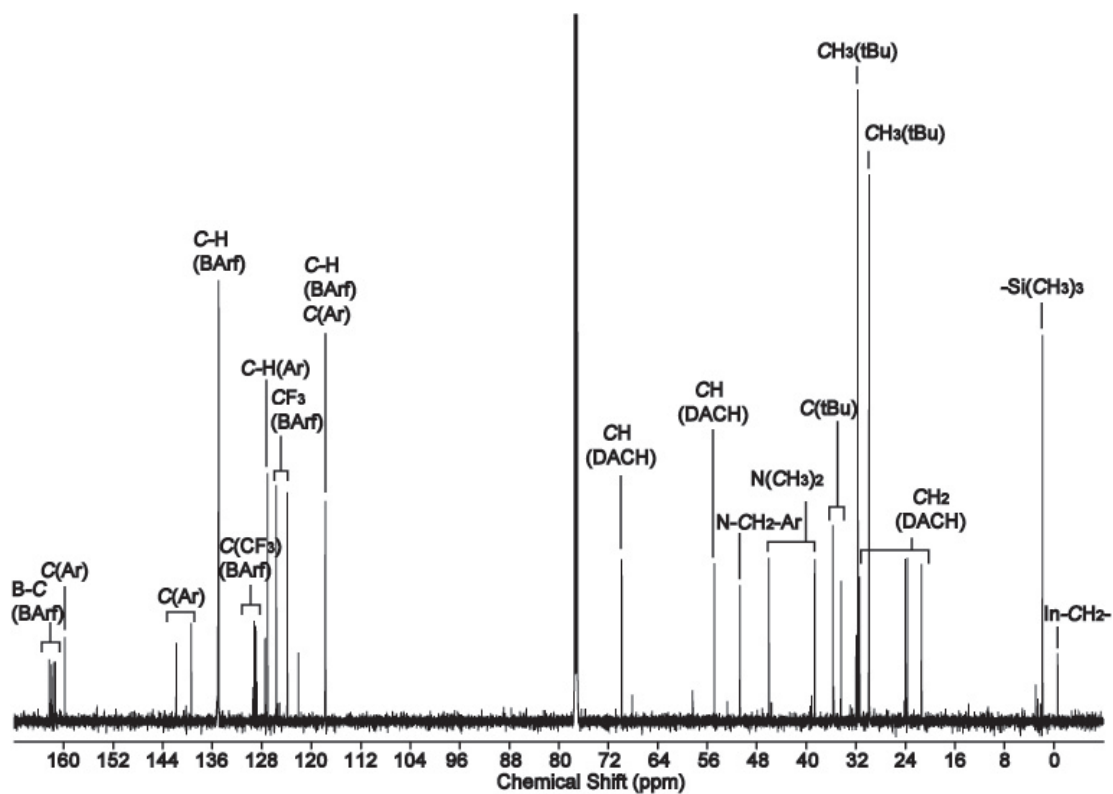


Figure C-2. (a) ${}^1\text{H}$ NMR, (b) ${}^{13}\text{C}\{{}^1\text{H}\}$ NMR, (c) ${}^1\text{H}$ - ${}^1\text{H}$ COSY, (d) ${}^1\text{H}$ - ${}^1\text{H}$ NOSEY (optimized mixing time: 400 ms), (e) ${}^1\text{H}$ - ${}^{13}\text{C}\{{}^1\text{H}\}$ HMQC NMR and (f) ${}^1\text{H}$ - ${}^{13}\text{C}\{{}^1\text{H}\}$ HMBC NMR spectrum of **14** $[(\text{NNO}_{\text{tBu}})\text{In}(\text{CH}_2\text{SiMe}_3)][\text{B}(\text{C}_6\text{F}_5)_4]$ (400 MHz, CDCl_3 , 25 $^\circ\text{C}$).

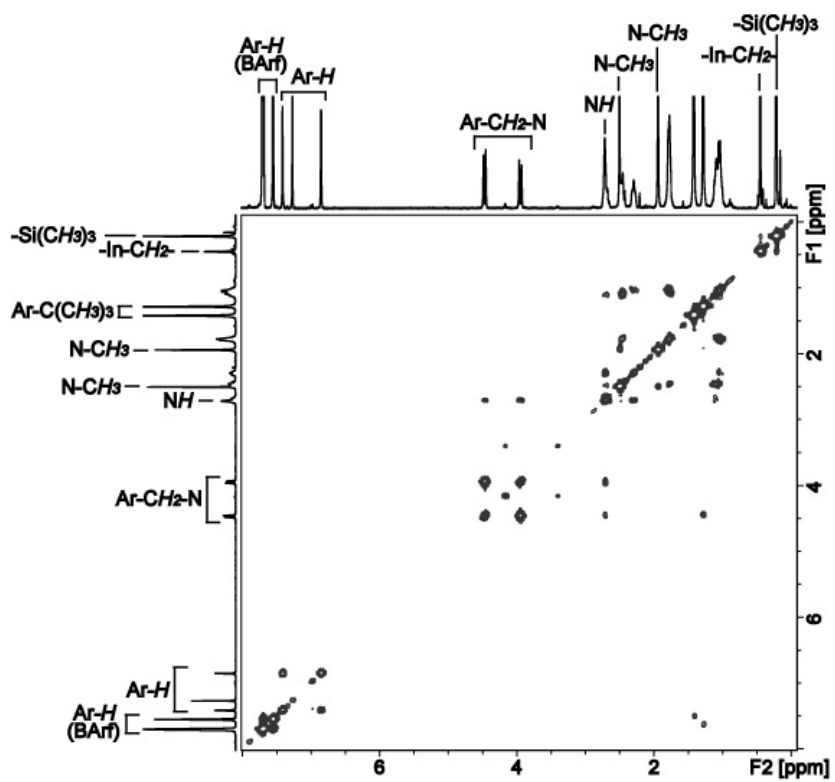
(a)



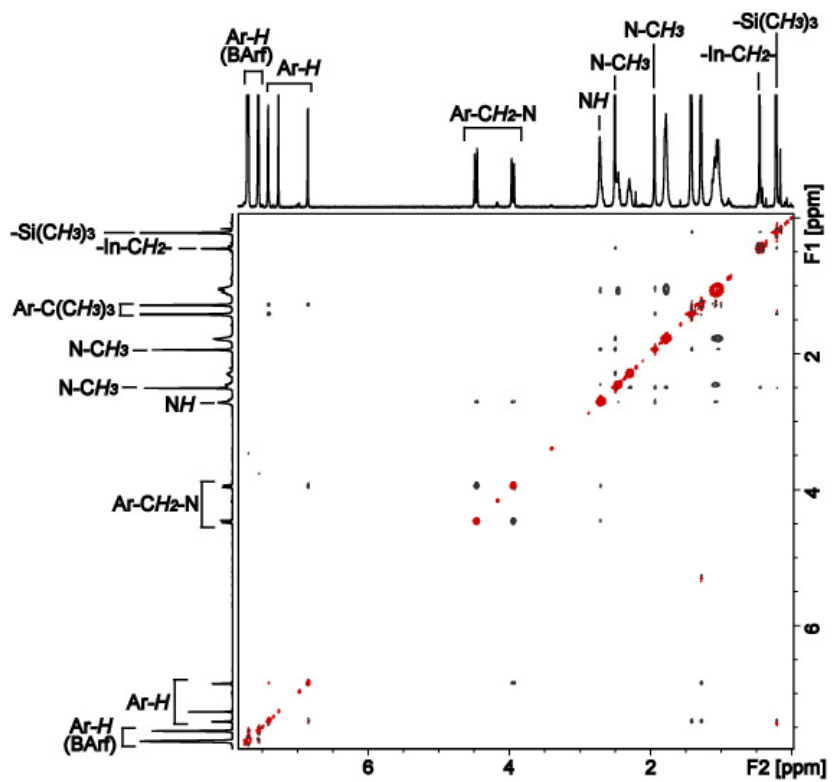
(b)



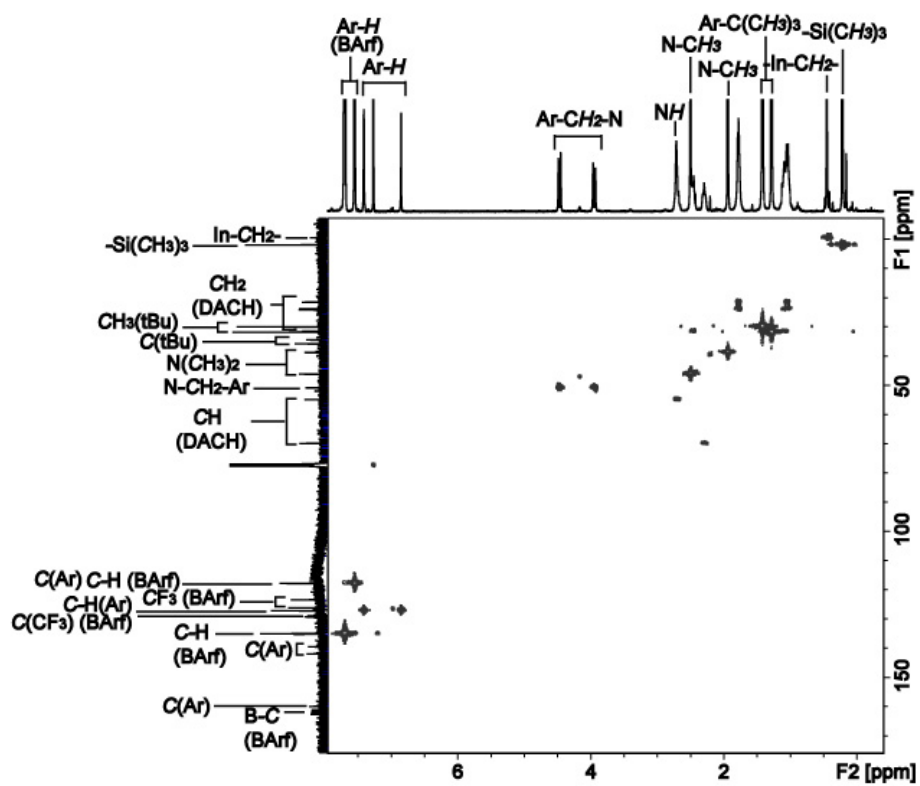
(c)



(d)



(e)



(f)

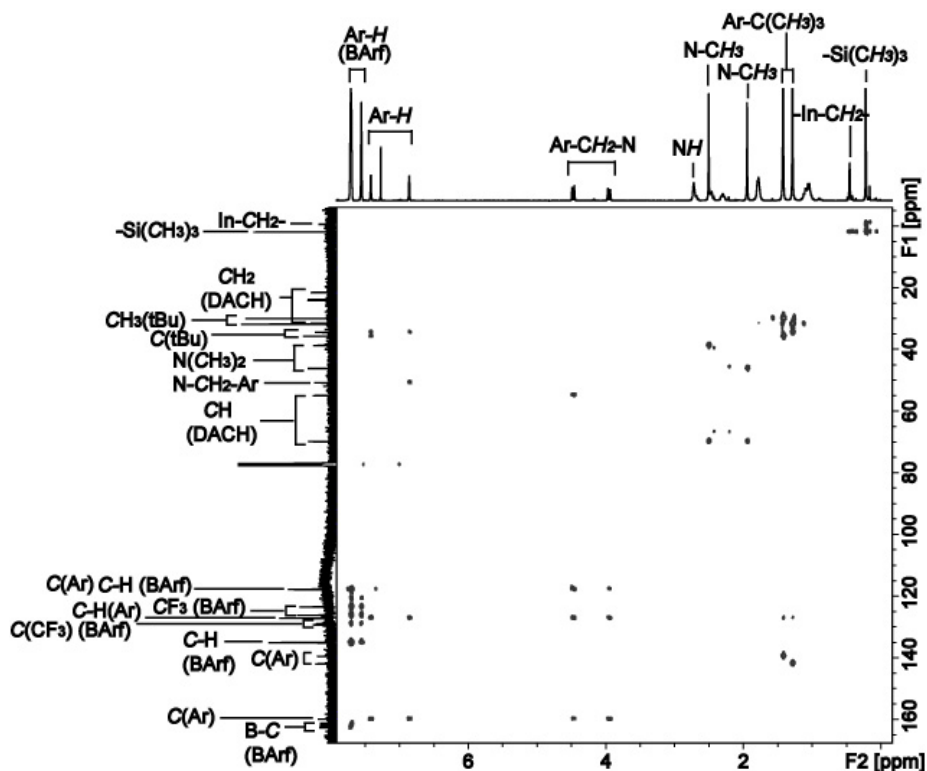
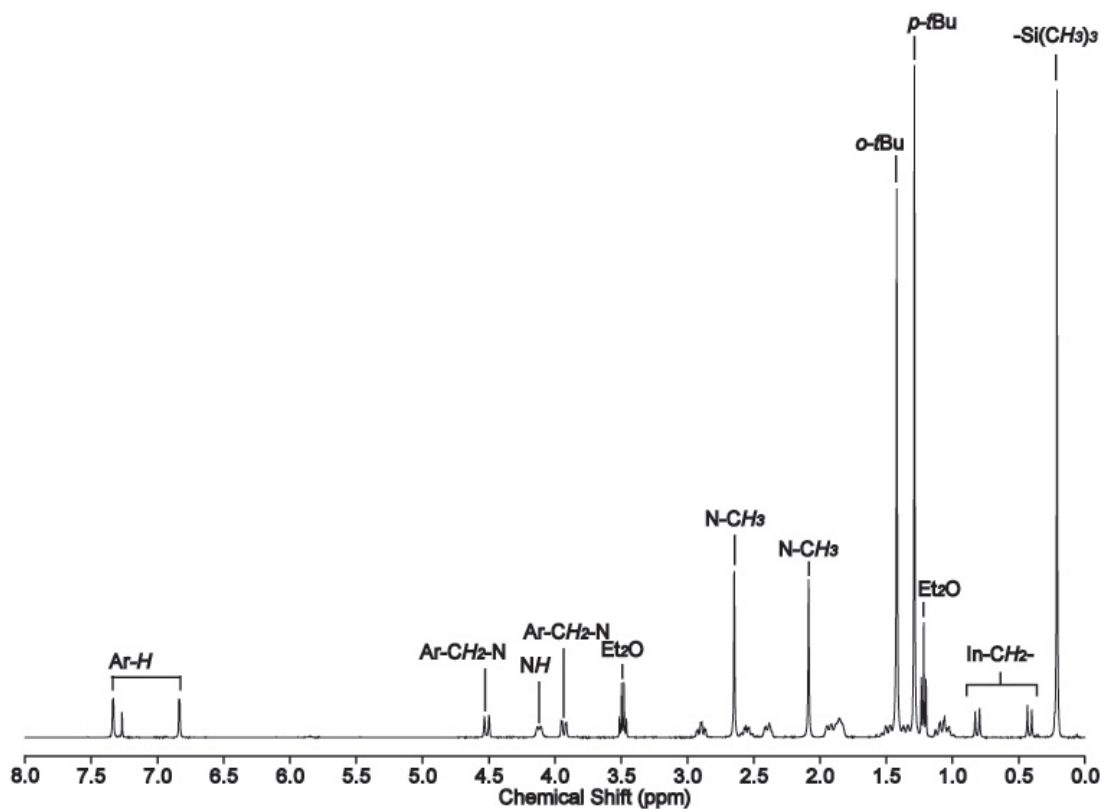
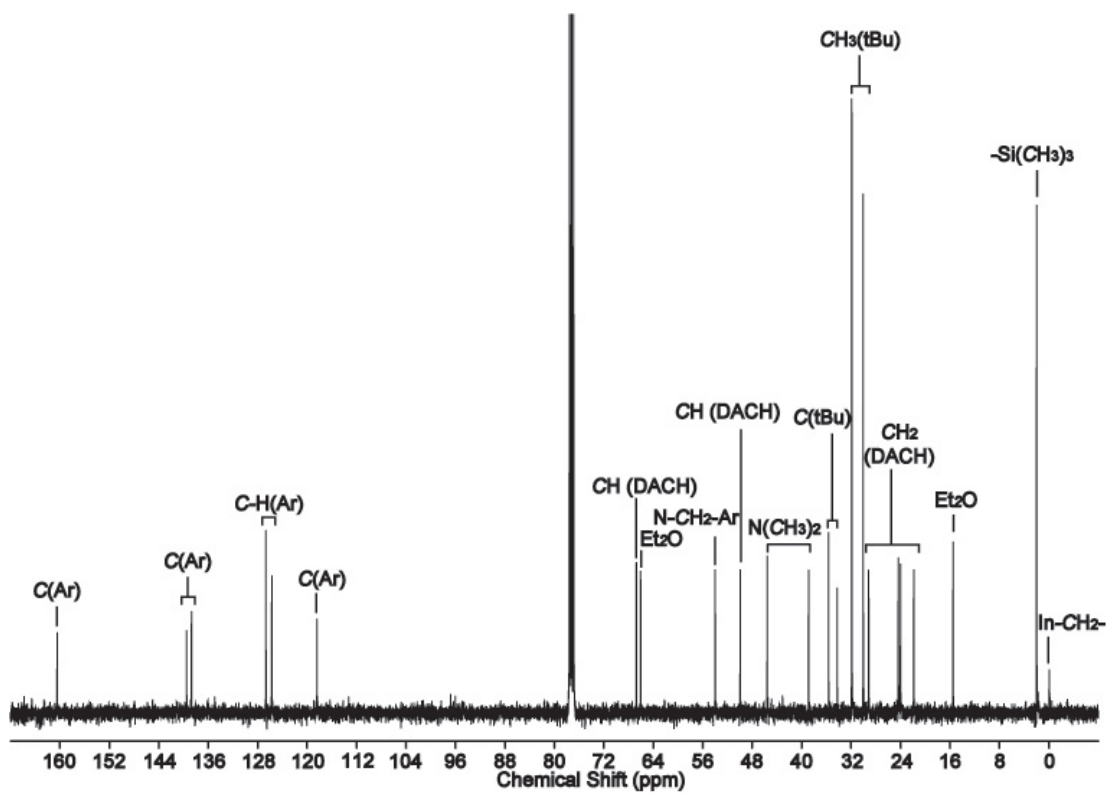


Figure C-3. (a) ^1H NMR, (b) $^{13}\text{C}\{^1\text{H}\}$ NMR, (c) ^1H - ^1H COSY, (d) ^1H - ^1H NOSEY (optimized mixing time: 400 ms), (e) ^1H - $^{13}\text{C}\{^1\text{H}\}$ HMQC NMR and (f) ^1H - $^{13}\text{C}\{^1\text{H}\}$ HMBC NMR spectrum of **15** [(NNO_{tBu})In(CH₂SiMe₃)] [BArf] (400 MHz, CDCl₃, 25 °C).

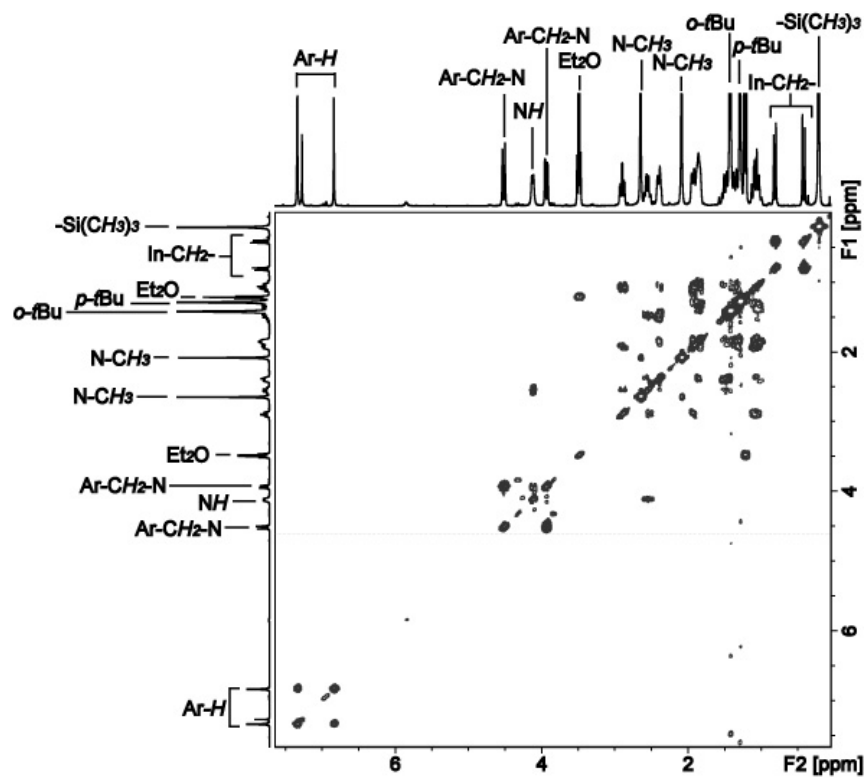
(a)



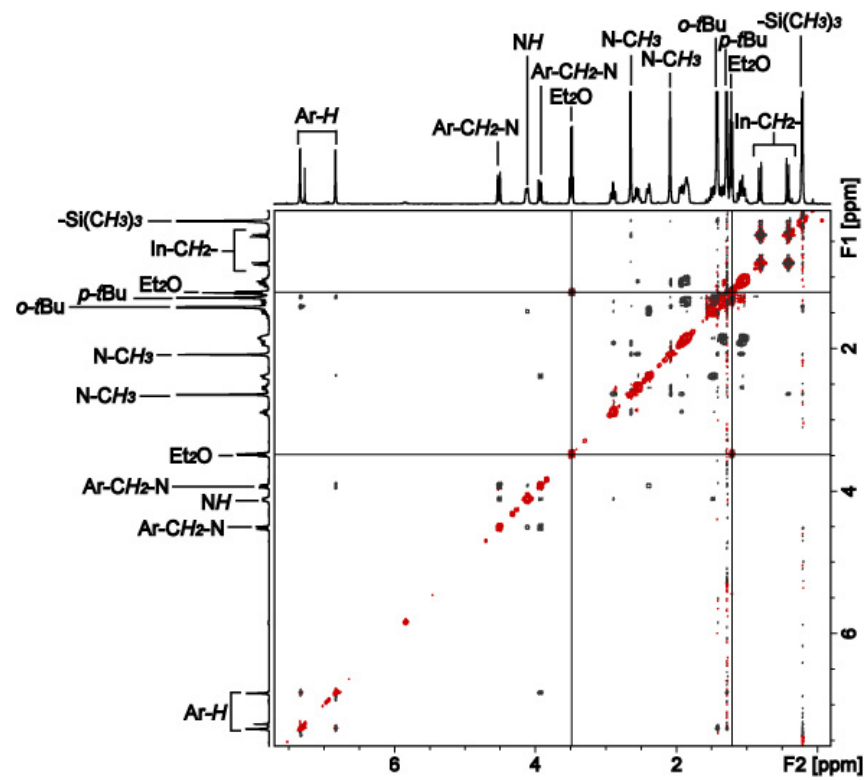
(b)



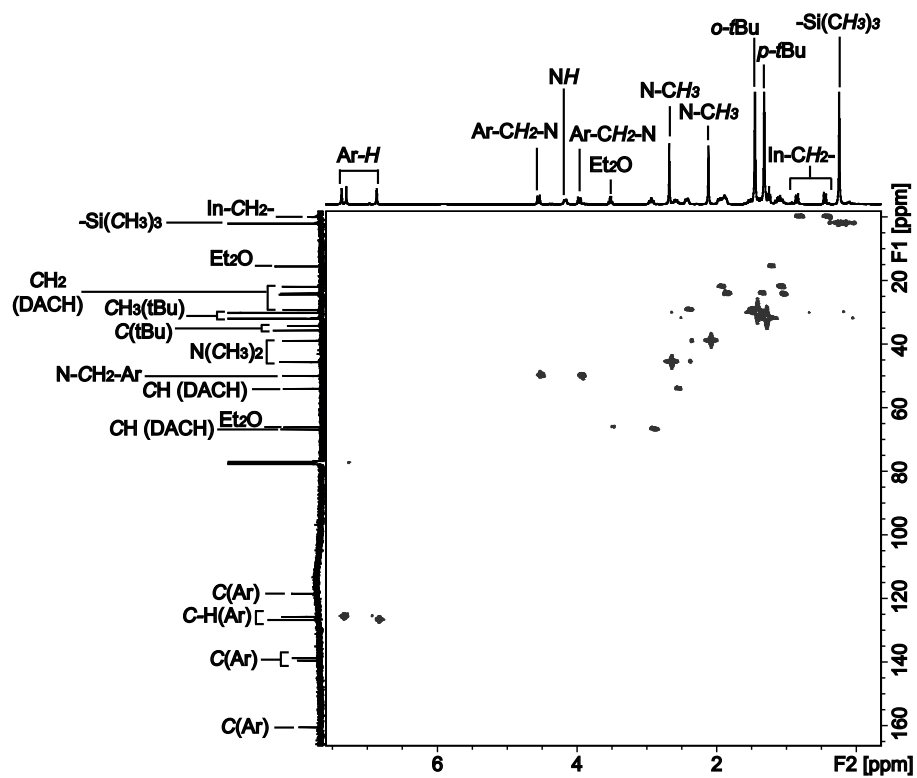
(c)



(d)



(e)



(f)

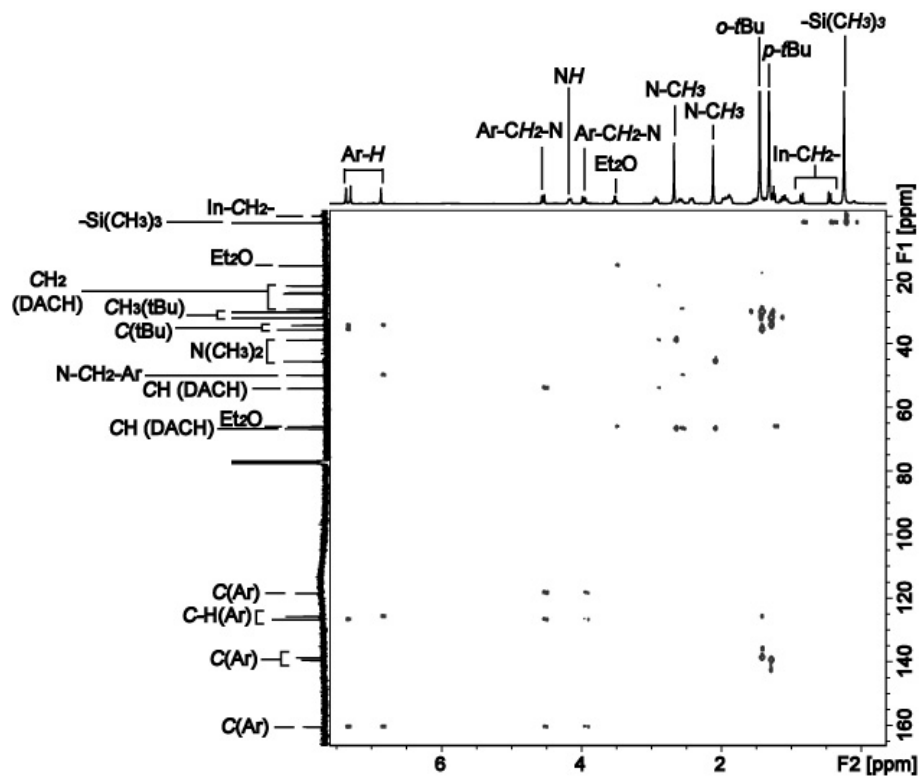


Figure C-4. (a) ^1H NMR, (b) $^{13}\text{C}\{^1\text{H}\}$ NMR, (c) ^1H - ^1H COSY, (d) ^1H - ^1H NOSEY (optimized mixing time: 400 ms), (e) ^1H - $^{13}\text{C}\{^1\text{H}\}$ HMQC NMR and (f) ^1H - $^{13}\text{C}\{^1\text{H}\}$ HMBC NMR spectrum of **16** [(NNO_{tBu}) $\text{In}(\text{CH}_2\text{SiMe}_3)$][PF_6] (400 MHz, CDCl_3 , 25 °C).

C.2 Selective crystal data for 13, 14 and 16.

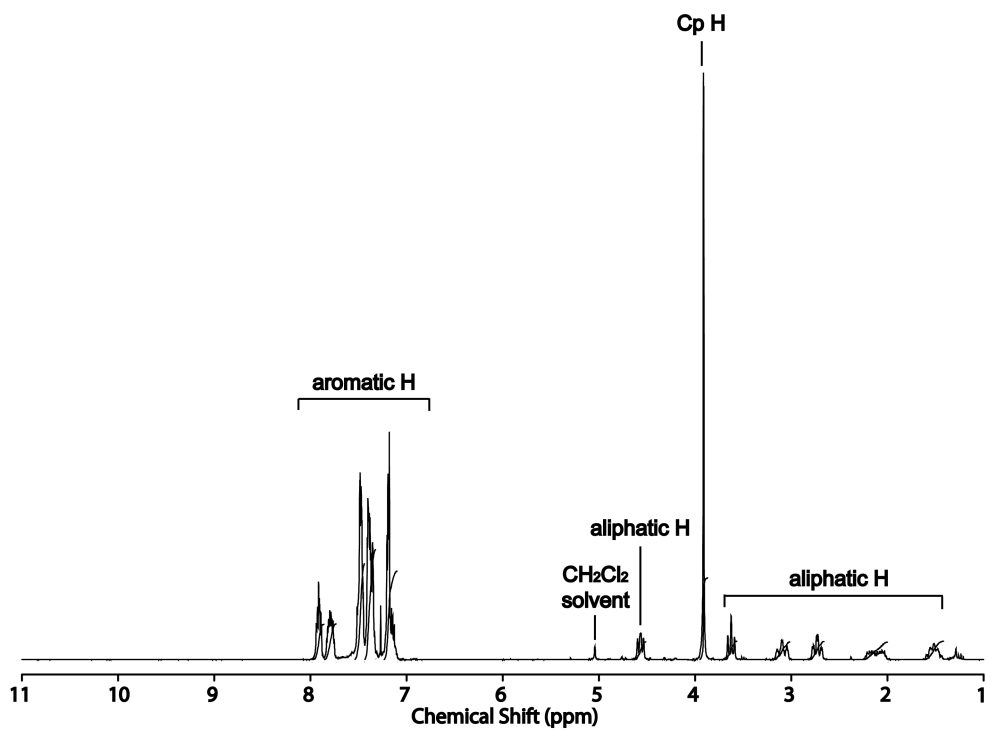
	13	14	16
empirical formula	C ₃₁ H ₆₁ InN ₂ OSi ₂	C ₁₁₁ H ₁₂₀ B ₂ F ₄₀ In ₂ N ₄ O ₃ Si ₂	C ₃₂ H ₆₀ F ₆ InN ₂ O ₂ PSi
fw	648.82	2625.55	780.69
<i>T</i> (K)	173	90	90
<i>a</i> (Å)	14.5173(5)	13.9210(5)	14.750(7)
<i>b</i> (Å)	22.1551(9)	16.0270(6)	14.750(0)
<i>c</i> (Å)	11.8658(4)	26.4150(9)	35.67(2)
<i>α</i> (deg)	90	91.0320(10)	90
<i>β</i> (deg)	106.121(2)	101.5490(10)	90
<i>γ</i> (deg)	90	91.7730(10)	90
volume (Å ³)	3666.4(2)	5769.7(4)	7762(7)
<i>Z</i>	4	2	8
cryst syst	monoclinic	triclinic	tetragonal
space group	<i>P</i> 2 ₁ / <i>c</i>	<i>P</i> -1	<i>P</i> 4 ₃ 2 ₁ 2
<i>d</i> _{calc} (g/cm ³)	1.175	1.511	1.336
<i>μ</i> (Mo Kα) (cm ⁻¹)	7.33	5.37	7.38
2 <i>θ</i> _{max} (deg)	57.5	59.1	65.2
absor corr (<i>T</i> _{min} , <i>T</i> _{max})	0.844, 0.929	0.743, 0.984	0.864, 0.929
total no. of reflns	36 742	157 071	96 058
no. of indep reflns (<i>R</i> _{int})	5 920 (0.038)	32 342 (0.049)	12 991 (0.037)
residuals (refined on <i>F</i> ²): <i>R</i> ₁ ; <i>wR</i> ₂	0.063, 0.098	0.055, 0.096	0.030, 0.059
GOF	1.204	1.049	1.148
no. obsrvns [<i>I</i> > 2σ(<i>I</i>)]	9933	7859	9476
residuals (refined on <i>F</i> ² : <i>R</i> ₁ ^{<i>a</i>} ; <i>wR</i> ₂ ^{<i>b</i>})	0.048, 0.093	0.036, 0.085	0.027, 0.058

$${}^a R_1 = \sum \|F_o\| - \|F_c\| / \sum \|F_o\|, {}^b wR_2 = [\sum (w(F_o^2 - F_c^2))^2 / \sum w(F_o^2)]^{1/2}$$

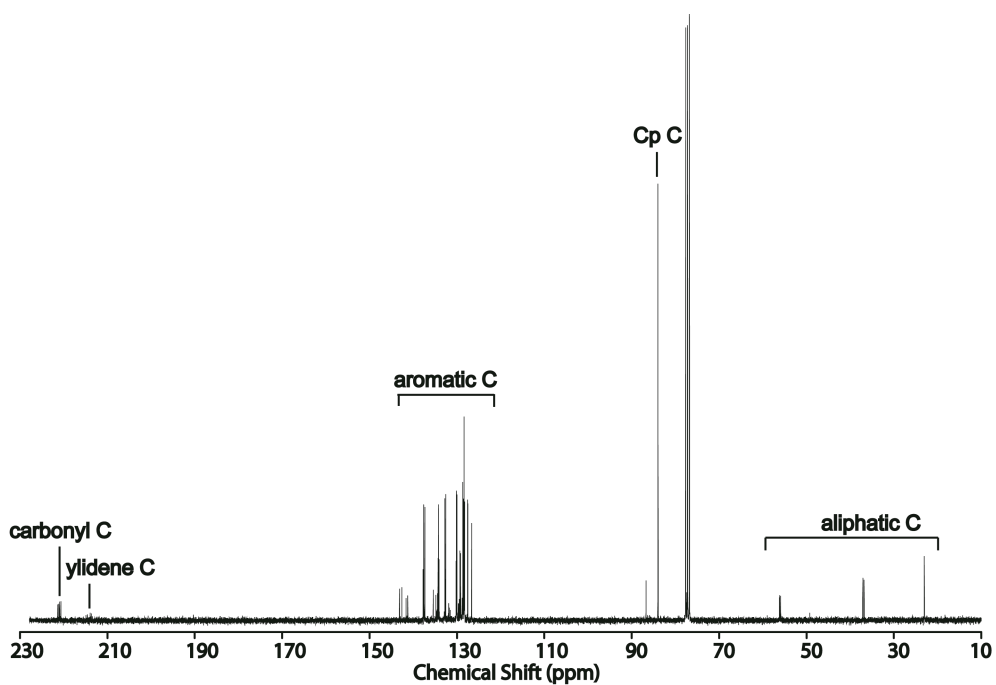
Appendix D

D.1 ^1H , $^{13}\text{C}\{^1\text{H}\}$ and $^{31}\text{P}\{^1\text{H}\}$ NMR spectra of 35, 36, 37 and 38

(a)



(b)



(c)

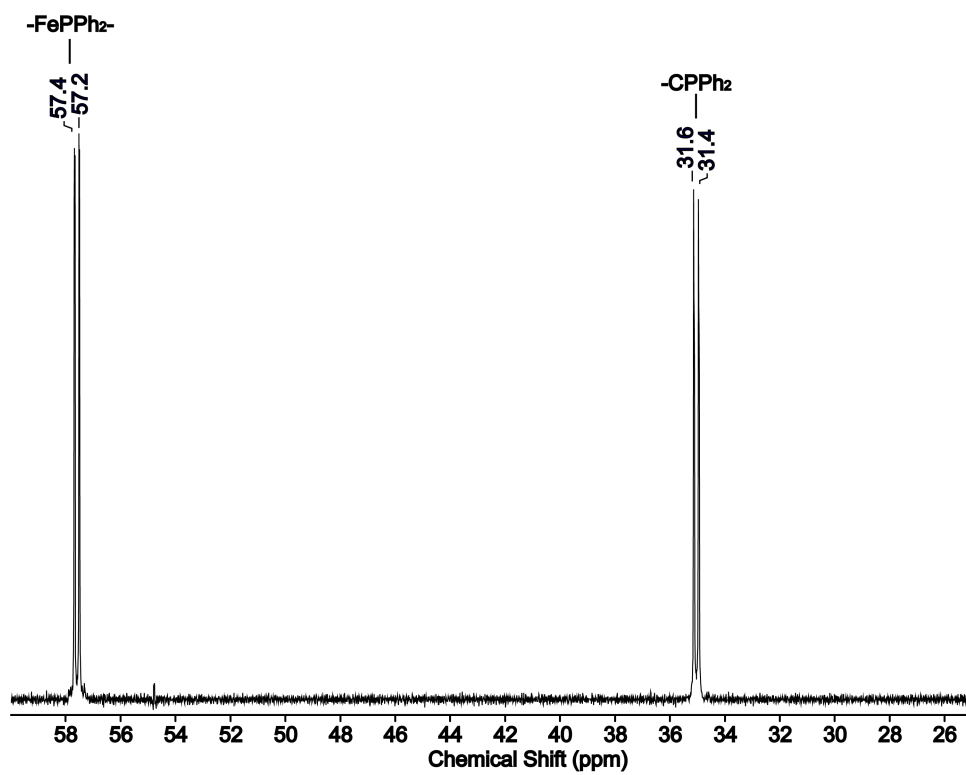
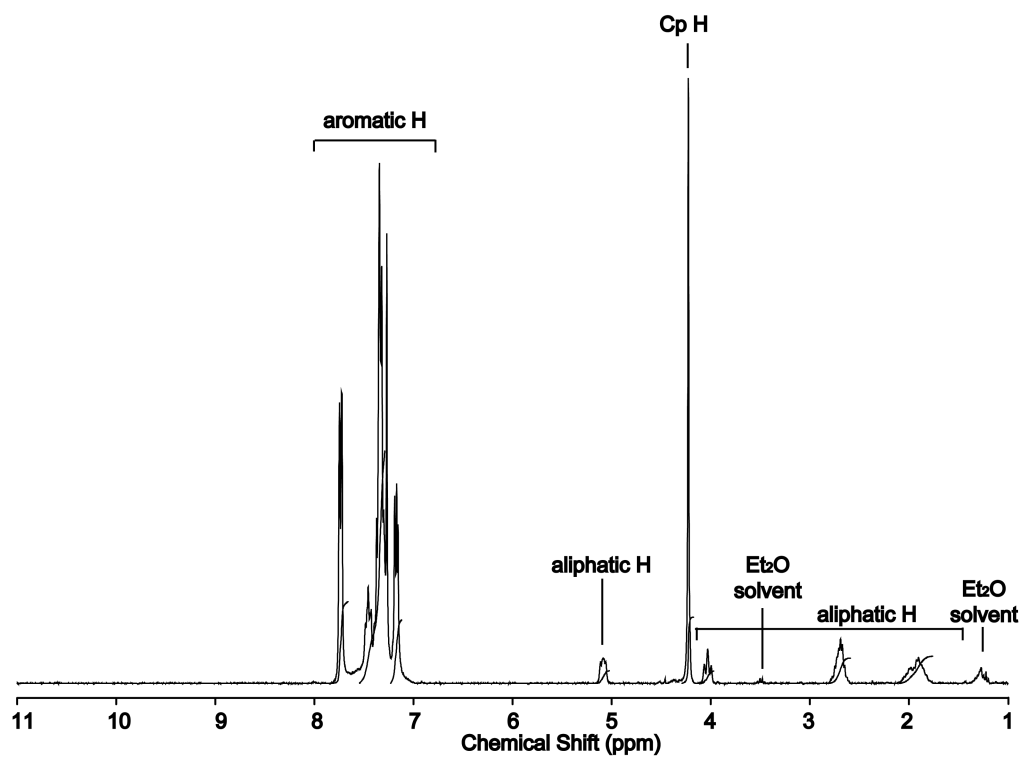
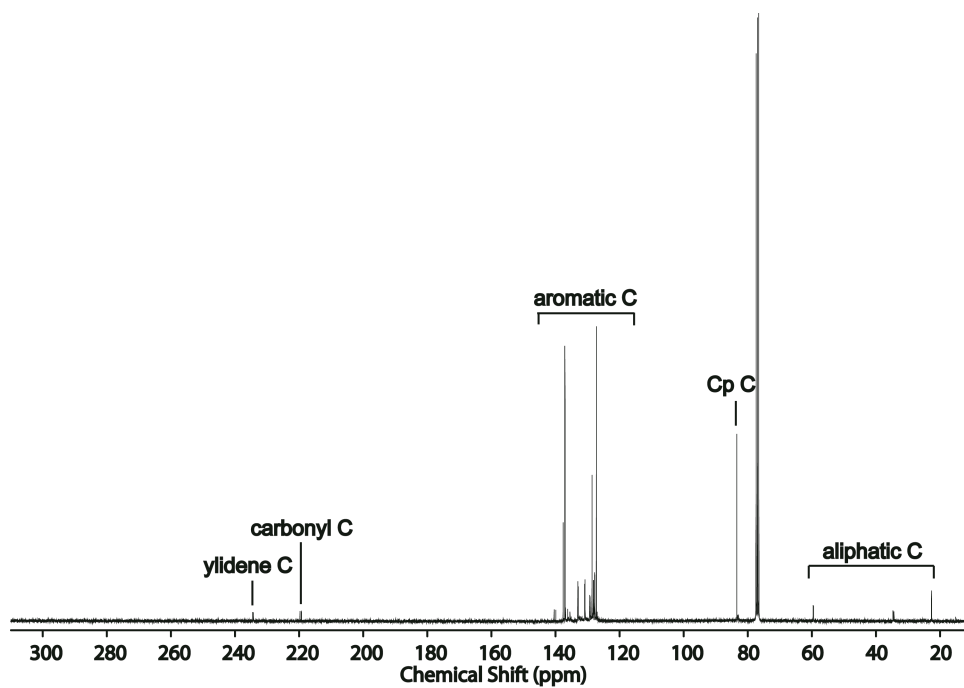


Figure D-1. ^1H , $^{13}\text{C}\{^1\text{H}\}$ and $^{31}\text{P}\{^1\text{H}\}$ NMR spectra of **35** in CDCl_3 at 25 °C.

(a)



(b)



(c)

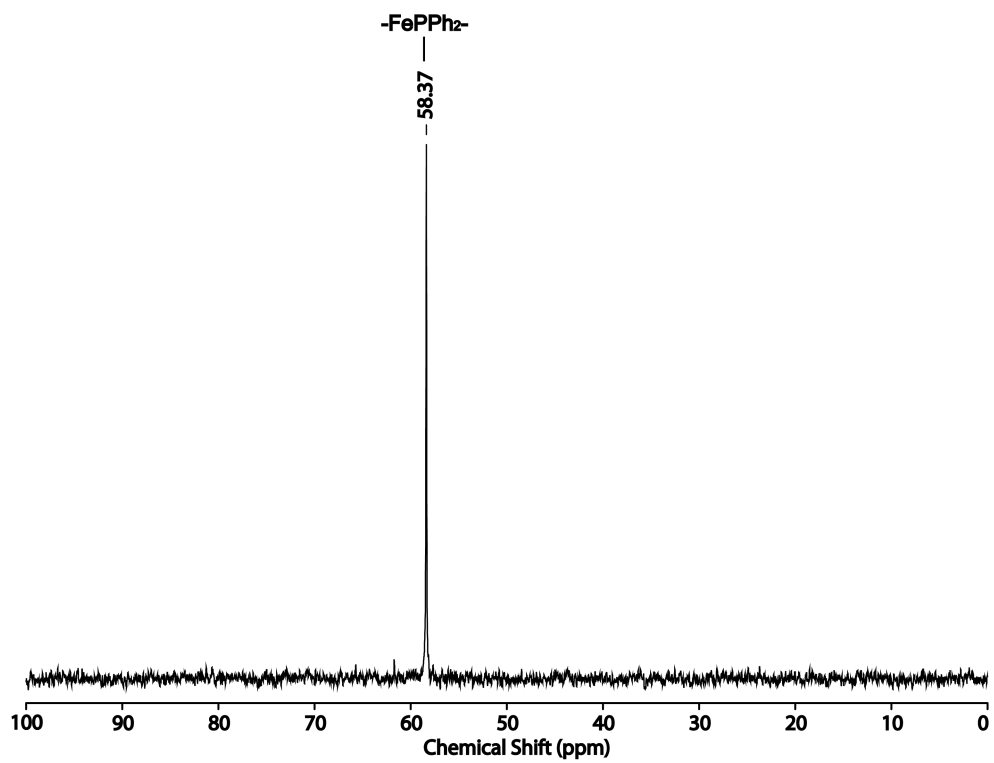
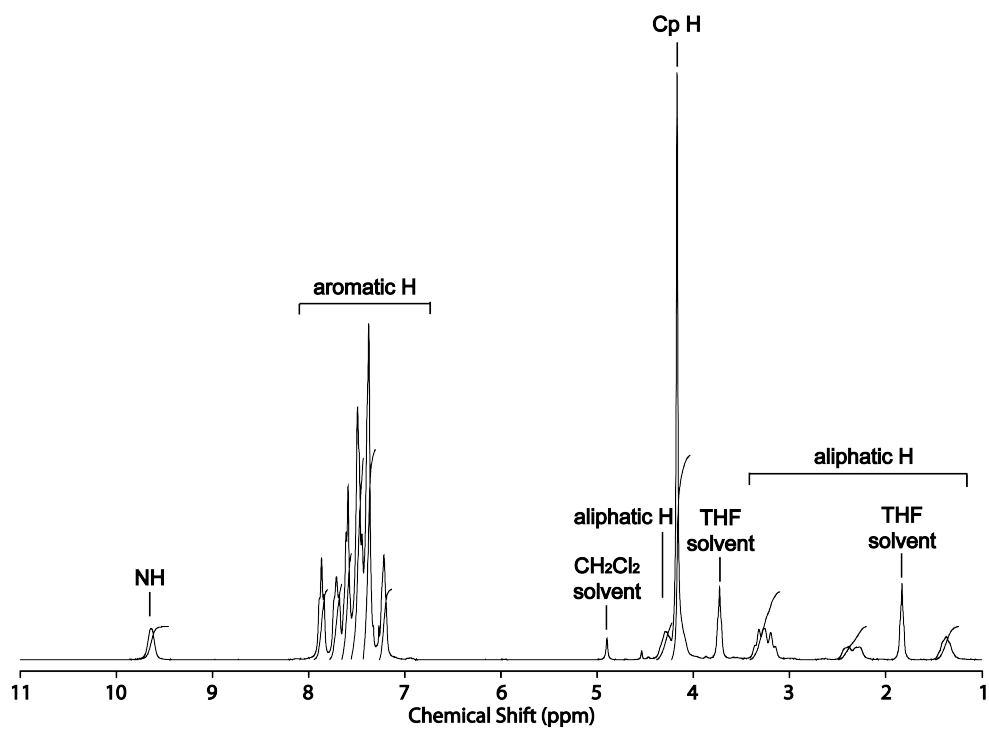
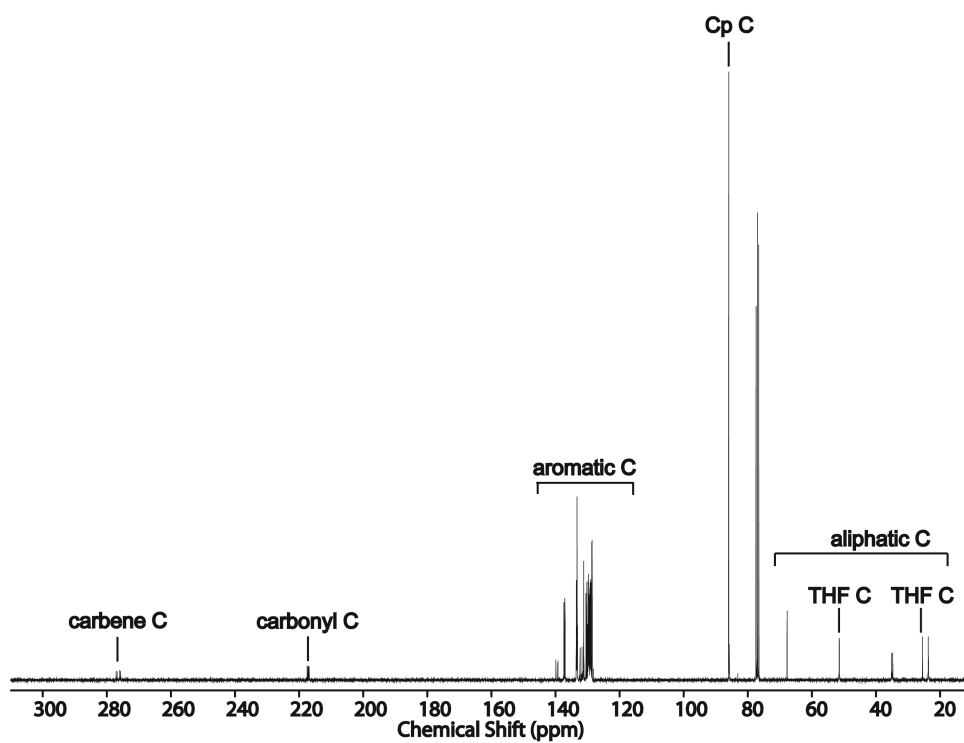


Figure D-2. ^1H , $^{13}\text{C}\{^1\text{H}\}$ and $^{31}\text{P}\{^1\text{H}\}$ NMR spectra of **36** in CDCl_3 at 25 °C.

(a)



(b)



(c)

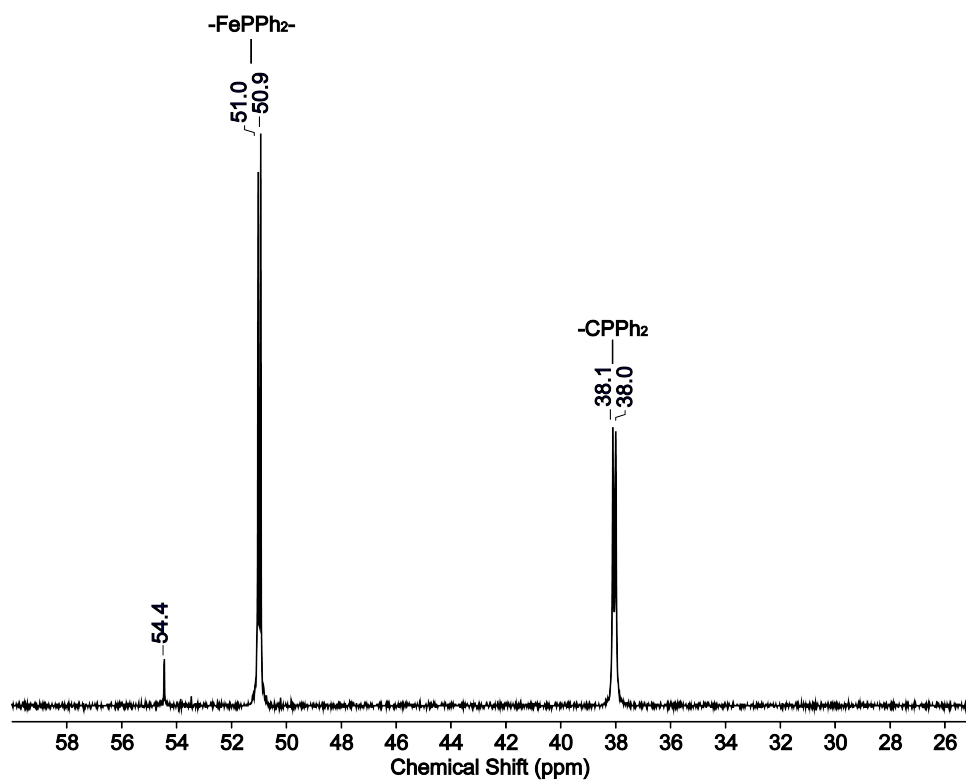
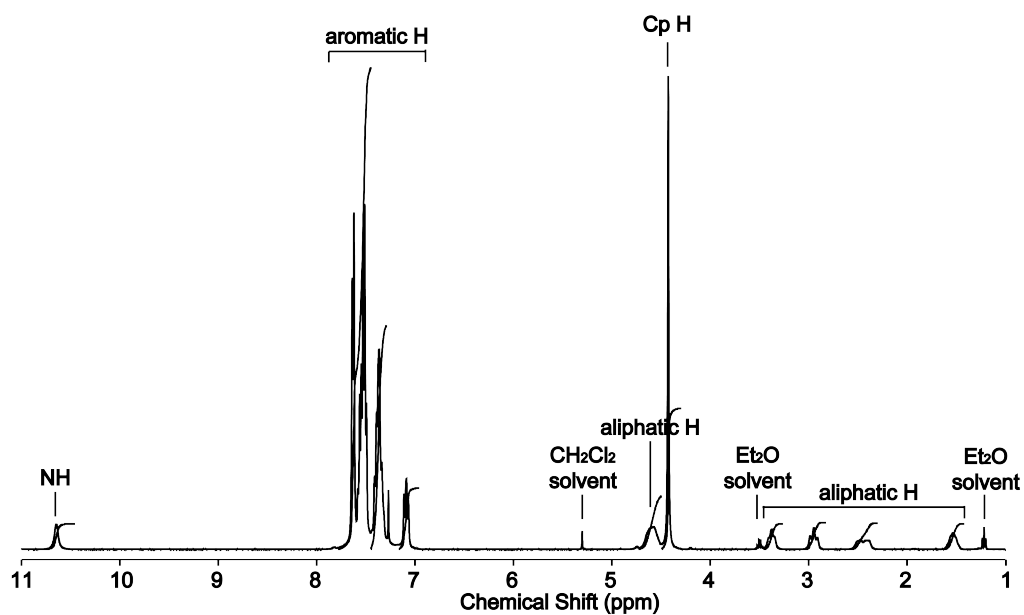
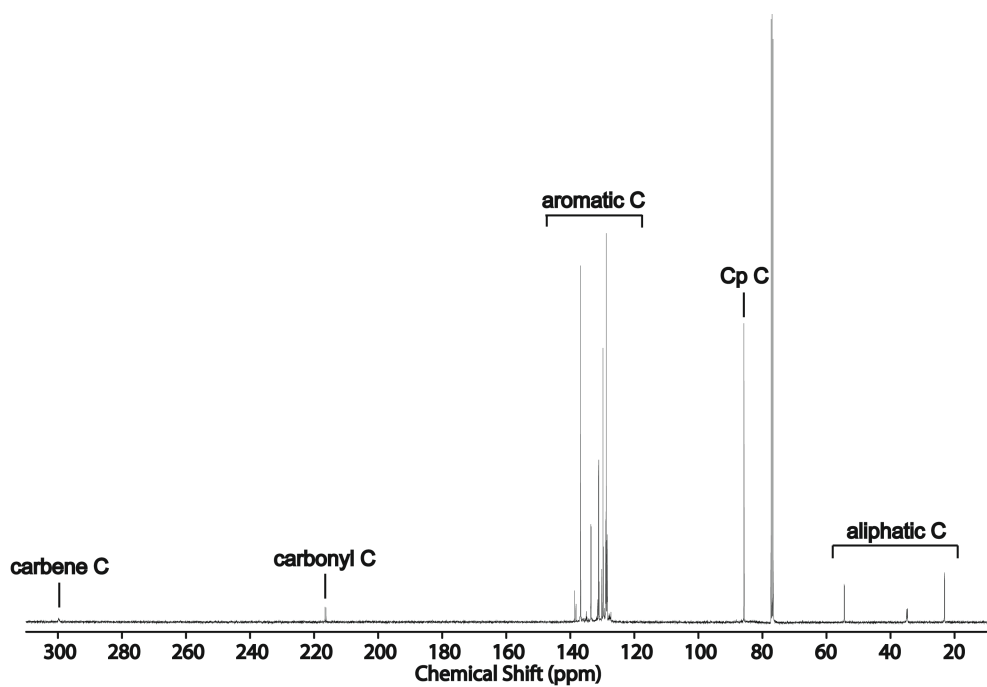


Figure D-3. (a) ^1H , (b) $^{13}\text{C}\{^1\text{H}\}$ and (c) $^{31}\text{P}\{^1\text{H}\}$ NMR spectra of **37** in CDCl_3 at 25 °C.

(a)



(b)



(c)

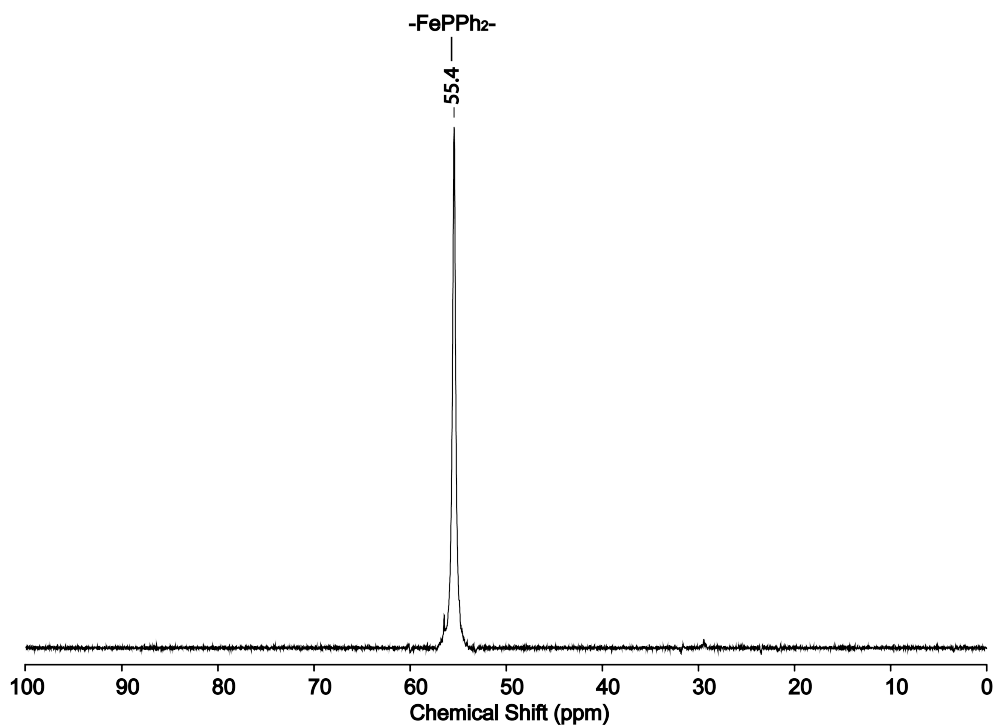


Figure D-4. (a) ^1H , (b) $^{13}\text{C}\{^1\text{H}\}$ and (c) $^{31}\text{P}\{^1\text{H}\}$ NMR spectra of **38** in CDCl_3 at 25 °C.

D.2 Overlaid $^{31}\text{P}\{^1\text{H}\}$ NMR spectra

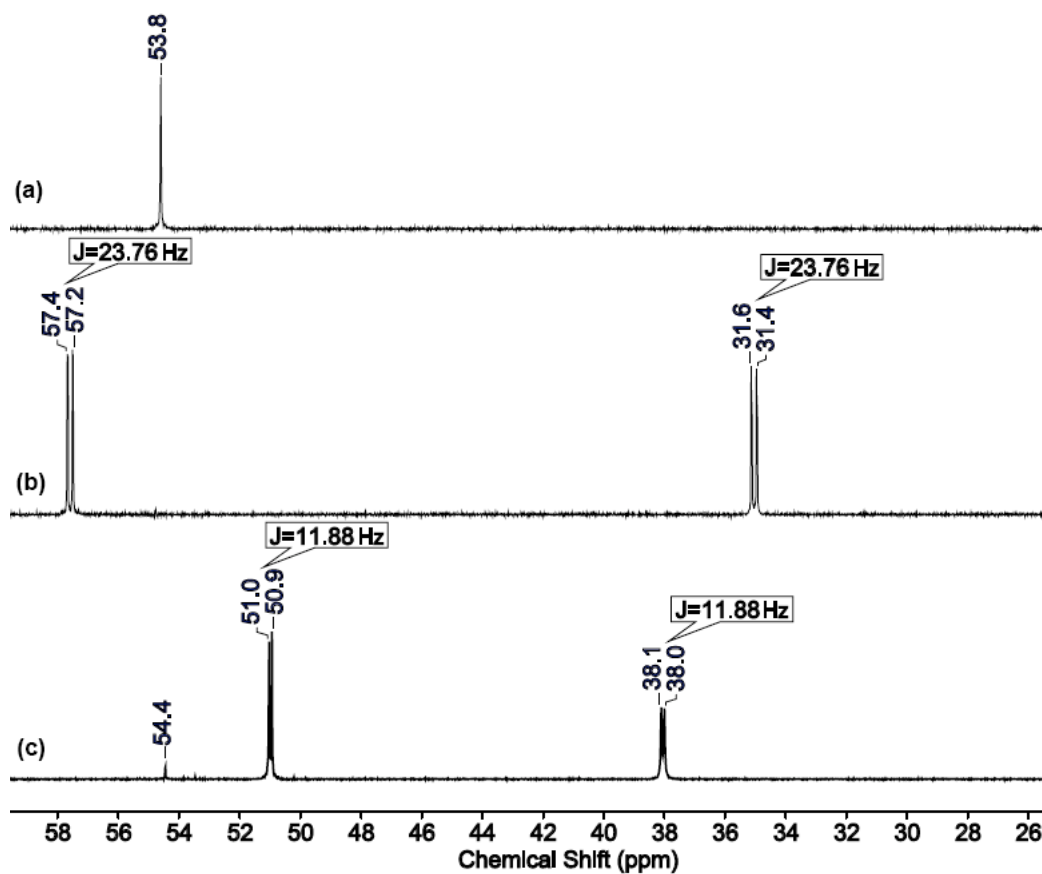


Figure D-5. Overlaid $^{31}\text{P}\{^1\text{H}\}$ NMR spectra of (a) the isocyanide complex **17**, (b) the acyclic (phosphino)(amino)carbanion complex **35**, and (c) the acyclic (phosphino)(amino)carbene complex **37** in CDCl_3 at 25 °C.

D.3 IR, $^{31}\text{P}\{^1\text{H}\}$ NMR and $^{13}\text{C}\{^1\text{H}\}$ NMR spectroscopic data for 16-38.

	Complexes	IR (cm^{-1})			$^{31}\text{P}\{^1\text{H}\}$ (ppm)	$^{13}\text{C}\{^1\text{H}\}$ (ppm)		
		$V_{\max}(\text{CO})$	$V_{\max}(\text{CN})$	$V_{\max}(\text{C=N})$		$^{13}\text{C}_{\text{carbonyl}}$	$^{13}\text{C}_{\text{carbanion}}$	$^{13}\text{C}_{\text{carbene}}$
17 ^a	$[\text{CpFe}(\text{CO})(\text{P}_{\text{Ph}}\text{CN})]^+\text{I}^-$	1998	2089		54.0	213.0 (d, $^2J_{\text{C-P}}=22.3$ Hz)		
18	$[\text{CpFe}(\text{CO})(\text{P}_{\text{t-butyl}}\text{CN})]^+\text{I}^-$	2001	2090		87.7	214.2 (d, $^2J_{\text{C-P}}=19.5$ Hz)		
19	$[\text{CpFe}(\text{CO})(\text{P}_{\text{t-butyl}}\text{C}_{\text{N}(\text{n-butyl})}\text{N}_{\text{H}})]^+\text{I}^-$	1950		1546	77.9	210.7 (d, $^2J_{\text{C-P}}=27.3$ Hz)		221.0 (d, $^2J_{\text{C-P}}=33.2$ Hz)
20	$[\text{CpFe}(\text{CO})(\text{P}_{\text{Ph}}\text{C}_{\text{NH}(\text{n-butyl})}\text{N}_{\text{H}})]^+\text{I}^-$	1949		1546	56.7	209.61 (d, $^2J_{\text{C-P}}=24.91$ Hz)		218.05 (d, $^2J_{\text{C-P}}=31.83$ Hz)
21	$[\text{CpFe}(\text{CO})(\text{P}_{\text{Ph}}\text{C}_{\text{N}(\text{nhexyl})_2}\text{N}_{\text{H}})]^+\text{I}^-$	1948		1535	55.9	210.00 (d, $^2J_{\text{C-P}}=20.96$ Hz)		219.16 (d, $^2J_{\text{C-P}}=36.99$ Hz)
22	$[\text{CpFe}(\text{CO})(\text{P}_{\text{Ph}}\text{C}_{\text{NH}(3\text{-methylphenyl})}\text{N}_{\text{H}})]^+\text{I}^-$	1954		1536	57.9	216.43 (d, $^2J_{\text{C-P}}=24.54$ Hz)		217.58 (d, $^2J_{\text{C-P}}=32.20$ Hz)
23	$[\text{CpFe}(\text{CO})(\text{PC}_{\text{N}(\text{chloroethyl})}\text{N}_{\text{H}})]^+\text{I}^-$	1959		1551	56.4	211.35 (d, $^2J_{\text{C-P}}=28.36$ Hz)		218.11 (d, $^2J_{\text{C-P}}=32.06$ Hz)
24	$[\text{CpFe}(\text{CO})(\text{PC}_{\text{N}(\text{chloropropyl})}\text{N}_{\text{H}})]^+\text{I}^-$	1952		1551	56.4	211.04 (d, $^2J_{\text{C-P}}=24.66$ Hz)		218.16 (d, $^2J_{\text{C-P}}=32.06$ Hz)
25	$[\text{CpFe}(\text{CO})(\text{PC}_{\text{NH}(\text{N}-5\text{Cy})}\text{N}_{\text{H}})]^+\text{I}^-$	1949		1487	57.0	211.54 (d, $^2J_{\text{C-P}}=27.60$ Hz)		218.81 (d, $^2J_{\text{C-P}}=29.14$ Hz)
26	$[\text{CpFe}(\text{CO})(\text{PC}_{\text{NH}(\text{N}-6\text{Cy})}\text{N}_{\text{H}})]^+\text{I}^-$	1952		1548	56.2	205.75 (d, $^2J_{\text{C-P}}=24.91$ Hz)		218.25 (d, $^2J_{\text{C-P}}=33.22$ Hz)
27	$\text{CpFe}(\text{CO})(\text{PC}_{\text{O}(\text{Me})}\text{N})$	1937		1566	60.6	221.08 (d, $^2J_{\text{C-P}}=31.83$ Hz)	198.03 (d, $^2J_{\text{C-P}}=33.22$ Hz)	
28	$\text{CpFe}(\text{CO})(\text{PC}_{\text{O}(\text{Et})}\text{N})$	1937		1561	61.1	221.22 (d, $^2J_{\text{C-P}}=32.06$ Hz)	197.64 (d, $^2J_{\text{C-P}}=30.83$ Hz)	
29	$\text{CpFe}(\text{CO})(\text{PC}_{\text{O}(\text{Pr})}\text{N})$	1936		1561	61.3	221.37 (d, $^2J_{\text{C-P}}=33.31$ Hz)	196.27 (d, $^2J_{\text{C-P}}=33.31$ Hz)	
30	$[\text{CpFe}(\text{CO})(\text{PC}_{\text{O}(\text{Me})}\text{N}_{\text{H}})]^+\text{BF}_4^-$	1960		1552	55.6	218.25 (d, $^2J_{\text{C-P}}=27.60$ Hz)		237.08 (d, $^2J_{\text{C-P}}=27.60$ Hz)
31	$[\text{CpFe}(\text{CO})(\text{PC}_{\text{O}(\text{Et})}\text{N}_{\text{H}})]^+\text{BF}_4^-$	1958		1551	55.6	218.09 (d, $^2J_{\text{C-P}}=27.13$ Hz)		236.34 (d, $^2J_{\text{C-P}}=29.59$ Hz)
32	$[\text{CpFe}(\text{CO})(\text{PC}_{\text{O}(\text{Pr})}\text{N}_{\text{H}})]^+\text{BF}_4^-$	1959		1544	56.0	217.92 (d, $^2J_{\text{C-P}}=28.36$ Hz)		234.63 (d, $^2J_{\text{C-P}}=25.89$ Hz)
33	$[\text{CpFe}(\text{CO})(\text{PC}_{\text{NO}-5\text{Cy}})]^+\text{Cl}^-$	1964		1523	55.8	217.62 (d, $^2J_{\text{C-P}}=26.66$ Hz)		229.00 (d, $^2J_{\text{C-P}}=28.50$ Hz)
34	$[\text{CpFe}(\text{CO})(\text{PC}_{\text{NO}-6\text{Cy}})]^+\text{Cl}^-$	1966		1534	56.3	217.97 (d, $^2J_{\text{C-P}}=29.06$ Hz)		231.32 (d, $^2J_{\text{C-P}}=29.06$ Hz)
35	$\text{CpFe}(\text{CO})(\text{P}_{\text{Ph}}\text{C}_{\text{P}(\text{Ph})_2}\text{N})$	1912		1561	31.51 (d, $^3J_{\text{P-P}}=23.76$ Hz) 57.28 (d, $^3J_{\text{P-P}}=23.76$ Hz) (dd, $^3J_{\text{C-P}}=16.91$, $^2J_{\text{C-P}}=20.42$ Hz) (dd, $^1J_{\text{C-P}}=70.57$, $^2J_{\text{C-P}}=23.96$ Hz)	221.04	214.3	
36	$[\text{CpFe}(\text{CO})(\text{P}_{\text{Ph}}\text{C}_{\text{P}(\text{Ph})_2}\text{N}_{\text{H}})]^+\text{BF}_4^-$	1956		1529	38.05 (d, $^3J_{\text{P-P}}=11.88$ Hz) 50.98 (d, $^3J_{\text{P-P}}=11.88$ Hz) (dd, $^2J_{\text{C-P}}=19.58$, $^3J_{\text{C-P}}=8.97$ Hz)	217.17		276.39 (dd, $^1J_{\text{C-P}}=61.20$, $^2J_{\text{C-P}}=23.66$ Hz)
37	$\text{CpFe}(\text{CO})(\text{P}_{\text{Ph}}\text{C}_{\text{Si}(\text{Ph})_3}\text{N})$	1915		1569	57.8	223.2 (br. s.)	218.3 (d, $^2J_{\text{C-P}}=26.4$ Hz)	
38	$[\text{CpFe}(\text{CO})(\text{P}_{\text{Ph}}\text{C}_{\text{Si}(\text{Ph})_3}\text{N}_{\text{H}})]^+\text{BF}_4^-$	1959		1518	55.4	216.4 (d, $^2J_{\text{C-P}}=32.3$ Hz)		299.4 (br. s.)

^a Ref³⁹⁷.

D.4 Selected crystallographic data for compounds 19, 21, 23, 26, 27, 34, 35, 36, and 38.

	19	21	23	26	27	34	35	36	38
empirical formula	C ₂₂ H ₄₀ N ₂ OPFeI•2CHCl ₃	C ₃₄ H ₄₈ FeIN ₂ OP	C ₂₄ H ₂₇ ClFeIN ₂ OP	C ₂₅ H ₂₈ N ₂ OPFeI•CH ₂ Cl ₂	C ₂₃ H ₂₄ NO ₃ FeP	C ₂₅ H ₂₇ NO ₂ PFeI	C ₃₅ H ₃₂ NOP ₂ Cl ₃ Fe	C ₄₀ H ₃₆ NOFePSi	C ₄₀ H ₃₇ BF ₄ FeNOPSi
fw	801.02	741.46	608.65	671.14	433.25	587.2	706.76	661.61	749.43
T (K)	173	173	173	173	173	173	173	173	173
a (Å)	15.1631(5)	12.9690(4)	20.2320(3)	8.6746(2)	7.4296(2)	8.6529(4)	8.2910(9)	20.407(3)	8.9075(3)
b (Å)	14.9065(5)	16.5713(6)	20.232	22.2743(8)	15.3027(5)	20.7218(8)	11.5242(15)	10.1257(12)	13.6417(4)
c (Å)	16.0890(6)	15.7782(5)	10.5999(2)	14.2245(5)	17.9529(6)	13.1388(6)	17.549(2)	15.793(2)	15.2165(4)
α (deg)	90	90	90	90	90	90	89.073(5)	90	97.466(2)
β (deg)	111.237(1)	104.923(2)	90	100.8600(10)	90	99.379(2)	81.920(4)	90	98.451(2)
γ (deg)	90	90	120	90	90	90	78.355(4)	90	107.810(2)
volume (Å ³)	3389.6(2)	3276.58(19)	3757.59(9)	2699.24(15)	2041.12(11)	2324.34(18)	6848.2(4)	3263.3(7)	1710.99(9)
Z	4	4	6	4	4	4	2	4	2
crystal system	monoclinic	monoclinic	trigonal	monoclinic	orthorhombic	monoclinic	triclinic	orthorhombic	triclinic
space group	<i>P</i> 2 ₁ / <i>c</i>	<i>P</i> 2 ₁ / <i>n</i>	<i>P</i> 6 ₅	<i>P</i> 2 ₁ / <i>c</i>	<i>P</i> 2 ₁ 2 ₁ 2 ₁	<i>C</i> <i>c</i>	<i>P</i> -1	<i>P</i> <i>na</i> 21	<i>P</i> -1
d _{calc} (g/cm ³)	1.570	1.448	1.614	1.652	1.410	1.678	1.444	1.347	1.455
μ (MoKα) (cm ⁻¹)	18.97	14.80	20.24	19.82	8.36	20.68	8.39	5.82	5.80
2θ _{max} (deg)	55.9	55.9	56.2	56.2	50.1	55.1	55.3	47.5	51.1
absorption correction (T _{min} , T _{max})	0.584, 0.738	0.541, 0.800	0.512, 0.641	0.573, 0.820	0.656, 0.882	0.502, 0.733	0.852, 0.927	0.926, 0.983	0.877, 0.955
total no. of reflections	65575	74450	69259	22180	12288	46854	40523	23026	21956
no. of indep reflections (R _{int})	8102 (0.038)	40387 (0.050)	6085 (0.035)	6535 (0.056)	3619(0.040)	30439(0.076)	7408 (0.033)	4952 (0.050)	6306 (0.046)
residuals (refined on F ² , all data):									
R ₁ ; wR ₂	0.048; 0.082	0.0492; 0.0834	0.0225; 0.0611	0.103; 0.236	0.054; 0.098	0.040; 0.073	0.043; 0.085	0.044; 0.062	0.0726; 0.1166
GOF	1.05	1.035	1.176	1.041	1.15	1.049	1.05	1	1.025
no. observations [I > 2σ(I)]	6513	6669	5874	4650	3193	4806	6263	4208	4741
residuals (refined on F ²): R ₁ ^a ; wR ₂ ^b	0.032; 0.072	0.0353; 0.0765	0.0207; 0.0603	0.0720; 0.216	0.045; 0.095	0.032; 0.071	0.033; 0.080	0.031; 0.058	0.048; 0.105

^a R₁ = Σ ||F_o| - |F_c|| / Σ |F_o|; ^b wR₂ = [Σ(w(F_o² - F_c²)²)/Σ w(F_o²)²]^{1/2}.